Behaviour of High Strength Steel Endplate Connections in Fire and after Fire

Xuhong Qiang

Behaviour of High Strength Steel

Endplate Connections

in Fire and after Fire

Proefschrift

ter verkrijging van de graad van doctor
aan de Technische Universiteit Delft,
op gezag van de Rector Magnificus prof. ir. K.C.A.M. Luyben,
voorzitter van het College voor Promoties,
in het openbaar te verdedigen
op dinsdag 16 juli 2013 om 12:30 uur

door

Xuhong QIANG

Master of Science in Structural Engineering, Tongji University, China

geboren te Qiqihar, China

Dit proefschrift is goedgekeurd door de promotor:

Prof.ir. F.S.K. Bijlaard

Copromotor:

Dr. M.H. Kolstein

Samenstelling promotiecommissie:

Rector Magnificus	voorzitter
Prof.ir. F.S.K. Bijlaard	Technische Universiteit Delft, promotor
Dr. M.H. Kolstein	Technische Universiteit Delft, copromotor
Prof.dr. Y. Luo	Tongji University
Prof.dr. J.M. Franssen	University of Liège
Prof.dr.ir. J.W.G. van de Kuilen	München University of Technology
Prof.ir. A.C.W.M. Vrouwenvelder	Technische Universiteit Delft
Ir. L. Twilt	TNO
Prof. dr.ir. J. Wardenier	Technische Universiteit Delft, reservelid

For my grandparents and my parents

Acknowledgements

At the exciting moment when my book is going to be printed, I would like to thank everyone who, in their different ways, gave me support, help and friendship.

First and foremost, I would like to express my deepest gratitude to my supervisors Prof. Frans Bijlaard and Dr. Henk Kolstein. It is really my great fortune to have conducted my PhD research under their supervisions. In the first one or two years, when I experienced the shock of culture and education system, both Prof. Bijlaard and Dr. Kolstein supported and guided me very patiently and cordially so that I could adapt to the Dutch way smoothly. In research, they always gave me the most freedom as long as they were convinced that I was running in the right direction. Their remarkable advocacy for independent research fully explored my research interests and capabilities. Their rigorous professional attitude and dedicated patience are my lifelong model. What I learned from my supervisors is much more than I expected.

I highly appreciate all members of my doctoral examination committee for their careful evaluation, helpful comments and taking the long journey to attend my defence. Special acknowledgements go to Prof. Yongfeng Luo, Ir. Leen Twilt, Prof. Jaap Wardenier and Prof. Jean-Marc Franssen.

Furthermore, I would like to thank my colleagues Sofia Teixeira de Freitas, Maarten Mulder, Ana Margarida Girao Coelho, Richard Pijpers, Carmen Sandhaas, Ayse Nesen Surmeli-Anac, Wolfgang Gard, Roland Abspoel, Geert Ravenshorst, Peter de Vries, Arjan van Rhijn and John Hermsen for their support, help and patience in academic discussion, culture talk, technical support, group excursion, lunch time, coffee break and dining out. Special gratitude goes to Caspar Groot, who taught me the story of art, aroused my interests on the art, showed me around many museums and helped me a lot in my daily life.

What is more, I would like to extend my faithful thanks to my dear friends Zhuqing Yu, Ning Li, Mingliang Li, Tingting Jiang, Yue Xiao, Huanhuan Mao, Jitang Fan, Zhan Zhang, Hailing Zhang and Yuan Zhang who I met in the Netherlands. Thank you so much for sharing cooking, travelling, our minds and our insights with each other, which makes my daily life more colorful, enjoyable and memorable.

Last but not the least, I am always grateful to my grandparents and my parents for their love, guidance, encouragement, understanding and support. You are my reason and my motivation forever. Sincere appreciation goes to Xu Jiang, my office mate and soul mate.

All in all, I deeply appreciate everyone who I met in my life. Without anyone of you, I cannot be the Xuhong of today. No matter when and where, I am just one email or one call away.

Xuhong Qiang
June 2013
Delft, the Netherlands

Summary

The aim of this research is to reveal more information and understanding on behaviour and failure mechanisms of high strength steel endplate connections (combining high strength steel endplates with either mild steel or high strength steel beams and columns in endplate connections) in fire and after fire, for an effective application of high strength structural steels in civil engineering as well as enhancing the fire safety of steel structures.

The research work consists of three main parts: (Part I) numerical validation of the research idea; (Part II) experimental study on mechanical properties of high strength structural steels in fire and after fire; (Part III) full-scale behaviour of high strength steel endplate connections in fire and after fire.

In Part I, the research idea of combining high strength steel endplate with mild steel beam and column in endplate connections is proposed and validated. A numerical modelling of endplate connections using ABAQUS/Standard was conducted, to reveal how high strength steel endplate connections behave in fire. The proposed FE modelling was further validated with fire test results on mild steel endplate connections reported by the University of Sheffield. On this basis, the performances of HSS endplate connections at ambient temperature and at elevated temperatures were further predicted and compared with those made of mild steel. It is found that the proposed research idea, combining HSS with mild steel in connections, may be used for further investigations of improving the behaviour of steel connections under fire conditions as well as promoting the application of HSS in civil engineering. Hence, the subsequent research is carried out .

In Part II, the experimental study on mechanical properties of high strength structural steels in fire and after fire is presented. Firstly, in order to provide convincing proof for safe fire-resistance design of high strength steel structures and validate the limited available research results in literature, an experimental research was performed on S460, S690 and S960, using both the steady state test method and the transient state test method. The elastic modulus, yield strength and ultimate strength of these three high strength structural steels at elevated temperatures up to 700°C under various conditions were obtained and compared with available literature and the recommendations of current leading

design standards for steel structures (i.e. EC3, AISC, AS 4100, ASCE and BS5950). The comparison of HSS with mild steels shows that the deterioration of mechanical properties of structural steels at elevated temperatures is dependent on steel grades and manufacturing method. Comparison with current European, American, Australian and former British design standards for steel structures shows that no current design standard may be used conservatively to conduct fire-resistance design of steel structures with high strength steel S460N, S690 or S960. Therefore, some unique predictive equations calculating reduction factors of mechanical properties for HSS S460, S690 and S960 at elevated temperatures were proposed and recommended for safe practical design and structural analysis. Moreover, a series of experimental studies were undertaken on three high strength steel grades S460, S690 and S960, to investigate their post-fire mechanical properties after cooling down from fire. Steady state tensile tests were undertaken after cooling down from various different fire temperatures up to 1000°C, to reveal the residual elastic modulus, yield strength, ultimate strength and post-fire stress–strain curves of S460, S690 and S960 after fire. The results showed that the steel grade has a significant influence on the post-fire residual mechanical properties of structural steels. Further, some separate predictive equations were proposed to determine the post-fire elastic modulus, yield strengths and ultimate strengths of S460, S690 and S960 respectively.

Finally, the behaviour of HSS endplate connections in fire and after fire is studied via experimental tests and numerical analysis in Part III. The full-scale tests on high strength steel endplate connections in fire and after cooling down from fire were carried out to reveal their characteristics. Their performance were compared with mild steel endplate connections. It is found that a proper thinner HSS endplate can enhance the connection's rotation capacity at ambient temperature, in fire and after fire (which guarantees the safety of an entire structure), and simultaneously achieve almost the same moment resistance with a mild steel endplate connection. In addition, a numerical study on HSS endplate connections in fire and after fire was conducted using ABAQUS/Standard. Validation of the numerical modelling against all representative experimental results conducted on moment-rotation relationship, failure mode and yield line pattern of connections showed good agreements. Hence the numerical analysis method can be used with confidence to predict the behaviour of high strength steel endplate connections under various fire conditions as well as at ambient temperature, and after cooling down from fire.

All in all, the mechanical properties of HSS S460, S690 and S960 in fire and after fire as well as the experimental and numerical study on high strength steel endplate connections in fire and after fire have been presented in this thesis. It offers a basis for structural engineers to conduct fire-resistance design of steel structures with high strength steels, and to perform accurate evaluation and safe reuse of constructional structures with members made of S460, S690 and S960 after fire as well.

Contents

Part III Full-scale behaviour of high strength steel endplate connections in fire and after fire

Chapter 6 Experimental study on HSS endplate connections at ambient temperature and in fire

Chapter 7 Numerical analysis of HSS endplate connections at ambient temperature and in fire

List of Notations

Latin

A	section area
A_s	tensile stress area of the bolt
d	nominal bolt diameter
e	distance from bolt hole to the adjacent end of endplate
E	elastic modulus
E_{20}	elastic modulus at ambient temperature
E_θ	elastic modulus at elevated temperature θ
E_θ / E_{20}	reduction factor of elastic modulus
$E_{P\theta}$	post-fire elastic modulus
$E_{P\theta} / E_{20}$	post-fire remaining factor of elastic modulus
F	force
$f_{u,b}$	tensile strength of bolt
f_{u20}	ultimate strength at ambient temperature
$f_{u\theta}$	ultimate strength at temperature θ
$f_{u\theta} / f_{u20}$	reduction factor of ultimate strength
$f_{uP\theta}$	post-fire ultimate strength
$f_{uP\theta} / f_{u20}$	post-fire remaining factor of ultimate strength
f_{y20}	yield strength at ambient temperature
$f_{y\theta}$	yield strength at temperature θ
$f_{y\theta} / f_{y20}$	reduction factor of yield strength
$f_{yP\theta}$	post-fire yield strength
$f_{yP\theta} / f_{y20}$	post-fire remaining factor of yield strength
h_b	height of beam section
h_c	height of column section
L	length
l_{eff}	effective length of endplate
p_1	distance of first bolt row and second bolt row
p_2	distance of second bolt row and third bolt row
M	moment
$M_{j,R}$	design moment resistance, plastic flexural resistance
S_j	secant stiffness
$S_{j,ini}$	initial rotational stiffness of connections
t	thickness
T	temperature
t_f	thickness of flange of a section
t_{fb}	thickness of beam flange
t_{fc}	thickness of column flange
t_w	thickness of web of a section

Greek

ϕ	rotation capacity of connections
ϕ_C	maximum rotation of connections
ϕ_{Mmax}	rotation corresponding to the maximum load
θ	temperature
θ_b	rotation of beam
θ_c	rotation of column
σ	stress
$\varepsilon_{11,av,b}$	maximum average principal strain
ε_u	ultimate strain
δ_{DTi}	deformation at *DTi*
η	stiffness modification coefficient

Subscript

b	beam or bolt
c	column
eng	engineering
ep	endplate
exp	experiment
f	flange
ini	initial
max	maximum
p	post-fire
Rd	design resistance
u	ultimate
w	web
y	yield

Abbreviations

CHS	circular hollow section
DT	displacement transducer
FE	finite element
HSS	high strength steel
PEEQ	equivalent plastic strain
RHS	rectangular hollow section
VHSS	very high strength steel

Chapter 1

Introduction

1.1 BACKGROUND

Fires in buildings often have enormous consequences on safety and economy. Structural fire safety is therefore a key consideration in the design of buildings and is attracting worldwide attention. Beam-to-column connections are important components of steel framed structures, as they are supposed to resist resultant forces at the end of the beam and transfer them into the columns and surrounding structural components. The fracture of a connection can cause the collapse of the connected beam, which may lead to a progressive collapse of the entire structure. Therefore the behaviour of connections in a building is of extreme significance, not only at ambient temperature but also under fire conditions.

In Europe, endplate connections are typical beam-to-column connections for steel buildings produced by welding at workshops and erected by bolting in situ. The simplicity and economy associated with its fabrication make this type of connection popular in steel structures. Rules for prediction of strength, stiffness and deformation capacity of endplate connections at ambient temperature have been included in current leading design standards, such as Eurocode 3 Part 1-8. According to Eurocode 3, for structural steels up to S460, plastic design of connections may be used. However, for steel grades higher than S460 up to S700 only elastic design of connections can be employed, which is very uneconomical for steel structures. This is due to the lack of experimental and theoretical evidence of the deformation capacities of these high strength steel (HSS) connections. Girao Coelho and Bijlaard have found that the high strength steel S690 endplate connections satisfy the design provisions for resistance and achieve reasonable rotation requirements at ambient temperature.

A recent research on mild steel endplate connections in fire, conducted by the University of Sheffield, reports that a thick endplate enhances the resistance of the endplate connection but significantly reduces the ductility of the connection under fire conditions, as shown in Fig.1.1. Based on this, a research idea is

proposed that using high strength steel to take place of mild steel as endplate material in endplate connections, to achieve similar connection load-bearing capacity, the required endplate thickness may be less. The thinner high strength steel endplate might make the endplate connection more ductile, which enhances the fire safety of the entire steel structure. In this thesis, the behaviour of high strength steel endplate connections in fire is investigated.
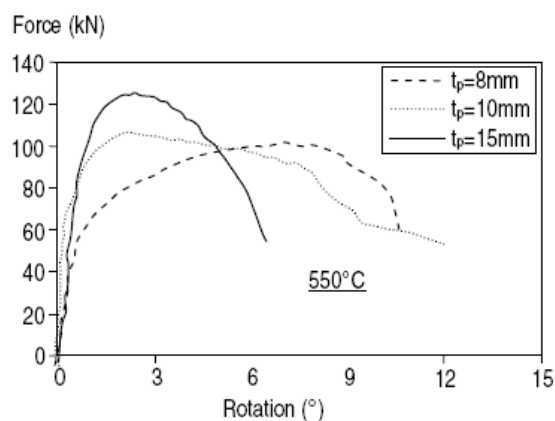
Fig.1.1. Effect of endplate thickness on endplate connections in fire by the University of Sheffield.

Provided that collapse does not occur when a steel structure is exposed to fire, the steel members will begin to cool once the fire starts to decay and the air temperature begins to decrease. Residual forces and deformations redevelop in steel structures during the cooling phase due to the shrinkage of the steel members, which might be a more dangerous condition than in fire. If all the structures exposed to fire are dismantled and then new alternates are built, it is wasteful and time-consuming; whereas if the post-fire structures are reused directly or simply reinforced, it may be safety-compromised, which makes people feel unsafe when they step into the structures. Whether the structures exposed to fire should be demolished, repaired or reused directly, a reliable evaluation is needed. Hence, the post-fire behaviour of high strength steel endplate connections is also studied in this thesis to reveal their residual performance after fire, which is a basis for evaluating the residual performance of an entire structure after cooling down from fire.

1.2 AIM OF THIS RESEARCH

In this research, a perspective of combining high strength steel endplate with mild steel beam and column in endplate connections is proposed and investigated. For comparison, the experimental study on mild steel connections is also carried out. The aim of this research is to reveal more information and understanding on behaviour and failure mechanisms in the tension zone of high

strength steel flush endplate connections in fire and after fire, for an effective application of high strength structural steels in civil engineering as well as enhancing the fire safety of steel structures. The mechanical properties of high strength structural steels S460, S690 and S960 in fire and after fire experimentally studied in this research can serve as fundamental data to numerically or theoretically simulate the performance of isolated connections or an entire structure with members made of high strength steels under fire conditions or after cooling down from fire. The experimental and numerical study on high strength steel endplate connections in fire and after fire are expected to be used by structural engineers as a basis to conduct safe fire-resistance design and accurate post-fire evaluation of steel structures with high strength steel members.

1.3 THESIS OUTLINE

This thesis consists of 10 chapters, as introduced below.

Chapter 2 gives a brief state-of-the-art on high strength structural steels in general, mechanical properties of high strength structural steels in fire, post-fire mechanical properties of high strength structural steels, beam-to-column endplate connections and endplate connections under fire conditions.

The research work consists of three main parts: (I) numerical validation of the research idea; (II) experimental study on mechanical properties of high strength structural steels in fire and after fire; (III) experimental and numerical study on high strength steel endplate connections in fire and after fire.

Part I , which consists of Chapter 3, introduces the numerical prediction of combining high strength steel endplate with mild steel beam and column in endplate connections both at ambient temperature and under fire conditions to validate the research idea. The focus is on the tensile zone of the flush endplate connections. The accuracy of this numerical modelling conducted by the commercial package ABAQUS was validated against the test results on mild steel flush endplate connections reported by Yu et al. from the University of Sheffield. Moreover, a parametric study on the effects of endplate thicknesses was carried out, and an achievement was obtained for improving the robustness of endplate connections under fire conditions.

Part II is divided into Chapters 4 and 5, describing the experimental study on mechanical properties of high strength structural steels S460, S690 and S960 in fire and after fire respectively. The aims of this experimental investigation presented in Chapter 4 are to reveal more information on HSS S460, S690 and S960 at elevated temperatures, to validate the accuracy of existing data for the mechanical properties of HSS in literature and to support related research projects aimed at studying the behaviour of HSS structures or composite structures with HSS members in fire. In this experimental investigation, both steady and transient state tensile tests were conducted on HSS S460, S690 and S960 at various temperatures ranging from 20°C to 700°C. The elastic modulus, yield strength and ultimate strength of HSS S460, S690 and S960 at various temperatures were obtained and compared with the recommendations of the leading design standards (i.e. EC3, AISC, AS4100, ASCE and BS5950 et al.). Further, several sets of predictive equations for mechanical properties of HSS S460, S690 and S960 under fire conditions based on test results and available literature are proposed. In Chapter 5, a series of experimental studies was undertaken on high strength steel S460, S690 and S960, to investigate their post-fire mechanical properties after cooling down from elevated temperatures up to 1000°C. Chapter 5 presents the details of the experimental study, the post-fire residual elastic modulus, yield and ultimate strengths, as well as stress-strain curves of S460, S690 and S960. The results from this study were compared with other steel grades obtained from current literature and design standards for steel structures. Further, separate sets of predictive equations are proposed for the deterioration of post-fire mechanical properties of HSS S460, S690 and S960.

Part III is dedicated to the experimental and numerical study on the behaviour of high strength steel endplate connections in fire and after fire, with the focus on the tensile zone. This part includes Chapters 6, 7, 8 and 9. In Chapter 6, the behaviour of high strength steel endplate connections in fire was studied through tests conducted at an elevated temperature of 550°C. The moment resistance, rotation capacity and failure mode according to moment of high strength steel endplate connections in fire and at ambient temperature were obtained via tests and compared with those of mild steel endplate connections. In Chapter 7, a numerical study on high strength steel endplate connections in fire conducted via the commercial package ABAQUS is described. The main characteristics of the finite element model, such as geometry, materials, mesh, element, contact interaction and analysis progress etc. are described in detail. The accuracy of this numerical modelling is validated against the experimental

results shown in Chapter 6. Chapter 8 presents the experimental study on the behaviour of high strength steel endplate connections after cooling down from fire. The post-fire moment resistance, rotation capacity and failure mode of high strength steel endplate connections after fire were obtained and compared with those of mild steel endplate connections after fire. The post-fire behaviour of high strength steel endplate connections was compared with that at ambient temperature without fire exposure to evaluate their residual performance after fire exposure. Chapter 9 introduces a numerical study on high strength steel endplate connections after fire, performed via the commercial package ABAQUS. The accuracy of this numerical modelling on moment-rotation relationship and failure modes was verified with the experimental study presented in Chapter 8.

Finally, the overall conclusions of this research project together with recommendations for future research work are summarized in Chapter 10.

The schematic outline overview of this thesis is shown in Fig.1.2.

Chapter 1
Introduction

Problem definition
Research objectives
Thesis outline

Chapter 2
Literature review

High strength structural steel
In-fire and post-fire mechanical property
Beam-to-column endplate connection

Part I: Numerical validation of research idea

Chapter 3
Numerical prediction of combining HSS with mild steel in endplate connections at ambient and elevated temperatures

Part II:
Experimental study on mechanical properties of HSS in fire and after fire

Chapter 4
Mechanical properties of high strength structural steel in fire

Chapter 5
Mechanical properties of high strength structural steel after

Part III:
Experimental and numerical study on HSS endplate connections in and after fire

Chapter 6
Experimental study on HSS endplate connections in fire

Tests at ambient and elevated temperatures
Moment-rotation relationship, rotation capacity and failure mode

Chapter 7
Numerical study on HSS endplate connections in fire

Finite element modelling
Validation against in-fire experimental results

Chapter 8
Experimental study on HSS endplate connections after fire

Full scale tests after cooling down
Post-fire behaviour of connections
Residual performance evaluation

Chapter 9
Numerical study on HSS endplate connections after fire

Finite element modelling
Validation against post-fire experimental results

Chapter 10 Conclusions and recommendations

Fig.1.2. Schematic outline of the thesis.

Chapter 2

Literature review

In this chapter, the state of the art about the relevant information of this research project is introduced, including: the definition, development and application of high strength structural steels, the mechanical properties of high strength structural steels in fire as well as after fire, beam-to-column endplate connections and the behaviour of endplate connections under fire conditions.

2.1 HIGH STRENGTH STRUCTURAL STEELS

The structural steel grade S355, which used to be considered as high strength steel (HSS) 20 years ago, is now the main constructional steel for hot rolled plates and H-sections in Europe. For the time being, the steels having a nominal yield stress equal to or more than 420 N/mm^2 are called high strength steel, based on the implication of the current European Standard for steel structures Eurocode 3 (EC3) [1, 2]. In the last decade, high strength steel has been applied in many structures all over the world because of its economical benefits in comparison to mild steels, which are hot-rolled carbon steels with normal strengths (see Table 2.1). Hence, HSS is gaining more and more attention in the market of constructional steel structures. In some significant structures and landmark constructions high strength steels have been employed, such as the New York Freedom Tower, the Beijing Bird's Nest Olympic Stadium and the French cable-stayed road-bridge Millau Viaduct.

Table 2.1: Typical examples and application of various structural steel types [3]

Yield strength (MPa)	Type	Other description	Typical examples	Potential application
< 420	Mild steel	Regular structural steel	S235, S275, S355	Buildings
420-600	Conventional high strength steel (CHSS)	High performance steel / High tensile steel	S420, S460, S550	Bridges, High rise buildings
700-1100	Very high strength steel (VHSS)	Ultra high strength steel / Super high strength steel	S690, S890, S960, S1100	Cranes, Bridges, High rise buildings

In Europe, the cost of building a structure usually depends more on fabrication, transportation and erection than on the price of raw material. In the construction of steel structures, HSS allows less material to be used, which reduces the volume of weld metals and correspondingly the time for welding. Further, less material has to be transported and the lighter weight simplifies the erection of structures. In some structural applications the light weight plays an important role, because the payload can be increased or the running expense can be decreased, in case of cranes and vehicles. What is more, an increasing international concern on environment protection leads to more attention on saving energy and raw materials. Thus, using HSS is a great environmental benefit in comparison with mild steel. Collin and Johansson [4] made an evaluation and proved that if the strength of steel material could be fully utilized, the cost of material would be decreased with the increase of material strength. With the development of processing and manufacturing technology, the cost of manufacturing high strength steel will be closer and closer to that of mild steels. So the material cost increase by using HSS is less than the benefits of its improved yield strength. The strength of structural steel can be very significant for certain applications with tensile forces (for instance cables and tension bars), whether for individual tensile members or for long span structural systems, as well as for short and stocky columns in high rise buildings, where the physical dimensions of structural members can be reduced by employing high strength structural steel. Therefore, it is economical to use HSS especially in structures where the strength can be almost utilized.
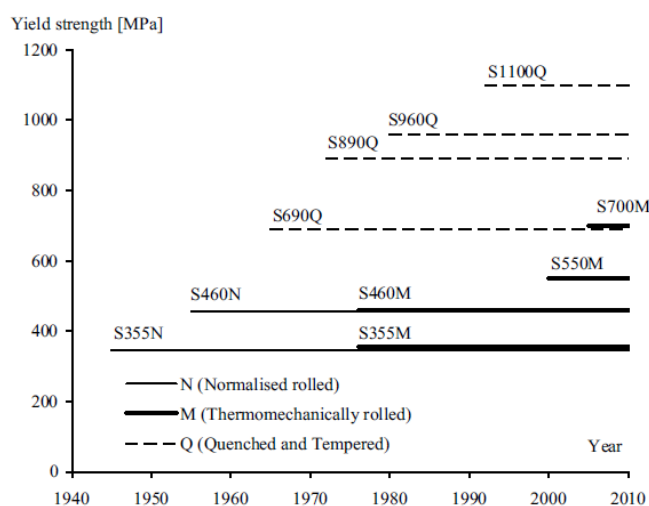
Fig. 2.1. Development of high strength structural steel grades [3].

With the development of architectural requirements, design techniques and numerical modelling, constructional structures have evolved significantly in practice, which calls for higher performance materials in constructions. The steel producer has developed structural steels with higher yield and tensile strengths than mild steels. The high strength of the structural steels is predominantly derived by heat treatment techniques in the manufacturing. Fig.2.1 shows the steel development of normalized steels (N-type), thermo-mechanically rolled steels (M-type) and quenched and tempered steels (Q-type) [3]. For the manufacturing of conventional high strength steels, steels are heated to 920°C, followed by air cooling. This process is called normalizing; for instance S460N is normalized steel with nominal yield strength of 460N/mm^2. An alternative procedure for obtaining high strength is thermo-mechanically rolling. The steels are rolled at relatively low temperatures and have excellent toughness and welding properties. The highest yield strengths are obtained by the quench and temper process. Very high strength steels (VHSS) with a nominal yield stress equal to or above 690N/mm^2 have been available for years, and they have been widely used in ship engineering, offshore structures and crane industry. However, the application of VHSS in building structures in the civil engineering field is not very common, due to lack of design knowledge and available shapes on the market as well as limited recommendations in current design standards all over the world. For the time being, several steel manufacturers make VHSS plate material with nominal yield strengths up to 1100MPa with plate thicknesses up to 40mm (See Tables 2.2 and 2.3); circular hollow sections (CHS) are available up to 890MPa, rectangular hollow sections (RHS) are up to 700MPa. At present, the availability of rolled H-sections is limited to 460MPa yield strength, as illustrated in [5].

Table 2.2: Available VHSS on the market (according to steel manufacturer product brochures)

Type	Manufacturer	Name	Yield Strength (MPa)
Plate material	Dillinger Hütte GTS	DILLIMAX	690, 890, 960, 1100
	Thyssen Krupp	N-A-XTRA XABO	700, 800, 890, 960, 1100
	SSAB	WELDOX	700, 800, 900, 960, 1100, 1300
	JFE	HITEN	690, 890
	Ilsenburger-Grobblech	MAXIL	690, 890, 960, 1100
Circular Hollow Sections (CHS)	Tenaris	TN 140	960
	Europipe	X100	690
	Vallourec-Mannessmann	FGS78WV-FGS90WV	770, 790, 890
Rectangular Hollow Sections (RHS)	Ruukki	Optim HS 700 MH	700

Table 2.3: Available VHSS material thickness

Plate material		CHS		RHS	
Strength (MPa)	Thickness (mm)	Strength (MPa)	Thickness (mm)	Strength (MPa)	Thickness (mm)
690	$4 < t < 200$	690	$t < 65$	690	$3 < t < 8$
890	$3 < t < 120$	890	$t < 40$		
960	$3 < t < 100$				
1100	$4 < t < 40$				

2.2 MECHANICAL PROPERTIES OF HIGH STRENGTH STRUCTURAL STEELS IN FIRE

Since the 9-11 World Trade Centre tragedy, a lot of researches have been carried out on the structural behaviour of building structures under fire conditions with the combined effects of weakening of materials, thermal restraint and accidental removal of some structural elements. As a basis of evaluating the performance of steel structures in fire, mechanical properties of some structural steels at elevated temperatures have been reported [6-11].

However, previous researches in literature mainly focus on mild steels. For high strength steels, only very limited information has been reported so far [12-16]. As a result, the fire-resistance design of steel structures with HSS is either too conservative or safety-compromised in practice, which seriously retards the application of HSS in civil engineering as well as leads to safety risk.

In the European design standard EC3 part 1-2 [1], it is assumed that the material properties of various structural steel grades at elevated temperatures can be evaluated uniformly. The predictions recommended by EC3 are based on test results mainly obtained from mild steels. However, previous researches [12-16] indicate that the elevated-temperature material properties of HSS are different from those of mild steels. Schneider and Lange [12-14] compared the yield strength reductions of HSS S460 at elevated temperatures obtained by some researchers with those from EC3 part 1-2 [1]. They pointed out that nearly all of the tested materials did not meet the specifications of EC3 part 1-2, because the specifications of EC3 part 1-2 are uniform for various steel grades and are based on test results mainly obtained from mild steels. Hence, using the recommendations from EC3 to carry out fire-resistance design of structural members made of HSS probably runs a risk. For the leading design standards all over the world, (i.e. European design standard EC3 part 1-2 [1], American standard AISC [17], Australian standard AS 4100 [18] and British standard BS5950 [19]), no design standard for steel structures has specified recommendations for HSS under fire conditions. Therefore, accurate material properties of various HSS grades at elevated temperatures are urgently needed in practical design, in order to keep pace with the development of modelling techniques for predicting the fire response of steel structures.

In civil engineering field, S460 is currently the most commonly used high strength structural steel. However, the researches on material properties of HSS S460 at elevated temperatures reported in English are very limited (i.e. some research results are only available in German or other languages) and mainly focused on two types, S460N and S460M. The difference between them is the delivery condition: S460N is normalized rolled, while S460M is thermo-mechanical rolled. Lange and Wohlfeil [11] conducted transient state tests on both S460N and S460M. Their stress-strain relationships at elevated temperatures up to 3% total strain were reported. They proved that the elevated temperature performance of S460M was better than S460N. Schneider and Lange [12-14] extended the above experimental investigation to 7 types of commercial HSS S460 with different chemical compositions and delivery

conditions, using both steady state and transient state test methods. They pointed out that EC3 overestimated the elevated-temperature yield strengths if used for S460. Outinen [8, 10] carried out a transient state test on S460M at elevated temperatures, and compared his experimental results of elastic modulus and yield strength with the recommendations of EC3. However, there is a considerable discrepancy between the different data available in literature (which will be presented in detail hereafter in Chapter 4), because of variations in test methods, heating conditions and data collection techniques. This results in a challenge for structural engineers to choose accurate elevated-temperature material properties of S460 for predicting response of steel structure under fire conditions.

In literature, the elevated-temperature mechanical properties of BISPLATE 80 were reported by Chen et al. [16], of which the yield strength is similar to HSS S690. For S690 under fire conditions no quantitative research result has been available by now. What is more, no report on elevated-temperature mechanical properties of other steel grade for HSS (i.e. S890, S960 and S1100 et al.) is available in literature.

In order to supply convincing proof for safe fire-resistance design of steel structures with HSS S460 and validate the available research results, an experimental research was conducted on S460N and will be introduced in Chapter 4, using both the steady state test method and the transient state test method. Furthermore, in order to reveal more information on HSS S690 and S960 at elevated temperatures, and to support related research projects aimed at studying the behaviour of HSS structures or composite structures under fire conditions, the experimental investigation on the mechanical properties of HSS S690 and S960 was conducted and presented in Chapter 4.

2.3 POST-FIRE MECHANICAL PROPERTIES OF HIGH STRENGTH STRUCTURAL STEELS

Due to numerous unpredictable fire hazards which happen almost every day all over the world, structural fire safety is currently one of the critical considerations in the design of building structures, especially for high-rise buildings, which are usually made of steel. Provided that collapse does not occur when a steel structure is exposed to fire, the steel members will begin to cool once the fire starts to decay and the atmosphere temperature begins to

decrease. Residual tensile forces and corresponding deformations redevelop in steel structures during the cooling phase and after cooling down, which might be more dangerous conditions than in fire. If all the structures exposed to fire would be dismantled and newly rebuilt, it is wasteful and time-consuming. However, if the post-fire structures are reused directly or simply reinforced, it is safety-compromised. Whether the structures exposed to fire should be demolished, repaired or reused directly, a reliable evaluation is needed. As a critical basis for evaluating performance of steel structures after fire, the post-fire material properties of structural steel are very significant.

As we know, steel has excellent mechanical properties at ambient temperature. However, like other materials, its strength and stiffness decrease with temperature. But steel can regain some of its original mechanical properties after cooling down from fire, which is very promising for the reuse of steel structures after fire.

The high-temperature mechanical properties of structural steel have been paid attention and investigated especially since the 9-11 Tragedy, although the researches mainly focus on mild steels. However, for post-fire mechanical properties of high strength steels, no research result has been available by now. Even for mild steels, research on their material properties after cooling down is very limited [8, 10]. In appendix B of British Standard 5950: Part 8(2003) [19], there is an advice about the reuse of structural steel after fire. According to this, hot finished steels and cast steel can be reused after fire if the distortions remain within the tolerances for straightness and shape. For mild steel S235 and S275, it is stated that they can be assumed to be able to regain at least 90% of their mechanical properties, without any confirmatory testing. Similarly, for S355, it is stated that it can be assumed at least 75% of the strength is regained after cooling from temperatures above 600°C. But no assumption or suggestion is given for high strength steels in any current design standard of steel structures.

Without reliable post-fire mechanical properties of high strength steels, the evaluation on behaviour of HSS structures after exposure to fire is not convincing. This will lead to an uneconomical consequence, either waste of money and energy or safety-compromised. Therefore, for practical design and evaluation, it is necessary and important to develop some recommendations for post-fire mechanical properties of high strength steels in the design standards of steel structures, such as BS5950 [19], EC3 part 1-2 [1] and so on. So an

experimental study was undertaken on three commonly used HSS grades S460 S690 and S960, as presented in Chapter 5, to investigate their post-fire mechanical properties after cooling down from elevated temperatures up to 1000°C .

2.4 BEAM-TO-COLUMN ENDPLATE CONNECTIONS

Beam-to-column connections are important components of any steel structure, as they are supposed to resist the resultant forces at the end of the beam and transfer these to the columns and surrounding structural components. Generally, the forces transmitted through the connections are axial and shear forces, bending and torsion moments. The bending moments are predominant in most cases, in comparison to axial and shear forces as well as torsion. Typical beam-to-column moment-resisting connections in steel structures include bolted endplate connections, bolted connections with (flange and/or web) angle cleats and welded connections. Their behaviour is represented by a moment vs. rotation curve (M-Φ) that describes the relationship between the applied bending moment, M and the corresponding rotation between the members, Φ. This curve defines three main structural properties: moment resistance, rotational stiffness and rotation capacity.

Connections can be divided into groups according to their structural properties. The European code for design of structural steel connections in buildings (Eurocode 3 Part 1-8) [2] classifies connections by strength (full strength, partial strength or pinned) and stiffness (rigid, semi-rigid or pinned, see Fig.2.2). A full strength connection exhibits a moment resistance at least equal to that of the connected members, while partial strength connections have lower strengths than the members. Nominally pinned connections are sufficiently flexible to be regarded as a pin for analysis purposes, i.e. they are not moment resisting and have nearly no rotational stiffness. A rigid connection is sufficiently stiff to neglect the effect of its deformation on the distribution of internal forces and bending moments in the structure. A semi-rigid connection is in between a rigid connection and a pin. The semi-rigid/partial strength design philosophy of connections usually leads to more economic and simple solutions. The use of this connection category in steel frames, however, is only feasible if they develop sufficient rotation capacity in order that the intended failure mechanism of the whole structure can be formed prior to failure of the connection.
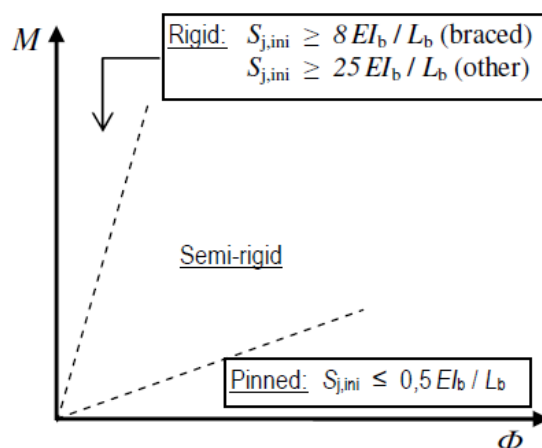
Fig.2.2 Classification of connections by stiffness in Eurocode 3 [2].

Endplate bolted connections are widely used in steel structures as moment-resistance connections; they usually fall in the semi-rigid/partial strength connection category. The simplicity and economy associated to their fabrication and erection made this connection typology quite popular in steel-framed structures. In Europe, steel bolted partial strength endplate connections are typical for buildings erected using welding at workshop and bolting on site. Hence the behaviour of endplate connections at ambient temperature has been widely studied by many researchers over years [20-25], according to experimental study or numerical study or a combination of both. Rules for prediction of strength and stiffness of this connection configuration at ambient temperature have been recommended in current leading design codes such as Eurocode 3, but they are mainly based on mild steel endplate connections. Girao Coelho and Bijlaard [26] have found that the high strength steel (HSS) S690 endplate connections satisfy the design provisions for resistance and achieve reasonable rotation demands at ambient temperature.

2.5 ENDPLATE CONNECTIONS UNDER FIRE CONDITIONS

The earliest experimental investigations on the performance of beam-to-column connections under fire conditions are rather limited in number, due to the high cost of the fire tests, limitations on the size of furnace used and difficulties in recording the deformation of steel connections. The current design procedures for bolted steel connections are based on moment-rotation relationships through isolated connection tests in fire. The experimental results from fire tests carried out on isolated connections provide very important fundamental data on the behaviour of beam-to-column connections in frame structures. In

literature, there are some experimental or numerical investigations or a combination of both available on the behaviour of endplate connections under fire conditions.

Experimental tests were conducted by Leston-Jones et al. [27] to develop moment-rotation relationships for flush endplate joints at elevated temperatures. Eleven tests were carried out, including two tests at ambient temperature, for both bare steel and composite joints. The details of their test specimens are presented in Fig.2.3. Results demonstrated that both the stiffness and moment capacity of the joint decreased with increasing temperature and there was a significant reduction in capacity for temperatures in the range of 500- 600° C. These tests provided useful data for connection modelling, but only for a limited range of details, using relatively small section sizes for comparison with earlier ambient temperature joint testing work by Davison et al. [28].
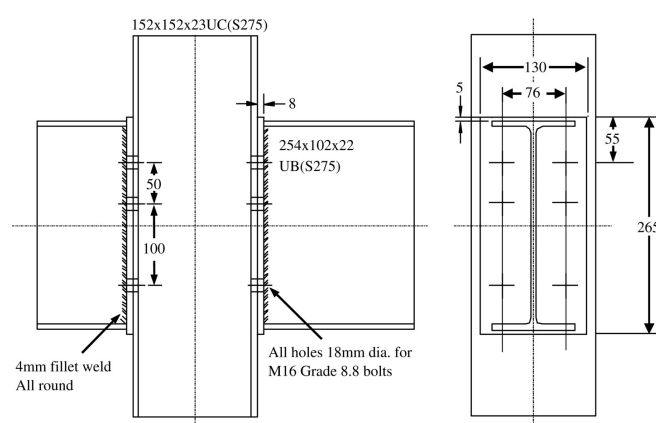
Fig.2.3 Connection details in Leston-Jones and Al-Jabri et al.'s test [27, 29]

A series of elevated temperature joint tests was conducted by Al-Jabri et al. [29] to study the influence of parameters such as member size, endplate type and thickness and composite slab characteristics, on the joint response in fire. The joint types included two flush endplate joints (one is the same as that shown in Fig.2.3, the other is illustrated in Fig.2.4 (a)) and one flexible endplate bare steel joint (see Fig.2.4(b)) and two flexible endplate composite joints (see Fig.2.4(c) and (d)). For each joint, a series of tests was carried out, each at a constant load level but with increasing furnace temperature. A family of moment-rotation-temperature curves via simplified mathematical expressions was established for each joint [30, 31], for instance see Fig.2.5.

16

(a) flush endplate connection

(b) flexible endplate bare steel connection

(c) flexible endplate composite connection Type 1

(d) flexible endplate composite connection Type 2
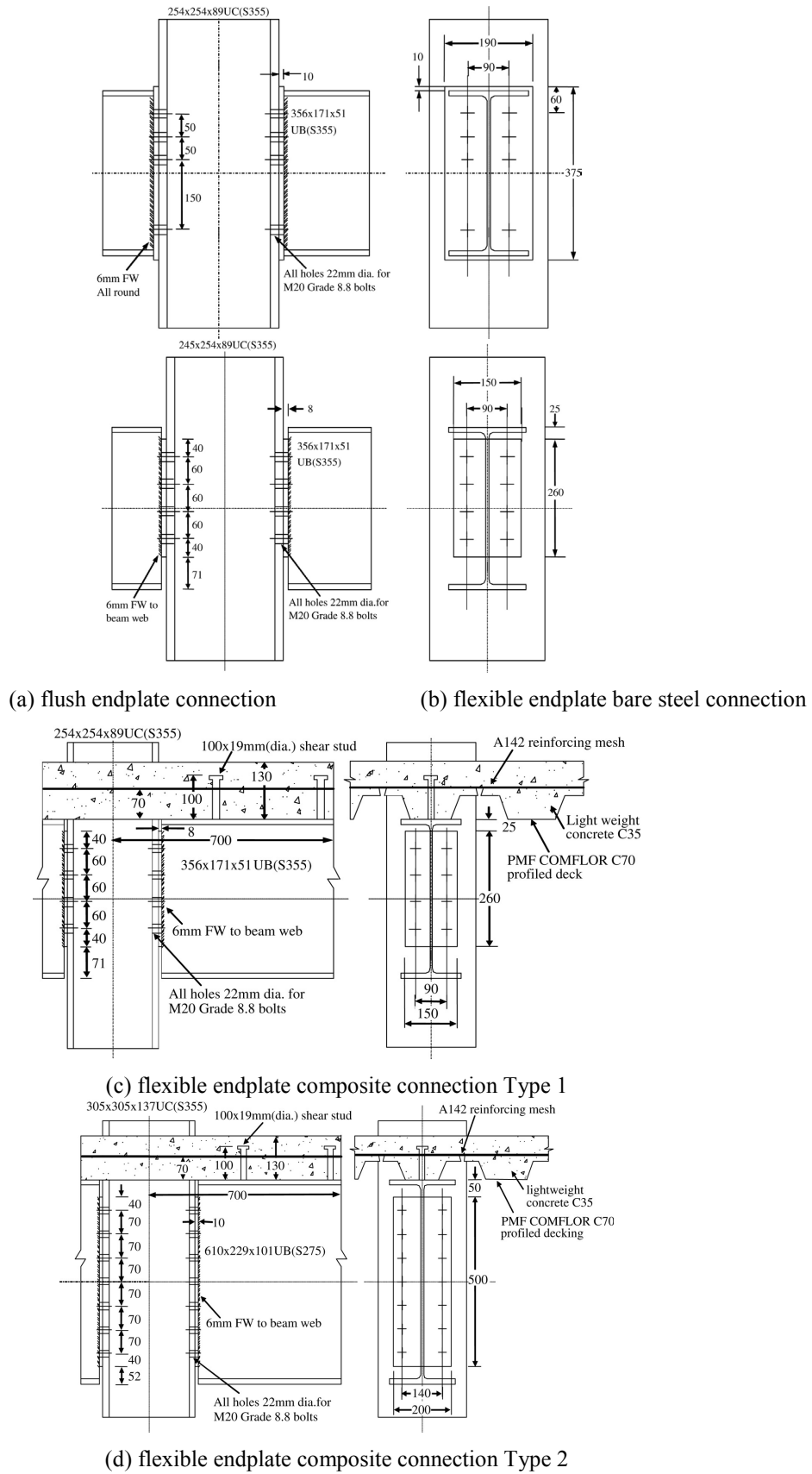
Fig.2.4 Connection details in Al-Jabri et al.'s test [29, 30]

17
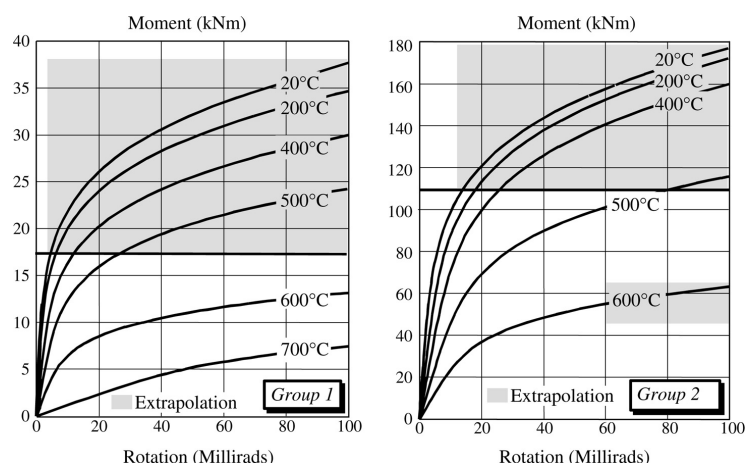
Fig.2.5. Moment–rotation–temperature curves for flush endplate bare-steel connections [30].

A series of full-scale fire tests was conducted on an eight-story composite building at the BRE Cardington Laboratories in Bedfordshire between 1995 and 1996; more detailed descriptions see [32-35]. In 2003, the seventh fire test at Cardington was carried out by Wald [36] on steel-framed structures, and the research efforts were focused on temperature distribution and damage mechanisms of connections under a natural fire. These connections were exposed to fire without protective materials, and then rupture of partial depth of endplate connections along welds and fracture of bolts in the fin plate connections were reported in this fire test, as shown in Fig.2.6. Local buckling of the beam bottom flange, shear buckling of beam webs and plastic deformation of the column flange were also found in these full-scale fire tests. All these failure mechanisms (for instance see Fig.2.7) indicate that considerable axial forces developed within the steel beams and that the robustness of steel connections against failure in fire is very important for maintaining structural integrity of a steel frame structure under fire conditions.

Fig.2.6. Failure modes of flexible end-plate and fin-plate joints in Cardington fire tests [37].

Fig.2.7. Cardington: overall frame deformation after a fire [37].

In 2004, Spyrou et al. [38, 39] reported the results of an experimental investigation on the performance of the tension and compression zones of steel joints at elevated temperatures. A total of 45 T-stubs were tested at elevated temperatures and 29 column web transverse compression tests. Simplified analytical models of both the tension and compression zone according to the 'component method' were developed at elevated temperatures, see Fig.2.8 (via taking into consideration of the reduction factors of structural materials at elevated temperatures) and compared with the experimental results. The analytical model for the tension T-stubs proved capable of predicting with reasonable accuracy the failure in any one of the three modes, see Fig.2.9: formation of plastic hinges in the flange near the web followed by bolt yield and fracture (Failure Mode I), formation of plastic hinges in the flanges near the web and the bolt lines followed by bolt yield and fracture (Failure Mode II), or bolt fracture with the flanges remaining elastic (Failure Mode III). Block et al. [40, 41] further developed the work on the compression zone, conducting tests focusing on the behaviour of column web in joints at elevated temperatures and refining the analytical model for this zone.
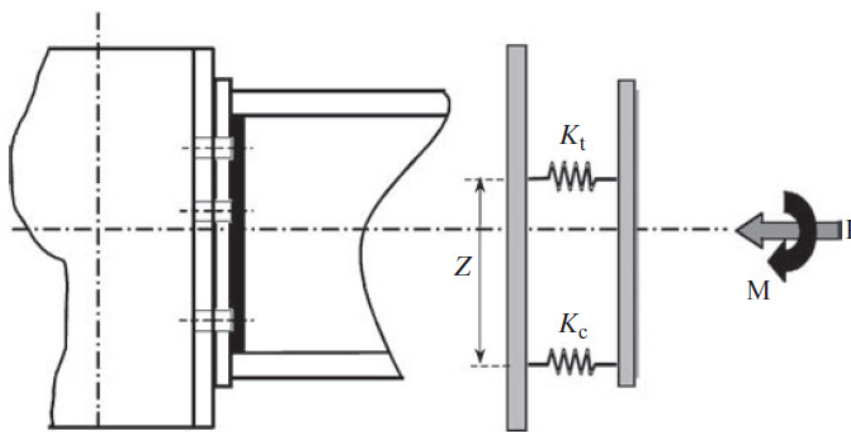
Fig.2.8. Spyrou's model of joint with axial force and moment [37].

19
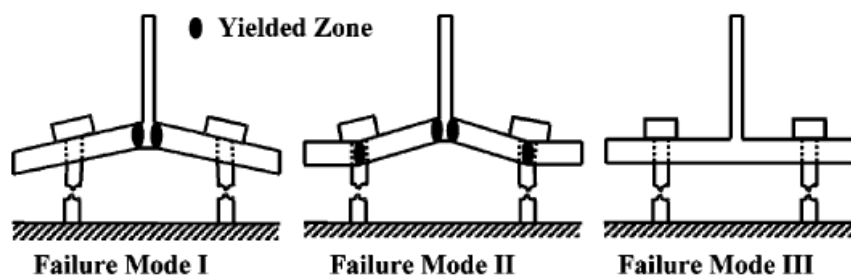
Fig.2.9. Failure modes for the tension T-stub flange [39].

Lou and Li [42] reported the results of two axially unrestrained cruciform tests conducted on 16mm thick extended endplates with M20 bolts under ISO834 fire conditions. The well-instrumented tests recorded temperature distributions and structural response and were used to validate nonlinear FE modelling. In their tests, these connections failed by buckling of the column web at ambient temperature; the failure mode changed at elevated temperatures to fracture of the bolts and yielding of the column web in tension.

From 2005 to 2008, the University of Sheffield and the University of Manchester conducted a joint research program with the aim of investigating the tying capacity and ductility of steel connections at elevated temperatures [37, 43-47]. Various levels of moment may be transferred through a connection, depending mainly on the connection type. For this purpose, the investigation adopted a test set-up, see Fig.2.10, in which the connections were subjected to combinations of tying and shear forces. Moments were generated at the connection from the lever arm of the applied force. In total, two types of endplate connections were studied: flush endplate connections and flexible endplate connections, see Fig.2.11. The behaviour of the connections at various elevated temperatures and subjected to different load combinations were given. Different failure modes were described, and their effects on the behaviour of the connections were illustrated and validated by numerical modeling via ABAQUS.
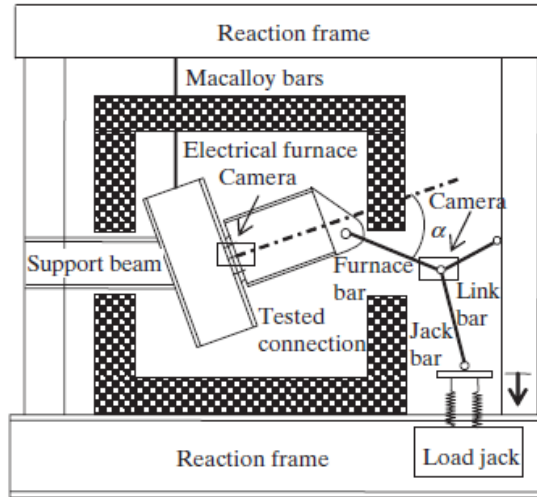
Fig.2.10.Schematic of electric furnace and test set-up for multi-directional loading tests [37].
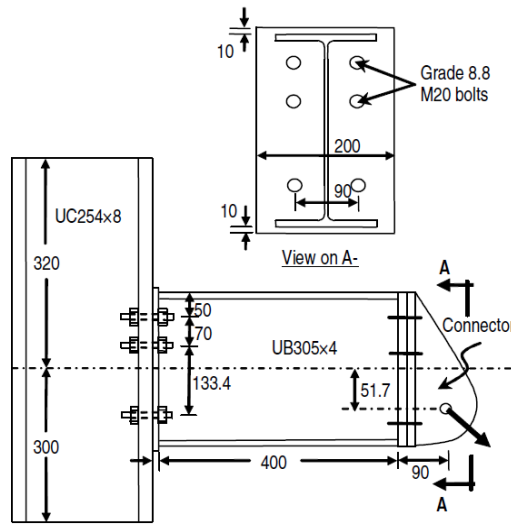
(a) flush endplate connection
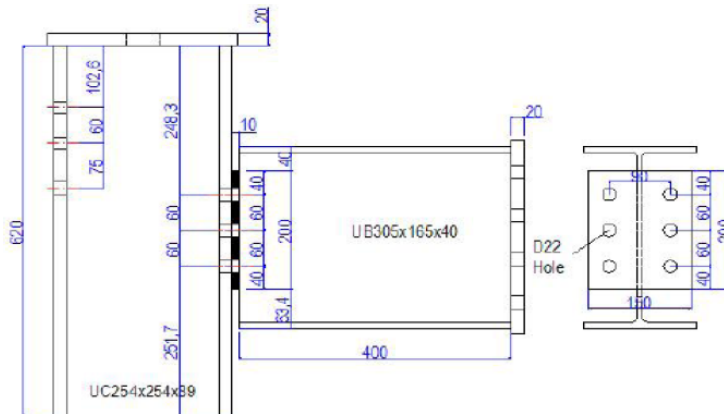
(b) flexible endplate connection

Fig.2.11. Details of flush endplate connection [44] and flexible endplate connection [47].

21

Recently, Strejček and co-authors [48] reported on an investigation of the behaviour of a column web component in shear at an elevated temperature in order to improve the simulation of steel connections subjected to fire conditions. An experimental study on an extended endplate connection exposed to ambient and elevated temperatures has been conducted to observe the behaviour of the column web component subjected to the interaction of bending moment and axial force, see Fig.2.12. In order to extend the study to other temperatures, a detailed finite element simulation was conducted. Their proposed model was validated against experimental results at both ambient and elevated temperatures see Fig.2.13. An analytical prediction approach, which has been established for the ambient temperature conditions, was extended to elevated temperature cases and compared with numerical predictions, as shown in Fig.2.14. Reasonably good agreement was obtained between the numerical and analytical models.
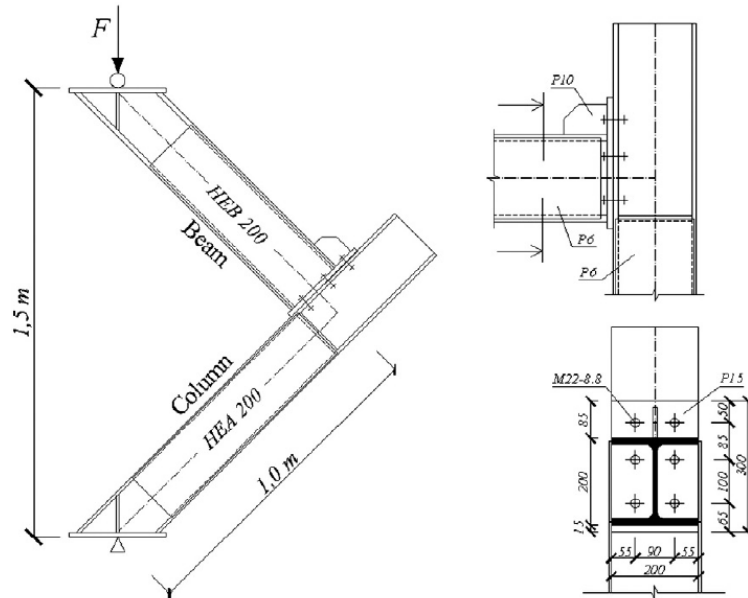
Fig.2.12. Details of the extended endplate connection and test set-up [48].
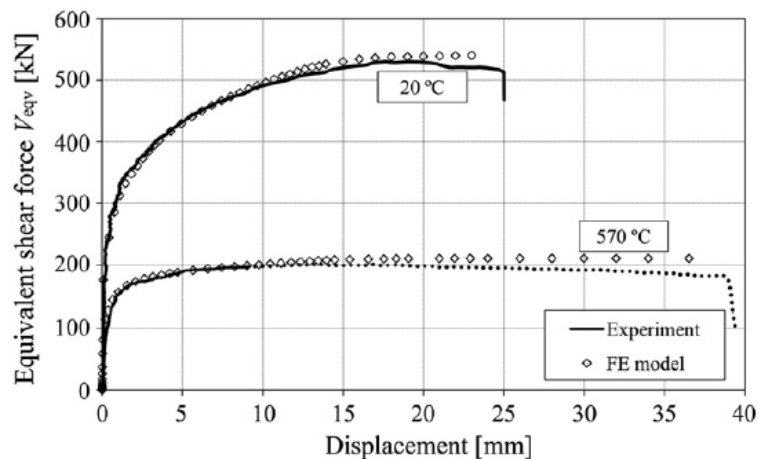
Fig.2.13. Comparisons between FE model and test results at ambient and elevated temperatures [48].

22
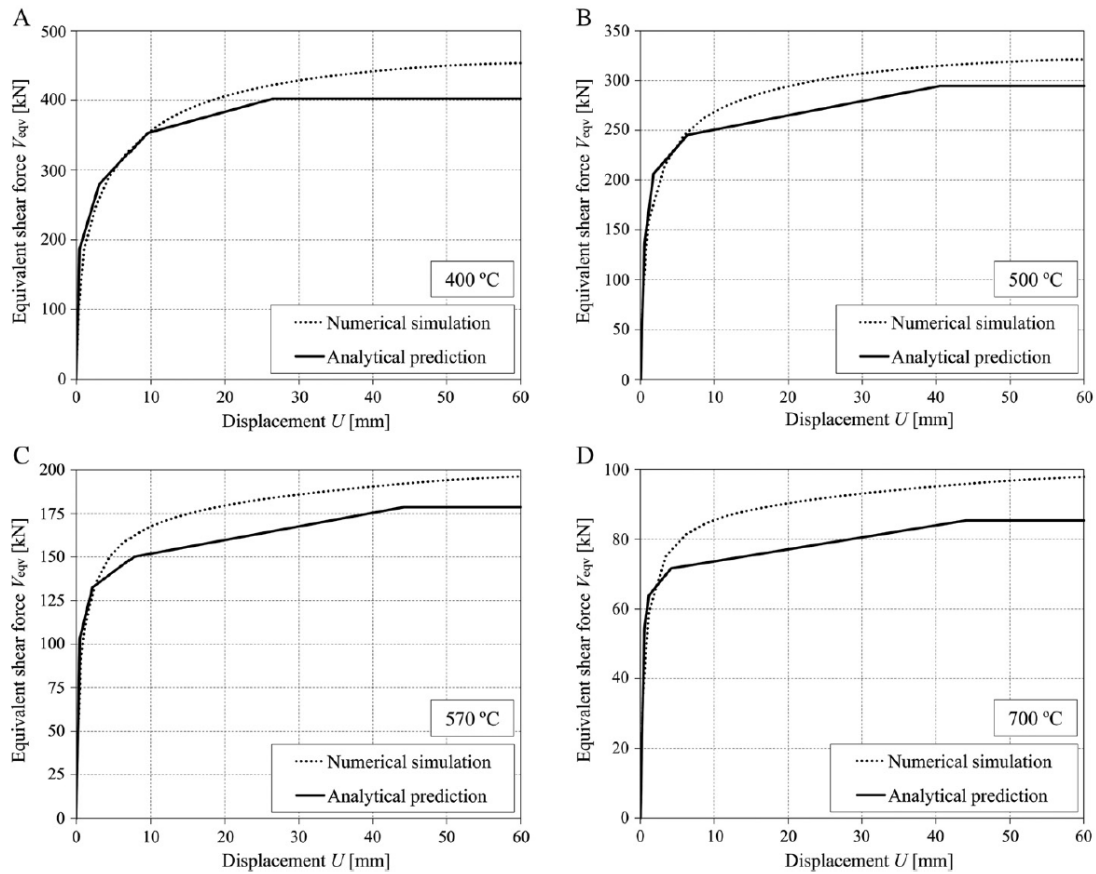
Fig.2.14. Comparison between analytical prediction and FEM results at elevated temperatures [48].

The available information on the behaviour of endplate connections under fire conditions in literature is for mild steels. No quantitative guidance on performance of high strength steel (HSS) endplate connection in fire has been available by now. In order to gain essential understanding and quantification on how HSS endplate connections behave not only at ambient but also at elevated temperatures, some researches are necessary to guide structural design engineers in practice for conducting fire-resistance design of HSS endplate connections.

23

2.6 REFERENCES

[1] European Committee for Standardization (CEN), Eurocode 3 - Design of steel structures - Part 1-2: General rules - Structural fire design, in, CEN, Brussels, 2005.

[2] European Committee for Standardization (CEN), BS EN 1993-1-8, Eurocode3: Design of steel structures, Part 1-8: Design of joints. British Standards Institution, Brussels , 2005.

[3] R.J.M. Pijpers, Fatigue strength of welded connections made of very high strength cast and rolled steels, Delft University of Technology, PhD Thesis, 2011.

[4] P. Collin, B. Johansson, Bridges in high strength steel, in, IABSE Symposium, Budapest, 2006, pp. 1-9.

[5] C. Weber, HISTAR, A new generation of high performance steel, Proceedings of the International Conference on Steel Structures of the 2000's, Istanbul, pp. 369-374.

[6] V. Kodur, M. Dwaikat, R. Fike, High-Temperature Properties of Steel for Fire Resistance Modeling of Structures, J Mater Civil Eng, 22 (2010) 423-434.

[7] J. Outinen, J. Kesti, P. Makelainen, Fire design model for structural steel S355 based upon transient state tensile test results, J Constr Steel Res, 42 (1997) 161-169.

[8] P. Makelainen, J. Outinen, J. Kesti, Fire design model for structural steel S420M based upon transient-state tensile test results, J Constr Steel Res, 48 (1998) 47-57.

[9] J. Outinen, Mechanical properties of structural steels at high temperatures and after cooling down, in: Laboratory of Steel Structures, Helsinki Univ. of Technology, Helsinki, Finland, 2007.

[10] J. Outinen, P. Makelainen, Mechanical properties of structural steel at elevated temperatures and after cooling down, Fire Mater, 28 (2004) 237-251.

[11] J. Outinen, O. Kaitila, P. Makelainen, High-temperature testing of structural steel and modelling of structures at fire temperatures, in, Helsinki Univ. of Technology Laboratory of Steel Structures, Helsinki, Finland, 2001.

[12] J. Lange, N. Wohlfeil, Examination of the mechanical properties of the microalloyed grain refined steel S 460 at elevated temperatures, Bautechnik, 84 (2007) 711-720.

[13] R. Schneider, J. Lange, Constitutive equations of structural steel S460 at high temperatures, in: Nordic steel construction conference 2009, Sweden, 2009, pp. 204-211.

[14] R. Schneider, J. Lange, Constitutive equations and empirical creep law of structural steel S460 at high temperatures, in: V. Kodur, J.M. Franssen (Eds.) Structures in fire 2010, DEStech Publication, Inc., East Lansing, 2010, pp. 703-710.

[15] R. Schneider, J. Lange, Material and creep behaviour of S460 in case of fire-experimental investigation and analytical modeling, in: F. Wald, K. Horova, J. Jirku (Eds.) international conference application of structural fire engineering, Cost, Prague, 2011, pp. 55-60.

[16] B. Young, J. Chen, B. Uy, Behavior of high strength structural steel at elevated temperatures, J Struct Eng-Asce, 132 (2006) 1948-1954.

[17] AISC, Specification for structural steel buildings, American Institution of Steel Construction, Chicago, 2005.

[18] AS, AS 4100, Australian Standards: Steel structures, Sydney, Australia, 1998.

[19] Institution BS, BS5950, Structural use of steelwork in building, Part 8: Code of practice for fire resistant design, London, 1998.

[20] L.Simoes da Silva, Aldina Santiago, Paulo Vila Real. Post-limit stiffness and ductility of end-plate beam-to-column joints. Computers and Structures 80(2002) 515-531.

[21] L.Simoes da Silva, A.M. Girao Coelho, Elisem Lucena Neto. Equivalent post-buckling models for the flexural behaviour of steel connections. Computers and Structures (2000) 615-624.

[22] C.M. Steenhuis, A.C.W.M. Vrouwenvelder, F. van Herwijnen, H.H. Snijder. Definitions of resistance and deformation capacity for non-sway steel and composite structures. Heron, Vol.47, No.1 (2002).

[23] F.S.K. Bijlaard. Requirements for welded and bolted beam-to-column connections in non-sway frames. Joints in Structural Steelwork, edited by J.H.Howlet, W.M. Jenkins and R. Stainsby, Pentech Press, London, United Kingdom, 1981.

[24] Y.J. Shi, S.L. Chan, Y.L. Wong. Modelling for moment rotations characteristics for end-plate connections. Journal of Structural Engineering, 1300-6 (1996).

[25] K. Weynand, J.P. Jaspart, M. Steenhuis. The stiffness model of revised Annex J of Eurocode 3. Proceedings of the Third International Workshop on Connections, Trento, Itlay (May 1995).

[26] A.M. Girao Coelho, F.S.K. Bijlaard, Experimental behaviour of high strength steel end-plate connections, Journal of Constructional Steel Research, 63(2007), 1228–1240.

[27] L.C. Leston-Jones, T. Lennon, R.J. Plank, I.W. Burgess. Elevated temperature moment–rotation tests on steelwork connections. Proc Inst Civ Engr Structs Bldgs 1997;122:410–419.

[28] J.B. Davison, P.A. Kirby, D.A. Nethercot. Rotational stiffness characteristics of steel beam to column connections. Journal of Constructional Steel Research, 8 (1987):17–54.

[29] K.S. Al-Jabri, T. Lennon, I.W. Burgess, R.J. Plank. Behaviour of steel and composite beam-column connections in fire. J Const Steel Res 46 (1998):1–3.

[30] K.S. Al-Jabri, I.W. Burgess, T. Lennon, R.J. Plank. Moment–rotation–temperature curves for semi-rigid joints. J Const Steel Res 61(2005):281–303.

[31] K.S. Al-Jabri. The behaviour of steel and composite beam-to-column connections in fire. PhD thesis, University of Sheffield, 2000.

[32] Armer GST, Moore DB. Full-scale testing on complete multi-storey structures. Struct Engnr. 1994; 72(2): 30–31.

[33] Moore DB, Lennon T. Fire engineering design of steel structures. Prog Struct Engnr Mater. 1997; 1(1): 4–9.

[34] Lennon T. Cardington Fire Tests: Survey of Damage to Eight Storey Building. Building Research Establishment: Garston, UK, 1997.

[35] Simms WI. The Cardington Fire Tests. London, 1998.

[36] F. Wald , L. Simoes da Silva, D.B. Moore , T. Lennon, M. Chladna, A. Santiago, M. Benes, and L. Borges. Experimental behaviour of a steel structure under natural fire, Fire Safety Journal, 41 (2006): 509-522.

[37] I.Burgess, J. B. Davison, G.Dong and S. Huang. The Role of Connections in the Response of Steel Frames to Fire, Structural Engineering International, 4 (2012):449-461.

[38] S. Spyrou, J. Davison, I.W. Burgess, R.J. Plank. Experimental and analytical investigation of the "compression zone" component within a steel joint at elevated temperatures. J Const Steel Res 2004;60(6):841–65.

[39] S. Spyrou, J. Davison, I.W. Burgess, R.J. Plank. Experimental and analytical investigation of the "tension zone" component within a steel joint at elevated temperatures. J Const Steel Res 2004;60(6):867–96.

[40] F.M. Block, J.B. Davison, I.W. Burgess, R.J. Plank. A component approach to modelling steelwork connections in fire: behaviour of column webs in compression. In: Proceedings of the ASCE structures congress, Nashville, 2004.

[41] F.M. Block, J.B. Davison, I.W. Burgess, R.J. Plank. High-temperature experiments on joint components. In: Proceedings of the 4th European conference on steel structures, Maastricht, the Netherlands, 2005.

[42] G.B. Lou, G.Q. Li. Non-linear finite element modelling of behaviour of extended end-plate bolted moment connections in fire. In: Proceedings of the fourth international workshop on structures in fire, Aveiro, Portugal, 2006. p. 327–43.

[43] I.W. Burgess, The Robustness of Steel Connections in Fire, Proceeding of ASCCS 2009, Leeds, 2009, 103-114.

[44] H. Yu, I.W. Burgess, J.B. Davison, and R.J. Plank. Experimental Investigation of the Behaviour of Flush Endplate Connections in Fire, Proceeding of Structures in Fire Workshop, Singapore, 2008.

[45] H. Yu, I.W. Burgess, J.B. Davison, and R.J. Plank. Tying Capacity of Web Cleat Connections in Fire. Part 1: Test and Finite Element Simulation, Engineering Structures, 2009, 31 (3), 651-663.

[46] H. Yu, I.W. Burgess, J.B. Davison, and R.J. Plank. Development of a Yield-Line Model for Endplate Connections in Fire, Journal of Constructional Steel Research, 2009, 65 (6), 1279-1289.

[47] Y. Hu, I.W. Burgess, J.B. Davison, and R.J. Plank. Modelling of flexible endplate connections in fire using cohesive elements, Proceeding of Structures in Fire Workshop, Singapore, 2008.

[48] M. Strejček, J. Řezníček, K. Tan, F. Wald. Behaviour of column web component of steel beam-to-column joints at elevated temperatures. Journal of Constructional Steel Research, 67 (2011) 1890–1899.

Part I

Numerical validation of research idea

Chapter 3

Numerical prediction of combining HSS with mild steel in endplate connections at ambient and elevated temperatures*1

3.1 INTRODUCTION

In Europe, endplate connections are typical beam-to-column connections for steel buildings erected by welding at workshops and bolting in situ. The simplicity and economy associated with their fabrication make this connection type popular in steel structures.

Rules for the prediction of strength and stiffness of endplate connections at ambient temperature have been included in current leading design codes, such as Eurocode 3 Part 1-8 [1], but they are mainly based on mild steel connections. Girao Coelho and Bijlaard [2] have found that the high strength steel (HSS) S690 endplate connections satisfy the design provisions for resistance and achieve reasonable rotation demands at ambient temperature. However, no quantitative guidance on HSS endplate connections under fire conditions is available in literature.

Recent research on bolted connections has revealed that bolt failure becomes critical at elevated temperatures, although the design for ambient temperature assumes more ductile failure [3-6], i.e. mild steel bolted connections are relatively brittle at elevated temperatures. So, making bolted connections more ductile at elevated temperatures is a significant mission for structural engineers, in order to improve the robustness of steel connections under fire conditions.

---

*1 This chapter has been accepted and will be published in Journal of Structural Fire Engineering [14].

In order to enhance fire safety of endplate connections, a numerical research has been conducted, combining HSS endplate with mild steel beam and column. In this chapter, the numerical modelling of HSS endplate connections is compared with that of mild steel endplate connections, to gain essential understanding and quantification on how HSS endplate connections behave at ambient and elevated temperatures. The accuracy of this numerical modelling was validated against the results of tests conducted by Yu et al. on mild steel flush endplate connections [3-6]. Moreover, a parametric study on the effects of endplate thicknesses was conducted, and an achievement was obtained for improving the rotation capacity of endplate connections at elevated temperatures.

3.2 TESTS AT UNIVERSITY OF SHEFFIELD

From 2005 to 2008, the University of Sheffield and the University of Manchester conducted a joint research project with the aim of investigating the capacity and ductility of steel connections at elevated temperatures [3-8]. In tests, they adopted a test setup in which the connections were subjected to a combination of tension and shear forces. Four types of simple beam-to-column connections were studied in their project. In order to illustrate the experimental behaviour of mild steel endplate connections at ambient and elevated temperatures, only the tests on flush endplate connections are used herein.

A detailed description of the test setup and test measurements was given previously [4]. The tests were performed in an electrical furnace of $1.0m^3$ internal capacity, as shown in Fig. 3.1. The specimens were heated slowly to the specified elevated temperature, and then loaded to fail at this constant temperature, i.e. under steady state fire condition. A special loading system was designed to allow very large rotation of the tested connection. When the head of the jack moves downward, it applies a tensile force to the end of the specimen through the action of the linkage. The loading jack was displacement-controlled. The applied load was measured from strain-gauges attached to the bars. The deformations of the connection were measured using a digital camera facing the connection through a glass window in the door of the oven.
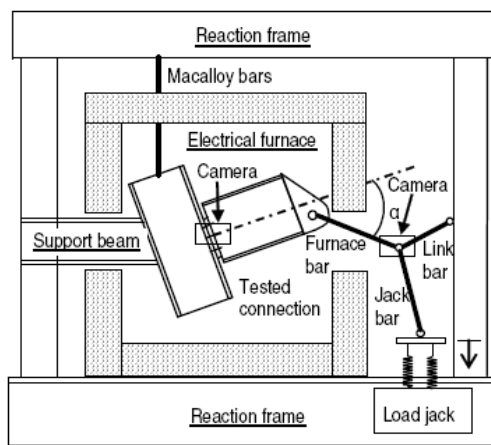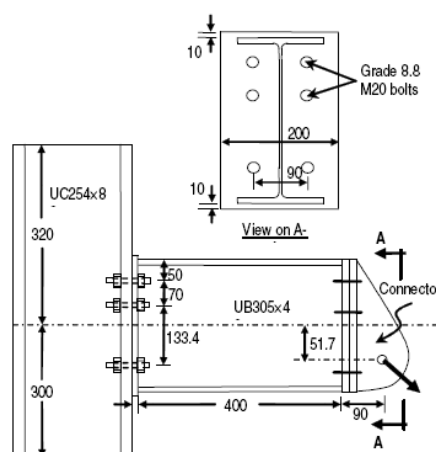
Fig.3.1. Test setup.   Fig.3.2. Flush endplate connection specimen.

Fig. 3.2 shows the details of a typical flush endplate connection in tests. In all cases, a UC254×89 section made of S355 was used for the column, and the beam section was UB305×165×40 made of S275.

3.3 FINITE ELEMENT ANALYSIS METHOD

The finite element software ABAQUS [9] was used to simulate the behaviour of endplate connections at ambient and elevated temperatures.

3.3.1 Geometric Details of Connections

The details of all connection components modelled in FEM were the same as those of the test specimens. Because the geometric details, loads, temperature distribution and boundary conditions were symmetric, half of the endplate connection was modelled, to reduce computer costs and shorten computing time. The components of this FE model are shown in Fig. 3.3, including bolt shank, nut, washer, endplate, beam and column. The bolt holes were modelled 2mm larger than the bolt shank diameter, and the hexagon bolt heads were modelled as cylinders for simplicity.

(a) Beam   (b) Column (c) Endplate (d) Bolt assembly (e) Assembled FE model
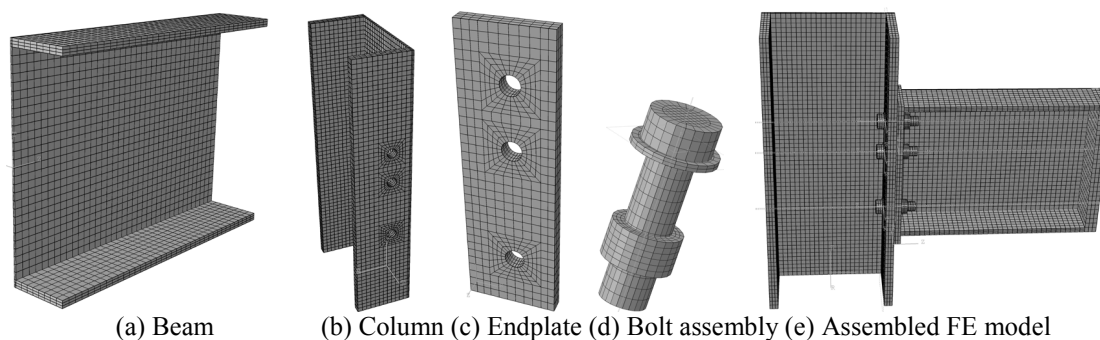
Fig.3.3. FE model and its mesh generation.

31

3.3.2 Mesh Generation and Element Type

There were 13 surface-to-surface contact interactions and 14 tie interactions in this model, and the materials were endowed with non-linear properties. These make this analysis sensitive to mesh, so the mesh should be fine enough. To capture accurate stress distribution in the region around bolt holes where failures would likely to initiate, an intensive mesh was created in the vicinity of bolt holes, as shown in Fig. 3.3(c). The whole connection was modelled using C3D8I elements, because of its excellence in simulating contact interactions, non-linear material properties and stress concentrations, which will be introduced in detail in Chapter 7.

3.3.3 Contact Interaction

To handle the contact interaction problem, the whole analysis process comprised 6 analysis steps. In the first step, the bolts, washers and endplate were temporarily restrained in all directions, and then a very small temporary load was applied to every bolt for restraining the bolt pairs temporarily. The temperature field for all components was 20°C. In the second step, the bolts, washers and the endplate were freed from any temporary restraint. In the third step, the pretension was applied to every bolt. In the fourth step, the length of every bolt was fixed. In the fifth step, the temperature field for all components was modified to a preselected temperature. (For the analysis at ambient temperature, the temperature field was kept constant.) In the sixth step, an equivalent surface traction converted from the actual inclined force with its preselected initial load angle was applied to the end of the beam. The first four steps helped contact interactions to be established smoothly, which is effective to decrease calculation time and eliminate errors.

Surface-to-surface contact, with a small sliding option, was used for all contact surfaces to fully transfer the load. The contact pairs in the endplate connection comprised the washers-to-column flange, column flange-to-endplate, endplate-to-nuts. The washer was tied to the bolt head in each bolt pair for simplicity and the nuts were tied to the corresponding bolt shanks.

3.3.4 Material Properties

In this FE modelling, the material properties of mild steels (including S275 and S355) and bolt pairs were the same with those reported by the University of Sheffield [6, 10-12]. The material properties of BISPLATE 80 (which is similar to S690) at elevated temperatures reported by Chen and Young [13]

were used for HSS. The detailed material properties at ambient temperature in this modelling are illustrated in Table 3.1.

Table 3.1: Material properties at ambient temperature used in FEM.

Material	Yield stress (N/mm^2)	Ultimate stress (N/mm^2)	Elastic modulus (kN/mm^2)	Poisson ratio
S275	275	450	205	0.3
S355	355	550	205	0.3
S690	690	877	223	0.3
Bolt	640	800	205	0.3

3.3.5 Loads

An additional endplate was modelled at the other end of the beam, just for applying surface traction, as shown in Fig. 3.3(e). The initial load angles used in these tests were also taken into consideration when applying the surface traction. The magnitude of pretension for each bolt agrees with the average reported in the experimental investigation [4, 6].

3.3.6 Welds

The welds between endplate and beam were modelled by tie restraint instead of solid modelling, in order to simplify the model, as illustrated afterwards in Fig.7.6.

3.4   VALIDATIONS   AGAINST   EXPERIMENTAL RESULTS

Validations of the numerical modelling were performed against Yu et al.'s experimental results on mild steel endplate connections both at ambient temperature and at elevated temperatures under steady-state conditions, to check the accuracy of the proposed numerical model.

3.4.1 At Ambient Temperature

In Yu et al.'s tests, at ambient temperature experimental results on 10mm S275 endplate with the initial load angle of 55 degree (10E55RS275) and 8mm S275 endplate with the initial load angle of 35 degree (8E35RS275) were available. So, the corresponding numerical modellings were conducted, using ABAQUS/Standard, based on the above-mentioned FE analysis.

The comparisons of the ultimate failure mode and the status of the corresponding components of 10E55RS275 are illustrated in Fig. 3.4 and Fig. 3.5, while those of 8E35RS275 are shown in Fig. 3.6 and Fig. 3.7. The force-connection rotation curves for both specimens are shown in Fig. 3.8.
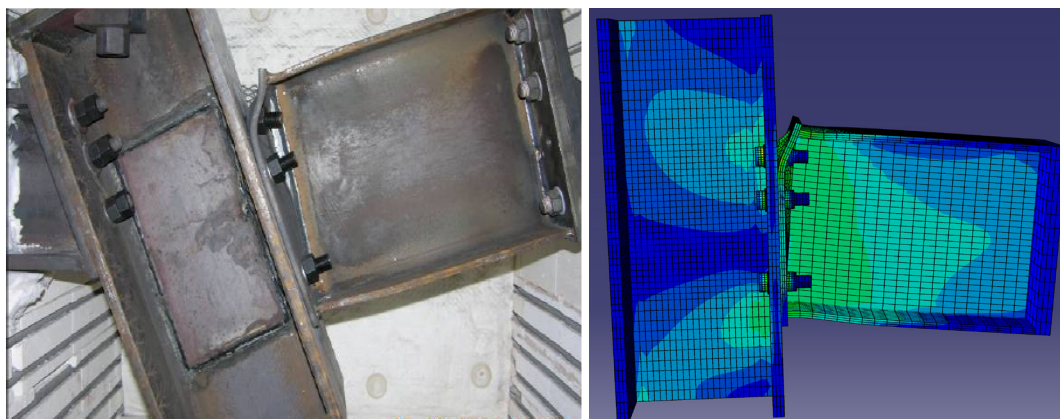
Fig.3.4. Ultimate failure mode of specimen 10E55RS275 at ambient temperature.
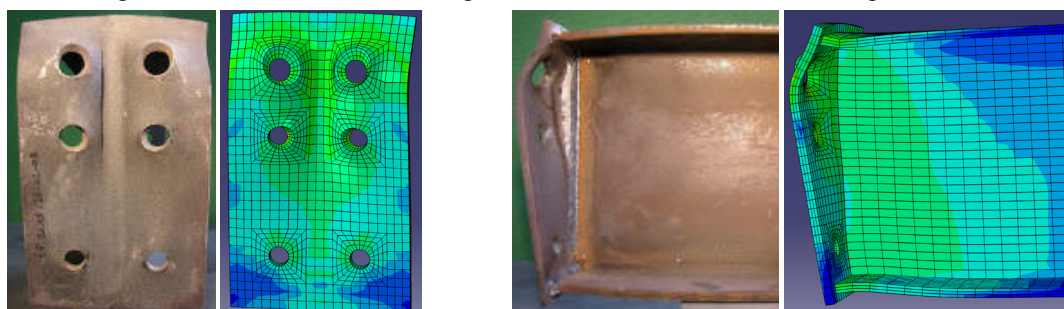
(a) Endplate

(b) Endplate and beam

(c) Bolt pairs

Fig.3.5. Components of connection 10E55RS275 after failure.
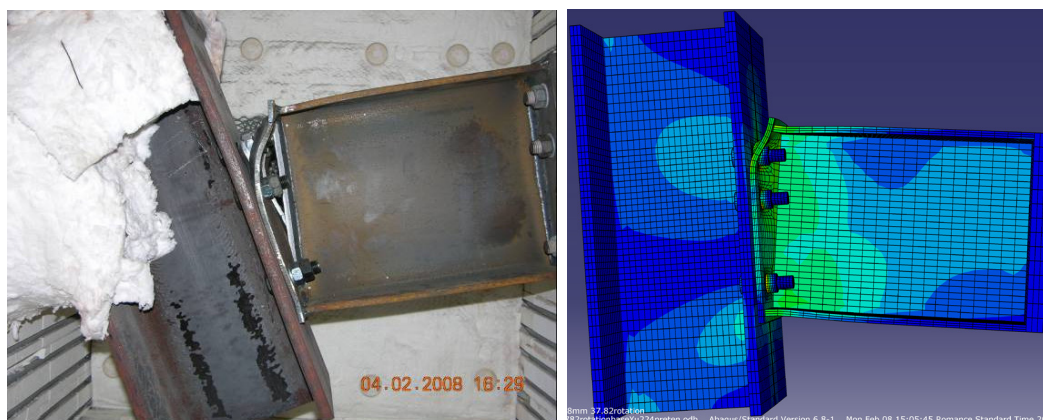
Fig.3.6. Comparison of ultimate failure mode of specimen 8E35RS275 at ambient temperature.

34

(a) Endplate   (b) Endplate and beam

(c) Bolt pairs
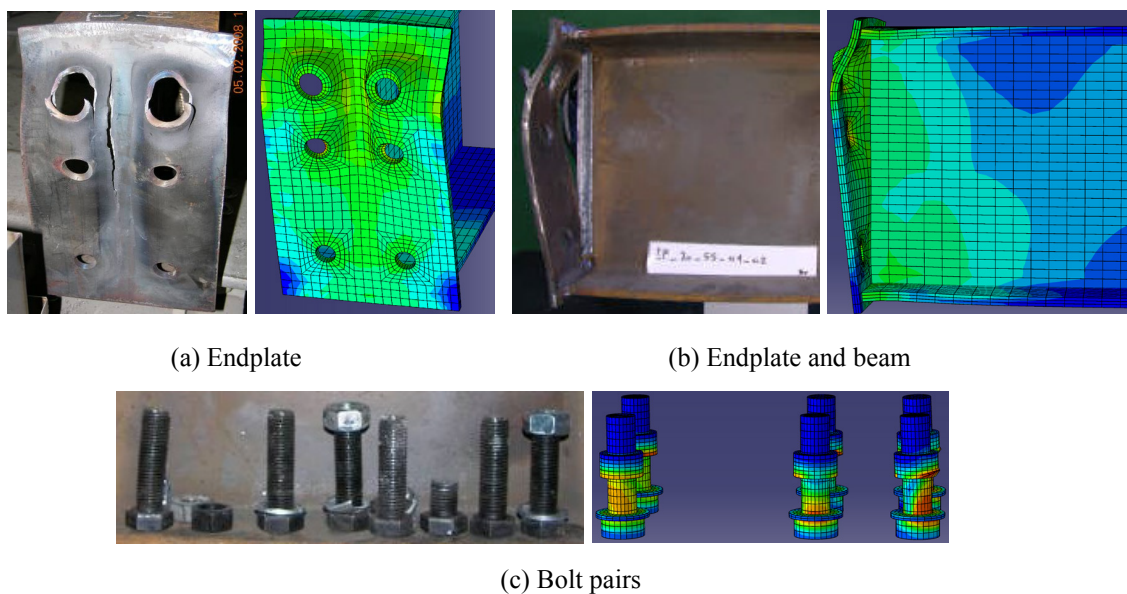
Fig.3.7. Components of connection 8E35RS275 after failure.

(a) 10E55RS275   (b) 8E35RS275
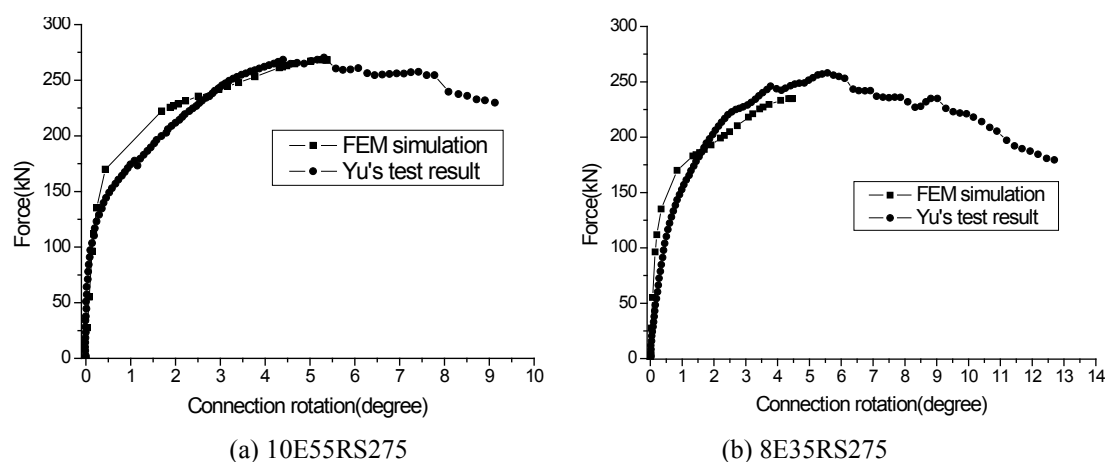
Fig.3.8. Force-rotation curves of connections at ambient temperature.

It can be seen that the FEM simulations and Yu et al.'s test results are in good agreement. For the two specimens, the maximal discrepancies between numerical simulations and experimental data are both about 10%. It can be concluded that the Finite Element modelling described here can simulate the response of endplate connections at ambient temperature with reasonable accuracy.

3.4.2 At Elevated Temperatures

In Yu et al.'s fire tests, the connection specimens (10mmS275 endplate connections) have been heated to two preselected elevated temperatures 450°C and 550°C, and then loaded till failure occurred. For each elevated temperature, the specimens were tested with three initial load angles (35degree, 45degree and 55degree). The corresponding numerical modellings are based on the above-mentioned FE analysis method as well.

The force-rotation capacities of 10mmS275 endplate connections at elevated temperatures obtained by FEM were compared with test results, as shown in Figs. 3.9-3.10. The following remarks can be drawn. This FE model cannot simulate the descending stage of force-rotation curves obtained in tests. For the first two stages of the semi-trilinear curves obtained by FEM simulations, they are in acceptable agreement with Yu et al.'s test results at 450°C and 550°C.

(a) 35°initial load angle

(b) 45°initial load angle

(c) 55°initial load angle
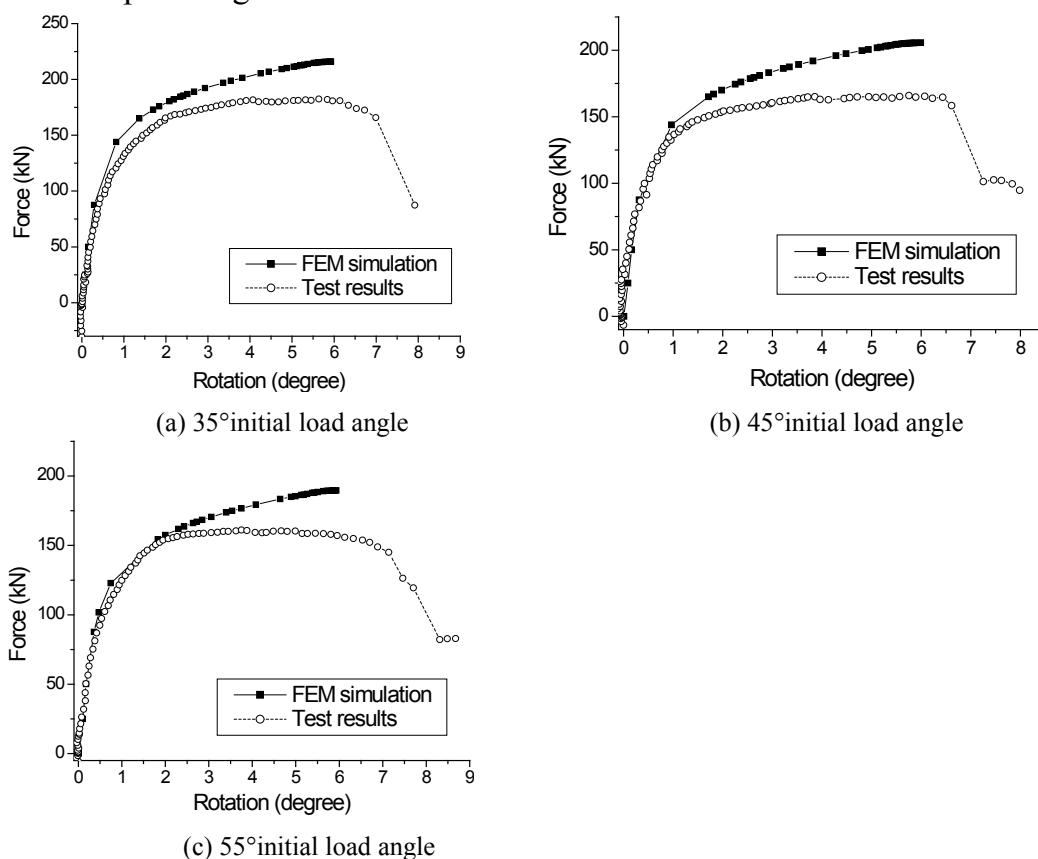
Fig.3.9. Force-rotation comparisons of 10mmS275 at 450°C.

(a) 35°initial load angle

(b) 45°initial load angle
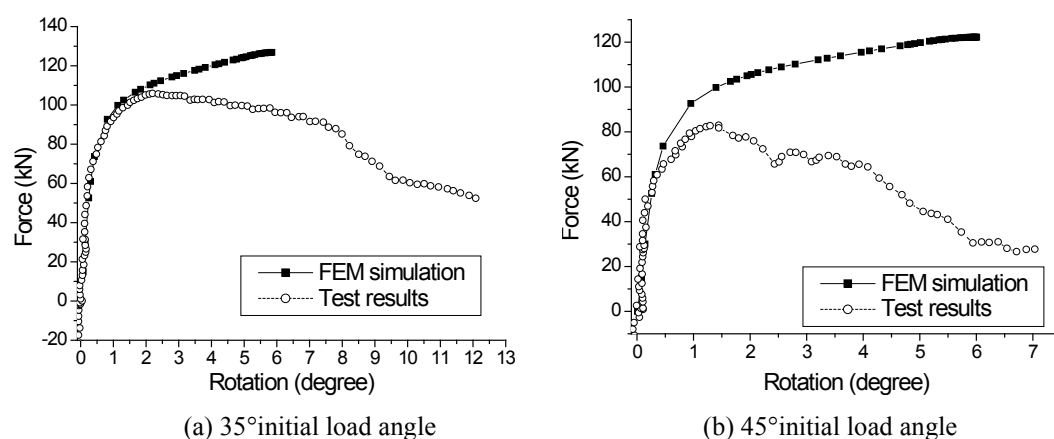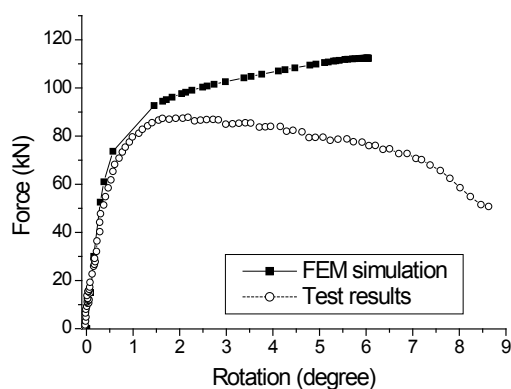
(c) 55°initial load angle

Fig.3.10. Force-rotation comparisons of 10mmS275 at 550°C.

3.4.3 Discussion of Discrepancies

The discrepancies between numerical results and test results need some discussions. Firstly, the true stress - true strain relationships for S275, S355 and high strength bolts used in FEM are transferred from test obtained results of elastic-plastic nature with strain-hardening. In fire tests, the connections were loaded at a very slow deflection rate (i.e. the specimens were loaded until failure in about 120 mins) at constant temperature, but there are no material properties of S275 corresponding to so slow steady-state conditions available in literature. The material properties used herein were obtained from previous material tests of the University of Sheffield, in which the strain rates were higher than those of Yu's full-scale connection tests. The deviations in material properties are responsible for resulting in the discrepancies of connection behaviour between numerical simulation and test results. Secondly, the welds between endplate and beam were not solidly modelled but treated by tie restraints. Hence, the failure of welds was not simulated in FEM. So, the discrepancy is attributable to this welds treatment, which indicates that the solid modelling of welds is necessary to improve the accuracy of numerical simulation. Thirdly, the amount of applied pretension for each bolt is the average given in Yu et al.'s tests. In actual tests, it is very difficult to induce exactly a predetermined bolt force by current pretension techniques. As a result, this may also be a reason for the discrepancies. Moreover, fabrication errors in the test specimens may also lead to deviations between the numerical and experimental results.

3.5 NUMERICAL PREDICTION OF HSS ENDPLATE CONNECTIONS

In this section, numerical modelling was conducted using the high strength steel BISPLATE 80 (which is similar to HSS S690) material property obtained from Chen and Young's tests [13] as endplate material, in order to predict the behaviour of HSS endplate connections both at ambient temperature and at elevated temperatures. For comparison, S275 is used as mild steel, to illustrate the behaviour of mild steel endplate connections under both conditions. The numerical modelled column is made of S355, and S275 is the material for the beam, which are the same with Yu's test specimens.

3.5.1 Connections with Same Endplate Thickness

3.5.1.1 At Ambient Temperature

The numerically simulated force-rotation capacities of HSS endplate connections at ambient temperature were compared with those of mild steel ones, with the same endplate thickness. The results for the initial load angle of 45 degree are illustrated in Fig. 3.11.

(a) 10mm thickness endplate   (b) 12mm thickness endplate

(c) 15mm thickness endplate
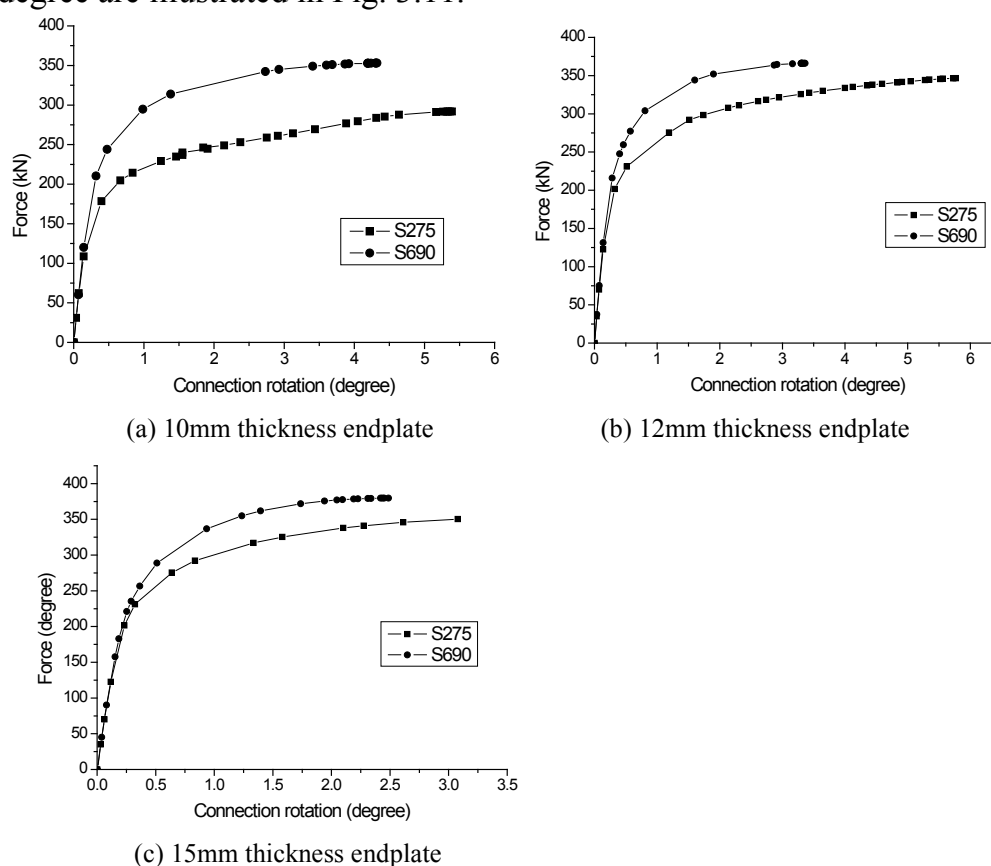
Fig.3.11.Comparisons of HSS and mild steel endplate connections at ambient temperature.

As we could expect, it is found that at ambient temperature the load-bearing capacities of HSS endplate connections are larger than those of mild steel connections using the same thickness of endplates, but the rotation capacity of the former is lower. So using the same thickness of HSS endplate in connections to take place of mild steel endplate at ambient temperature is proved not effective to improve rotation capacity of connections.

3.5.1.2 At Elevated Temperatures

For the same endplate thickness, the force-rotation capacity of HSS endplate connections at elevated temperatures obtained in the numerical simulation was compared with that of mild steel ones, as presented in Fig. 3.12. The numerical results for 10mm endplate with the initial load angle of 55 degree at 450°C and 550°C are illustrated.

| (a) at 450°C | (b) at 550°C |
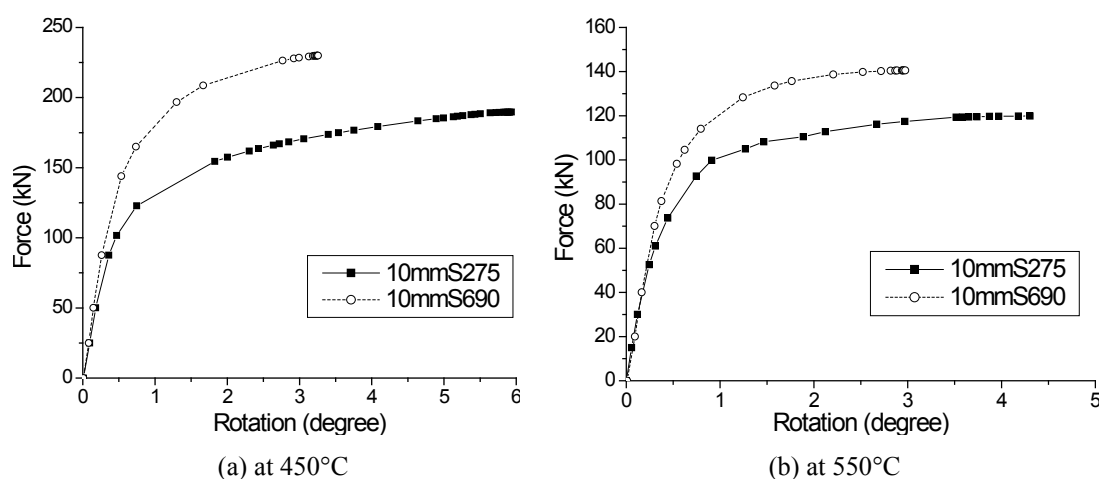
Fig.3.12.Comparisons of HSS and mild steel endplate connections at elevated temperatures.

Similar to those at ambient temperature, it is found that at elevated temperatures the load-bearing capacities of HSS endplate connections are also higher than mild steel endplate connections with the same endplate thickness, but the rotation capacity of the former is worse. It is obvious that using the same thickness HSS endplate instead of a mild steel endplate in connections is not effective to improve the rotation capacity of endplate connections at elevated temperatures.

3.5.2 Parametric Study on Endplate Thickness

To investigate the thickness effect of endplate on strength and ductility of connections, a parametric study both at ambient temperature and at elevated temperatures was conducted using the proposed FE model. In this numerical analysis, BISPLATE 80 (similar to S690) [13] was considered as HSS endplate

material, while mild steel endplate material was S275. The parameter concerned, i.e. thickness of endplate, was varied.

3.5.2.1 At Ambient Temperature

The obtained force-rotation capacities of HSS S690 endplate connections with various endplate thicknesses at ambient temperature were compared with those of mild steel S275 endplate connections, as shown in Fig. 3.13.
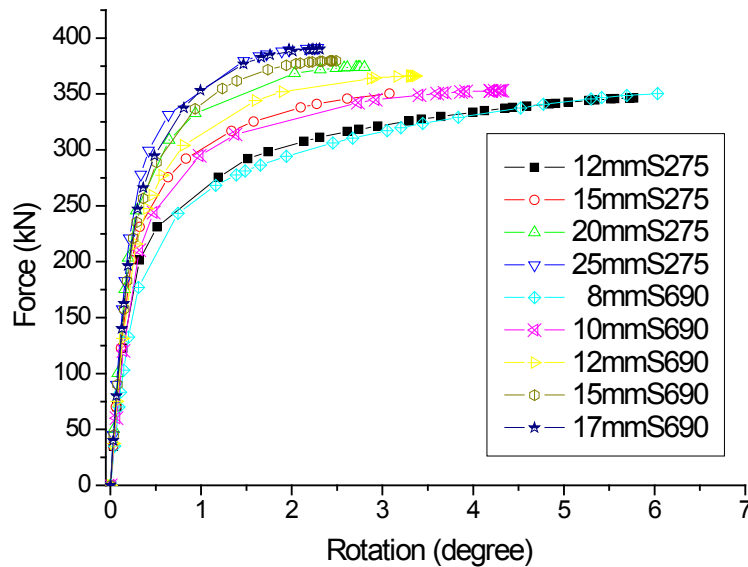
Fig.3.13. Effects of endplate thicknesses at ambient temperature.

It can be seen that the 8mm thickness S690 endplate connection (8mmS690) is as strong as the 12mm thickness S275 endplate connection (12mmS275) in load-bearing, but the rotation capacity of the former is higher. Similar conclusions can be drawn for the other three comparison pairs: 10mmS690-15mmS275, 12mmS690-20mmS275 and 17mmS690-25mmS275.

These results show that at ambient temperature the connection with a thin HSS endplate enhances its rotation capacity and simultaneously achieves the same resistance as that with a thick mild steel one. This is positive for improving the ductility of endplate connections at ambient temperature, and also indicates a beneficial research idea for enhancing the ductility of endplate connections at elevated temperatures.

3.5.2.2 At Elevated Temperatures

At elevated temperatures (i.e. 450°C and 550°C), the numerically simulated force-rotation capacities of various thicknesses of HSS endplate connections were compared with those of mild steel endplate connections, as shown in Fig. 3.14. A similar conclusion can be drawn from Fig. 3.14 like that at ambient

temperature: at elevated temperatures, a thinner HSS endplate provides the same load-bearing capacity as that of a mild steel endplate connection, but enhances the rotation capacity of the connection. This quantitative achievement is positive for improving the fire-resistance design of endplate connections at elevated temperatures.
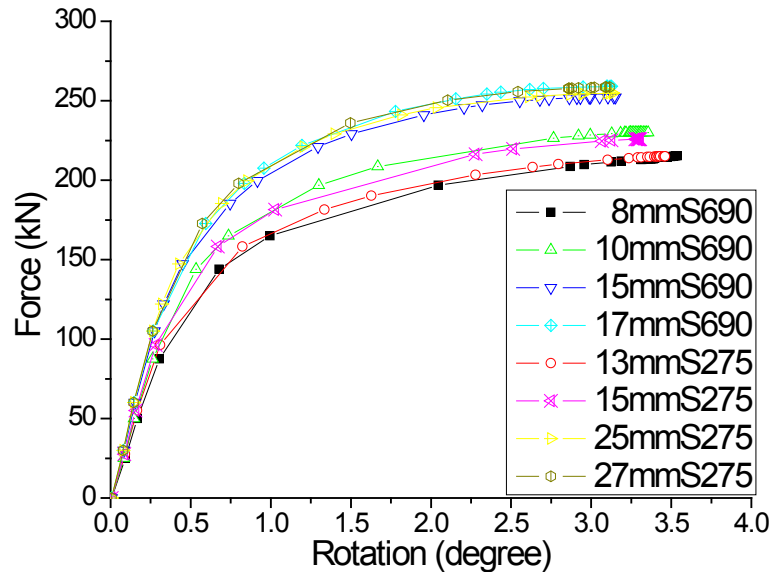
(a)450°C
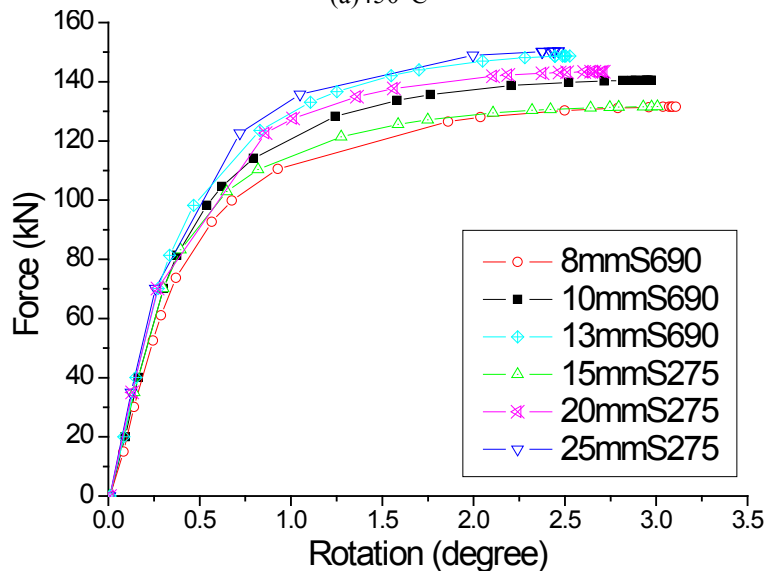
(b) 550°C

Fig.3.14. Effects of endplate thicknesses at elevated temperatures.

3.6 CONCLUSION

This chapter reports on a FE modelling of endplate connections using ABAQUS/Standard, in order to predict the performances of endplate connections combining HSS with mild steel at ambient and elevated temperatures. The results may be used as a basis for investigating how HSS

41

endplate connections behave not only under normal conditions but also under fire conditions. This research widens the perspective of fire resistance on steel connections as well. The following conclusions can be drawn.

The challenge of numerical modelling contact interactions is solved successfully, considering material and geometric non-linear effects. The proposed FE modelling is verified appropriate to simulate mild steel endplate connections at ambient and elevated temperatures with reasonable accuracy. On this basis, the performances of HSS endplate connections at ambient temperature and at elevated temperatures are further predicted and compared with those of mild steel ones.

It is found that a proper thinner HSS endplate has the potential to enhance the connection's rotation capacity both at ambient temperature and at elevated temperatures, and simultaneously achieve almost the same load-bearing capacity as a mild steel endplate connection. The proposed research idea, combining HSS with mild steel in connections, may be used for further investigation of improving the behaviour of steel connections under fire conditions as well as effective application of HSS in civil engineering.

By the present modelling method, the critical locations of endplate connections can be identified, but the occurrence of component failure cannot be predicted.

3.7 REFERENCES

[1] European Committee for Standardization (CEN), BS EN 1993-1-8, Eurocode3: Design of steel structures, Part 1-8: Design of joints. British Standards Institution, Brussels , 2005.

[2] A.M. Girao Coelho and F.S.K. Bijlaard, Experimental behaviour of high strength steel end-plate connections, Journal of Constructional Steel Research, 63 (9), 1228-1240 .

[3] I.W. Burgess, The Robustness of Steel Connections in Fire. Proceeding of the Ninth International Conference on Steel Concrete Composite and Hybrid Structures, (2009) July 8-10; Leeds, UK.

[4] H. Yu, I.W. Burgess, J.B. Davison and R.J. Plank, Experimental Investigation of the Behaviour of Flush Endplate Connections in Fire, Proceeding of the Fifth International Conference Structures in Fire, (2008) May 28-30; Singapore.

[5] H. Yu, I.W. Burgess, J.B. Davison and R.J. Plank, Development of a Yield-Line Model for Endplate Connections in Fire, Journal of Constructional Steel Research, 65 (6), 1279-1289.

[6] Y. Hu, J.B. Davison, I.W. Burgess and R.J. Plank, Experimental Study on Flexible End Plate Connections in Fire, Proc. 5th European Conference on Steel Structures, Graz, Austria, 1007-1012.

[7] H. Yu, I.W. Burgess, J.B. Davison and R.J. Plank, Tying Capacity of Web Cleat Connections in Fire. Part 1: Test and Finite Element Simulation, Engineering Structures, 31 (3), 651-663.

[8] H. Yu, I.W. Burgess, J.B. Davison and R.J. Plank, Tying Capacity of Web Cleat Connections in Fire. Part 2: Development of Component-Based Model, Engineering Structures, 31 (3), 697-708.

[9] Abaqus Analysis User's Manual, 6.8 version.

[10] Y. Hu, J.B. Davison, I.W. Burgess and R.J. Plank, Comparative Study of the Behaviour of BS 4190 and BS EN ISO 4014 Bolts in Fire, ICSCS 2007, Manchester, 587-592.

[11] A. Renner, The effect of strain-rate on the elevated-temperature behaviour of structural steel. Research dissertation. University of Sheffield, UK, 2005.

[12] Y. Theodorou, Mechanical properties of grade 8.8 bolts at elevated temperatures. Master's dissertation. University of Sheffield, UK, 2003.

[13] J. Chen, B. Young, B. Uy, Behavior of high strength structural steel at elevated temperatures. J. Struct Eng (2006) 1948-1954.

[14] X. Qiang, F.S.K. Bijlaard, M.H. Kolstein, L. Twilt, Numerical analysis of high strength steel endplate connections at ambient and elevated temperatures, Journal of Structural Fire Engineering. (accepted, in press)

Part II

Experimental study on mechanical properties of high strength structural steels in fire and after fire

Chapter 4

Mechanical properties of high strength structural steels in fire

4.1 INTRODUCTION

In the European design standard for steel structures Eurocode 3 part 1-2 [1], it is assumed that the material properties of various structural steel grades (i.e. S235, S275, S355, S420 and S460) at elevated temperatures can be evaluated uniformly. Afterwards, the Eurocode 3 part 1-12 [2] extends Eurocode 3 (EC3) up to S700, including S500, S550, S620 and S690. The predictions on the deterioration of material properties of structural steels in fire recommended by EC3 are based on test results mainly obtained from mild steels (i.e. S235, S275 and S355). However, previous researches [3-7] indicate that the elevated-temperature material properties of high strength steels (HSS) are different from those of mild steels. Hence, using the recommendations from EC3 to perform fire-resistance design of structural members made of HSS might run a risk. Not only the European design standards (Eurocode 3 part 1-2 [1] and Eurocode 3 part 1-12 [2]) but also American standards ASCE [8] and AISC [9], Australian standard AS 4100 [10] and British standard BS 5950 [11], current design standards for steel structures do not specify the recommendations for HSS under fire conditions. Therefore, accurate material properties of various constructional high strength steel grades at elevated temperatures are urgently needed in practical design, in order to keep pace with the development of modelling techniques for predicting the fire response of steel structures made of HSS as well as the application of HSS in structural engineering field.

In order to supply convincing proof for a safe fire-resistance design of steel structures with HSS and validate the limited available research results in literature, an experimental research was conducted on S460, S690 and S960, using both the steady state test method and the transient state test method. The elastic modulus, yield strength and ultimate strength of these three high strength structural steels at elevated temperatures were obtained from the tests

and compared with available literature and the recommendations of leading design standards for steel structures (i.e. EC3 [1], ASCE [8], AISC [9], AS 4100 [10] and BS 5950 [11]).

4.2 MECHANICAL PROPERTIES OF S460 IN FIRE[*1]

4.2.1 Experimental Study

4.2.1.1 Test device

The tensile tests at various fire temperatures were conducted using a Gleeble 3800 System, which is a fully integrated digital closed loop control thermal and mechanical testing system, as shown in Fig. 4.1. In this system, the test specimens are heated by an electrical current through the specimens. The direct resistance heating system can heat specimens at rates of up to 10,000°C/second, or can hold steady-state equilibrium temperatures. In this experimental study, the heating rate used is according to the standard fire based on Eurocode 1 EN 1991-1-2 [12], which is in the range of 5-50°C/min. The heating rates of nature fire of buildings are originally derived from standard fire conditions, by taking into account of the environment, density of combustible materials and ventilation in or around the building structures. The Gleeble 3800 has a digital control system, which provides all signals necessary to control the thermal and mechanical test variables simultaneously through the digital closed-loop thermal and mechanical servo systems. In this study, 3 pairs of thermocouples applied to the test coupons provided signals for accurate feedback control of the specimen temperatures, see Fig. 4.3b. The Gleeble 3800 mechanical system is an integrated hydraulic servo system, capable of exerting as much as 200kN of static force in compression or 100kN in tension. A non-contact laser extensometer was used to obtain the strain of the specimen. The experimental process was controlled by some predefined programming options using QuikSim Software. All the data obtained from the tests (i.e. force, stroke, deformation, strain, temperature and time) were recorded and could be monitored during testing.

[*1] This section has been published in two journal papers of X.Qiang et al. [25, 26].

Fig.4.1. Test device-Gleeble 3800 system.
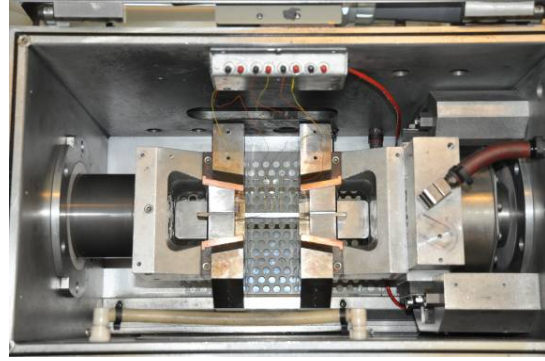
Fig.4.2. Tensile test set-up in the furnace of Gleeble 3800.

(a) Test coupons
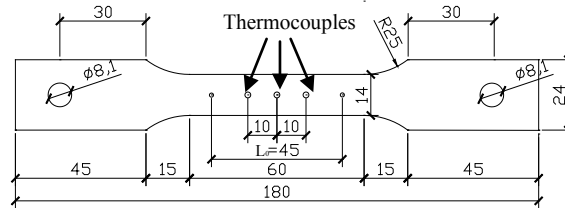
(b) Dimensions

Fig.4.3. Tensile test coupon and dimensions.

4.2.1.2 Test material and specimen

All test specimens were cut from an S460NL steel sheet ordered for this experimental study with a nominal thickness of 5mm. S460NL is weldable normalized steel for steel constructions, with high yield strength and high toughness, produced in compliance with EN 10025-3 [13]. *S460NL* is the grade designation abbreviation of this steel, where *S* means structural steel, *460* is its minimum yield strength, *N* means normalized rolled delivery condition, and *L* means low notch toughness testing temperature. The chemical composition of the tested high strength steel S460N is shown in Table 4.1. The shapes and dimensions of the specimens were prepared in accordance with EN 10002-5 [14]. As shown in Fig. 4.3, one hole was provided at each end of the specimen in order to fix it to the grips of the Gleeble 3800 by using two steel bars. Three thermocouples were welded on the surface of the specimen to measure its temperature, as shown in Fig. 4.3b.

Table 4.1: Actual chemical composition of HSS S460N material (%).

C	Si	Mn	P	S	Cr	Cu
0.172	0.483	1.500	0.012	0.005	0.020	0.025
N	Nb	Ni	Ti	V	Al	Mo
0.0051	0.046	0.018	0.002	0.087	0.037	0.002

4.2.1.3 Test method

To assess the mechanical properties of structural steels exposed to fire, the method is usually to conduct tensile tests either under steady state or transient state. Compared to the transient state test method, the steady state test method is more commonly used in research, as it is easier to perform and provides the stress-strain curves directly. However, the transient state test method is considered to be more realistic in simulating the performance of steel components in fire, as a realistic heating rate for fire exposed steel members can be taken into account. In order to compare the difference between these two methods, both the steady state test method and the transient state test method were applied in this experimental study.

4.2.1.4 Test procedure

In the steady state test, the specimen was heated up to a specified temperature and then loaded in tension until it failed while maintaining the same temperature. The heating rate used herein was uniform 50°C/min, and the preselected temperatures were 100°C, 200°C, 300°C, 350°C, 400°C, 450°C, 500°C, 550°C, 600°C, 650°C and 700°C. After reaching the preselected temperature, approximately 10mins was required for the temperature to stabilize, to ensure a uniform temperature within the central part of the specimen. After that, the tensile load was applied to the specimen until it failed. In the steady state tests, strain-control was used according to the strain obtained from the extensometer. The strain rate used herein was 0.005/min, which satisfied the requirement of ASTM Standard E21-09 [15]. Three repetitive tests were carried out under each fire condition. In order to compare the elevated temperature effect on mechanical properties of S460N, tensile tests were conducted at ambient temperature as well.

In the transient state test, the specimen was under a constant tensile load while the temperature rose until failure occurred. The used stress levels were preselected: 100, 150, 200, 250, 300, 350, 400, 450, 500, 600, 650, 700, 750 and 800MPa. For each condition, three repetitive tests were conducted. The heating rate in all transient state tests was 10°C/min, which corresponds to normally fire-protected steel members [16]. The total strain and temperature of the specimen during the whole test procedure were recorded. The thermal elongation of the specimen (determined according to the recommendations of Eurocode 3 Part 1-2 [1]) is subtracted from the total measured strain, and then the strains of the specimen at various temperatures could be obtained. Under

some constant stress level, the strain-temperature curves obtained from transient-state tests can be transferred to stress-strain curves at various elevated temperatures, by the direct-relationship method which Maljaars et al. [17] and Outinen [18-21] used in their previous researches, see Fig.4.4. It is necessary to mention that the accuracy of the stress-strain curves under transient state fire conditions is influenced by the errors in the measurement of the deformation and the thermal elongation of the measuring equipment. The measuring errors add up and sometimes are in the order of magnitude of the stress-induced elongation. That is why, Maljaars [22] recommended to employ three-point bending tests to determine the elastic modulus of aluminum in fire, since the errors in measuring the elastic deflection in bending tests is relatively small in comparison to the errors in measuring the elongation in tensile tests.
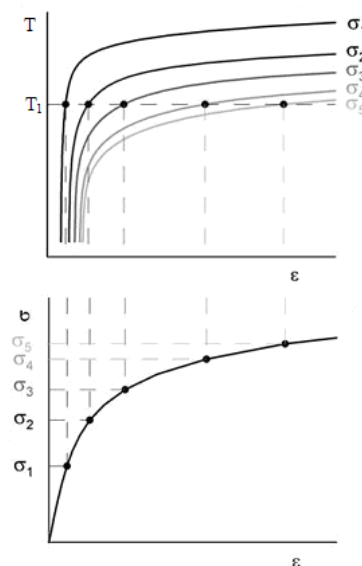
Fig.4.4. Transient state stress–strain derivation [17].

4.2.2 Experimental Results and Discussion

4.2.2.1 Stress-strain curves

The stress-strain curves of S460 at various fire temperatures obtained from this steady state test are plotted in Fig. 4.5. The stress-strain curves of S460 under various transient state conditions transferred from the experimentally obtained strain-temperature curves under various constant stress levels are presented in Fig.4.6. The raw data of test results are presented in Stevin Report 6-13-1 [23].

(a) full range

(b) within the strain range from 0 to 3%
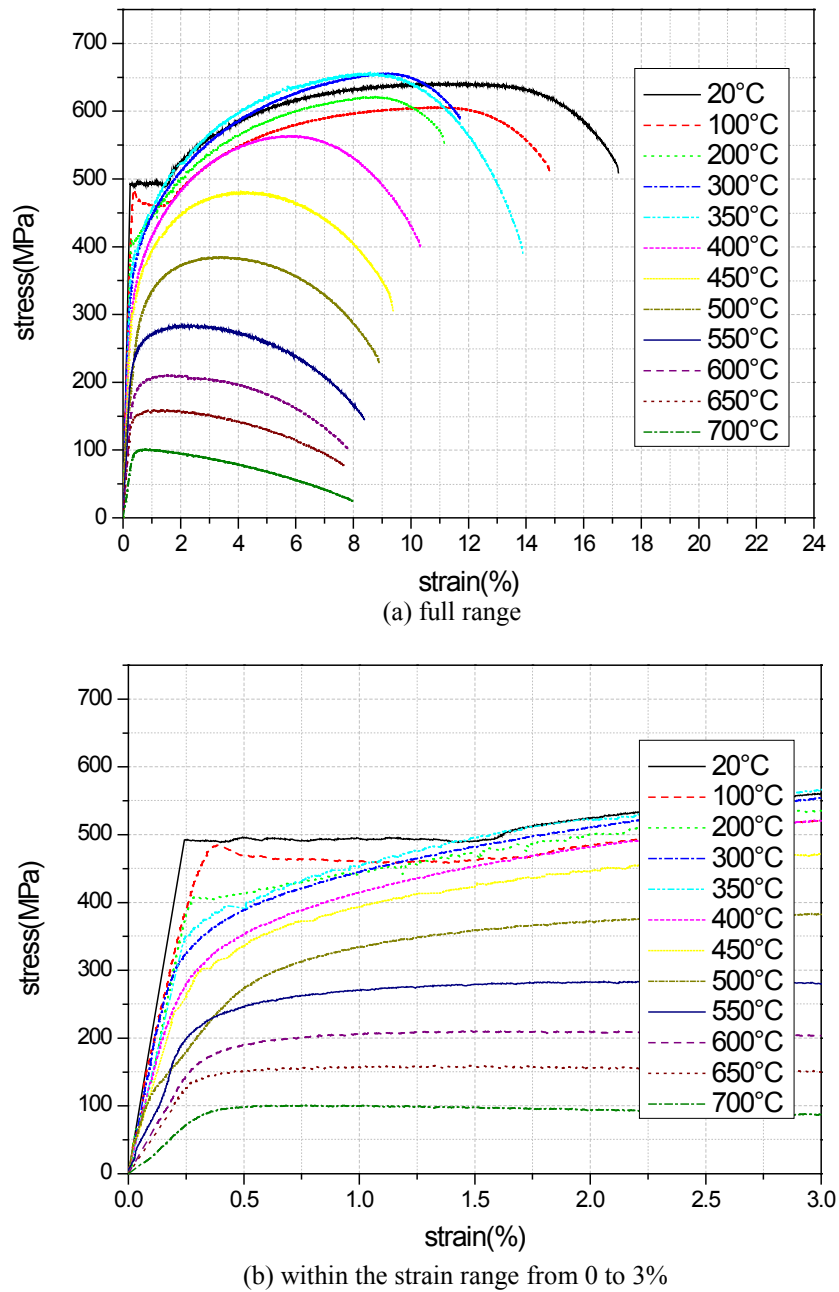
Fig.4.5. Stress-strain curves of S460N at elevated temperatures under steady state.
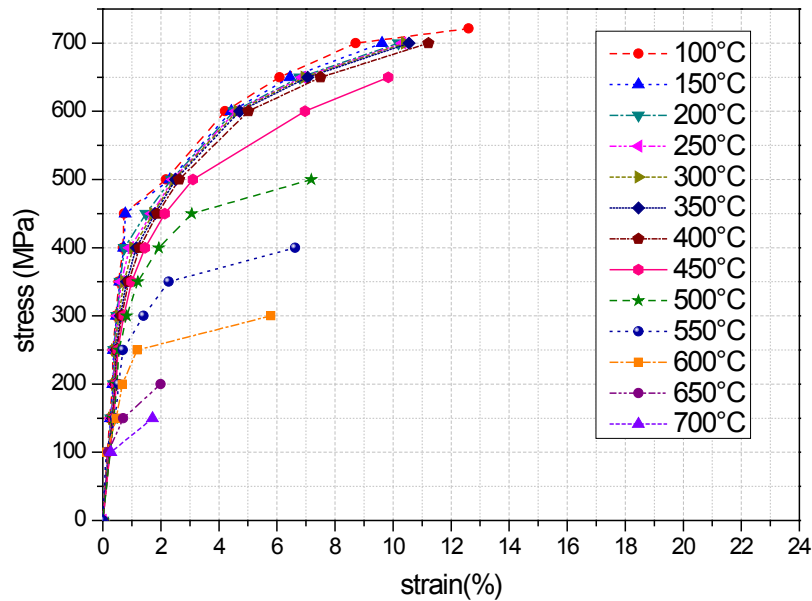
(a) full range
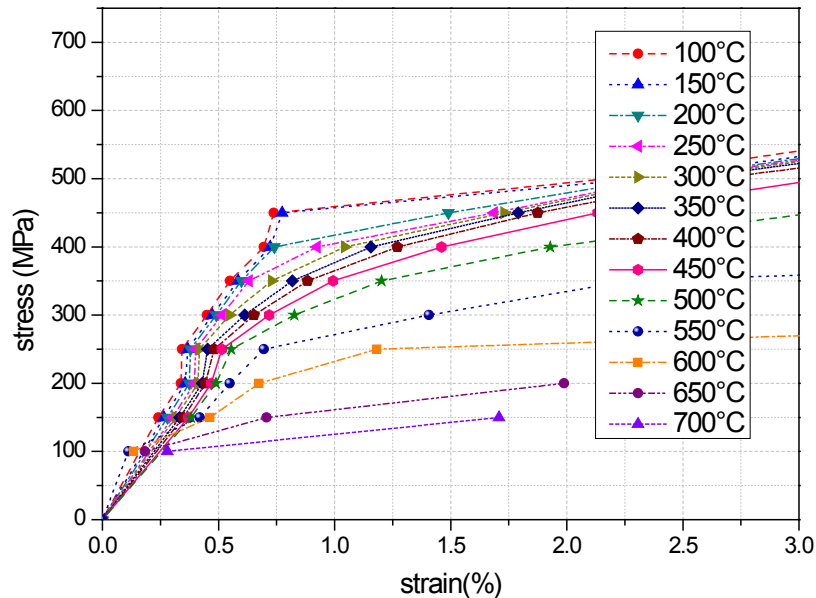
(b) within the strain range from 0 to 3%

Fig.4.6. Stress-strain curves of S460N at elevated temperatures under transient state.

4.2.2.2 Failure mode

Typical failure mode of high strength steel S460N tensile specimens at various elevated temperatures obtained from steady state tests in this experimental study is shown in Fig. 4.7. It can be seen that for all specimens necking appeared before failure. No brittle failure was observed for all temperatures from 20°C up to 700°C.
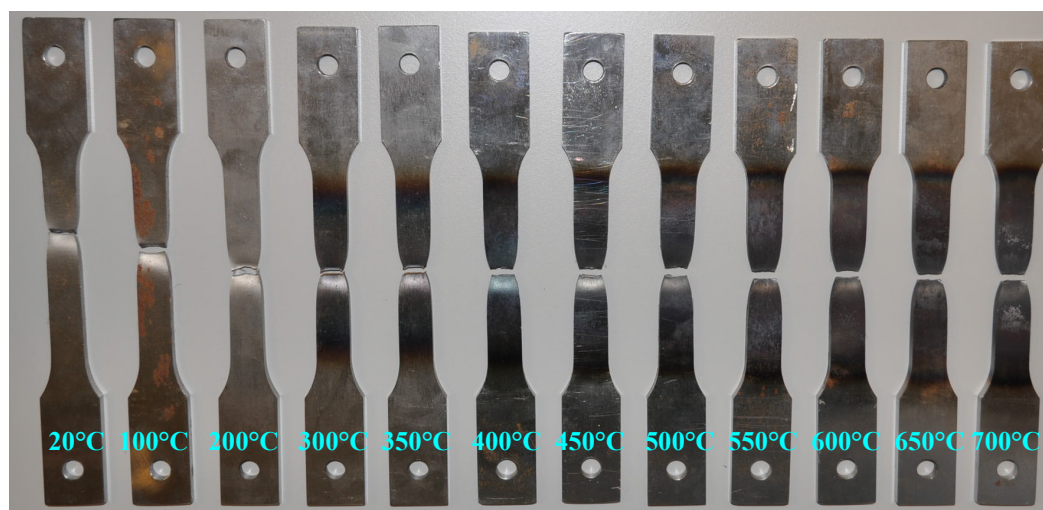
Fig.4.7. Failure mode of S460N specimens under steady state fire condition at various fire temperatures.

Typical failure mode of high strength structural steel S460N tensile specimens under transient state fire condition at various stress levels obtained from this experimental study is shown in Fig.4.8. It can be seen that for all specimens necking appeared before failure. No brittle failure is observed for all stress levels up to 800MPa, which is very promising for fire safety of steel structures with HSS S460N. The elevated temperature at which the specimen fails under a constant tensile stress level is called failure temperature at this specified stress level under transient state fire condition. The failure temperatures of HSS S460N at various stress levels up to 800MPa obtained herein are presented in Table 4.2. It is observed that S460N specimens under very high stress levels fail at a very low fire temperature, especially when the stress level is beyond 750MPa. However, within its nominal yield stress level, S460N fails at a fire temperature in excess of 500°C.
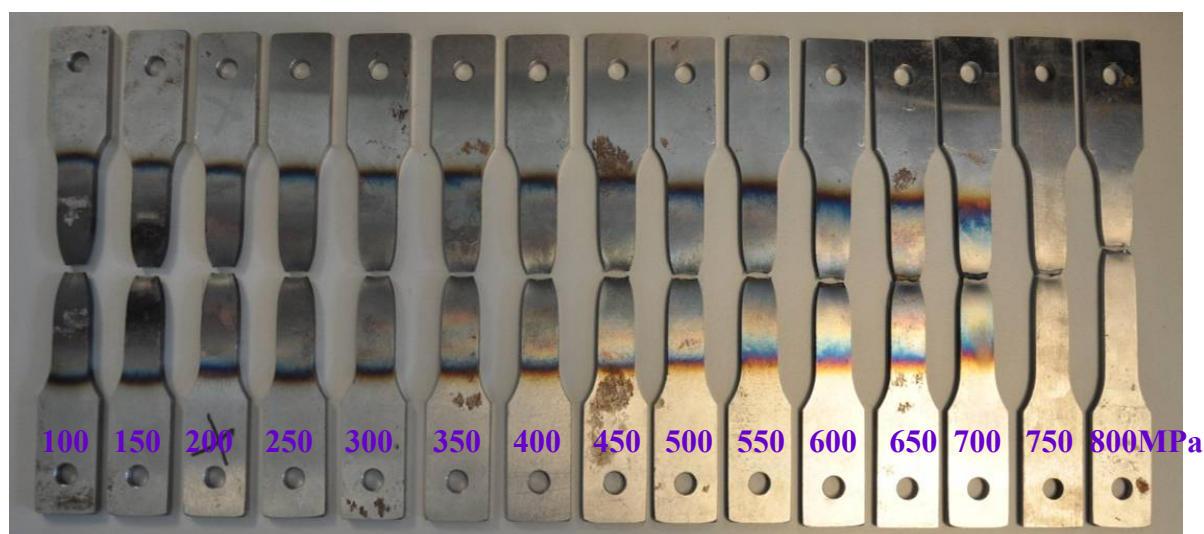
Fig.4.8. Failure mode of S460N specimens under transient state fire condition at various stress levels.

Table 4.2: Failure temperatures of S460N at various stress levels under transient state fire condition

Stress level (MPa)	Failure temperature (°C)
100	789
150	700
200	682
250	621
300	600
350	592
400	555
450	511
500	495
550	488
600	440
650	420
700	381
750	140
800	58

4.2.2.3 Elastic modulus

The decrease of elastic modulus with increasing temperature affects the load-bearing capacity of steel structures significantly. Therefore, it is important to understand the deterioration of elastic modulus at elevated temperatures quantitatively, in order to be able to evaluate the performance of steel structures under fire conditions and correspondingly conduct safe fire-resistance design.

At elevated temperatures the elastic modulus of structural steel is determined from the stress-strain curve at the corresponding temperature, based on the tangent modulus of the initial elastic linear curve, as shown in Fig.4.9. The deterioration of elastic modulus at elevated temperatures is represented by a reduction factor at corresponding temperature. The reduction factor of the elastic modulus is determined by the ratio of the elastic modulus at some elevated temperature E_θ to that at ambient temperature E_{20}. In European, American and Australian design standards, reduction factors are recommended for fire-resistance design and evaluation of steel structures because of their simplicity. Therefore, the reduction factors of elastic modulus $\frac{E_\theta}{E_{20}}$ for S460N at various elevated temperatures were obtained from this experimental study and presented in Table 4.3.
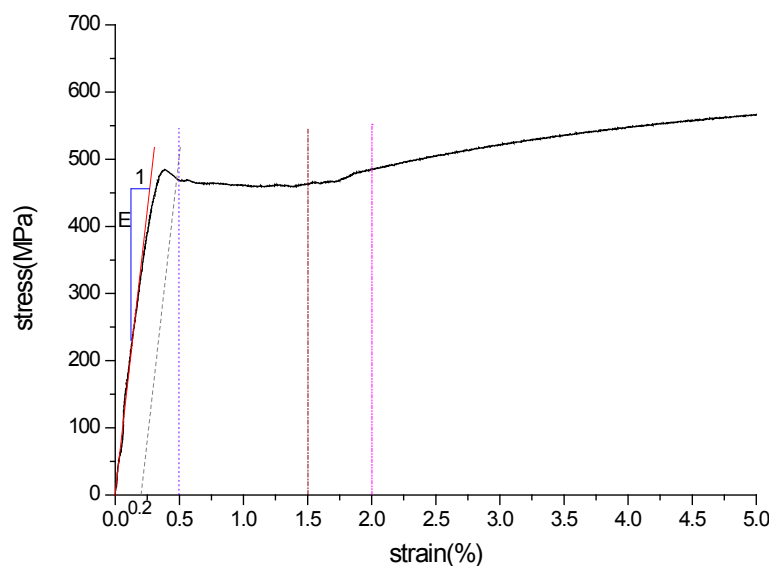
Fig.4.9. Mechanical properties determination of structural steel.

Table 4.3: Elastic modulus and reduction factors of S460N at elevated temperatures.

Steady state test			Transient state test		
temperature (°C)	elastic modulus (MPa)	reduction factor	temperature (°C)	elastic modulus (MPa)	reduction factor
20	202812	1.000	20	201925	1.000
100	199770	0.985	100	199704	0.989
200	178677	0.881	200	175675	0.870
300	161974	0.799	300	159925	0.792
350	144372	0.712	350	141751	0.702
400	135621	0.669	400	134482	0.666
450	117225	0.578	450	118126	0.585
500	103205	0.509	500	97328	0.482
550	75852	0.374	550	72491	0.359
600	59019	0.291	600	54924	0.272
650	50390	0.248	650	44827	0.222
700	31008	0.153	700	26654	0.132
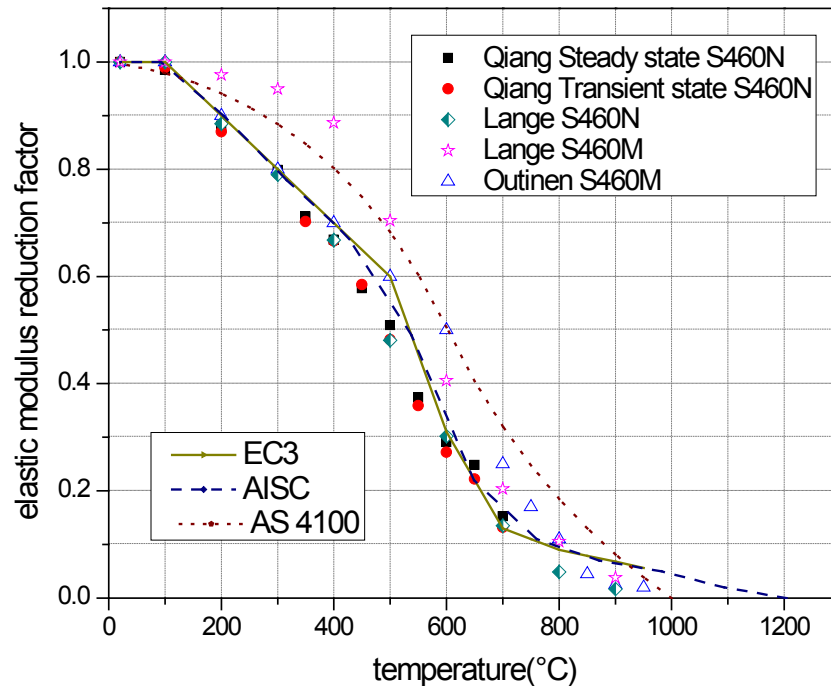
Fig.4.10. Comparison of E-modulus reduction factors of S460 at elevated temperatures.

The reduction factors of elastic modulus obtained from this experimental study are compared with some current leading design standards (i.e. EC3 [1], AISC [9] and AS 4100 [10]) and the available data of HSS S460 in literature [3-6, 18-21], as shown in Fig. 4.10. As introduced in Chapter 2, the difference between S460M and S460N is on the delivery condition. The suffix *M* means thermo-mechanical rolled delivery condition, while the suffix *N* means normalized rolled delivery condition. The comparison in Fig.4.9 confirms that the elastic modulus of S460M at elevated temperatures is higher than that of S460N. For S460N, the results from Lange agree very well with this present experimental study. In comparison to current design standards, AS 4100 is generally non-conservative for HSS S460, except the results from Lange for S460M below 500°C. EC3 and AISC are generally conservative for S460M, but non-conservative for S460N. And the recommendations of AS 4100 on elastic modulus of structural steels at elevated temperatures are not applicable to HSS S460, neither S460M nor S460N.

4.2.2.4 Yield strength

In current leading design standards, the reduction factors of yield strength recommended by EC3 [1] are based on the strain level of 2.0%, while in BS 5950 [11] different reduction factors are given based on three strain levels 0.5%, 1.5% and 2.0%. In AISC [9], ASCE [8] or AS 4100 [10], no specification on strain level accompanies the given reduction factors for yield strength. The yield strength at elevated temperatures used herein was defined

based on the total strain of 2.0%, to agree with the commonly used method in literature. The reduction factors of yield strength at elevated temperatures were calculated by the ratio of yield strength at elevated temperatures $f_{y\theta}$ to that at ambient temperature f_{y20}. The yield strength reduction factors $\dfrac{f_{y\theta}}{f_{y20}}$ of S460N at elevated temperatures from both the steady state test and the transient state test are shown in Table 4.4.

Table 4.4: Yield strength reduction factors of S460N at elevated temperatures.

Steady state test		Transient state test	
temperature (°C)	reduction factor	temperature (°C)	reduction factor
20	1.000	20	1.000
100	0.987	100	0.989
-	-	150	0.975
200	0.994	200	0.970
-	-	250	0.966
300	1.001	300	0.962
350	0.984	350	0.958
400	0.949	400	0.942
450	0.877	450	0.899
500	0.739	500	0.771
550	0.559	550	0.639
600	0.415	600	0.495
650	0.313	650	0.381
700	0.187	700	0.247

In literature, Outinen [18-20] provided the reduction factors of yield strength for S460M obtained from transient state tests, while Lange and Wohlfeil [3] offered reduction factors of yield strength for both S460M and S460N under a transient state test method. Schneider and Lange [4-6] conducted both steady state and transient state tests on three S460N grades with different chemical compositions, to get their stress-strain relationships up to 3% strain at various temperatures. The reduction factors of yield strength are compared with those reported by other researchers in Fig.4.11, and the recommended values from current steel structure design standards are also included. It can be observed that the yield strength reduction factors of S460M at elevated temperatures are higher than those of S460N. The results under both steady state and transient

58

state obtained from this experimental study agree reasonably with each other. There are also good agreements between the research results of this experimental study and that given by Schneider and Lange [4-6] on S460N. The reduction factors recommended in EC3, BS 5950 and AISC are similar, but they are generally non-conservative for S460N in comparison to this experimental result and literature. This comparison also shows that the predictions of ASCE and AS 4100 are not accurate enough for S460.
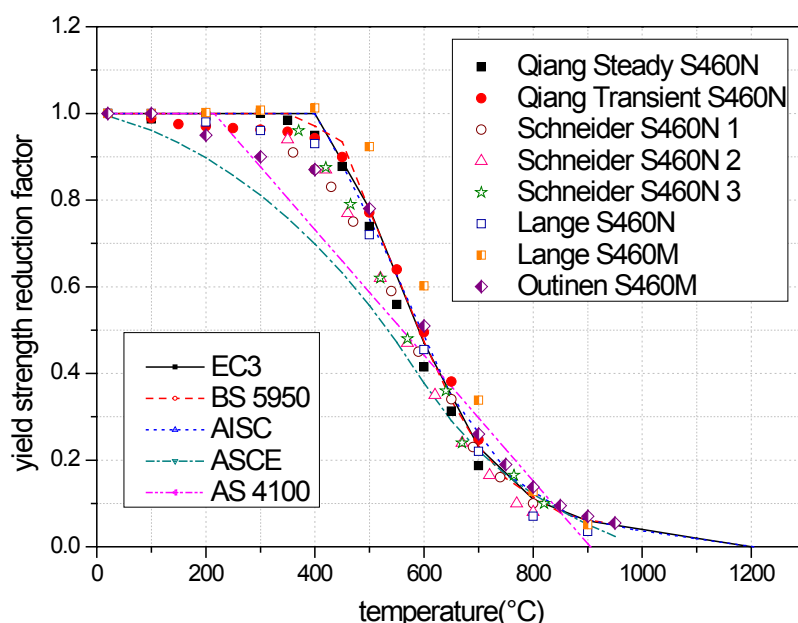
Fig.4.11. Comparison of yield strength reduction factors with current standards and literature on S460.

The reduction factors of yield strength for S460N obtained from this study are also compared with those of various mild steels previously given by Makelainen and Outinen [18-20, 24] as shown in Fig.4.12. The results for S460M reported by Outinen [18-20] and the recommended values of EC3 are also included as reference. This comparison shows that there is a considerable discrepancy in the reduction factors for different steel grades at elevated temperatures. It seems that only the reduction factors for mild steels S235 and S355 can be predicted accurately by EC3. This is because the recommendations of EC3 were mainly obtained from tests on mild steels S235, S275 and S355. Hence, the recommendations of EC3 part 1-2 [1] on yield strength reduction factors of structural steels in fire are confirmed not to be accurate enough for HSS S460. Similar to EC3, no current design standard for steel structures has any specific statements on the difference of various structural steel grades, which could result in risks to conduct fire-resistance design of steel structures with high strength structural steels.
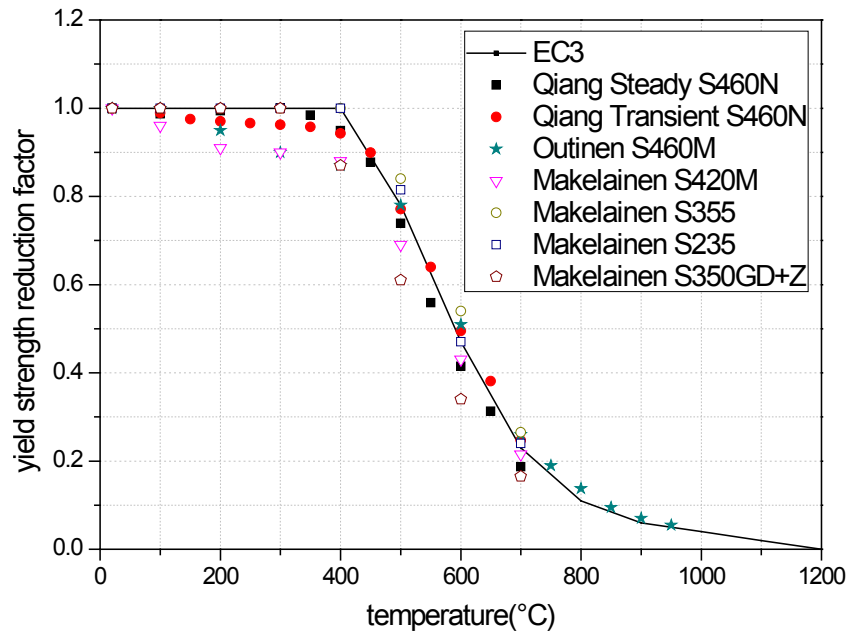
Fig.4.12. Comparison of yield strength reduction factors of S460 with literature on mild steels.

4.2.2.5 Ultimate strength

Table 4.5: Ultimate strength and reduction factors of S460N at elevated temperatures.

Steady state test			Transient state test		
temperature (°C)	ultimate strength (MPa)	reduction factor	temperature (°C)	ultimate strength (MPa)	reduction factor
20	640	1.000	20	723	1.000
100	605	0.945	100	722	0.998
-	-	-	150	701	0.969
200	621	0.969	200	700	0.968
-	-	-	250	700	0.968
300	655	1.023	300	700	0.968
350	656	1.024	350	700	0.968
400	563	0.880	400	700	0.968
450	480	0.750	450	649	0.897
500	385	0.601	500	501	0.693
550	284	0.443	550	402	0.556
600	210	0.328	600	305	0.421
650	159	0.249	650	201	0.278
700	101	0.157	700	149	0.206

The ultimate strength reduction factors were calculated based on the ratio of ultimate strength at a particular elevated temperature $f_{u\theta}$ to that at ambient

temperature f_{u20}. The ultimate strengths and their reduction factors at elevated temperatures $\dfrac{f_{u\theta}}{f_{u20}}$ obtained under steady state and transient state are given in Table 4.5. They are compared with the recommendations of American design standard AISC [9], as shown in Fig.4.13. The reduction factors of ultimate strength for S460N are generally below the recommendations of AISC. In AISC the recommendations for the ultimate strength reduction factors obtained mainly from mild steels are uniform for all structural steel grades, which are proved to be not conservative for evaluating HSS S460N under fire condition. Thus some specified recommendations are necessary for S460N as well as other high strength steel grades, to accurately predict their material properties at elevated temperatures.
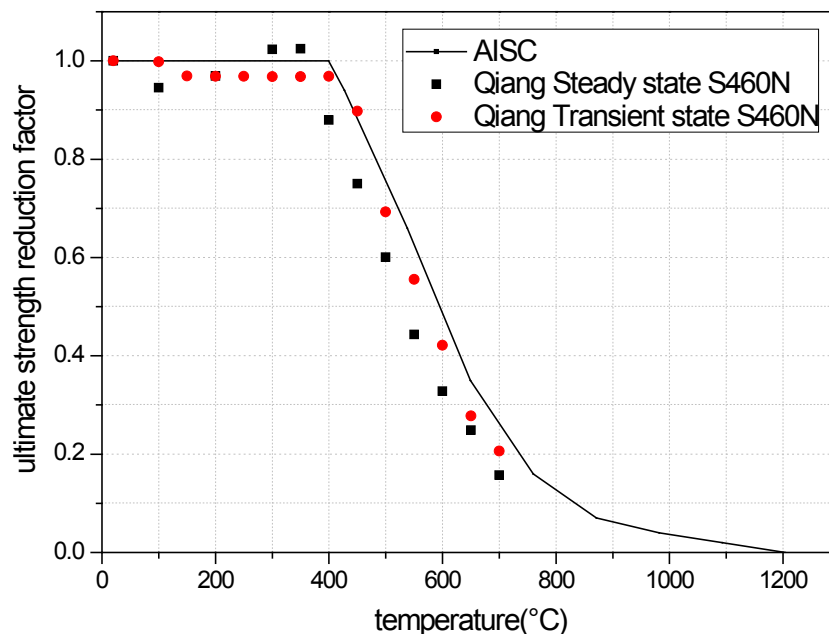
Fig.4.13. Comparison of ultimate strength reduction factors of S460 with AISC.

4.2.3 Predictive Equations

By now there have not been standard test methods for evaluating elevated-temperature mechanical properties of structural steels and this leads to researchers using their own test methods to obtain the elevated-temperature properties of structural steels. Hence, the discrepancies in literature introduce a challenge to designers, who use the material properties as a basis to model the behaviour of steel structures in fire. In numerical modelling and theoretical analysis of steel structures under fire conditions, the elastic modulus, yield strength and ultimate strength play important roles. However, as

61

aforementioned the reduction factors recommended in current design standards are not accurate enough to predict these mechanical properties of high strength structural steels. Therefore, several sets of predictive equations for S460 based on test results and available literature are proposed herein, for accurate evaluating the fire performance of steel structures with HSS S460. As elevated temperature was the main reason causing the deterioration of material properties of steel, the equations were developed as a function of the elevated temperature θ, which specimens have been exposed to.

4.2.3.1 Elastic modulus

A new predictive equation is proposed based on this experimental study and Lange et al.'s research on S460N to present the deterioration of elastic modulus at elevated temperatures, as shown below. The predictions of Equation 4.1 are compared with available research results of S460 in literature, see Fig.4.14. The comparison shows that good agreement between Equation 4.1 and the test results of S460N exists. It can be found that using Equation 4.1 to predict the elastic modulus reduction factors for S460M at elevated temperatures is very conservative but safe. So Equation 4.1 is a conservative estimation of S460M.

$$20 \leq \theta \leq 100, \ \frac{E_\theta}{E_{20}} = 1.003 \text{-} 1.625 \times 10^{-4} \theta \tag{4.1a}$$

$$100 < \theta \leq 900, \ \frac{E_\theta}{E_{20}} = 2.961 \times 10^{-9} \theta^3 - 4.317 \times 10^{-6} \theta^2 + 3.867 \times 10^{-4} \theta + 0.986 \tag{4.1b}$$
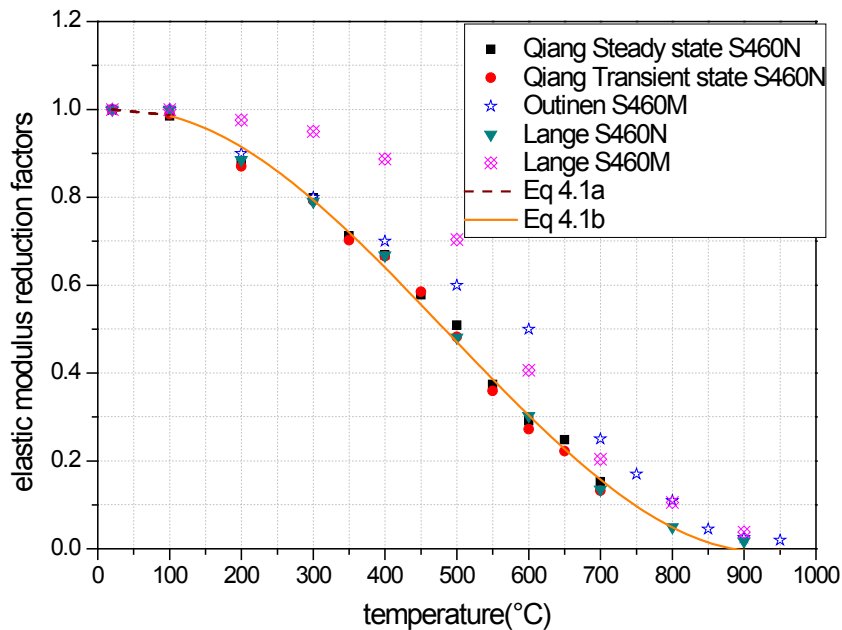
Fig.4.14. Validation of predicted elastic modulus reduction factors for S460.

4.2.3.2 Yield strength

$$20 \leq \theta \leq 350, \quad \frac{f_{y\theta}}{f_{y20}} = 1.001 - 1 \times 10^{-4} \theta \tag{4.2a}$$

$$350 < \theta \leq 900, \quad \frac{f_{y\theta}}{f_{y20}} = -1.672 \times 10^{-11} \theta^4 + 5.135 \times 10^{-8} \theta^3 - 5.41 \times 10^{-5} \theta^2 + 2.138 \times 10^{-2} \theta - 1.835$$

$$\tag{4.2b}$$

Equation 4.2 is developed based on the available results on elevated-temperature yield strengths for S460N in literature [4-6] and this experimental study. In Fig.4.15, the predictions of Equation 4.2 for yield strength reduction factors are compared with available researches on HSS S460, including S460N and S460M. It can be seen that Equation 4.2 agrees well with the available research results for S460N. Except the yield strength in the range of 200-400°C from Outinen's research, Equation 4.2 can be conservatively used to predict the yield strength of S460M at elevated temperatures as well. The exceptions are attributed to the abnormal results in the temperature range of 200-400°C given by Outinen [19], because S460M should behave better than S460N at elevated temperatures on yield strength.
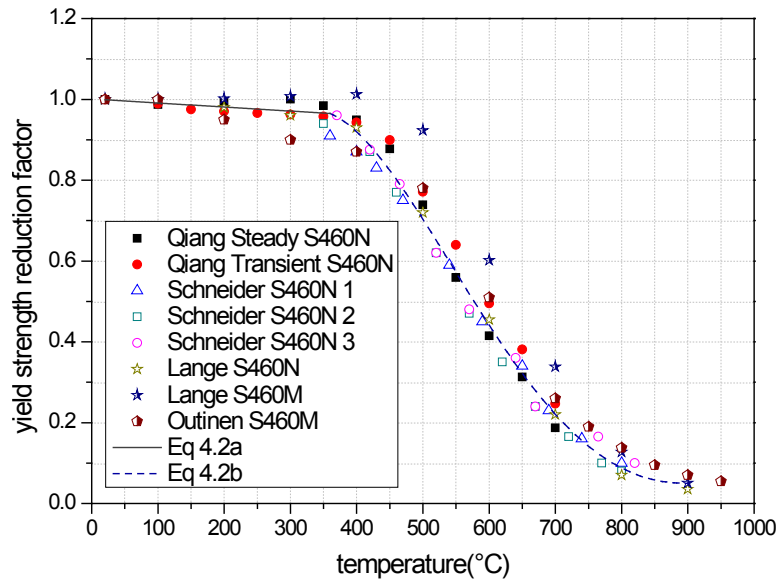
Fig.4.15. Validation of predicted yield strength reduction factors for S460.

4.2.3.3 Ultimate strength

$$20 \leq \theta \leq 350, \quad \frac{f_{u\theta}}{f_{u20}} = 1 - 1.855 \times 10^{-5} \theta \tag{4.3a}$$

$$350 < \theta \leq 700, \quad \frac{f_{u\theta}}{f_{u20}} = -7.097 \times 10^{-11} \theta^4 + 1.73 \times 10^{-7} \theta^3 - 1.526 \times 10^{-4} \theta^2 + 5.52 \times 10^{-2} \theta - 5.985$$

$$\tag{4.3b}$$

Based on this experimental study, Equation 4.3 is obtained to predict the reduction factors of ultimate strength for S460N at elevated temperatures. Fig.4.16 shows that there is good agreement between the predictions of Equation 4.3 and the test results.
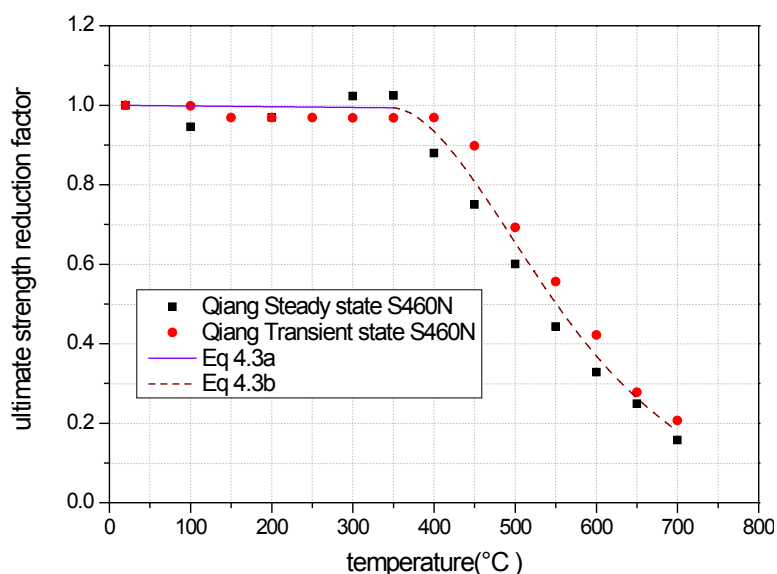
Fig.4.16. Validation of predicted ultimate strength reduction factors for S460 with test results.

4.3 MECHANICAL PROPERTIES OF S690 IN FIRE[*2]

4.3.1 Experimental Study

4.3.1.1 Test device

The test device used for tensile tests on HSS S690 in fire is the same with that used for HSS S460, as introduced in Section 4.2.1.1.

4.3.1.2 Test material and specimen

All test specimens were cut from an S690QL steel sheet ordered for this study with a nominal thickness of 5mm. S690QL is a high strength structural steel produced in compliance with EN 10025-6 [28]. This material is heat-treated using the quenched and tempered process and has good bending and welding properties. *S690QL* is the grade designation abbreviation of this steel, where *S* means structural steel, *690* is its minimum yield strength, *Q* means quenching and tempering, and *L* means low notch toughness testing temperature. The chemical composition of the tested high strength steel S690 is shown in Table 4.6. The shapes and dimensions of the specimens were prepared in accordance with EN 10002-5 [8] and ASTM standard E21-09 [9], as same as that of S460 see Fig. 4.3.

[*2] This section has been published in one journal paper of X.Qiang et al. [27].

Table 4.6: Chemical composition of HSS S690QL material

C	Si	Mn	P	S	Cr	Cu	Mo
0.160	0.210	0.850	0.012	0.001	0.350	0.030	0.200
N	Nb	Ni	Ti	V	Al-g	B-g	Zr
0.0026	0.025	0.050	0.006	0	0.093	0.0024	0

4.3.1.3 Test method

Similar as that for HSS S460, both the steady state test method and the transient state test method were applied for HSS S690 in this experimental study.

4.3.1.4 Test procedure

In the steady state tests, the heating rate was 50°C/min. The preselected temperatures were 100°C, 200°C, 300°C, 400°C, 500°C, 550°C, 600°C and 700°C respectively. The procedure of steady state tests of S690 was as same as that of S460, see 4.2.1.4.

In transient state tests, the stress levels used herein for S690 were preselected; they were 100, 200, 250, 300, 400, 500, 600, 650, 700, 800, 850 and 900MPa. The procedure of transient state tests of S690 was as same as that of S460, see 4.2.1.4.

4.3.2 Experimental Results and Discussion

4.3.2.1 Stress-strain curves

The stress-strain curves of S690 at various fire temperatures obtained from this steady state test are plotted in Fig. 4.17. The stress-strain curves of S690 under various transient state conditions transferred from the experimentally obtained strain-temperature curves under various constant stress levels are presented in Fig.4.18.
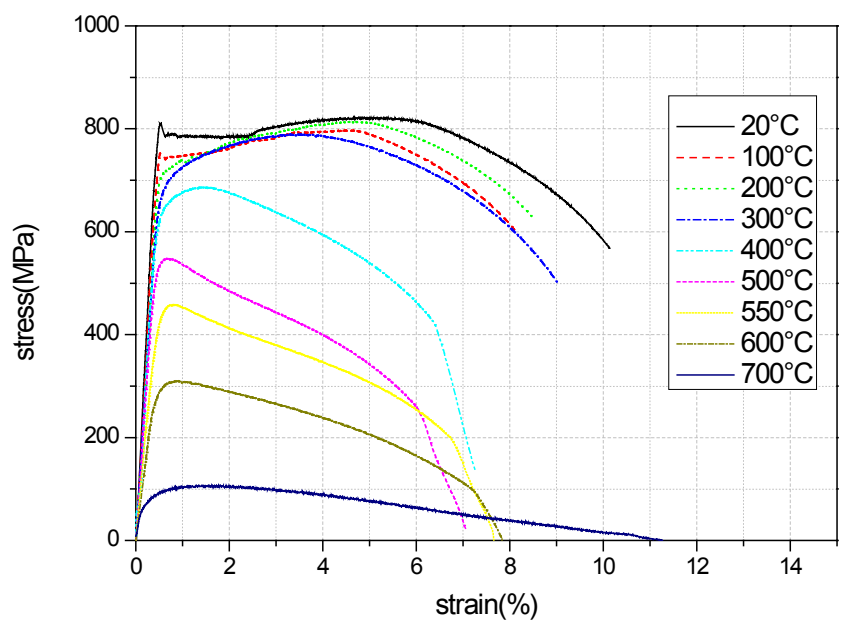
(a) full range
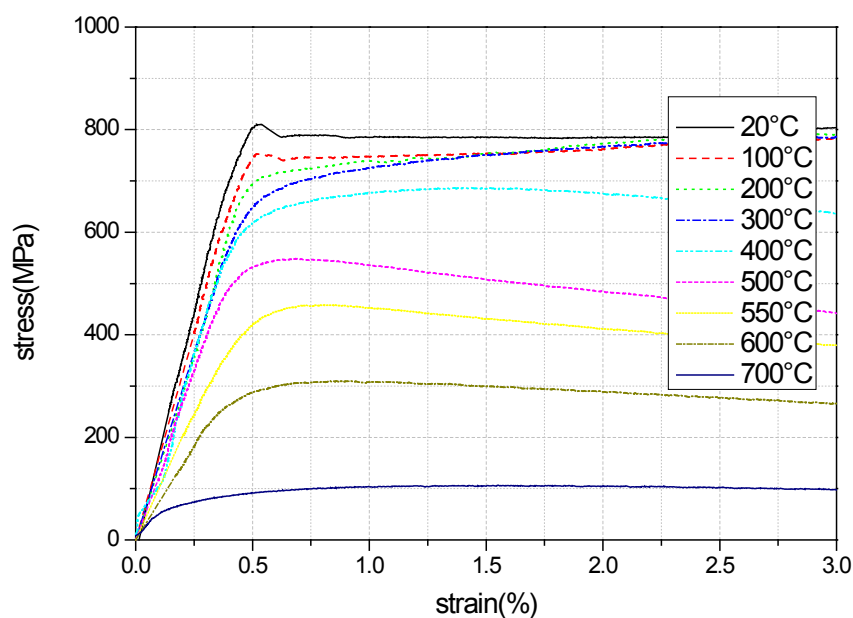
(b) within the strain range of 3%

Fig.4.17. Stress-strain curves of S690 at various temperatures under steady state.

(a) full range

(b) within the strain range of 3%
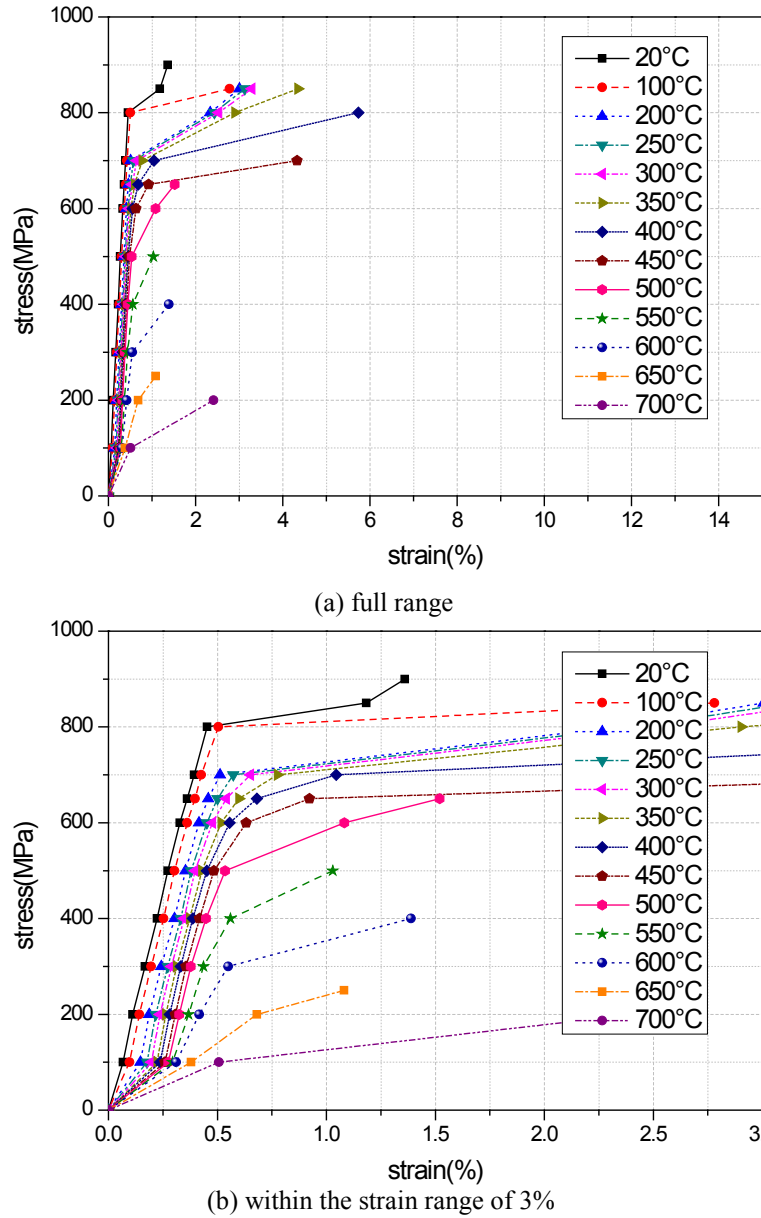
Fig.4.18. Stress-strain curves of S690 at various temperatures under transient state.

4.3.2.2 Failure mode

Typical failure mode of high strength steel S690 tensile specimens at different elevated temperatures obtained from steady state test in this investigation is shown in Fig. 4.19. It can be seen that for all specimens necking appeared before failure. No brittle failure is observed for all temperatures from 20°C up to 700°C, which is promising for fire safety of steel structures with HSS S690.
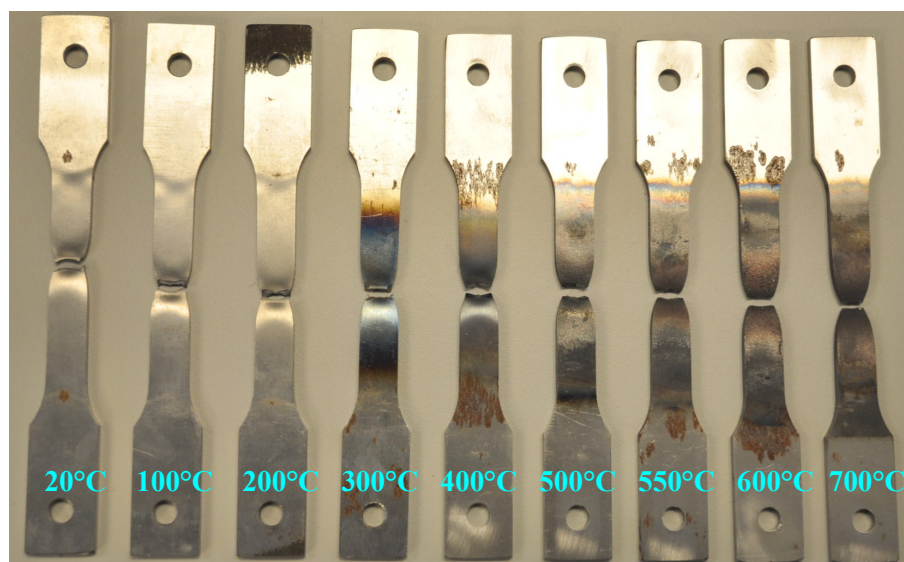
Fig.4.19. Failure mode of S690 specimens at elevated temperatures under steady state condition.
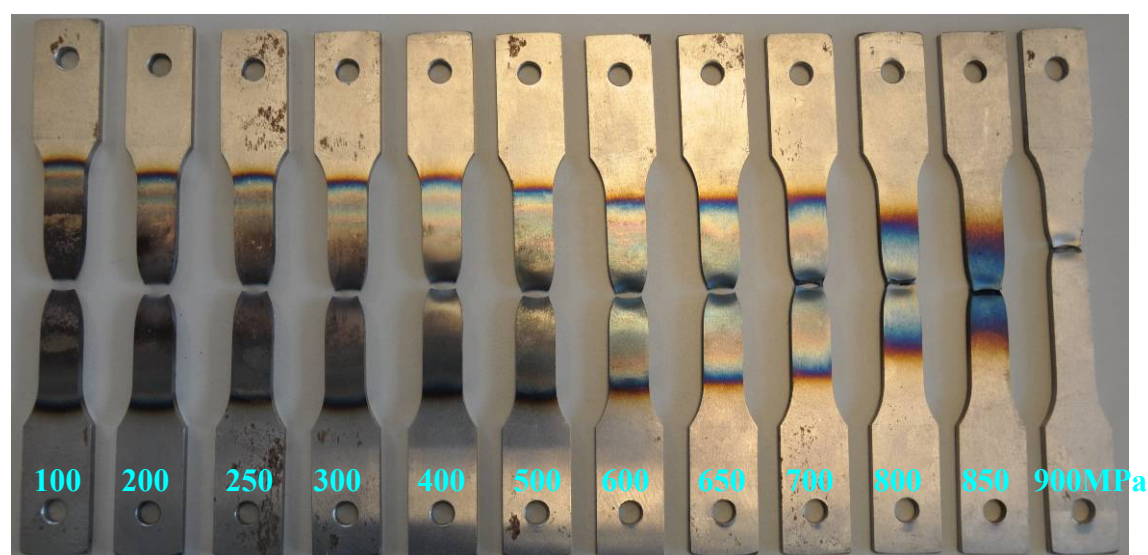
Fig.4.20. Failure mode of S690 specimens at various stress levels under transient state condition.

Typical failure mode of high strength structural steel S690 tensile specimens under transient state fire condition at various stress levels obtained from this experimental study is presented in Fig.4.20. It can be seen that for all specimens necking appeared before failure. No brittle failure can be observed for all stress levels up to 900MPa, which is very promising for fire safety of steel structures with HSS S690. The fire temperature at which the specimen fails under a constant tensile stress level is called failure temperature at this specified stress level under transient state fire condition. The failure temperatures of HSS S690 at various stress levels up to 900MPa obtained herein are presented in Table 4.7. It can be found that when S690 specimen is under very high tensile stress levels, it fails at very low fire temperature, especially when the stress level is around 900MPa. However, within its nominal yield stress level, S690 fails at the fire temperature in excess of 470°C.

Table 4.7: Failure temperatures of S690 at various stress levels under transient state fire condition

Stress level (MPa)	Failure temperature (°C)
100	775
200	702
250	685
300	623
400	602
500	562
600	520
650	507
700	470
800	399
850	368
900	83

4.3.2.3 Elastic modulus

The elastic modulus and their reduction factor at elevated temperatures of S690 obtained from steady state and transient state tests are presented in Table 4.8.

Table 4.8: Elastic modulus and reduction factors of S690 at elevated temperatures.

Steady state test			Transient state test		
Temperature (°C)	Elastic modulus (MPa)	Reduction factor	Temperature (°C)	Elastic modulus (MPa)	Reduction factor
20	204690	1.000	20	205890	1.000
100	204592	1.000	100	202267	0.982
200	179146	0.875	200	178874	0.869
-	-	-	250	176515	0.857
300	171819	0.839	300	173242	0.841
-	-	-	350	160829	0.781
400	158608	0.775	400	151457	0.736
-	-	-	450	142459	0.692
500	140127	0.685	500	133146	0.647
550	111788	0.546	550	110642	0.537
600	76105	0.372	600	76238	0.370
-	-	-	650	42027	0.204
700	28848	0.141	700	20480	0.099

The results from this experimental study are compared with some current standards (i.e. EC3, AISC and AS 4100) and the available research result of HSS BISPLATE 80 [7], as shown in Fig. 4.21. It appears that the reduction factors of the elastic modulus given in EC3 and AISC are generally conservative when used to predict the elastic modulus of HSS S690, and the prediction of AS 4100 is non-conservative for HSS S690.
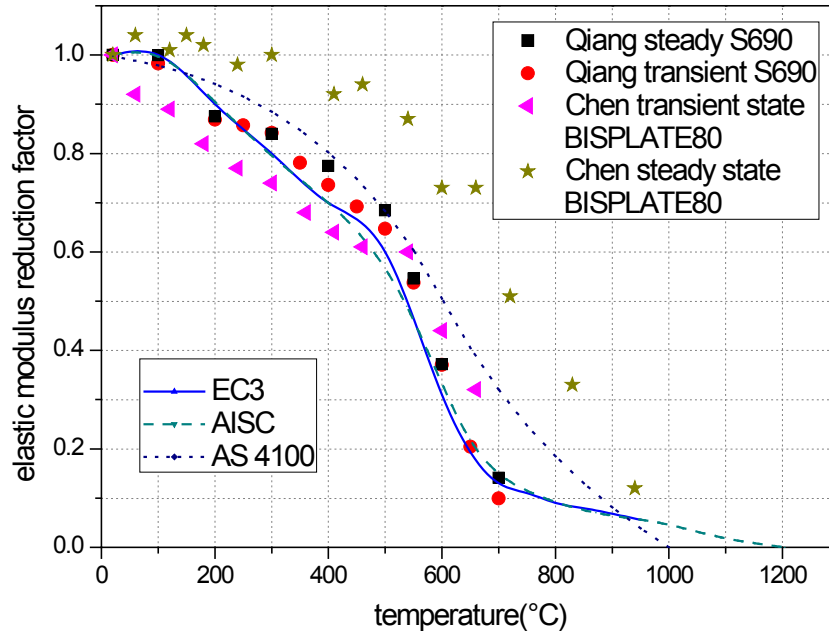
Fig. 4.21. Comparison on E-modulus of S690 at elevated temperatures.

Chen and Young conducted material tests at elevated temperatures on high strength steel BISPLATE 80 [7], the nominal yield strength of which is similar to S690Q. Their proposed reduction factors obtained from transient state tests are conservative when the temperature is below 500°C in comparison with the results of this current study for HSS S690, and their predictions overestimate the elastic modulus of HSS S690 when temperature is above 500°C. However, their steady state test results are non-conservative if used for S690, also for their own transient state test results. Therefore, it is apparent that the reduction factors of the elastic modulus obtained from HSS BISPLATE 80 are not applicable to HSS S690.

4.3.2.4 Yield strength

In current design standards, the reduction factors of yield strength recommended by EC3 are based on the strain level 2.0%, and in BS 5950 different reduction factors are given based on three strain levels 0.5%, 1.5% and 2.0%. In AISC, ASCE and AS 4100, no specification on strain level accompanies the given reduction factors for yield strength. Due to the absence of a well-defined yield point, the elevated-temperature yield strengths at strain levels 0.2%, 0.5%, 1.5% and 2.0% were used by researchers. Hence, the yield strengths of HSS S690 at above four strain levels were obtained from this experimental investigation for comparison. The definitions of yield strengths at corresponding strain levels are described in Fig. 4.9. The 0.2% yield strength ($f_{0.2}$) is the intersection point of the stress-strain curve and the proportional line offset by 0.2% strain. In addition, the stresses at 0.5%, 1.5% and 2.0% strain

levels are determined from the intersection of the stress-strain curve and a vertical line at the specified strain levels.

The yield strengths and reduction factors $\dfrac{f_{y\theta}}{f_{y20}}$ of HSS S690 at elevated temperatures from both the steady state test and transient state test are shown in Table 4.9.

Table 4.9: Yield strength reduction factors of S690 at various fire temperatures.

Steady state test					Transient state test				
Temperature (°C)	Reduction factors				Temperature (°C)	Reduction factor			
	0.2%	0.5%	1.5%	2.0%		0.2%	0.5%	1.5%	2.0%
20	1.000	1.000	1.000	1.000	20	1.000	1.000	1.000	1.000
100	0.947	0.874	0.958	0.968	100	0.985	0.989	0.910	0.923
200	0.884	0.854	0.956	0.982	200	0.863	0.878	0.836	0.868
-	-	-	-	-	250	0.858	0.875	0.831	0.861
300	0.879	0.751	0.952	0.975	300	0.837	0.872	0.826	0.855
-	-	-	-	-	350	0.803	0.839	0.813	0.839
400	0.794	0.794	0.864	0.850	400	0.797	0.812	0.786	0.798
-	-	-	-	-	450	0.758	0.763	0.730	0.738
500	0.628	0.605	0.655	0.624	500	0.627	0.631	0.716	0.716
550	0.554	0.438	0.557	0.533	550	0.540	0.542	0.554	0.554
600	0.380	0.345	0.382	0.371	600	0.396	0.397	0.445	0.445
-	-	-	-	-	650	0.295	0.213	0.278	0.278
700	0.100	0.114	0.133	0.133	700	0.163	0.228	0.203	0.203

The reduction factors of yield strengths at different strain values obtained from the above two methods are compared with European, American, Australian and British design standards, as described in Fig. 4.22- Fig. 4.25.
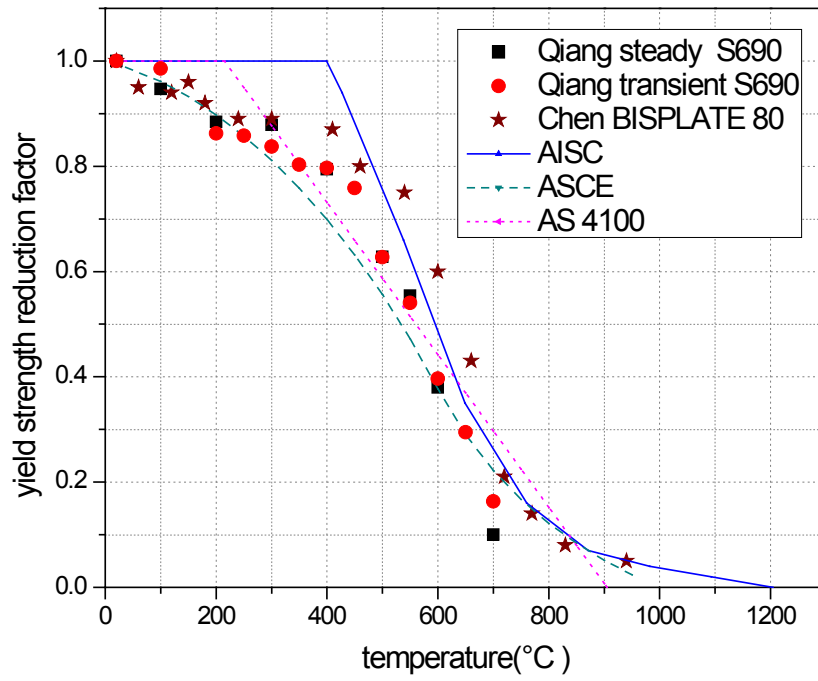
Fig.4.22. Yield strength reduction factors of S690 vs. temperatures at strain level 0.2%.
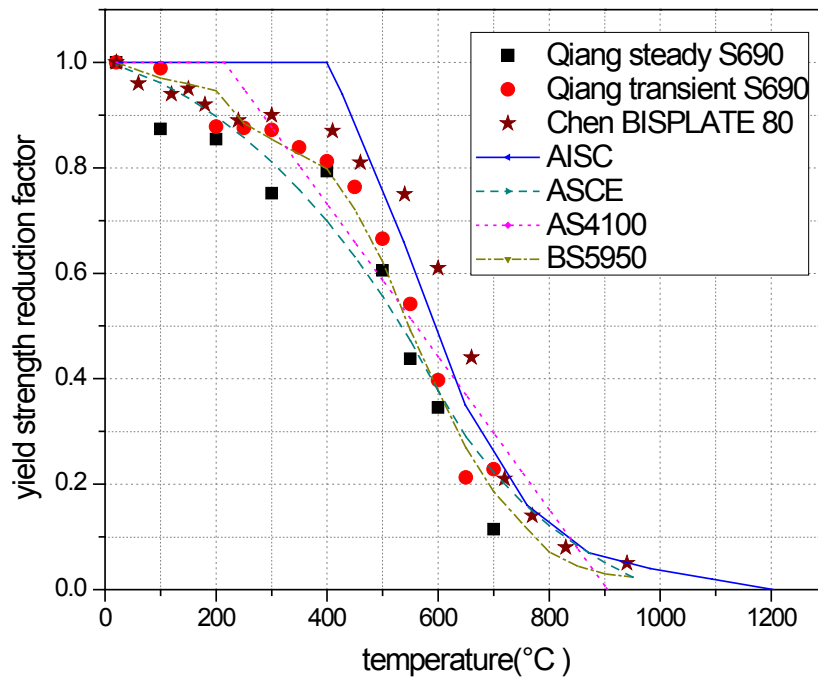
Fig.4.23. Yield strength reduction factors of S690 vs. temperatures at strain level 0.5%.
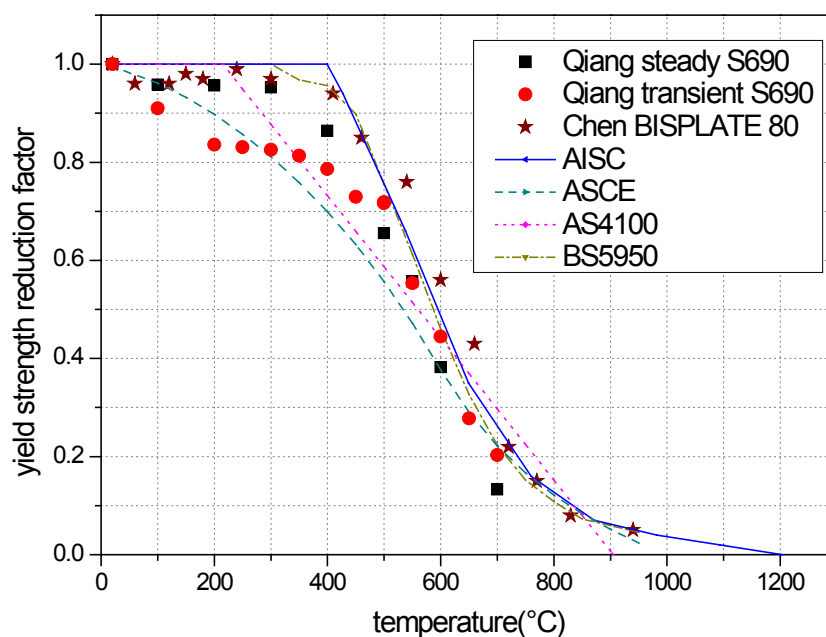
Fig.4.24. Yield strength reduction factors of S690 vs. temperatures at strain level 1.5%.
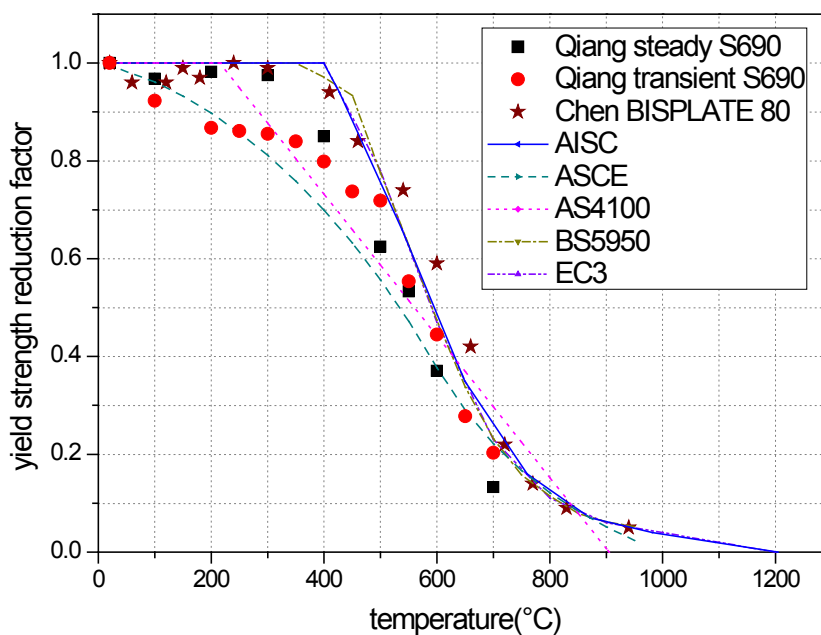
Fig.4.25. Yield strength reduction factors of S690 vs. temperatures at strain level 2.0%.

In Fig. 4.22 it can be seen that the prediction of AISC is always non-conservative for the yield strength of S690 at strain level 0.2%, while the prediction of AS 4100 is conservative from 400°C to 550°C but non-conservative for other temperatures, and similarly ASCE is conservative from 300°C to 550°C. Fig. 4.23 demonstrates that at strain level 0.5% the prediction of AISC is generally non-conservative, and the prediction of BS5950 is generally similar to the results under transient state condition but non-conservative for those under steady state condition except for temperatures from 400°C to 600°C, AS 4100 is conservative from 350°C to 500°C but non-

conservative for other temperatures. As shown in Fig. 4.24 at strain level 1.5%, the predictions of AISC and BS5950 are non-conservative, AS 4100 is conservative from 400°C to 550°C but not the case for other temperatures, while ASCE is conservative from 300°C to 550°C but not the case for other temperatures. Fig. 4.25 shows that at strain level 2.0% the prediction of EC3 is non-conservative, and the predictions of other standards are similar to the conclusion obtained at the strain level 1.5%.

At the above 4 different strain levels, the yield strength reduction factors of BISPLATE 80 obtained by Chen and Young [7] are generally non-conservative in comparison to those of S690 from this experimental investigation.

From the comparison of this investigation with current design standards and available research on HSS BISPLATE 80, it can be concluded that the reduction of yield strength at elevated temperatures depends on steel grades and manufacture methods. Thus, it is necessary to propose separate reduction factors of yield strength for different high strength steel grades.

4.3.2.5 Ultimate strength

Table 4.10: Ultimate strength and reduction factors of S690 at elevated temperatures.

Steady state			transient state		
temperature (°C)	ultimate strength (Mpa)	reduction factor	temperature (°C)	ultimate strength (Mpa)	reduction factor
20	821	1.000	20	899	1.000
100	796	0.970	100	850	0.946
200	814	0.991	200	850	0.946
-	-	-	250	850	0.946
300	789	0.961	300	850	0.946
-	-	-	350	850	0.946
400	680	0.828	400	800	0.890
-	-	-	450	700	0.779
500	548	0.668	500	650	0.723
550	458	0.558	550	501	0.558
600	310	0.377	600	399	0.444
-	-	-	650	252	0.281
700	107	0.130	700	201	0.223

The ultimate strength reduction factors were calculated based on the ratio of ultimate strength at a particular elevated temperature $f_{u\theta}$ to that at ambient temperature f_{u20}. The ultimate strengths and their reduction factors $\dfrac{f_{u\theta}}{f_{u20}}$ at

various elevated temperatures obtained under steady state and transient state are given in Table 4.10.

The ultimate strength reduction factors of HSS S690 obtained from this experimental study are compared with those of HSS BISPLATE 80 reported by Chen and Young [7], and also with the prediction of American standard AISC [9]. The comparison is presented in Fig. 4.26, from which it can be found that the prediction of AISC is not conservative for S690. Moreover, the ultimate strength reduction factors of BISPLATE 80 are generally higher than those of S690 for both transient state and steady state. It means neither the recommendation of AISC nor the reduction factor for BISPLATE 80 is safe when used to predict the ultimate strength of S690 at elevated temperatures.
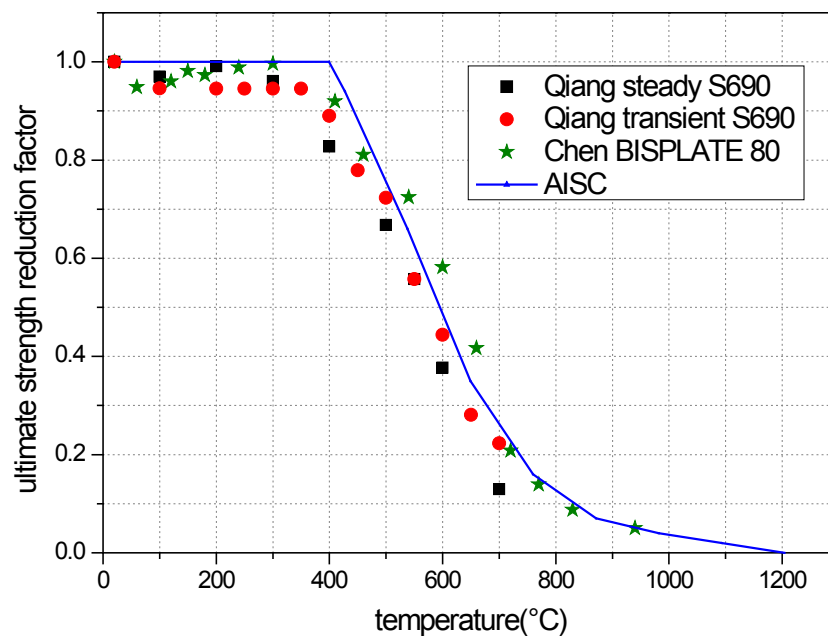
Fig.4.26. Comparison of ultimate strength reduction factors.

4.3.3 Predictive Equations

Some specified predictive equations were worked out to describe the deteriorations of mechanical properties of HSS S690 exposed to various fire temperatures, in order to offer an accurate choice for structural engineers to perform safe fire-resistance design of steel structures with S690. The deterioration of mechanical properties of mild steels exposed to fire are usually represented by the reduction factor at the corresponding fire temperature, so some unique predictive equations for calculating the reduction factors of mechanical properties of S690 were developed based on the experimental results. As fire temperature was the main cause of the deterioration of material

properties of steel, the equations were developed as a function of the elevated temperature θ, which specimens have been exposed to.

4.3.3.1 Elastic modulus

Equation 4.4 is proposed based on the experimental results to present the deterioration of the elastic modulus of S690 exposed to fire temperatures in the form of reduction factors, as shown below. The predictions of Equation 4.4 are compared with experimental results and shown in Fig. 4.27, in which the recommendations of European, American and Australian design standards are also included as reference. It shows that reasonably good agreement between Equation 4.4 and experimental results exists.

$$20 \le \theta \le 100, \ \frac{E_\theta}{E_{20}} = 1.005\text{-}2.25 \times 10^{-4}\theta \tag{4.4a}$$

$$100 < \theta \le 700, \ \frac{E_\theta}{E_{20}} = -3.66 \times 10^{-9}\theta^3 + 1.962 \times 10^{-6}\theta^2 - 9.12 \times 10^{-4}\theta + 1.031 \tag{4.4b}$$
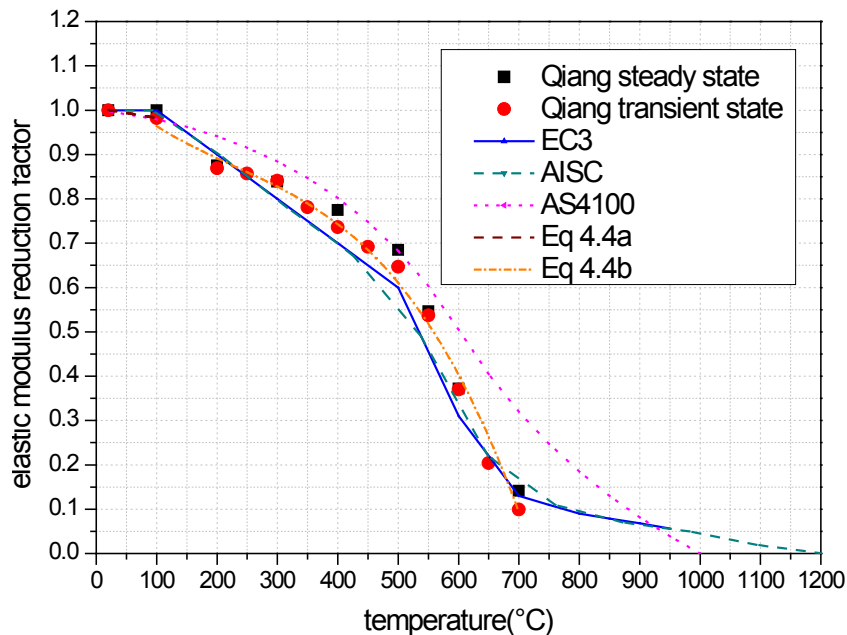
Fig.4.27. Validation of predictive equation on elastic modulus reduction factors of S690 in fire.

4.3.3.2 Yield strength

Since the deviations between yield strength reduction factors of S690 under steady state fire conditions and that under transient state fire conditions are not small, two sets of equations are developed based on the experimental results at the strain level of 2.0%, to predict the deterioration of yield strength of S690 exposed to fire. Equation 4.5 is developed to present the yield strength reduction factors of S690 under steady state fire conditions. Its predictions are compared with test results and described in Fig. 4.28, where the

76

recommendations of European, American, Australian and British design standards are also included as reference. The comparison shows that there is good agreement between Equation 4.5 and test results under steady state fire conditions.

$$20 \le \theta \le 300, \ \frac{f_{y\theta}}{f_{y20}} = 0.991 - 6.038 \times 10^{-5}\theta \tag{4.5a}$$

$$300 < \theta \le 700, \ \frac{f_{y\theta}}{f_{y20}} = 7.355 \times 10^{-9}\theta^3 - 1.31 \times 10^{-5}\theta^2 + 5.185 \times 10^{-3}\theta + 0.4 \tag{4.5b}$$
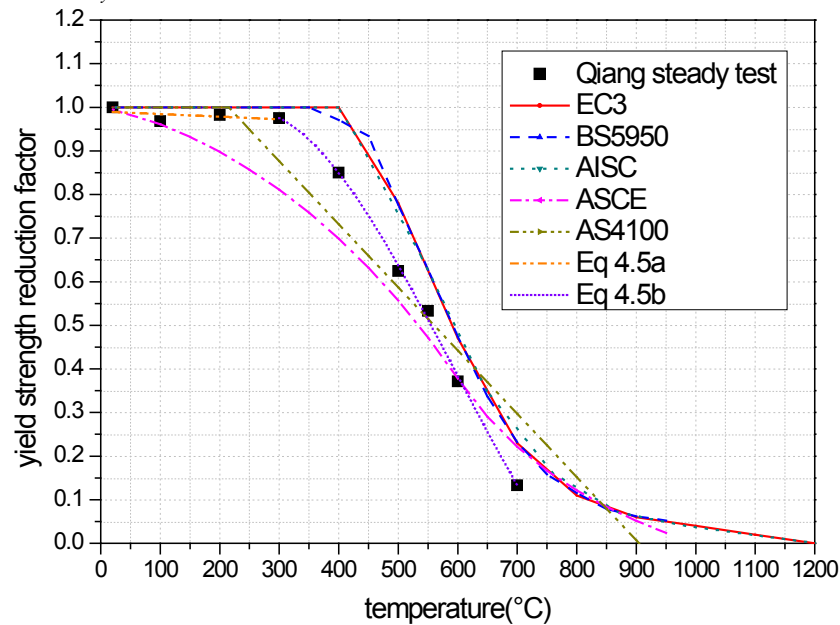
Fig.4.28. Validation of predictive equation on yield strength reduction factors of S690

under steady state fire.

Equation 4.6 is proposed to present the yield strength reduction factors of S690 under transient state fire condition. Its predictions are compared with test results and described in Fig. 4.29, where the recommendations of European, American, Australian and British design standards are also included as reference. The comparison shows that good agreement between Equation 4.6 and test results under transient state condition exists.

$$20 \le \theta \le 500, \ \frac{f_{y\theta}}{f_{y20}} = 0.996 - 5.321 \times 10^{-4}\theta \tag{4.6a}$$

$$500 < \theta \le 700, \ \frac{f_{y\theta}}{f_{y20}} = 3.504 \times 10^{-6}\theta^2 - 6.818 \times 10^{-3}\theta + 3.251 \tag{4.6b}$$
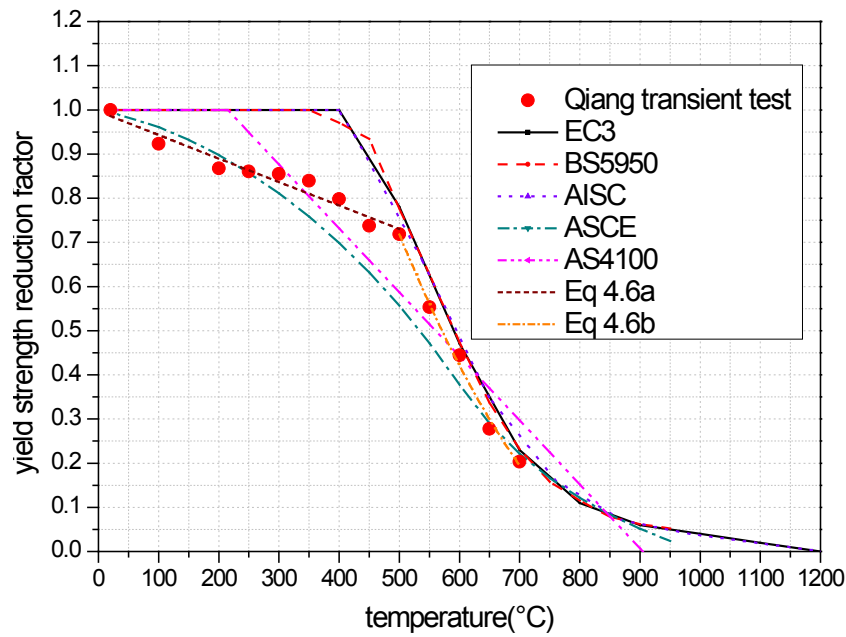
Fig.4.29. Validation of predictive equation on yield strength reduction factors of S690 under transient state fire.

4.3.3.3 Ultimate strength

Equation 4.7 is worked out to present the ultimate strength reduction factors of HSS S690 exposed to various fire temperatures up to 700°C. Its predictions are compared with test results and shown in Fig. 4.30, where the recommendations of American design standard AISC are also included as reference. The comparison shows that there is good agreement between Equation 4.7 and experimental results.

$$20 \leq \theta \leq 350, \quad \frac{f_{u\theta}}{f_{u20}} = 1.003 - 1.649 \times 10^{-4}\theta \tag{4.7a}$$

$$350 < \theta \leq 700, \quad \frac{f_{u\theta}}{f_{u20}} = -1.915 \times 10^{-6}\theta^2 - 2.442 \times 10^{-4}\theta + 1.27 \tag{4.7b}$$
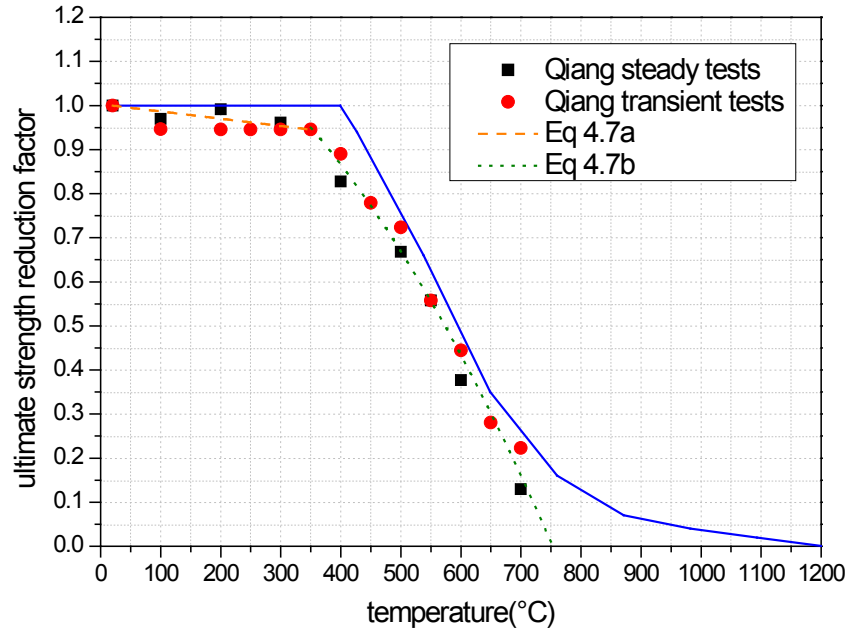
Fig.4.30. Validation of predictive equation on ultimate strength reduction factors of S690 in fire.

4.4 MECHANICAL PROPERTIES OF S960 IN FIRE

4.4.1 Experimental Study

4.4.1.1 Test device

The test device used for tensile tests on HSS S960 is the same as that for HSS S460 and S690, as shown in Section 4.2.1.1.

4.4.1.2 Test material and specimen

All test specimens were cut from a S960QL steel sheet ordered for this study with a nominal thickness of 5mm. S960QL is a very high strength structural steel produced in compliance with EN 10025-6 [28]. The material is heat-treated using the quenched and tempered process and has good bending and welding properties. *S960QL* is the grade designation abbreviation of this steel, where *S* means structural steel, *960* is its minimum yield strength, *Q* means quenching and tempering, and *L* means low notch toughness testing temperature. The chemical composition of the tested very high strength steel S960 is shown in Table 4.11. The shapes and dimensions of the specimens were prepared in accordance with EN 10002-5 [13] and ASTM standard E21-09 [14], as same as those of S460 and S690 see Fig. 4.3.

Table 4.11: Chemical composition of VHSS S960QL material (%).

C	Si	Mn	P	S	Cr	Cu	Mo
0.180	0.390	1.430	0.008	0.0009	0.580	0.020	0.450
N	Nb	Ni	Ti	V	Al-g	B-g	
0.0047	0.022	0.050	0.004	0.030	0.044	0.0001	

4.4.1.3 Test method

In this experimental study for VHSS S960, both the steady state test method and the transient state test method were performed, similar as those for HSS S460 and S690.

4.4.1.4 Test procedure

In the steady state tests, the heating rate was 50°C/min, and the preselected temperatures were 100°C, 200°C, 300°C, 400°C, 500°C, 550°C, 600°C, 650°C and 700°C respectively. The procedure of steady state tests of S960 was as same as those of S460 and S960, see 4.2.1.4.

In transient state tests, the stress levels used herein for S960 were 100, 200, 300, 400, 500, 600, 700, 750, 800, 850, 900, 950 and 1000MPa. The procedure of transient state tests of S960 was as same as those of S460 and S960, see 4.2.1.4.

4.4.2 Experimental Results and Discussion

4.4.2.1 Stress-strain curves

The stress-strain curves of S960 at various fire temperatures obtained from this steady state test are plotted in Fig. 4.31. The stress-strain curves of S960 under various transient state conditions transferred from the experimentally obtained strain-temperature curves under various constant stress levels are presented in Fig.4.32.
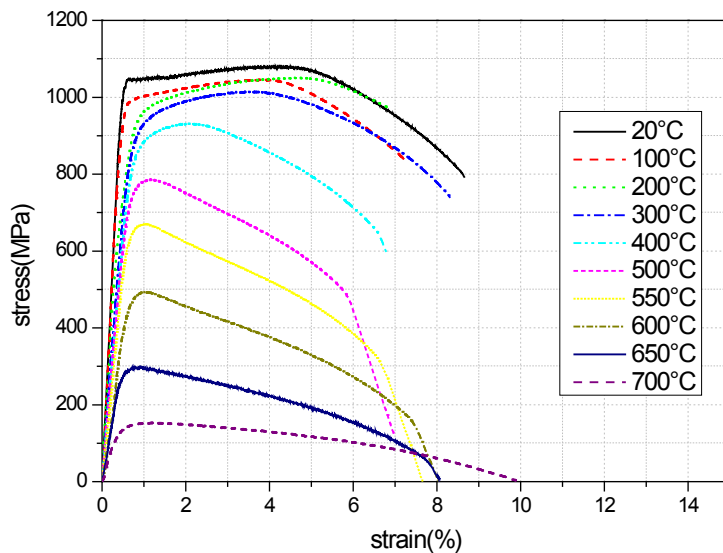
(a) full range
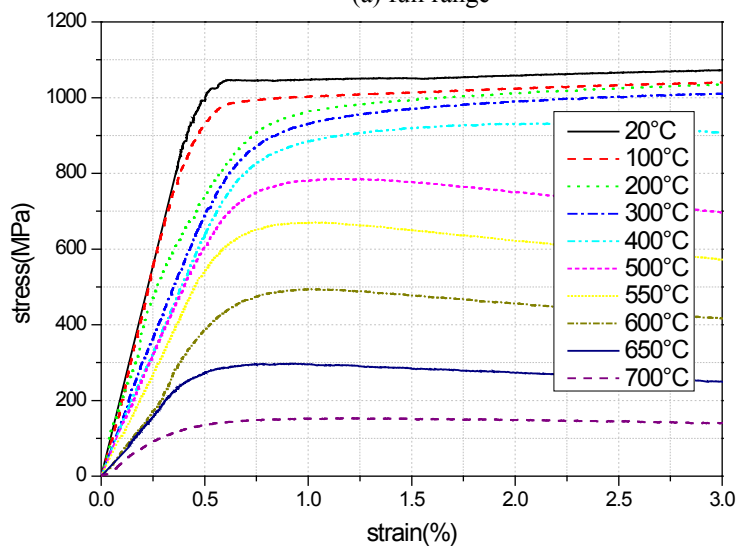
(b) within strain range of 3%

Fig.4.31. Stress-strain curves of S960 at various temperatures under steady state.
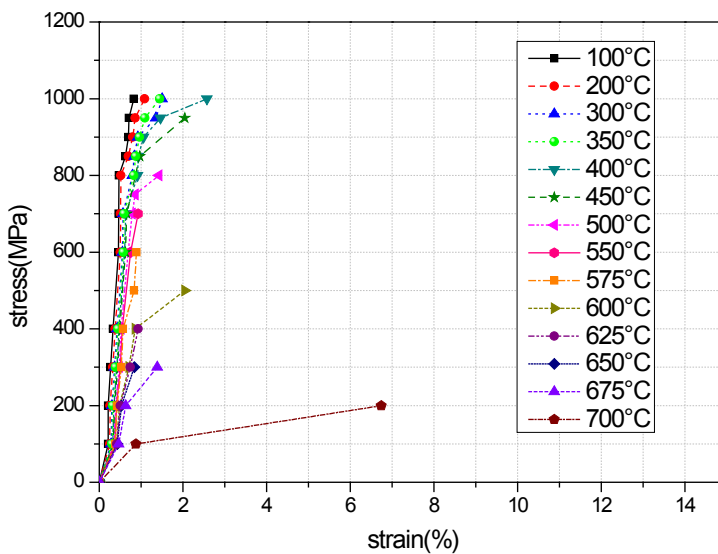
Fig.4.32. (a) full range
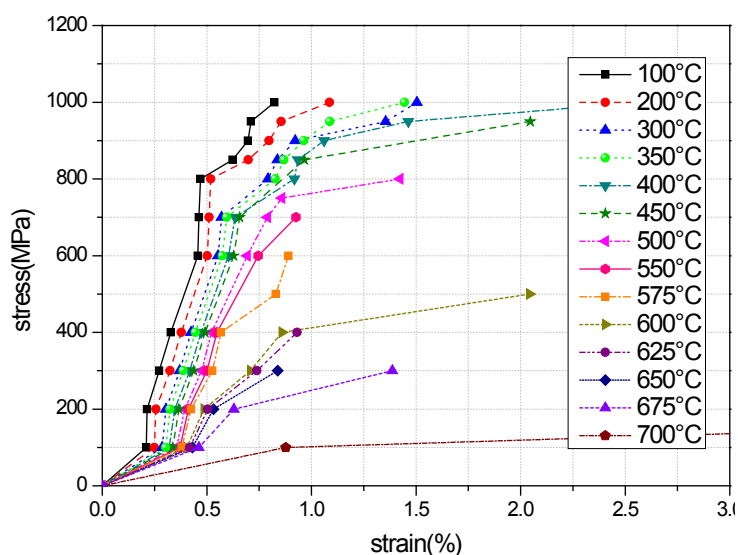
(b) within strain range of 3%

Fig.4.32. Stress-strain curves of S960 at various temperatures under transient state.

4.4.2.2 Failure mode

The typical failure mode of very high strength steel S960 tensile specimens at various elevated temperatures obtained from the steady state test in this study is shown in Fig. 4.33. It can be seen for all specimens necking appeared before failure. No brittle failure can be observed for all temperatures from 20°C up to 700°C, which is promising for fire safety of steel structures with VHSS S960.

Fig.4.33. Failure mode of S960 specimens at elevated temperatures under steady state condition.

The typical failure mode of very high strength structural steel S960 tensile specimens under transient state fire conditions at various stress levels obtained from this experimental study is presented in Fig.4.34. It can be seen that for all specimens necking appeared before failure. No brittle failure can be observed

for any stress levels up to 1000MPa, which is very promising for fire safety of steel structures with VHSS S960. The fire temperature at which the specimen fails under a constant tensile stress level is called failure temperature at this specified stress level under transient state fire condition. The failure temperatures of S960 at various stress levels up to 1000MPa obtained in this study are presented in Table 4.12. It can be found that within its nominal yield stress level under transient state, S960 fails at fire temperatures in excess of 400°C.
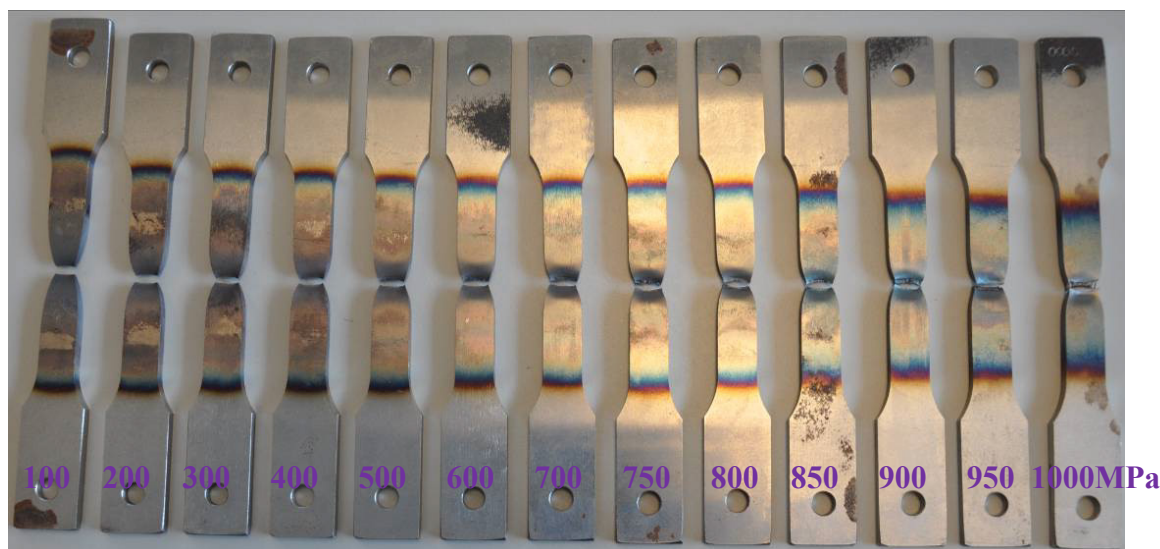
Fig.4.34. Failure modes of S960 specimens at various stress levels under transient state condition.

Table 4.12: Failure temperatures of S960 at various stress levels under transient state fire condition

Stress level (MPa)	Failure temperature (°C)
100	800
200	700
300	690
400	665
500	613
600	602
700	594
750	584
800	580
850	545
900	540
950	430
1000	402

4.4.2.3 Elastic modulus

The elastic modulus and its reduction factor at elevated temperatures of S960 obtained from the steady state and transient state tests are shown in Table 4.13.

Table 4.13: Elastic modulus and reduction factors of S960 at elevated temperatures.

Steady state test			Transient state test		
Temperature (°C)	Elastic modulus (MPa)	Reduction factor	Temperature (°C)	Elastic modulus (MPa)	Reduction factor
20	213586	1.000	20	213586	1.000
100	211141	0.989	100	213764	1.001
200	185292	0.868	200	184325	0.863
300	172992	0.810	300	173432	0.812
-	-	-	350	161055	0.754
400	154812	0.725	400	150819	0.706
-	-	-	450	149254	0.699
500	115089	0.539	500	126152	0.591
550	106959	0.501	550	108696	0.509
600	70059	0.328	600	62893	0.294
-	-	-	625	59121	0.277
650	51096	0.239	650	48900	0.229
700	36084	0.169	700	21601	0.101

The results from this experimental study are compared with some current leading design standards for steel structures (i.e. EC3, AISC and AS 4100), as shown in Fig. 4.35. It appears that the reduction factors of the elastic modulus given in EC3 and AISC are generally conservative when used to predict the elastic modulus of VHSS S960; the prediction of AS 4100 is non-conservative for VHSS S960.
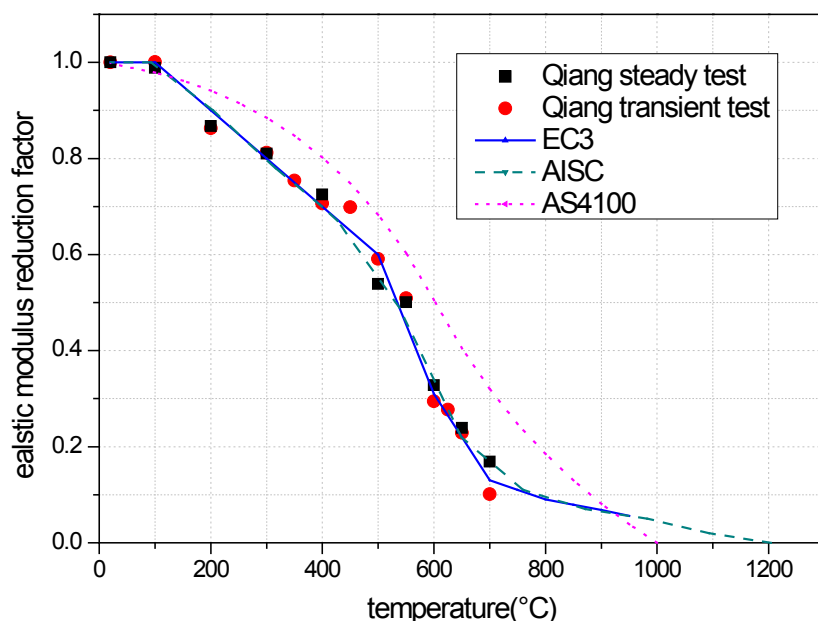
Fig. 4.35. Comparison on E-modulus of S960 at elevated temperatures.

4.4.2.4 Yield strength

In current design standards for steel structures, the reduction factors of yield strength recommended by EC3 are based on the strain level 2.0%, and in BS 5950 different reduction factors are given based on three strain levels 0.5%, 1.5% and 2.0%. In AISC, ASCE and AS 4100, no specification on strain level accompanies the given reduction factors for yield strength. Due to the absence of a well-defined yield point, the elevated-temperature yield strengths at strain levels 0.2%, 0.5%, 1.5% and 2.0% were used by researchers. Hence, the yield strengths of VHSS S960 at above four strain levels were obtained from this experimental study for comparison. The definitions of yield strengths at corresponding strain levels are described in Fig. 4.9. The 0.2% yield strength ($f_{0.2}$) is the intersection point of the stress-strain curve and the proportional line offset by 0.2% strain. In addition, the stresses at 0.5%, 1.5% and 2.0% strain levels are determined from the intersection of the stress-strain curve and a vertical line at the specified strain levels.

The yield strength reduction factors $\dfrac{f_{y\theta}}{f_{y20}}$ of VHSS S960 at elevated temperatures from both the steady state test and the transient state test are shown in Table 4.14.

Table 4.14: Yield strength reduction factors of VHSS S960 at various fire temperatures.

Steady state test					Transient state test				
Temperature (°C)	Reduction factors				Temperature (°C)	Reduction factor			
	0.2%	0.5%	1.5%	2.0%		0.2%	0.5%	1.5%	2.0%
20	1.000	1.000	1.000	1.000	20	1.000	1.000	1.000	1.000
100	0.947	0.899	0.964	0.968	100	0.953	0.807	0.951	0.945
200	0.904	0.714	0.945	0.956	200	0.925	0.800	0.951	0.945
300	0.859	0.673	0.923	0.936	300	0.863	0.732	0.949	0.943
-	-	-	-	-	350	0.857	0.715	0.946	0.940
400	0.819	0.622	0.874	0.880	400	0.813	0.701	0.913	0.928
-	-	-	-	-	450	0.806	0.697	0.874	0.909
500	0.734	0.590	0.738	0.710	500	0.740	0.605	0.763	0.788
550	0.631	0.513	0.618	0.589	550	0.679	0.576	0.718	0.721
600	0.472	0.364	0.454	0.431	600	0.462	0.251	0.513	0.569
650	0.280	0.259	0.271	0.259	650	0.345	0.263	0.391	0.401
700	0.138	0.130	0.144	0.141	700	0.102	0.192	0.206	0.210

The yield strength reduction factors of S960 at different strain values obtained from the above two methods are compared with European, American, Australian and British design standards, as described in Fig. 4.36- Fig. 4.39.
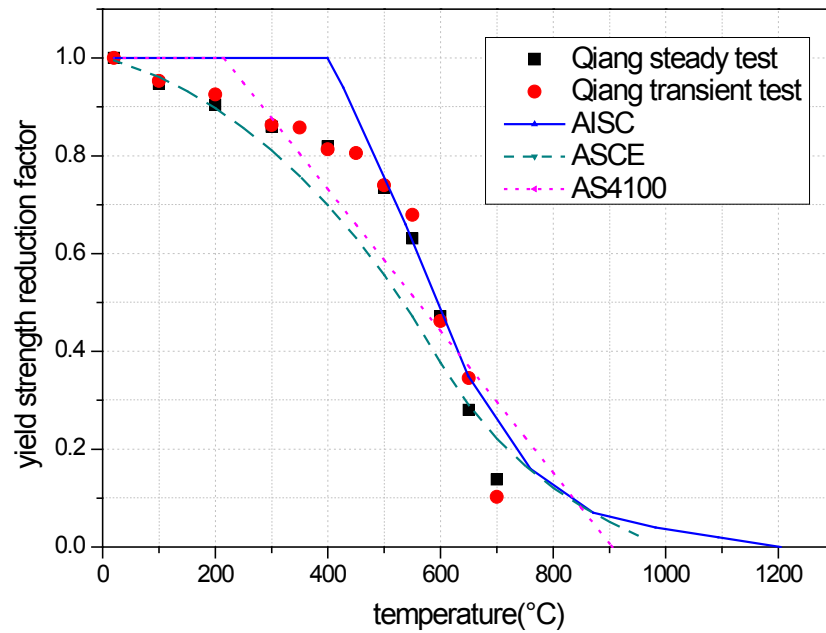
Fig.4.36. Yield strength reduction factors of S960 vs. temperatures at strain level 0.2%.
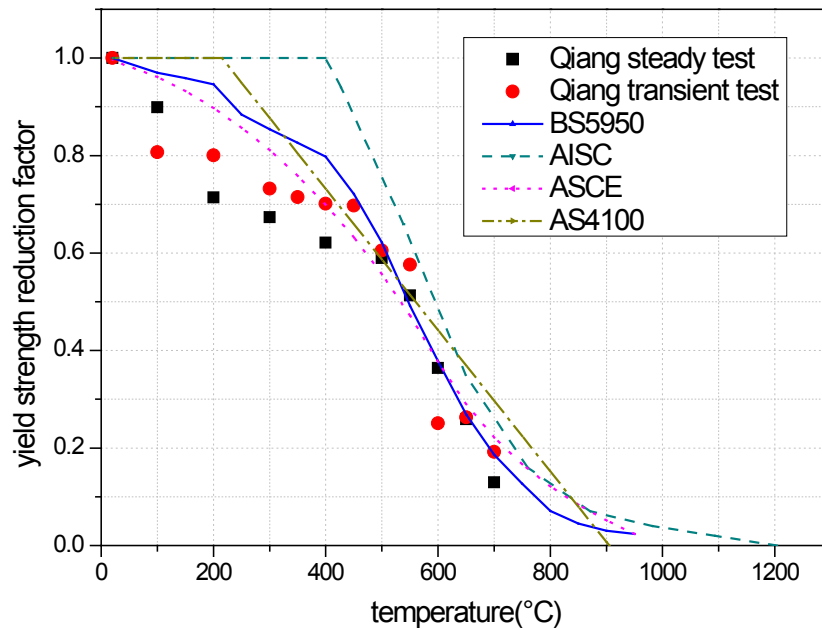
Fig.4.37. Yield strength reduction factors of S960 vs. temperatures at strain level 0.5%.
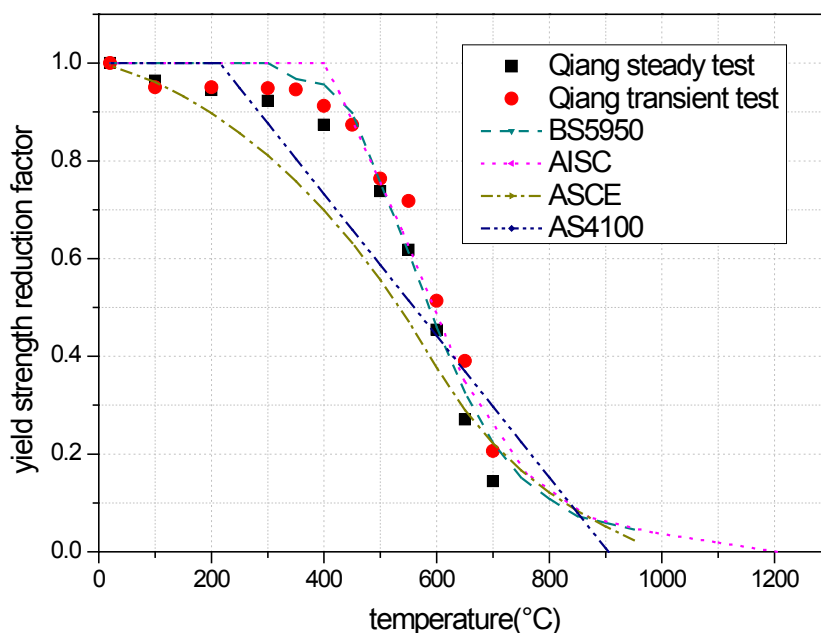
Fig.4.38. Yield strength reduction factors of S960 vs. temperatures at strain level 1.5%.
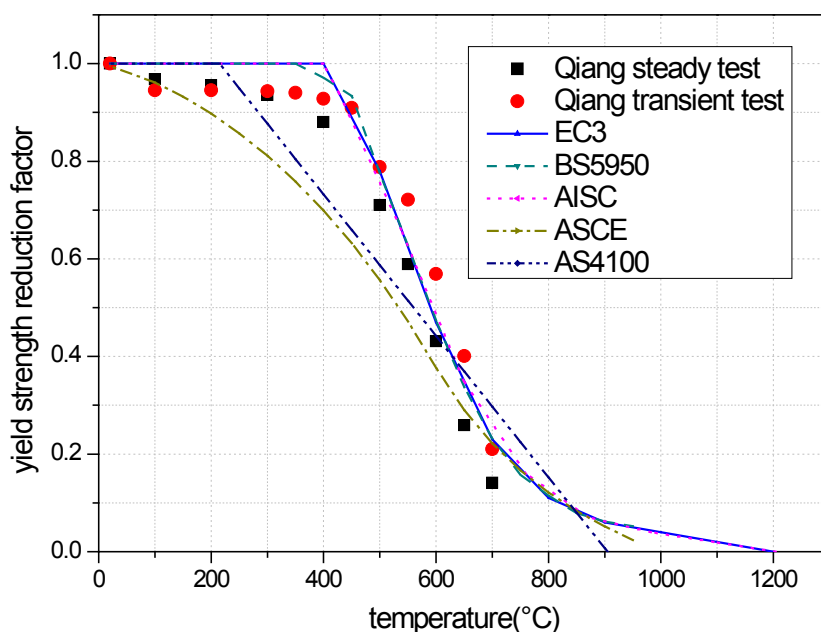
Fig.4.39. Yield strength reduction factors of S960 vs. temperatures at strain level 2.0%.

In Fig. 4.36 it can be seen that the prediction of AISC is always non-conservative for the yield strength of S960 at strain level 0.2%, while the prediction of AS 4100 is conservative from 350°C to 600°C but non-conservative for other temperatures, and similarly ASCE is conservative from 300°C to 600°C. Fig. 4.37 demonstrates that at strain level 0.5% the prediction of AISC is generally non-conservative, and the prediction of BS5950 is generally non-conservative when the temperature is below 500°C, while ASCE is generally non-conservative except at fire temperatures ranging between

450°C and 550°C; AS 4100 is conservative from 450°C to 550°C but non-conservative for other temperatures. As shown in Fig. 4.38 at strain level 1.5%, the predictions of AISC and BS5950 are non-conservative when the fire temperature is below 400°C, AS 4100 is conservative from 300°C to 600°C but not the case for other temperatures, while ASCE is generally conservative except at 700°C. Fig. 4.39 shows that at strain level 2.0% the prediction of EC3 is non-conservative when the fire temperature is below 400°C, and the predictions of other standards are similar to the conclusion obtained at strain level of 1.5%.

From the comparison of test results with current leading design standards which were mainly obtained from mild steels, it can be concluded that the reduction of yield strength at elevated temperatures depends on the steel grades. Thus, it is necessary to propose separate reduction factors of yield strength for high strength steel grades.

4.4.2.5 Ultimate strength

The ultimate strength reduction factors were calculated based on the ratio of ultimate strength at a particular elevated temperature $f_{u\theta}$ to that at ambient temperature f_{u20}. The ultimate strengths of S960 and their reduction factors $\dfrac{f_{u\theta}}{f_{u20}}$ at various elevated temperatures obtained under steady state and transient state are given in Table 4.15.

Table 4.15: Ultimate strength and reduction factors of S960 at elevated temperatures.

steady state			transient state		
temperature (°C)	ultimate strength (MPa)	reduction factor	temperature (°C)	ultimate strength (MPa)	reduction factor
20	1079	1.000	20	1079	1.000
100	1048	0.971	100	1000	0.927
200	1052	0.975	200	1000	0.927
300	1016	0.942	300	1000	0.927
-	-	-	350	1000	0.927
400	934	0.866	400	1000	0.927
-	-	-	450	950	0.880
500	786	0.728	500	800	0.741
550	670	0.621	550	700	0.649
600	494	0.458	600	500	0.463
650	296	0.274	650	300	0.278
700	153	0.142	700	200	0.185
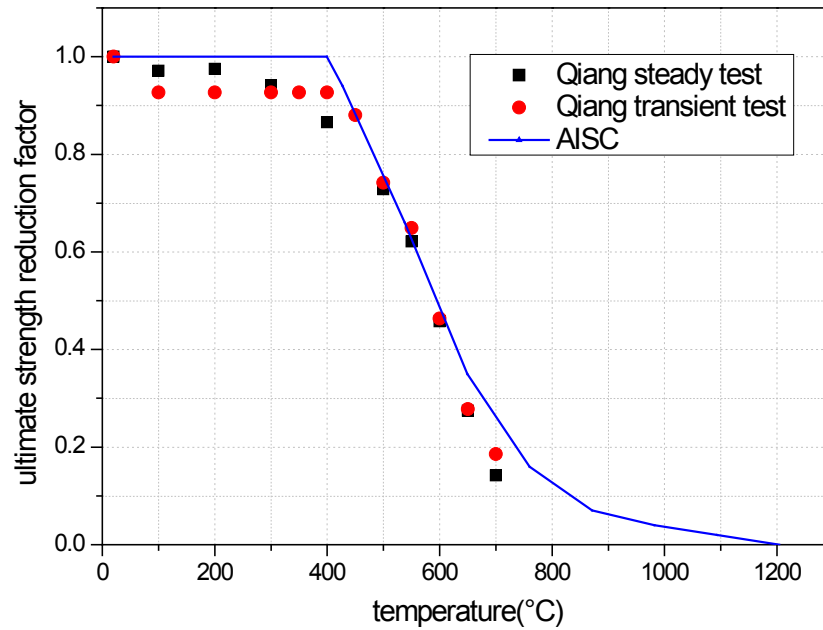
Fig.4.40. Comparison on yield strength reduction factors of S960 at elevated temperatures.

The ultimate strength reduction factors of VHSS S960 obtained from this experimental study are compared with the recommendation of American standard AISC [9]. The comparison is presented in Fig. 4.40, from which it can be found that the prediction of AISC is not conservative for S960 when the temperature is below 400°C or beyond 600°C, which means the recommendation of AISC is not always conservative when used to predict the ultimate strength of S960 exposed to fire.

4.4.3 Predictive Equations

Some specified predictive equations were developed herein based on the experimental results to describe the deteriorations of mechanical properties of VHSS S960 exposed to various fire temperatures, in order to offer an accurate choice for structural engineers to conduct safe fire-resistance design of steel structures with S960. As the elevated temperature was the main reason causing the deterioration of material properties of steel, the equations were developed as a function of the elevated temperature θ, which specimens have been exposed to.

4.4.3.1 Elastic modulus

Equation 4.8 is developed based on the experimental results to present the deterioration of the elastic modulus of S960 exposed to fire temperatures in the form of reduction factors, as shown below. The predictions of Equation 4.8 are compared with experimental results and shown in Fig. 4.41. It can be observed that good agreement between Equation 4.8 and experimental results exists.

$$20 \le \theta \le 100, \quad \frac{E_\theta}{E_{20}} = 1.003 - 1.375 \times 10^{-4}\theta \qquad (4.8a)$$

$$100 < \theta \le 700, \quad \frac{E_\theta}{E_{20}} = -1.8 \times 10^{-9}\theta^3 + 2.319 \times 10^{-7}\theta^2 - 5.845 \times 10^{-4}\theta + 1.021 \qquad (4.8b)$$
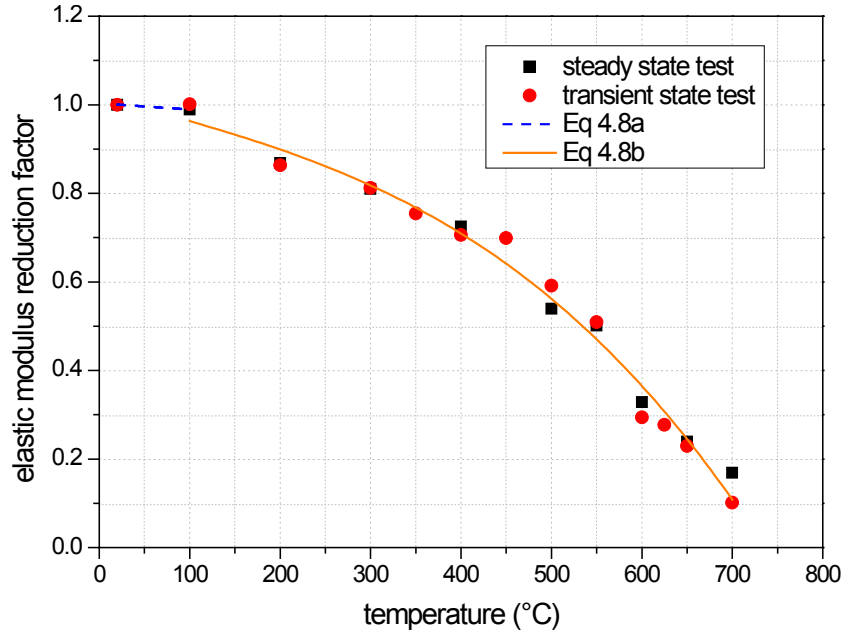
Fig.4.41. Validation of predictive equation on elastic modulus reduction factors of S960 in fire.

4.4.3.2 Yield strength

Since the deviations between yield strength reduction factors of S960 under steady state fire conditions and those under transient state fire conditions are not small, two sets of equations were developed based on the experimental results at strain level of 2.0%, to predict the deterioration of yield strength of S960 exposed to fire. Equation 4.9 is proposed to present the yield strength reduction factors of S960 under steady state fire condition, while Equation 4.10 is developed to present those of S960 under transient state fire condition. Their predictions are compared with test results and described in Fig. 4.42. The comparison shows that there is good agreement between Equation 4.9 and test results under steady state fire condition, and Equation 4.10 is in good agreement with the test results under transient state fire condition. For conservative consideration, Equation 4.9 is recommended for presenting the deterioration of the yield strength reduction factor of S960 exposed to fire.

$$20 \le \theta \le 400, \quad \frac{f_{y\theta}}{f_{y20}} = 1.006 - 2.834 \times 10^{-4}\theta \qquad (4.9a)$$

$$400 < \theta \le 700, \quad \frac{f_{y\theta}}{f_{y20}} = -3.21 \times 10^{-6} \theta^2 + 9.75 \times 10^{-4} \theta + 1.011 \tag{4.9b}$$

$$20 \le \theta \le 400, \quad \frac{f_{y\theta}}{f_{y20}} = 1.004 - 1.818 \times 10^{-4} \theta \tag{4.10a}$$

$$400 < \theta \le 700, \quad \frac{f_{y\theta}}{f_{y20}} = -6.024 \times 10^{-6} \theta^2 + 4.205 \times 10^{-3} \theta + 0.216 \tag{4.10b}$$
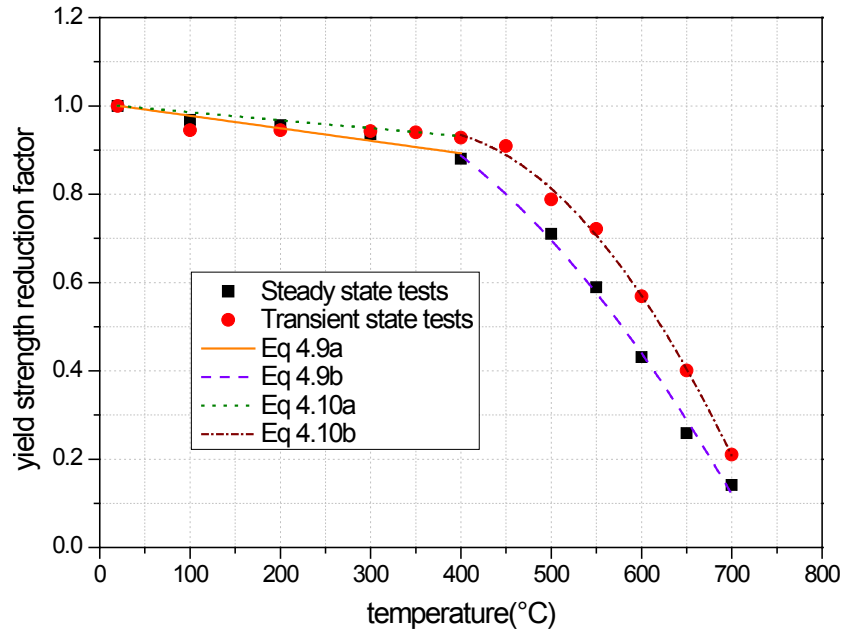
Fig.4.42. Validation of predictive equations on yield strength reduction factors of S960 in fire.

4.4.3.3 Ultimate strength
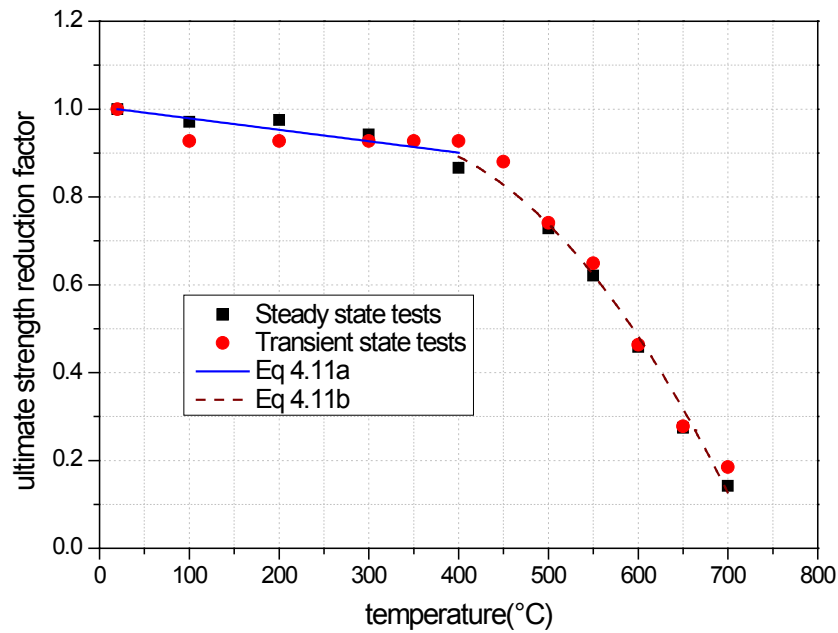
Fig.4.43. Validation of predictive equation on ultimate strength reduction factors of S960 in fire.

91

Equation 4.11 is worked out to present the ultimate strength reduction factors of VHSS S960 exposed to various fire temperatures up to 700°C. Its predictions are compared with test results and shown in Fig. 4.43. The comparison shows that there is good agreement between Equation 4.11 and experimental results.

$$20 \le \theta \le 400, \quad \frac{f_{u\theta}}{f_{u20}} = 1.005 - 2.607 \times 10^{-4} \theta \tag{4.11a}$$

$$400 < \theta \le 700, \quad \frac{f_{u\theta}}{f_{u20}} = -5.055 \times 10^{-6} \theta^2 + 3.01 \times 10^{-3} \theta + 0.497 \tag{4.11b}$$

4.5 DISCUSSION

4.5.1 Elastic Modulus Reduction Factor

The elastic modulus reduction factors of HSS S460, S690 and S960 at elevated temperatures are compared with each other and with the current leading design standards EC3, AISC and AS 4100, see Fig.4.44. It can be observed that there are some deviations among the reduction factors of the elastic modulus for these three high strength steel grades at elevated temperatures. The comparison with current leading design standards shows that AS 4100 is generally non-conservative for the aforementioned three high strength steel grades, while the recommendations of EC3 and AISC are similar to each other and generally conservative for S690 and S960 but not for S460 in the elevated temperature range between 350°C to 600°C.
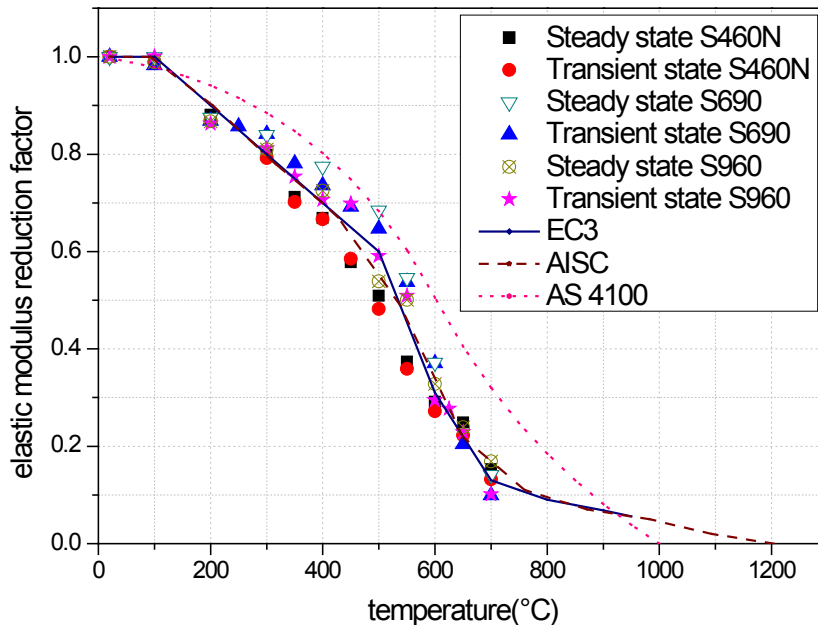
Fig.4.44. Comparison on elastic modulus reduction factors of S460, S690 and S960.

4.5.2 Yield Strength Reduction Factor

In Fig.4.45, the yield strength reduction factors at 2.0% strain level of HSS S460, S690 and S960 at elevated temperatures are compared with each other and with the current leading design standards EC3, BS5950, AISC, ASCE and AS 4100. It can be seen that some deviations exist among the reduction factors of yield strength for these three high strength steel grades at elevated temperatures. Moreover, the recommended values of EC3, BS5950 and AISC are similar to each other and generally non-conservative for these three high strength steel grades. The most conservative one in current leading design standards is ASCE, which is generally conservative for these aforementioned three high strength steels as well. Therefore, for the time being, for simple conservative evaluation the recommendation of ASCE on yield strength reduction factors in fire can be used for high strength structural steels when the elevated temperature is below 700°C, although not very accurate but safe.
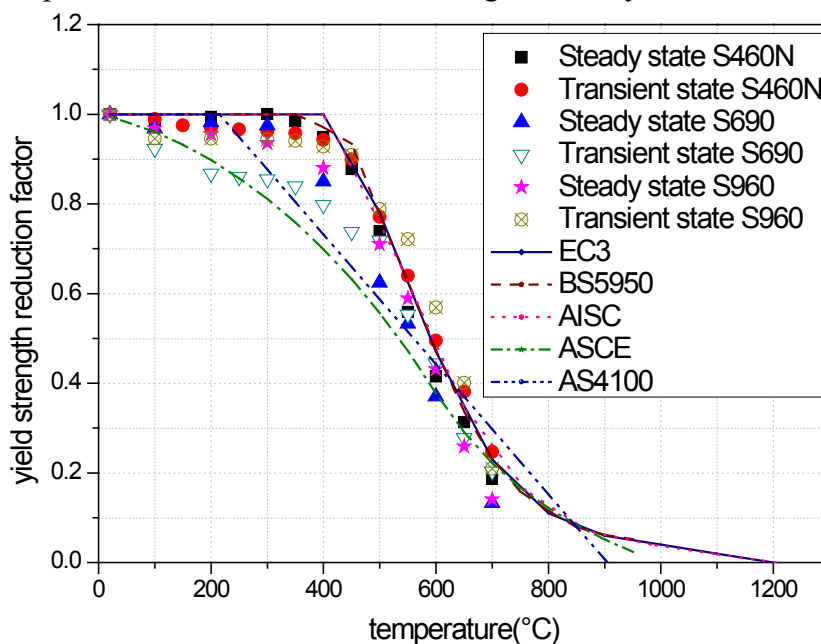
Fig.4.45. Comparison on yield strength reduction factors of S460, S690 and S960.

4.5.3 Ultimate Strength Reduction Factor

In current leading design standards, only AISC has some recommendations on ultimate strength reduction factors for structural steels in fire. Therefore the comparison of S460, S690, S960 and AISC is presented in Fig.4.46. The deviations among these three high strength steel grades can be observed. Further, the recommendation of AISC on ultimate strength reduction factors is generally non-conservative. Hence some accurate and safe recommendations

on ultimate strength reduction factors for various high strength steels should be proposed in current leading design standards for steel structures.
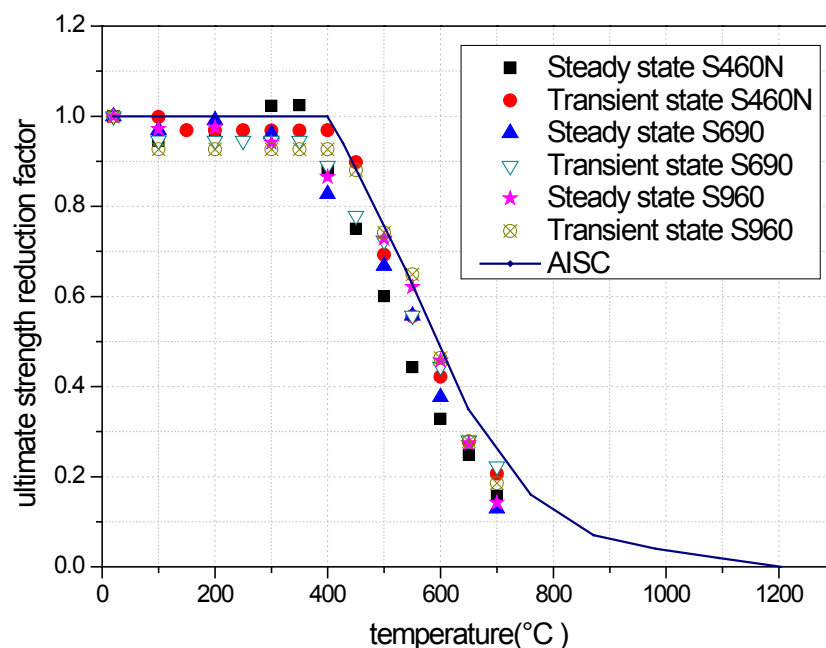
Fig.4.46. Comparison on ultimate strength reduction factors of S460, S690 and S960.

4.6 CONCLUSION

This chapter presents a detailed experimental study on the mechanical properties of high strength structural steels S460N, S690 and S960 exposed to fire. Tensile tests were conducted on the specimens at various elevated temperatures. The elevated-temperature elastic modulus, yield and ultimate strengths and typical failure mode of the aforementioned high strength steels were obtained. The comparison of HSS with mild steels shows that the deterioration of mechanical properties of structural steels at elevated temperatures is dependent on steel grades and manufacturing method. Comparison with European, American, Australian and British design standards for steel structures shows that no current design standard can be accurately used to conduct fire-resistance design of steel structures with high strength steel S460N, S690 or S960. For simple conservative evaluation, the recommendation of ASCE on yield strength reduction factors in fire can be used for high strength structural steels S460N, S690 and S960 when the elevated temperature is below 700°C. But it is not the case for other mechanical properties, neither elastic modulus nor ultimate strength. Comparison with design standards revealed the necessity of including recommendations on the deterioration of mechanical properties in fire for high strength structural steels in current leading design standards. Therefore, unique predictive equations

calculating reduction factors of mechanical properties for HSS S460N, S690 and S960 at elevated temperatures were proposed and recommended for safe practical design and analysis. Furthermore, no brittle failure mode was observed for all specimens made of HSS S460, S690 and S960 at various elevated temperatures up to 700°C, which is very promising for the fire safety of steel structures with members made of HSS. This chapter also highlights the necessity of more researches on mechanical properties at elevated temperatures for all high strength structural steel grades used in constructions, such as S890, S1100 etc.

4.7 REFERENCES

[1] CEN, Eurocode 3 - Design of steel structures - Part 1-2: General rules - Structural fire design, CEN, Brussels, 2005.

[2] CEN, Eurocode 3 - Design of steel structures - Part 1-12: Additional rules for the extension of EN 1993 up to steel grades S700, Brussels, 2004.

[3] J. Lange, N. Wohlfeil, Examination of the mechanical properties of the microalloyed grain refined steel S460 at elevated temperatures, Bautechnik, 84 (2007) 711-720.

[4] R. Schneider, J. Lange, Constitutive equations of structural steel S460 at high temperatures, in: Nordic steel construction conference 2009, Sweden, 2009, pp. 204-211.

[5] R. Schneider, J. Lange, Constitutive equations and empirical creep law of structural steel S460 at high temperatures, in: V. Kodur, J.M. Franssen (Eds.) Structures in fire 2010, DEStech Publication, Inc., East Lansing, 2010, pp. 703-710.

[6] R. Schneider, J. Lange, Material and creep behaviour of S460 in case of fire-experimental investigation and analytical modeling, in: F. Wald, K. Horova, J. Jirku (Eds.) international conference application of structural fire engineering, Cost, Prague, 2011, pp. 55-60.

[7] J. Chen, B. Young, B. Uy, Behavior of high strength structural steel at elevated temperatures. J. Struct Eng (2006) 1948-1954.

[8] ASCE, Structural fire protection, New York, 1992.

[9] AISC, Specification for structural steel buildings, American Institution of Steel Construction, Chicago, 2005.

[10] AS, AS 4100, Australian Standards: Steel structures, Sydney, Australia, 1998.

[11] B.S. Institution, BS5950, Structural use of steelwork in building, Part 8: Code of practice for fire resistant design, London, 1998.

[12] CEN, EN 1991-1-2, Eurocode 1 - Actions on structures- Part 1-2: General actions - Actions on structures exposed to fire, Brussels, 2002.

[13] CEN, EN 10025-3, Hot rolled products of structural steels - Part 3: Technical delivery conditions for normalized/normalized rolled weldable fine grain structural steels, in, Brussels, 2004.

[14] CEN, EN 10002-5, Metallic materials-Tensile testing-Part 5: Method of testing at elevated temperature, Brussels, 1992.

[15] ASTM, E21-09, Standard test methods for elevated temperature tension tests of metallic materials, West Conshohocken, United States, 2009.

[16] J.Witteveen, L. Twilt, F.S.K. Bijlaard. Theoretical and experimental analysis of steel structures at elevated temperatures. International association for bridge and structural engineering, Tokyo, September 6-11th, 1976.

[17] J. Maljaars, L. Twilt, F. Soetens, Flexural buckling of fire exposed aluminium columns, Fire Safety J, 44 (2009) 711-717.

[18] J. Outinen, Mechanical properties of structural steels at high temperatures and after cooling down, Laboratory of Steel Structures, Helsinki Univ. of Technology, Helsinki, Finland, 2007.

[19] J. Outinen, P. Makelainen, Mechanical properties of structural steel at elevated temperatures and after cooling down, Fire Mater, 28 (2004) 237-251.

[20] J. Outinen, O. Kaitila, P. Makelainen, High-temperature testing of structural steel and modelling of structures at fire temperatures, Helsinki Univ. of Technology Laboratory of Steel Structures, Helsinki, Finland, 2001.

[21] J. Outinen, J. Kesti, P. Makelainen, Fire design model for structural steel S355 based upon transient state tensile test results, J Constr Steel Res, 42 (1997) 161-169.

[22] J. Maljaars, Local buckling of slender aluminum sections exposed to fire, PhD thesis, Eindhoven University of Technology, 2008.

[23] X. Qiang, Stevin Report 6-13-1, Experimental results of high strength steel endplate connections in fire and after fire, Delft University of Technology, 2013.

[24] P. Makelainen, J. Outinen, J. Kesti, Fire design model for structural steel S420M based upon transient-state tensile test results, J Constr Steel Res, 48 (1998) 47-57.

[25] X. Qiang, F.S.K. Bijlaard, M.H. Kolstein, Deterioration of mechanical properties of high strength structural steel S460N under steady state fire condition, Materials and Design, 36(2012) 438-442.

[26] X. Qiang, F.S.K. Bijlaard, M.H. Kolstein, Deterioration of mechanical properties of high strength structural steel S460N under transient state fire condition, Materials and Design, 40(2012) 521-527.

[27] X. Qiang, F.S.K. Bijlaard, M.H. Kolstein, Dependence of mechanical properties of high strength steel S690 on elevated temperatures, Construction and Building Materials, 30 (2012) 73–79.

[28] CEN, European Standard EN 10025-6. Hot rolled products of structural steels - Part 6: Technical delivery conditions for flat products of high yield strength structural steels in the quenched and tempered condition, Brussels, 2009.

Chapter 5

Mechanical properties of high strength structural steels after fire

5.1 INTRODUCTION

As mentioned in Chapter 2, no recommendation is given for post-fire mechanical properties of high strength steels in any current design standard of steel structures all over the world. Without reliable post-fire mechanical properties of high strength structural steels, the evaluation on behaviour of HSS structures after exposure to fire is not convincing. This will lead to an uneconomical consequence, either waste of money and energy or safety-compromised. Therefore, it is significant to add accurate material properties of HSS after cooling down to some corresponding design standards, such as BS5950 [9], EC3 part 1-2 [10], EC3 part 1-2 [11] and so on.

A series of experimental studies was undertaken on three high strength steel grades S460, S690 and S960, to investigate their post-fire mechanical properties after cooling down from elevated temperatures up to 1000°C. This chapter presents the details of the experimental study, the post-fire remaining elastic modulus, yield and ultimate strengths, and stress-strain curves of HSS S460, S690 and S960. The results from this study were compared with other steel grades obtained from current literature and British design standard BS5950 [9]. Further, separate sets of predictive equations were proposed in this chapter for the deterioration of post-fire mechanical properties of S460, S690 and S960.

5.2 MECHANICAL PROPERTIES OF S460 AFTER FIRE[1]

5.2.1 Experimental Study

---

[1] This section has been published in one journal paper of X.Qiang et al. [20].

5.2.1.1 Test device

The heating of specimens was conducted in a temperature-controlled electrical furnace, as shown in Fig. 5.1. The post-fire tensile tests at room temperature were conducted using a Gleeble 3800 System, which is a fully integrated digital closed loop control thermal and mechanical testing system, as shown in Fig. 4.1. Gleeble 3800 has a digital control system, which provides all signals necessary to control mechanical test variables through the mechanical servo system. In this study, 3 pairs of thermocouples provided signals for accurate feedback control of specimen temperatures, see Fig. 4.3b. The Gleeble 3800 mechanical system is an integrated hydraulic servo system capable of exerting as much as 200kN of static force in compression or 100kN in tension. In the tensile rig of Gleeble 3800, the tension is applied by using two loading rods as shown in Fig. 4.2. The right loading rod is fixed while the left loading rod moves left to apply tension to the specimens. At the end of both loading rods, one pair of clamps and a steel bar are used to fix the specimens.

Fig.5.1. Temperature-controllable furnace.

5.2.1.2 Test material and specimen

All test specimens were cut from an S460NL steel sheet ordered for this experimental study with a nominal thickness of 5mm. S460NL is weldable normalized steel for steel constructions, with high yield strength and high toughness, produced in compliance with EN 10025-3 [12]. *S460NL* is the grade designation abbreviation of this steel, where *S* means structural steel, *460* is its minimum yield strength, *N* means normalized rolled delivery condition, and *L* means low notch toughness testing temperature. The chemical composition of the tested high strength steel S460N is shown in Table 4.1. The shapes and dimensions of the specimens were prepared in accordance with EN 10002-5 [13] and ASTM standard E21-09 [14]. As shown in Fig. 4.3, one hole was provided at each end of the specimen in order to fix it to the grips of Gleeble 3800 by using two steel bars.

5.2.1.3 Test method

The method to assess the mechanical properties of steels is to conduct tensile coupon tests under transient state or steady state. Although the transient state test method is considered more realistic in simulating a real fire to buildings, the steady state test method is more commonly used because it is easier to perform than the transient state test method as well as provides the stress-strain curves directly. In this post-fire material research the steady state test method was used, in which the specimen was heated up to a pre-specified temperature then cooled down to ambient temperature, and after that a tensile load was applied until failure at ambient temperature.

5.2.1.4 Test procedure

Firstly in the temperature-controlled electrical furnace, as shown in Fig. 5.1, the specimens were heated from ambient temperature to a pre-selected temperature under the heating rate of 10°C/min, which corresponds to normally fire-protected steel members [15]. In this study, 11 elevated temperatures were selected for investigating S460, i.e. 300°C, 400°C, 500°C, 600°C, 650°C, 700°C, 750°C, 800°C, 850°C, 900°C and 1000°C. After reaching every pre-selected elevated temperature, approximately 10mins holding time was required for the uniform temperature achieved in the whole specimen. Then the specimens were cooled to ambient temperature, after which the tensile tests were applied by the Gleeble 3800 System at ambient temperature until failure. In the tensile tests, strain-control was used and the strain rate employed herein was 0.005/min, which satisfies the requirement of ASTM Standard E 21-09 [14]. The experimental process was controlled by some predefined programming options using QuikSim Software. All the data obtained from the tests (i.e. force, stroke, strain, temperature and time) were recorded by a computer and could be monitored during testing. Three repetitive tests were conducted under each post-fire condition. For comparison, tensile tests were also conducted at ambient temperature on specimens that were not exposed to elevated temperatures.

5.2.2 Experimental Results and Discussion

5.2.2.1 Stress-strain curves

The post-fire stress-strain curves of S460 after cooling down from various fire temperatures obtained from this steady state test are plotted in Fig. 5.2.

(a) full range

(b) within strain range of 3%
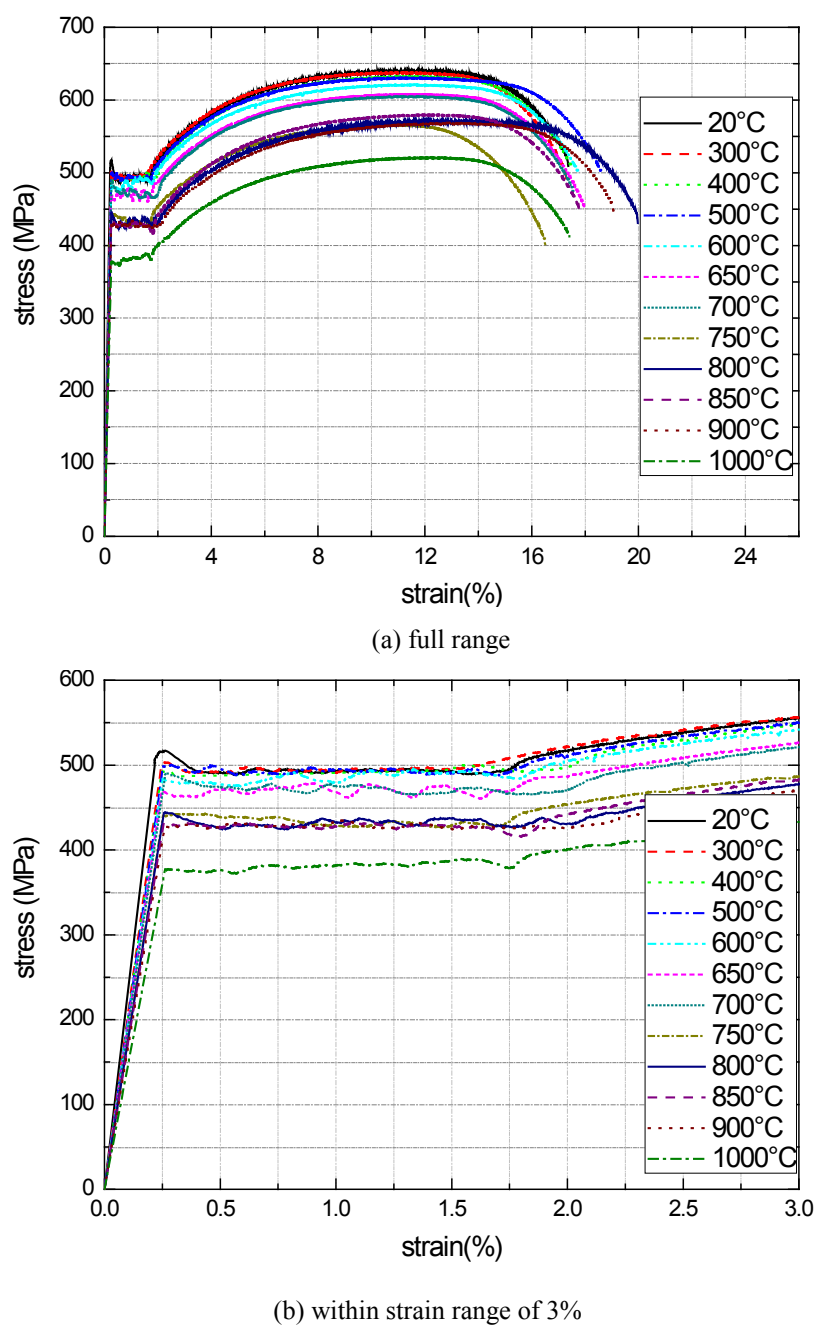
Fig.5.2. Stress-strain curves of S460N after cooling down from various fire temperatures.

5.2.2.2 Failure mode

Fig. 5.3 shows the failure mode of HSS S460 tensile specimens tested at ambient temperature after cooling down from elevated temperatures up to 1000°C. For comparison, the failure modes of HSS S460 without exposure to fire are also included. It can be seen that every specimen shows ductile failure with necking; no brittle failure is observed no matter how high temperature the specimen was exposed to. This is very promising for the safety of steel structures with HSS S460 going through a fire disaster.
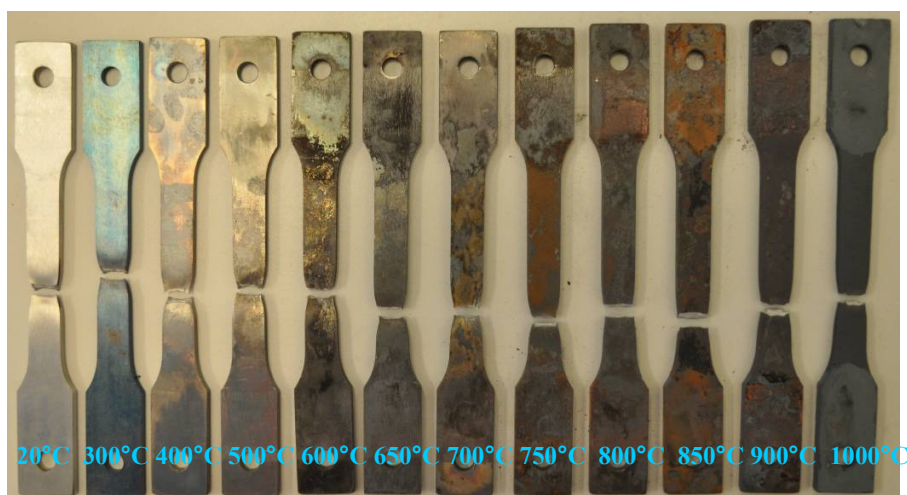
Fig.5.3. Failure modes of S460 tensile specimens after exposed to various elevated temperatures.

5.2.2.3 Elastic modulus

At elevated temperatures, the elastic modulus of steel is determined from the stress-strain curve, based on the initial slope, see Fig. 4.9. Similarly, the elastic modulus of post-fire steel is also obtained from the stress-strain curve of steel after exposure to a certain elevated temperature. The deterioration of steel properties at elevated temperatures is represented by reduction factors at the corresponding temperature, while the post-fire material properties of steel are representative by remaining factors. The elastic modulus remaining factor of steel is calculated as the ratio of the elastic modulus after cooling down from some elevated temperature ($E_{P\theta}$) to that at ambient temperature without having been exposed to fire (E_{20}). The elastic modulus and remaining factors of HSS S460 after exposure to fire obtained from this investigation are given in Table 5.1. It shows that when HSS S460 is cooled down after exposed to elevated temperatures below 600°C, it can regain its elastic modulus. But beyond 600°C, there is a considerable degradation of its elastic modulus. It is interesting to note that at least 85% of the elastic modulus is regained after cooling down from temperatures up to 800°C for HSS S460, and at least 70% for temperatures up to 1000°C.

Table 5.1: Post-fire elastic modulus and remaining factors of S460.

Temperature (°C)	E-modulus (MPa)	Remaining factor
20	202619	1.000
300	202300	0.998
400	198870	0.981
500	194910	0.962
600	191320	0.944
650	190000	0.938
700	186140	0.919
750	176184	0.870
800	173660	0.857
850	170780	0.843
900	163980	0.809
1000	144470	0.713

5.2.2.4 Yield strength

In current design standards, the reduction factors of yield strength recommended by EC3 [10] are based on the strain level of 2.0%; and in BS 5950 [9] different reduction factors are given based on three strain levels 0.5%, 1.5% and 2.0%. In AISC [16], ASCE [17] or AS 4100 [18], no specification on strain level accompanies the given reduction factors for yield strength. In this study, the yield strengths were determined using the 0.2% proof stress method as well as the 0.5%, 1.5% and 2% total strain methods.

After exposure to various elevated temperatures, the post-fire remaining yield strengths of S460 are presented in Table 5.2. The yield strength remaining factors after cooling down from elevated temperatures were calculated as the ratio of yield strength at elevated temperatures ($f_{yP\theta}$) to that at ambient temperature (f_{y20}), and the results based on different strain methods are listed in Table 5.2. It is observed that the post-fire yield strengths of S460 are almost not affected until the fire has achieved temperatures above 600°C. For HSS S460 at least 75% of its yield strength can be preserved after cooling from temperatures up to 1000°C, which is positive for the reuse of steel structures made of HSS S460 after fire. For safe consideration, a conservative suggestion is recommended to use 90% of the nominal yield strength for post-fire S460 if it has been exposed to fire temperatures below 600°C. Therefore, if steel members made of HSS S460 are exposed to fire temperatures below 600°C and their distortions remain within the tolerances for straightness and shape, they are reusable after fire.

Table 5.2: Post-fire remaining yield strengths (MPa) and remaining factor of S460.

Temperature	yield strength (MPa)				remaining factor			
(°C)	0.2%	0.5%	1.5%	2.0%	0.2%	0.5%	1.5%	2.0%
20	490	495	490	524	1.000	1.000	1.000	1.000
300	490	496	495	521	1.000	1.002	1.010	0.995
400	489	489	495	498	0.997	0.988	1.011	0.951
500	494	496	490	509	1.007	1.002	1.000	0.972
600	480	478	492	506	0.980	0.966	1.005	0.965
650	466	472	474	473	0.950	0.954	0.968	0.903
700	474	474	471	472	0.968	0.959	0.960	0.901
750	442	439	430	455	0.901	0.887	0.876	0.868
800	428	425	437	432	0.874	0.858	0.891	0.824
850	427	427	428	441	0.871	0.863	0.873	0.843
900	427	424	425	426	0.871	0.858	0.867	0.813
1000	374	375	387	400	0.763	0.758	0.790	0.764

5.2.2.5 Ultimate strength

The tensile tests were carried out until specimen failed; thus the remaining factors for ultimate strengths were calculated as the ratio of ultimate strength after cooling down from elevated temperature ($f_{uP\theta}$) to that at ambient temperature (f_{u20}). Table 5.3 presents the remaining ultimate strengths of S460 after exposure to elevated temperatures up to 1000°C. The results show that when S460 is exposed to elevated temperatures below 600°C it can regain its nominal ultimate strength after cooling down. Even when HSS S460 is exposed to temperatures as high as 1000°C, it can regain at least 80% of its ultimate strength.

Table 5.3:Post-fire ultimate strengths (MPa) and remaining factors of S460.

Temperature (°C)	Ultimate strength	Remaining factor
20	640	1.000
300	638	0.996
400	637	0.995
500	631	0.985
600	621	0.970
650	608	0.950
700	605	0.945
750	566	0.884
800	571	0.892
850	580	0.906
900	568	0.887
1000	521	0.814

5.2.2.6 Comparison with available literature

The information available concerning the remaining mechanical properties of structural steel after fire or after exposure to elevated temperatures is very limited. In British Standard 5950-8 (2003) Annex B [9], there are some recommendations for the reuse of steel after fire. It recommends that for S235

and S275 at least 90% of the mechanical strength is regained irrespective of the temperatures attained (even after heating to above 1000°C). For S355 it can be assumed that at least 75% of the strength is regained on cooling from temperatures above 600°C. For certain grades of cold finished steels it is stated that they can regain 90% of the original nominal strength. BS5950 has some suggestions on cast steel, reinforcing and pre-stressing steels as well, but no mention about the current high strength steels. For the time being, there is no other design standard for steel structures offering suggestions on the reuse of steel structures after exposure to fire. Outinen [2, 3] conducted tensile tests on S355 and S350 which were taken from steel members after testing at elevated temperatures up to 710°C. Outinen pointed out that if the distortions of a steel structure were within the tolerance limits, the strength of the material was still adequate. It is a pity that no quantitative material property data was reported on his tests.

The tests presented herein show that if S460 is exposed to fire temperatures below 600°C, it can regain its strength after cooling down. For safe considerations, a conservative use of 90% of its nominal strength is recommended for evaluating its remaining post-fire strength. When the elevated temperature is beyond 600°C, S460 can regain at least 75% of its yield strength and ultimate strength, even when cooled from temperatures up to 1000°C. So, using the recommendations of BS5950 based on mild steels to evaluate the remaining strength of HSS is dangerous. Better recommendations for evaluating the material properties of HSS after fire and the possibilities of their reuse are required. Hence, the following predictive equations were developed.

5.2.3 Predictive Equations

Several sets of predictive equations for remaining post-fire mechanical properties of S460 based on test results and available literature are proposed herein, for accurate evaluating the post-fire performance of steel structures with HSS S460. As fire temperature was the main reason causing the deterioration of material properties of steel, the equations were developed as a function of the highest fire temperature θ, which specimens have been exposed to.

5.2.3.1 Elastic modulus

A predictive equation Eq.5.1 for HSS S460 is proposed to present the deterioration of remaining elastic modulus after exposure to elevated

temperatures up to 1000°C. Fig.5.4 shows that there is a good agreement between Eq.5.1 and the test results.

$$20 \leq \theta \leq 600, \quad \frac{E_{P\theta}}{E_{20}} = 1.002 - 7.926 \times 10^{-5}\theta \tag{5.1a}$$

$$600 < \theta \leq 1000, \quad \frac{E_{P\theta}}{E_{20}} = -7.721 \times 10^{-7}\theta^2 + 6.683 \times 10^{-4}\theta + 0.823 \tag{5.1b}$$
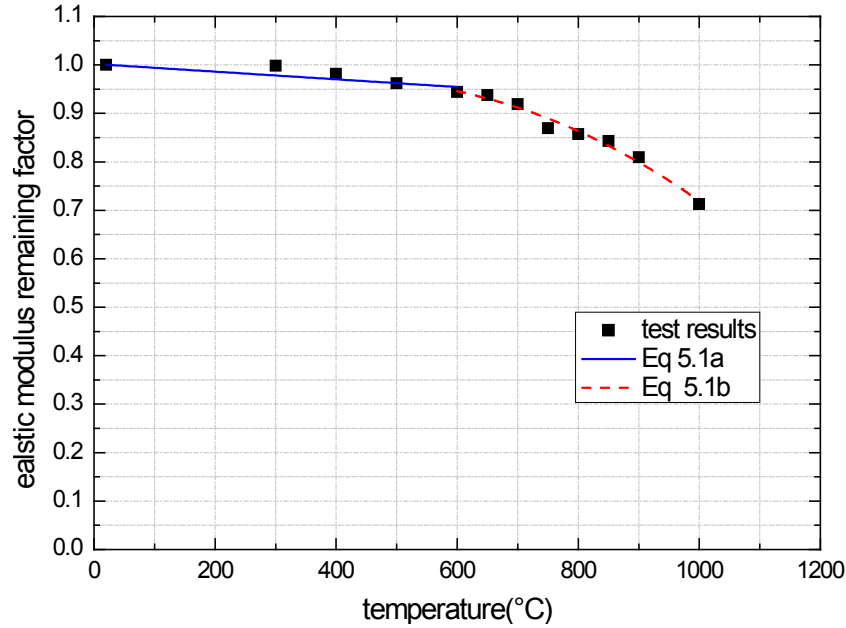
Fig.5.4. Comparison of predicted elastic modulus remaining factor from Eq.5.1 with test results.

5.2.3.2 Yield strength

Although four strain levels (0.2%, 0.5%, 1.5% and 2%) were considered in determining the yield strength, only the remaining factors based on the 0.2% proof stress method were employed herein for deriving the empirical equation, see Eq.5.2. Fig. 5.5 shows that a good agreement exists between the predictions of Eq.5.2 and test results.

$$20 \leq \theta \leq 600, \quad \frac{f_{yP\theta}}{f_{y20}} = 1.001 - 3.46 \times 10^{-5}\theta \tag{5.2a}$$

$$600 < \theta \leq 1000, \quad \frac{f_{yP\theta}}{f_{y20}} = -5.227 \times 10^{-7}\theta^2 + 3.299 \times 10^{-4}\theta + 0.967 \tag{5.2b}$$
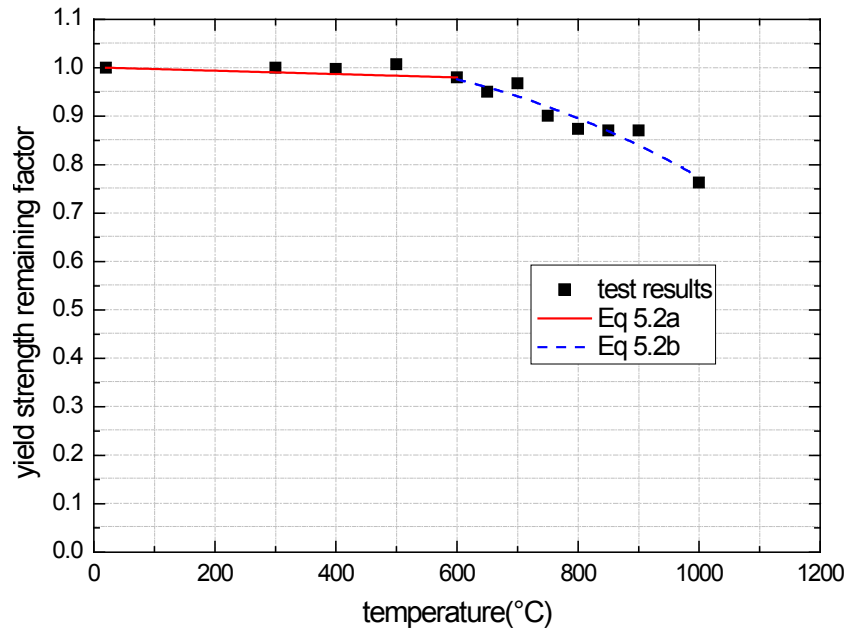
Fig.5.5. Comparison of predicted yield strength remaining factor from Eq.5.2 with test results.

5.2.3.3 Ultimate strength

The predictive equation for ultimate strength of S460 after fire is presented in Eq.5.3, and compared with test results as shown in Fig. 5.6. It can be observed that Eq.5.3 is reasonably in line with test results.

$$20 \le \theta \le 600, \quad \frac{f_{uP\theta}}{f_{u20}} = 1.001 - 5.192 \times 10^{-5} \theta \tag{5.3a}$$

$$600 < \theta \le 1000, \quad \frac{f_{uP\theta}}{f_{u20}} = -1.668 \times 10^{-7} \theta^2 - 7.514 \times 10^{-5} \theta + 1.069 \tag{5.3b}$$
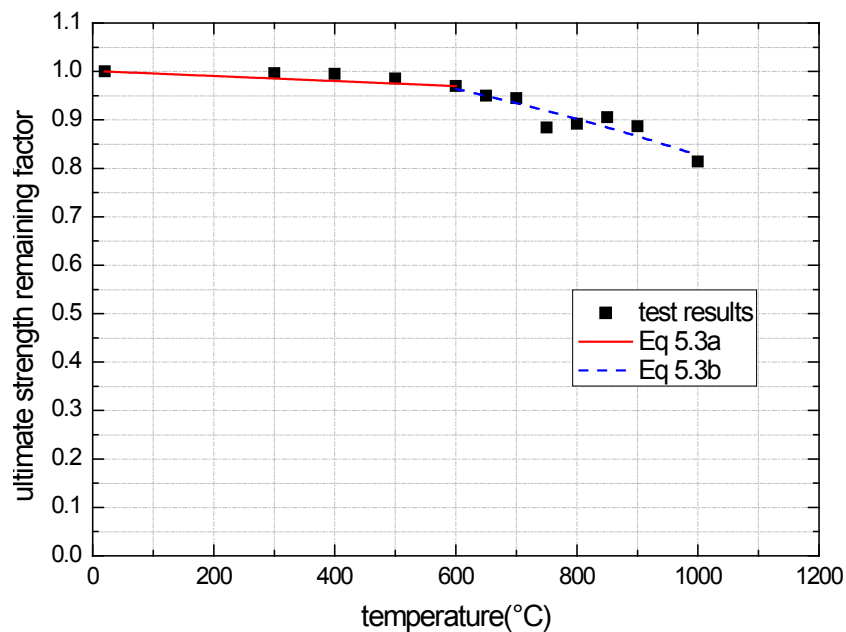
Fig.5.6. Comparison of predicted ultimate strength remaining factor from Eq.5.3 with test results.

108

5.3 MECHANICAL PROPERTIES OF S690 AFTER FIRE[*2]

5.3.1 Experimental Study

5.3.1.1 Test device

The test device used for tensile tests on S690 after fire was the same with that for HSS S460, as shown in Section 5.2.1.1.

5.3.1.2 Test material and specimen

All test specimens were cut from an S690QL steel sheet ordered for this study with a nominal thickness of 5mm. S690QL is a high strength structural steel produced in compliance with EN 10025-6 [19]. The material is heat-treated using the quenched and tempered process and has good bending and welding properties. *S690QL* is the grade designation abbreviation of this steel, where *S* means structural steel, *690* is its minimum yield strength, *Q* means quenching and tempering, and *L* means low notch toughness testing temperature. The chemical composition of the tested high strength steel S690 is shown in Table 4.6. The shapes and dimensions of the specimens were prepared in accordance with EN 10002-5 [13] and ASTM standard E21-09 [14], as same as that of S460, see Fig. 4.3.

5.3.1.3 Test method

Similar as that for S460, the steady state test method was employed for post-fire tensile tests of S690 in this experimental study.

5.3.1.4 Test procedure

The post-fire tensile test procedure for HSS S690 was the same with that for HSS S460. The heating process was conducted in the temperature-controlled electrical furnace, as shown in Fig. 5.1. The specimens were heated from ambient temperature to a pre-selected temperature under heating rate of 10°C/min, which corresponds to normally fire-protected steel members [15]. In this study, 13 elevated temperatures were selected for investigating S690, i.e. 100°C, 200°C, 300°C, 400°C, 500°C, 600°C, 650°C, 700°C, 750°C, 800°C, 850°C, 900°C and 1000°C. The test procedure for S690 is as same as that of S460, as presented in Section 5.3.1.4.

[*2] This section has been published in one journal paper of X.Qiang et al. [20].

5.3.2 Experimental Results and Discussion

5.3.2.1 Stress-strain curves

The stress-strain curves of HSS S690 after cooling down from various fire temperatures obtained from this series of tests are plotted in Fig. 5.7.

(a) full range

(b) within strain range of 3%
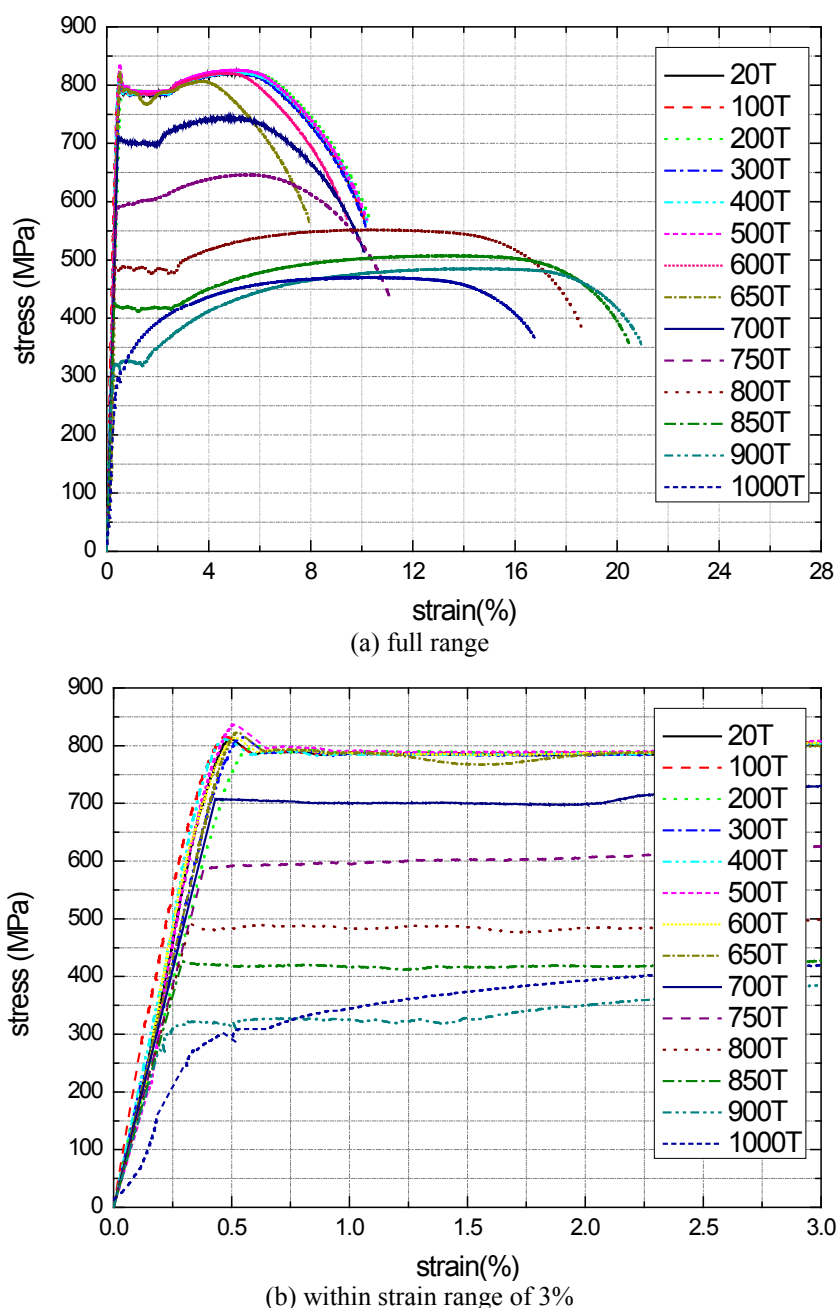
Fig.5.7. Stress-strain curves of S690 after cooling down from various fire temperatures.

5.3.2.2 Failure mode

Typical failure mode of high strength steel S690 after cooling down from various elevated temperatures obtained in this investigation is shown in Fig. 5.8. It shows that for all specimens necking appeared before failure. No brittle

failure could be observed for all temperatures from 20°C up to 1000°C, which is promising for the reuse of steel structures with HSS S690 after fire.
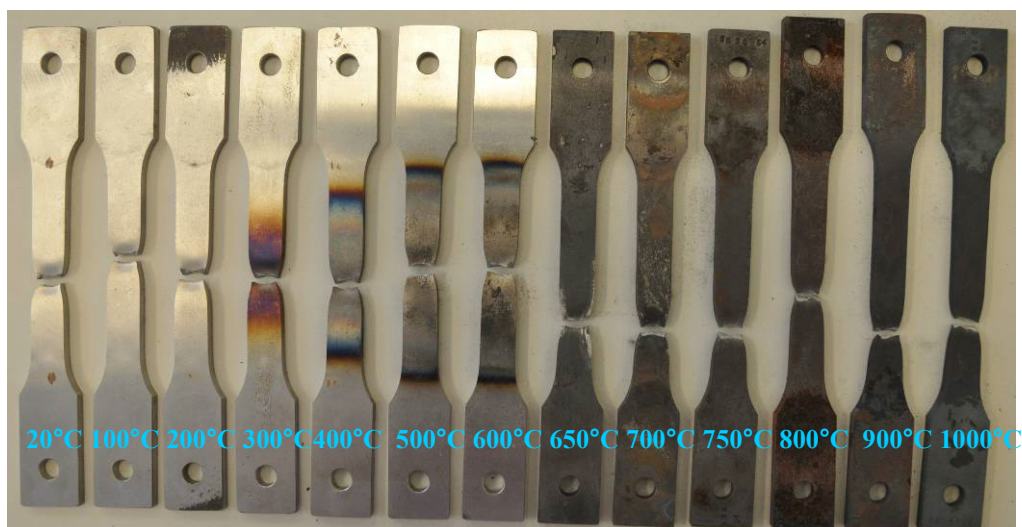
Fig.5.8. Failure mode of S690 tensile specimens after exposure to various elevated temperatures.

5.3.2.3 Elastic modulus

Table 5.4: Post-fire elastic modulus and remaining factors of S690.

Temperature (°C)	E-modulus (MPa)	Remaining factor
20	212490	1.000
100	211800	0.997
200	210808	0.992
300	210400	0.990
400	208900	0.983
500	205900	0.969
600	203500	0.958
650	195250	0.919
700	184761	0.870
750	168879	0.795
800	160010	0.753
850	149520	0.704
900	142538	0.671
1000	137063	0.645

The elastic modulus and remaining factors of HSS S690 after having been exposed to various fire conditions obtained from this investigation are listed in Table 5.4.

Fig. 5.9 presents the variation of elastic modulus remaining factors after cooling down from various elevated temperatures up to 1000°C for both S460 and S690. As seen in Fig. 5.12, when S460 and S690 are cooled down after exposure to elevated temperatures below 600°C, they can regain their elastic modulus. But beyond 600°C, there is a considerable degradation of its elastic

modulus for both S460 and S690, and it seems that S690 loses its elastic modulus more quickly. The quenched and tempered condition for manufacturing S690 is responsible for the difference of remaining elastic modulus between S460N and S690Q. It is interesting to note that at least 75% of the elastic modulus is regained after cooling from temperatures up to 800°C for both S460 and S690, and at least 60% for temperatures up to 1000°C.
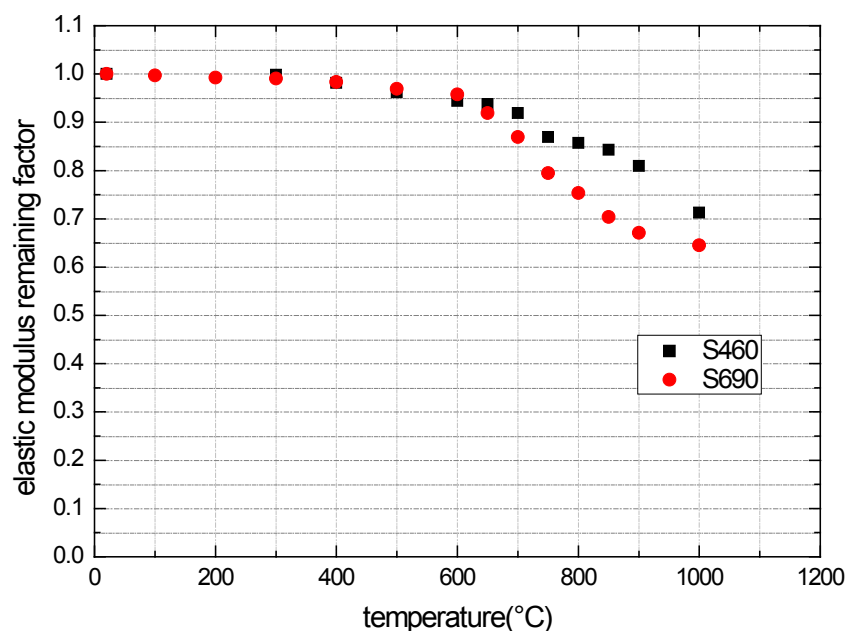
Fig.5.9. Elastic modulus remaining factors of S460 and S690.

5.3.2.4 Yield strength

After exposure to various elevated temperatures, the post-fire remaining yield strengths and their remaining factor of S690 are presented in Table 5.5.

Table 5.5: Post-fire yield strength and remaining factors of S690.

Temperature	Yield strength (MPa)				Remaining factor			
(°C)	0.2%	0.5%	1.5%	2.0%	0.2%	0.5%	1.5%	2.0%
20	789	806	784	786	1.000	1.000	1.000	1.000
100	787	801	787	787	0.998	0.994	1.004	1.002
200	787	782	789	789	0.998	0.971	1.006	1.004
300	785	781	781	781	0.995	0.970	0.997	0.995
400	786	806	788	786	0.997	1.000	1.005	1.001
500	786	807	790	790	0.997	1.002	1.007	1.005
600	785	802	783	786	0.995	0.995	0.999	1.001
650	793	800	769	783	1.006	0.993	0.981	0.997
700	705	707	702	698	0.894	0.877	0.895	0.889
750	591	591	603	608	0.749	0.733	0.769	0.775
800	484	484	486	486	0.614	0.600	0.619	0.618
850	420	420	417	418	0.532	0.521	0.531	0.532
900	320	321	375	394	0.405	0.399	0.478	0.502
1000	301	301	328	351	0.381	0.373	0.419	0.447
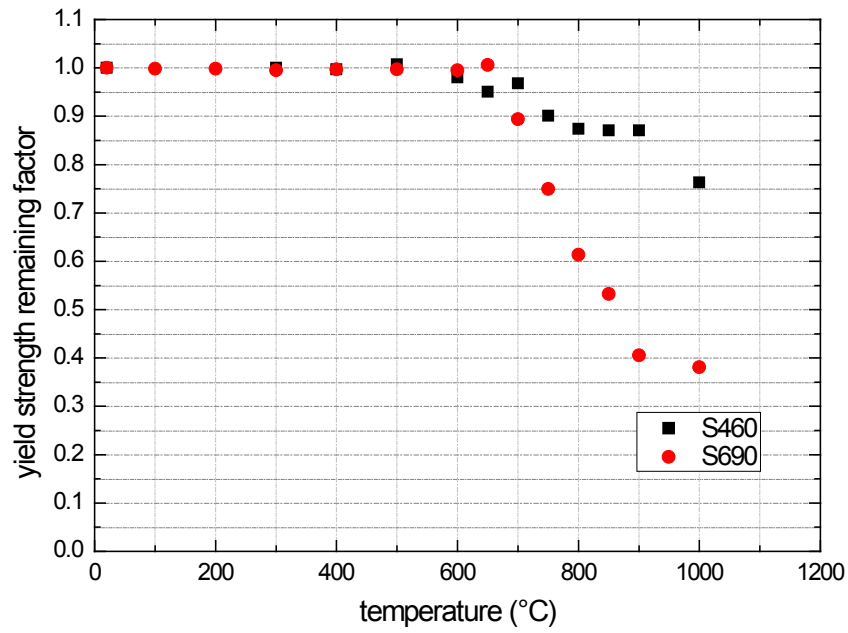
a) 0.2% proof stress method
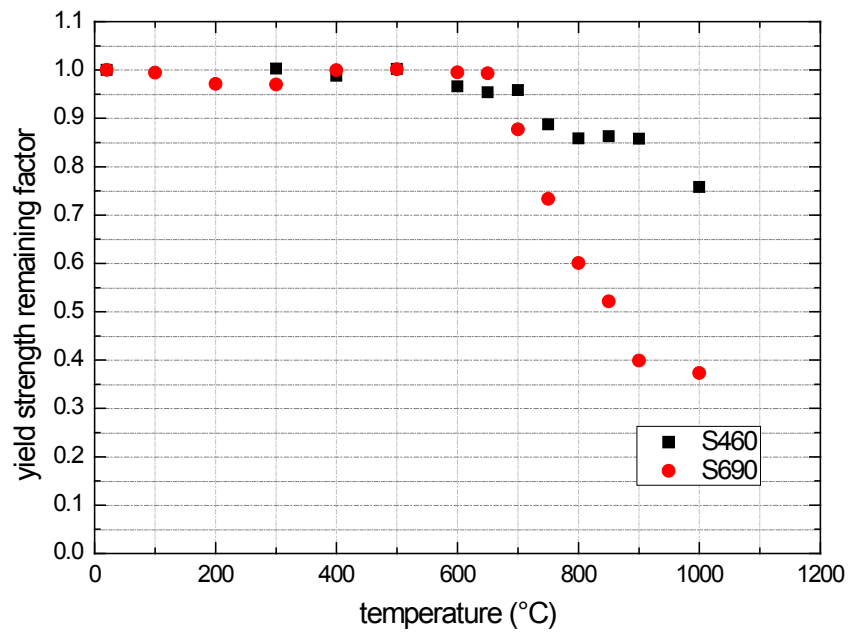
b) 0.5% total strain method
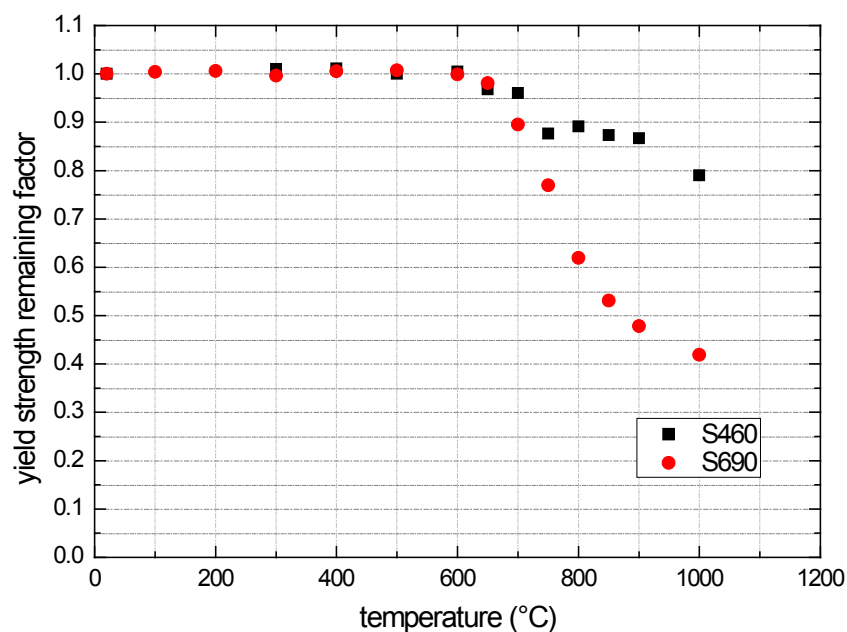
c) 1.5% total strain method
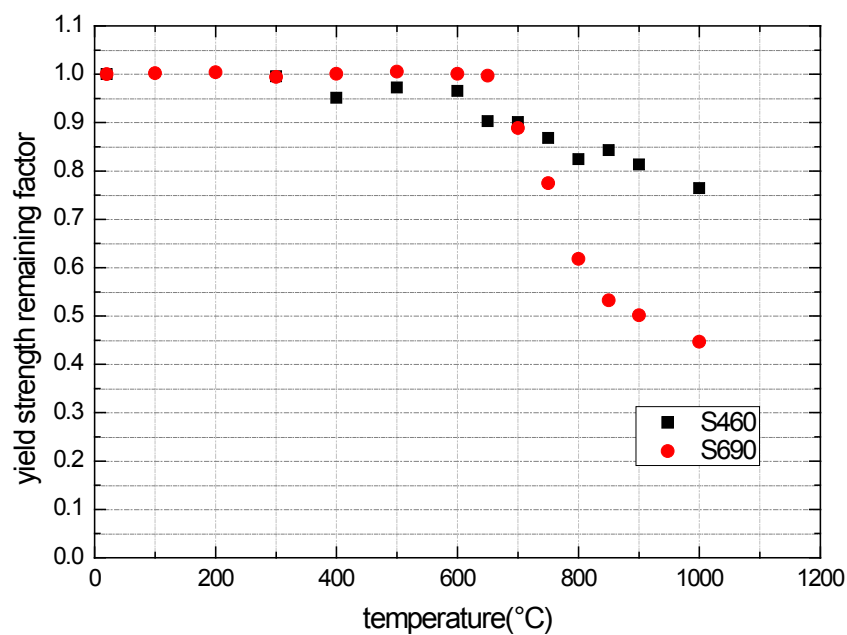
d) 2.0% total strain method

Fig.5.10. Yield strength remaining factors of S460 and S690 based on various strain methods.

Fig. 5.10 shows the deterioration of remaining yield strength with temperatures for both S460 and S690. As seen in Fig. 5.10, the post-fire yield strengths of S460 and S690 are almost not affected until they have achieved temperatures above 600°C. When they are cooled down from elevated temperatures above 600°C, S460 regains a higher percentage of yield strength than S690. For S460 at least 75% of its yield strength can be preserved after cooling from temperatures up to 1000°C, but it is much less for S690. The quenched and tempered process used in manufacturing S690 is the reason for the different rates of strength degradation between these two high strength steels. Based on

114

this study, both S460 and S690 can regain their nominal yield strength if they are exposed to temperatures below 600°C, which is positive for the reuse of HSS structures after fire. For safe consideration, a conservative suggestion is proposed to use 90% of the nominal yield strength for post-fire S690 if it has been exposed to fire temperatures below 600°C. Hence, if members made of HSS S690 are exposed to fire temperatures below 600°C and their distortions remain within the tolerances for straightness and shape, they are reusable after fire.

5.3.2.5 Ultimate strength

Table 5.6 presents the remaining ultimate strengths and their remaining factors of HSS S690 after exposure to elevated temperatures up to 1000°C. Fig. 5.11 compares the remaining factors of the ultimate strength of S690 with those of S460. The results show that when S460 and S690 are exposed to elevated temperatures below 600°C, they can regain their nominal ultimate strength after cooling down. If the temperature is beyond 600°C, S690 loses its ultimate strength more quickly than S460. For S460, even if it is exposed to temperatures as high as 1000°C, it can regain at least 80% of its ultimate strength. For S690 its remaining ultimate strength is only about 55% after cooling down from 1000°C elevated temperature. It is also the result of quench and tempering which S690 experienced during the manufacture process.

Table 5.6: Post-fire ultimate strengths (MPa) and remaining factors of S690.

Temperature (°C)	Ultimate strength	Remaining factor
20	820	1.000
100	823	1.003
200	823	1.003
300	822	1.002
400	820	0.999
500	821	1.001
600	820	1.000
650	807	0.983
700	743	0.906
750	646	0.788
800	552	0.673
850	507	0.619
900	485	0.592
1000	470	0.573
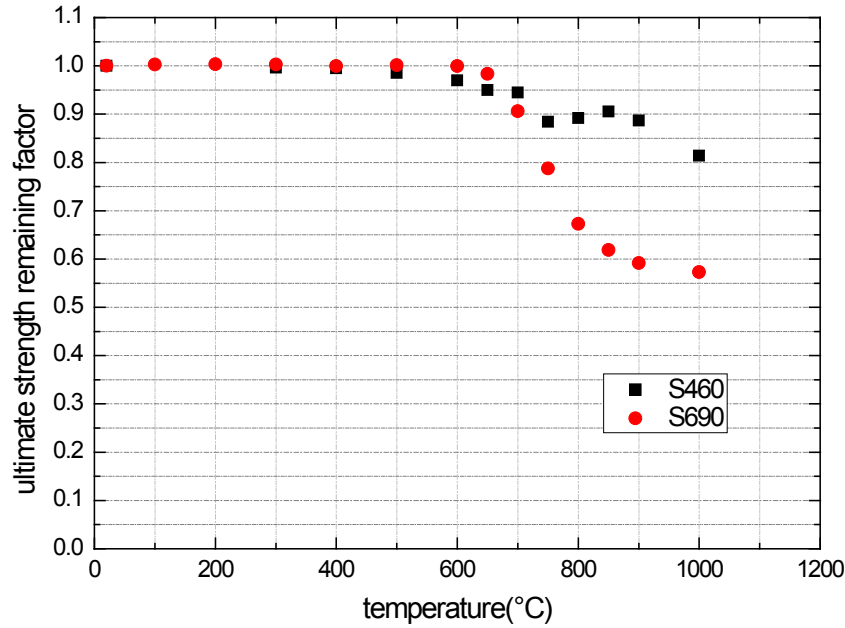
Fig.5.11. Post-fire ultimate strength remaining factors of S460 and S690.

5.3.3 Predictive Equations

In this section, some specified predictive equations were worked out to describe the remaining mechanical properties of HSS S690 after cooling down from various fire temperatures in the form of remaining factors, in order to offer an accurate choice for structural engineers to evaluate the performance of steel structures with HSS S690 after fire. As the fire temperature was the main reason causing the deterioration of post-fire material properties of steel, the equations were developed as a function of the highest fire temperature θ, which specimens have been exposed to.

5.3.3.1 Elastic modulus

For the remaining elastic modulus of S690 after fire, the predictions from Eqs.5.4 are compared with test results obtained from this study in Fig. 5.12. This figure shows that there is good agreement between the proposed equations and the test results. Therefore it is recommended to use Eqs.5.4 to determine the post-fire remaining elastic modulus of S690 after exposure to elevated temperatures up to 1000°C.

$$20 \leq \theta \leq 600, \quad \frac{E_{P\theta}}{E_{20}} = 1.001 - 6.461 \times 10^{-5} \theta \qquad (5.4a)$$

$$600 < \theta \leq 1000, \quad \frac{E_{P\theta}}{E_{20}} = 6.27 \times 10^{-9} \theta^3 - 1.38 \times 10^{-5} \theta^2 + 8.95 \times 10^{-3} \theta - 0.806 \qquad (5.4b)$$
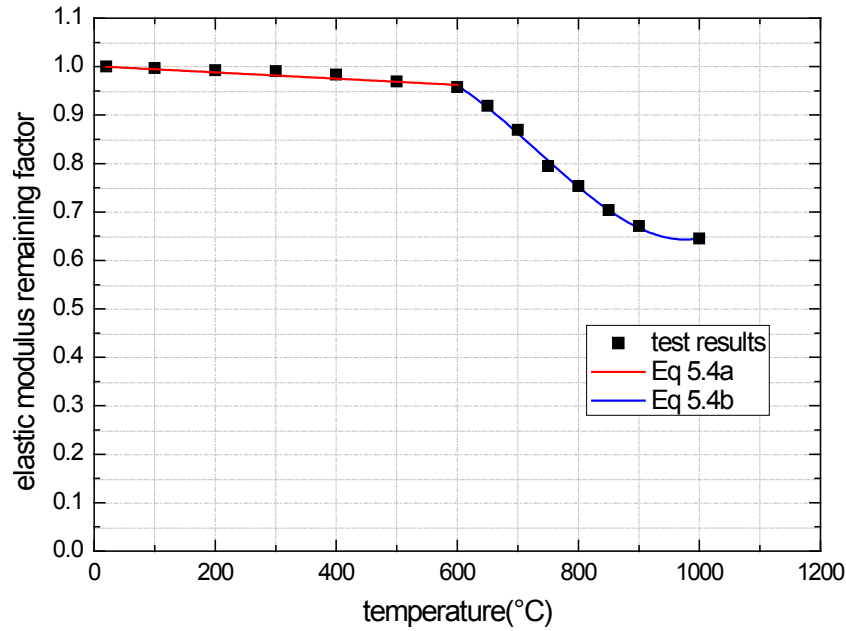
Fig.5.12. Comparison of predicted elastic modulus remaining factor from Eq.5.4 with test results.

5.3.3.2 Yield strength

Although in tests four strain levels (0.2%, 0.5%, 1.5% and 2%) were considered in determining the yield strength, only the remaining factors based on the 0.2% proof stress method were used in deriving the empirical equations for post-fire yield strength of S690, see Eqs.5.5.

$$20 \leq \theta < 650, \ \frac{f_{yP\theta}}{f_{y20}} = 1.000 \tag{5.5a}$$

$$650 \leq \theta \leq 1000, \ \frac{f_{yP\theta}}{f_{y20}} = 1.80 \times 10^{-8} \theta^3 - 4.03 \times 10^{-5} \theta^2 + 2.74 \times 10^{-2} \theta - 4.711 \tag{5.5b}$$

Fig. 5.13 compares the predictions of Eq.5.5 with test results on the post-fire remaining yield strength of S690. It can be observed that the proposed equations agree well with the test results. So Eq.5.5 is recommended to determine the post-fire remaining yield strength of S690 after cooling down from elevated temperatures up to 1000°C.
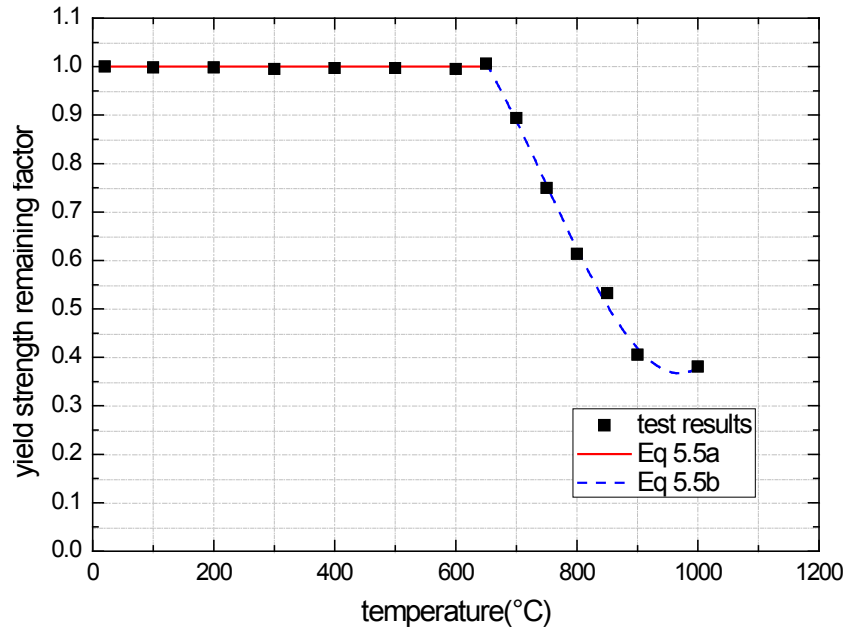
Fig.5.13. Comparison of predicted yield strength remaining factor from Eqs.5.5 with test results.

5.3.3.3 Ultimate strength

Equation 5.6 was proposed to describe the ultimate strength remaining factors of HSS S690 after cooling down from various fire temperatures up to 1000°C. Fig. 5.14 compares the predictions of Eq.5.6 for S690 with test results on its post-fire remaining ultimate strength. It seems that the proposed equations agree well with the test results. And Eq.5.6 is not very complicated in practical use. Therefore it is recommended to determine the post-fire remaining ultimate strength of HSS S690 after cooling down from elevated temperatures up to 1000°C.

$$20 \le \theta \le 600, \ \frac{f_{uP\theta}}{f_{u20}} = 1.000 \tag{5.6a}$$

$$600 < \theta \le 1000, \ \frac{f_{uP\theta}}{f_{u20}} = -1.24 \times 10^{-10}\theta^4 + 4.13 \times 10^{-7}\theta^3 - 5.077 \times 10^{-4}\theta^2 + 0.271\theta - 52.21$$

$$\tag{5.6b}$$
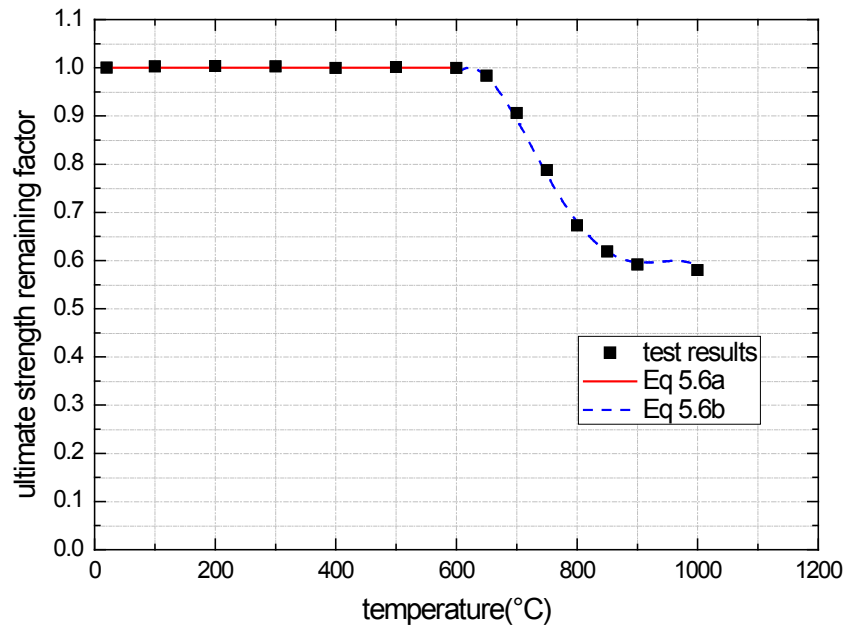
Fig.5.14. Comparison of predicted ultimate strength remaining factor from Eq.5.6 with test results.

5.4 MECHANICAL PROPERTIES OF S960 AFTER FIRE[*3]

5.4.1 Experimental Study

5.4.1.1 Test device

The test device used for post-fire tensile tests on HSS S960 is the same with that for HSS S460 and S690, as introduced in Section 5.2.1.1.

5.4.1.2 Test material and specimen

All test specimens were cut from an S960QL steel sheet ordered for this study with a nominal thickness of 5mm. S960QL is a very high strength structural steel produced in compliance with EN 10025-6 [19]. The material is heat-treated using the quenched and tempered process and has good bending and welding properties. *S960QL* is the grade designation abbreviation of this steel, where *S* means structural steel, *960* is its minimum yield strength, *Q* means quenching and tempering, and *L* means low notch toughness testing temperature. The chemical composition of the tested very high strength steel S960 is shown in Table 4.11. The shapes and dimensions of the specimens were prepared in accordance with EN 10002-5 [13] and ASTM standard E21-09 [14], the same as those of S460 and S690 see Fig. 4.3.

[*3] This section has been published in a journal paper of X.Qiang et al. [21].

5.4.1.3 Test method

As same as that for HSS S460 and S690, the steady state test method was employed for post-fire tensile tests of VHSS S960 in this experimental study.

5.4.1.4 Test procedure

The post-fire tensile test procedure for VHSS S960 was the same with that for HSS S460 and S690. The heating process was conducted in the temperature-controlled electrical furnace, as shown in Fig. 5.1; the specimens were heated from ambient temperature to a pre-selected temperature under the heating rate of 10°C/min. In this study, 11 elevated temperatures up to 1000°C were selected, i.e. 300°C, 400°C, 500°C, 600°C, 650°C, 700°C, 750°C, 800°C, 850°C, 900°C and 1000°C. 100°C and 200°C were excluded, because after cooling down from 100°C and 200°C, the post-fire performance of steels was proved not affected [20]. The test procedure for S960 is as same as those of S460 and S960, as presented in Section 5.2.1.4.

5.4.2 Experimental Results

5.4.2.1 Stress-strain curves

The post-fire stress-strain relationships of VHSS S960 obtained from this experimental study are plotted in Fig. 5.15. Its post-fire mechanical properties were investigated based on the stress-strain curves, as described in this section. It is worthwhile to note that when cooled down from fire temperatures below 800°C, the post-fire stress-strain curves of S960 exhibit a similar yield plateau to that at ambient temperature. However, beyond 800°C the post-fire stress-strain curves are of the gradual yielding type and there is an obvious increase in the post-fire strengths at 800°C and gradual decrease again afterwards.

Fig.5.15. (a) full range

120

(b) within strain range of 3%
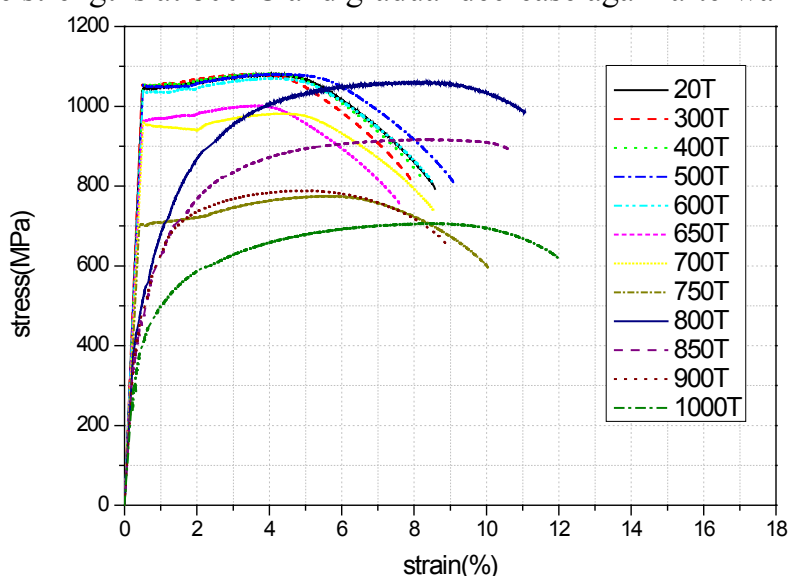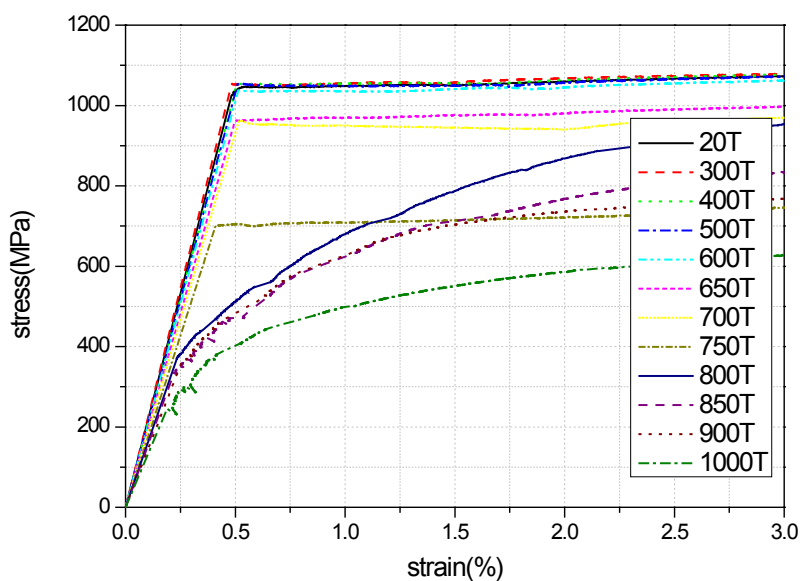
Fig.5.15. Stress-strain curves of S960 after cooling down from various fire temperatures.

5.4.2.2 Failure mode

Fig. 5.16 shows the failure mode of S960 tensile test specimens conducted at ambient temperature after cooling down from elevated temperatures up to 1000°C, for comparison, the failure mode of S960 without having been exposed to fire is also included. It is found that every specimen shows ductile failure with necking; no brittle failure was observed no matter how high a temperature the specimen is exposed to. This observation is promising for the safety of steel members made of S960 going through fire disaster.

Fig.5.16. Failure mode of S960 tensile specimens after exposure to various elevated temperatures.

5.4.2.3 Elastic modulus

The elastic modulus and remaining factors of VHSS S960 after exposure to fire up to 1000°C obtained from this study are given in Table 5.7. As seen in Table 5.7, when S960 is cooled down after exposure to elevated temperatures below 600°C, it is able to regain its elastic modulus. But beyond 600°C, there is a considerable degradation of its remaining elastic modulus. It is interesting to note that for S960 at least 75% of the elastic modulus is regained after cooling from temperatures up to 800°C, and at least 60% for temperatures up to 1000°C.

Table 5.7: Post-fire elastic modulus and their remaining factors of S960.

Temperature (°C)	E-modulus (MPa)	Remaining factor
20	213586	1.000
300	217287	1.017
400	208889	0.978
500	206272	0.966
600	201870	0.945
650	193695	0.907
700	186649	0.874
750	171418	0.803
800	160587	0.752
850	151339	0.709
900	141275	0.661
1000	138648	0.649

5.4.2.4 Yield strength

In this study, the yield strengths were determined using the 0.2% proof stress method as well as the 0.5%, 1.5% and 2% total strain methods. After exposure to various elevated temperatures, the post-fire remaining yield strengths of S960 at the above four strain levels are presented in Table 5.8. The yield strength remaining factors after cooling down from elevated temperatures are calculated as the ratio of yield strength at elevated temperatures ($f_{yP\theta}$) to that at ambient temperature (f_{y20}), and the results based on different strain methods are given in Table 5.8 as well. As shown in Table 5.8, S960 can regain its nominal yield strength if it is exposed to temperatures below 600°C, which is positive for the reuse of steel structures with VHSS S960 after fire. For safe consideration, a conservative suggestion is proposed to use 90% of the nominal yield strength for post-fire S960 if steel structures are exposed to fire temperatures below 600°C. Therefore, if members made of S960 are exposed to fire temperatures below 600°C and their distortions remain within the tolerances for straightness and shape, they are reusable after fire.

In addition, it is interesting to note that at strain levels of 1.5% and 2.0% the post-fire yield strength of S960 after cooling down from 800°C increases considerably, and the corresponding yield strengths after cooling down from temperatures higher than 800°C decrease gradually again. It attributes to the microstructure change in the material of S960.

Table 5.8: Post-fire yield strengths and their remaining factors of S960.

Temperature	Yield strength (MPa)				Remaining factor			
(°C)	0.2%	0.5%	1.5%	2.0%	0.2%	0.5%	1.5%	2.0%
20	1045	1041	1052	1058	1.000	1.000	1.000	1.000
300	1052	1054	1058	1068	1.006	1.012	1.006	1.010
400	1050	1054	1052	1058	1.004	1.012	1.000	1.000
500	1054	1054	1052	1058	1.008	1.012	1.000	1.000
600	1035	1039	1041	1045	0.990	0.998	0.990	0.988
650	967	965	977	981	0.925	0.926	0.929	0.927
700	755	753	807	807	0.722	0.723	0.767	0.763
750	701	705	716	722	0.671	0.677	0.680	0.682
800	629	581	826	909	0.601	0.558	0.785	0.859
850	529	512	786	869	0.506	0.492	0.747	0.822
900	388	400	570	601	0.371	0.385	0.542	0.568
1000	384	394	552	587	0.367	0.379	0.525	0.555

5.4.2.5 Ultimate strength

Table 5.9: Post-fire ultimate strengths and their remaining factors of S960.

Temperature (°C)	Ultimate strength	Remaining factor
20	1079	1.000
300	1080	1.001
400	1082	1.002
500	1074	0.995
600	1070	0.991
650	1002	0.928
700	983	0.911
750	776	0.719
800	1060	0.982
850	917	0.849
900	788	0.730
1000	695	0.644

The tensile tests were carried out until the specimen failed; therefore the remaining factors for ultimate strengths are calculated as the ratio of ultimate strength after cooling down from elevated temperature ($f_{uP\theta}$) to that at ambient temperature (f_{u20}). Table 5.9 presents the remaining ultimate strengths and their remaining factors after exposure to elevated temperatures up to 1000°C. The results show that when S960 is exposed to elevated temperatures below 600°C it is able to regain its nominal ultimate strength after cooling down. Even when it is exposed to temperatures as high as 1000°C, S960 can regain at least 60% of its original ultimate strength. Similar to yield strength, the post-fire ultimate

strength increases after cooling down from a fire temperature of 800°C and decreases after cooling down from higher fire temperatures.

5.4.3 Discussion

In literature, the information available concerning the remaining mechanical properties of structural steels after fire or after being exposed to elevated temperatures is very limited. In British Standard 5950-8 (2003) Annex B [9], there are some recommendations for the reuse of steel after fire. It recommends that for S235 and S275 at least 90% of the mechanical strength is regained irrespective of the temperatures attained (even after heating to above 1000°C). For S355 it can be assumed that at least 75% of the strength is regained after cooling from temperatures above 600°C. For certain grades of cold finished steels it is said that they can regain 90% of the original nominal strength. BS5950 has some suggestions on cast steel, reinforcing and pre-stressing steels as well, but no mention is made for the current high strength steels or very high strength steels. For the time being, it seems no other design standard for steel structures gives any suggestions on the reuse of steel structures after exposure to fire.

Outinen [2, 3] conducted tensile tests on S355 and S350 which were taken from steel members after testing at elevated temperatures up to 710°C. Outinen pointed out that if the distortions of a steel structure were within the tolerance limits, the strength of the material was still adequate. It is a pity that no sufficient quantitative material property data was reported.

The above available information about the post-fire material performance of mild steels was compared with that of VHSS S960 obtained from this study, and also with the previous study on S460N and S690Q [20].

5.4.3.1 Comparison of post-fire elastic modulus with available literature
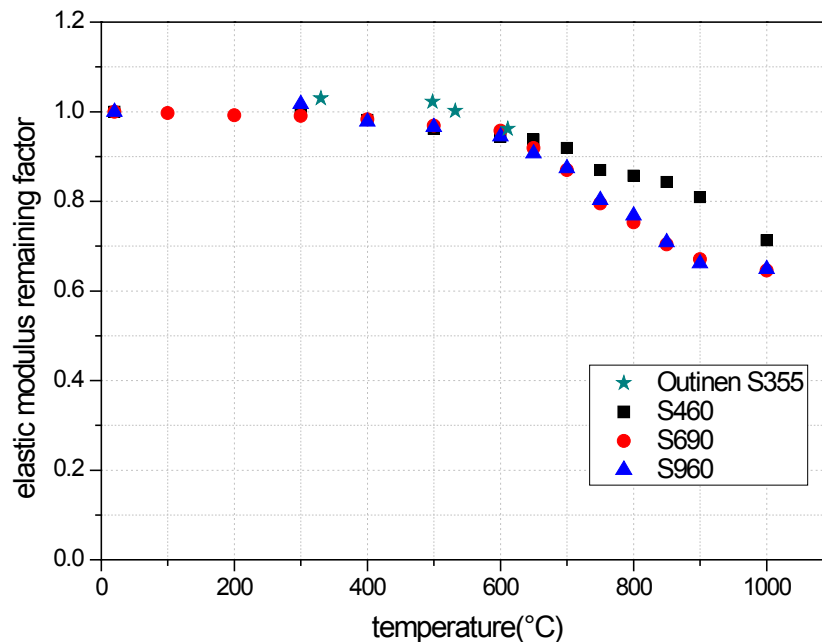

Fig.5.17. Comparison of post-fire elastic modulus remaining factors.

The post-fire elastic modulus of S960 were compared with those of S355 [2, 3], S460N and S690Q in the form of remaining factors, as shown in Fig. 5.17. It can be seen that the post-fire elastic modulus remaining factors of mild steel S355, HSS S460, S690 and S960 are similar if they are cooled down from fire temperatures below 600°C. They all have the ability to regain at least 90% of their original elastic modulus. In addition, it can be found that the post-fire elastic modulus remaining factors of VHSS S960 are similar to those of HSS S690 when cooling down from temperatures above 600°C, but different from those of HSS S460.

5.4.3.2 Comparison of post-fire yield strength with available literature

The post-fire yield strengths of VHSS S960 were compared with those of S355, S460N, S690Q and the recommendations of British design standard BS5950 for mild steels S235 and S275 in the form of remaining factors. The comparisons of remaining factors according to the 0.2% proof stress method, 0.5% total strain method, 1.5% total strain method and 2.0% total strain method were all conducted and presented in Fig. 5.18. It is found that the recommendation of BS5950 for mild steels S235 and S275 is not applicable for HSS S460, HSS S690 or VHSS S960. And the recommendation of BS5950 for mild steel S355 is applicable for HSS S460, conservative but safe. However it is too dangerous to be applicable for HSS S690 and VHSS S960, especially when cooling down from fire temperatures beyond 700°C. In addition, it can be seen that the post-fire yield strength remaining factors of S960 are similar to

those of S690 at strain levels 0.2% and 0.5%. But at strain levels 1.5% and 2.0% it is not the case for cooling down from temperatures in excess of 800°C. All in all, the post-fire remaining yield strength of steels is dependent on steel grade and manufacture method.
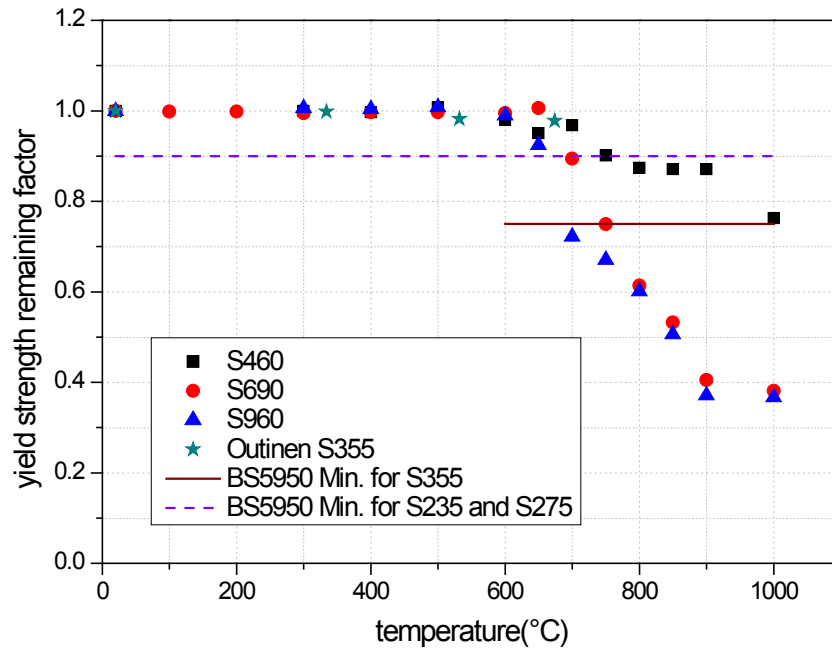
a) 0.2% proof stress method

b) 0.5% total strain method
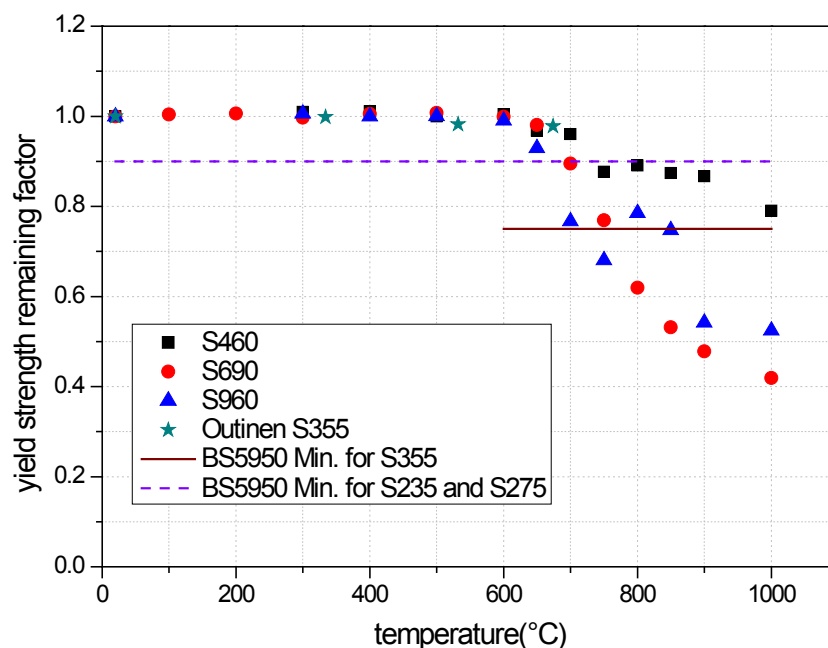
c)1.5% total strain method
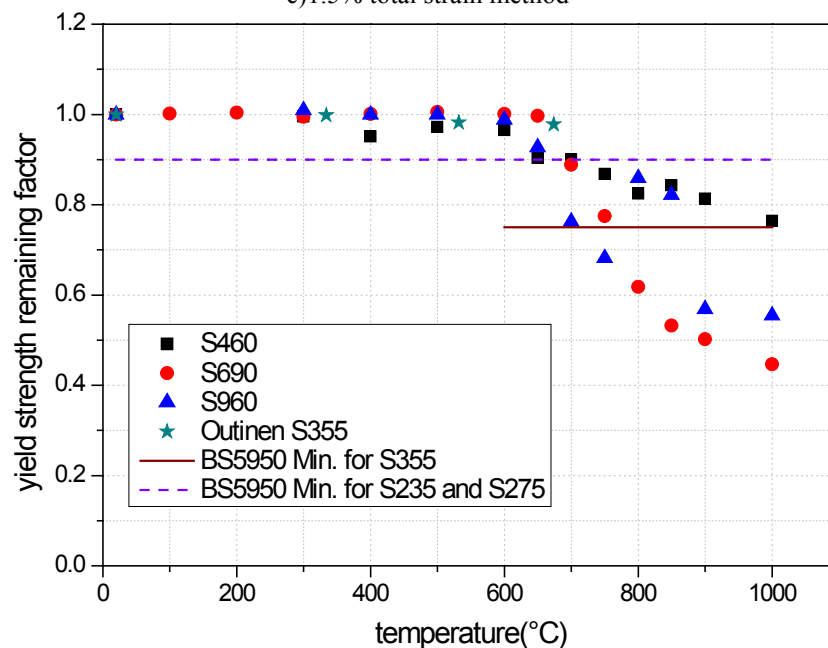
d) 2.0% total strain method

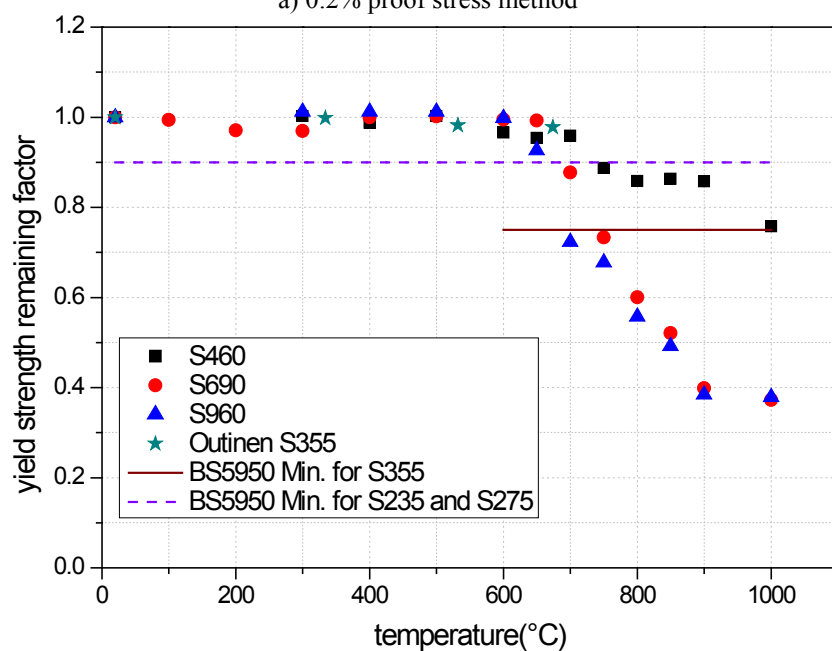Fig.5.18. Comparison of post-fire yield strength remaining factors.

5.4.3.3 Comparison of post-fire ultimate strength with available literature

The post-fire ultimate strengths of VHSS S960 were compared with those of S460N, S690Q and the recommendations of British design standard BS5950 for mild steels S235, S275 and S355 in the form of remaining factors, as described in Fig. 5.19. It can be observed that the recommendation of BS5950 for mild steels S235 and S275 is not applicable for HSS S460, VHSS S690 or VHSS S960. And the recommendation of BS5950 for mild steel S355 is applicable for HSS S460, conservative but safe; however not for VHSS S690

and VHSS S960, especially when cooling down from fire temperatures beyond 700°C. Furthermore, the post-fire ultimate strength remaining factors of VHSS S960 are similar to those of S690 when cooling down from fire temperatures below 800°C, but not the case when cooing down from temperatures above 800°C. A conclusion can be drawn is that the post-fire remaining ultimate strength of steels is dependent on steel grade and manufacture method.
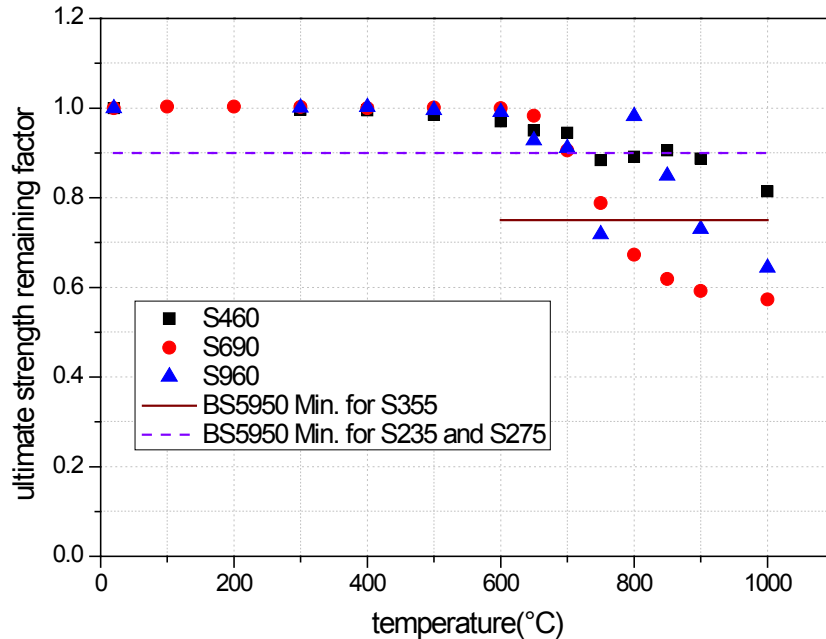
Fig.5.19. Comparison of post-fire ultimate strength remaining factors.

Therefore, using the recommendations of BS5950 for mild steels to evaluate the remaining performance of very high strength steels is dangerous. There should be some unique suggestions for evaluating the mechanical properties of VHSS S960 after fire and the possibility of its reuse. Hence, the following predictive equations were developed.

5.4.4 Predictive Equations

As fire temperature is the main cause of the deterioration of material properties of steel, the predictive equations were developed as a function of the highest fire temperature θ that specimens have been exposed to. Figs 5.23-5.25 show that the proposed predictive equations agree well with the experimental results and therefore are able to accurately predict the post-fire performance of VHSS S960.

5.4.4.1 Elastic modulus

Since the elastic modulus remaining factors of S960 are very similar to those of S690, the predictive equation (Eq.5.7) proposed for evaluating the remaining elastic modulus of S690 is compared with the test results from this study as

shown in Fig. 5.20. This figure shows that there is a good agreement between the proposed equations and the test results of S960. Eq.5.7 is not complicated in practical use. Therefore it is recommended to use Eq.5.7 to determine the post-fire remaining elastic modulus of VHSS S960 after exposure to fire temperatures up to 1000°C.

$$20 \le \theta \le 600, \quad \frac{E_{P\theta}}{E_{20}} = 1.001 - 7.125 \times 10^{-5} \theta \tag{5.7a}$$

$$600 < \theta \le 1000, \quad \frac{E_{P\theta}}{E_{20}} = 6.27 \times 10^{-9} \theta^3 - 1.38 \times 10^{-5} \theta^2 + 8.95 \times 10^{-3} \theta - 0.806 \tag{5.7b}$$
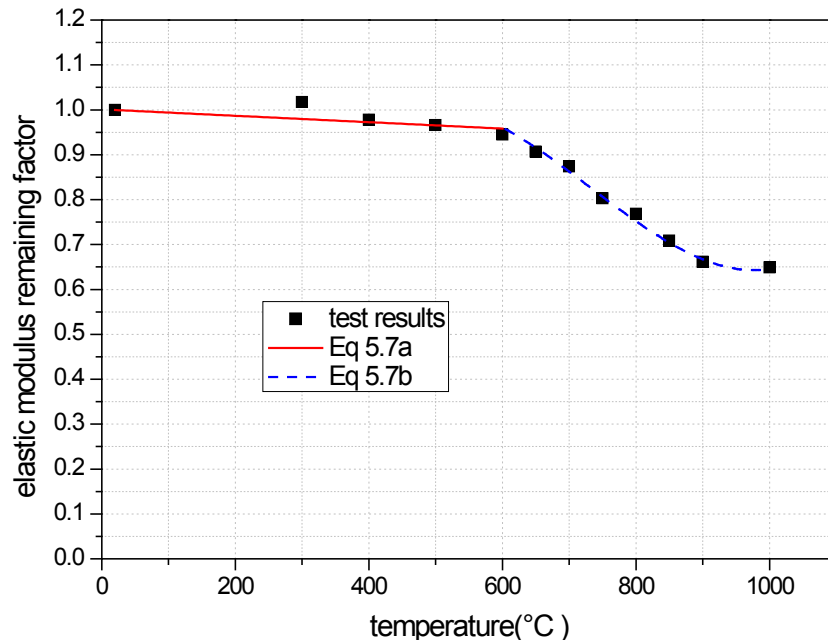
Fig.5.20. Comparison of predicted elastic modulus remaining factor from Eq.5.7 with test results.

5.4.4.2 Yield strength

Though four strain levels (0.2%, 0.5%, 1.5% and 2%) were considered in determining the yield strength, only the remaining factors based on the 0.2% proof stress method are used in deriving the empirical equations. Two sets of predictive equations are worked out for the post-fire remaining yield strength of S960 and compared with test results in Fig. 5.21. Eqs.5.8 is more accurate according to all test data, but sometimes not conservative. For conservative consideration, Eqs.5.9 is recommended for practical use, to determine the post-fire remaining yield strength of S960 after cooling down from fire temperatures up to 1000°C.

$$20 \le \theta \le 600, \quad \frac{f_{yP\theta}}{f_{y20}} = 1.0 \tag{5.8a}$$

$$600 < \theta \leq 1000, \; \frac{f_{yP\theta}}{f_{y20}} = 8.157 \times 10^{-9}\theta^3 - 1.685 \times 10^{-5}\theta^2 + 9.388 \times 10^{-3}\theta - 0.333 \quad (5.8b)$$

$$20 \leq \theta \leq 600, \; \frac{f_{yP\theta}}{f_{y20}} = 1.0 \quad (5.9a)$$

$$600 < \theta \leq 1000, \; \frac{f_{yP\theta}}{f_{y20}} = 4.4 \times 10^{-6}\theta^2 - 8.637 \times 10^{-3}\theta + 4.596 \quad (5.9b)$$
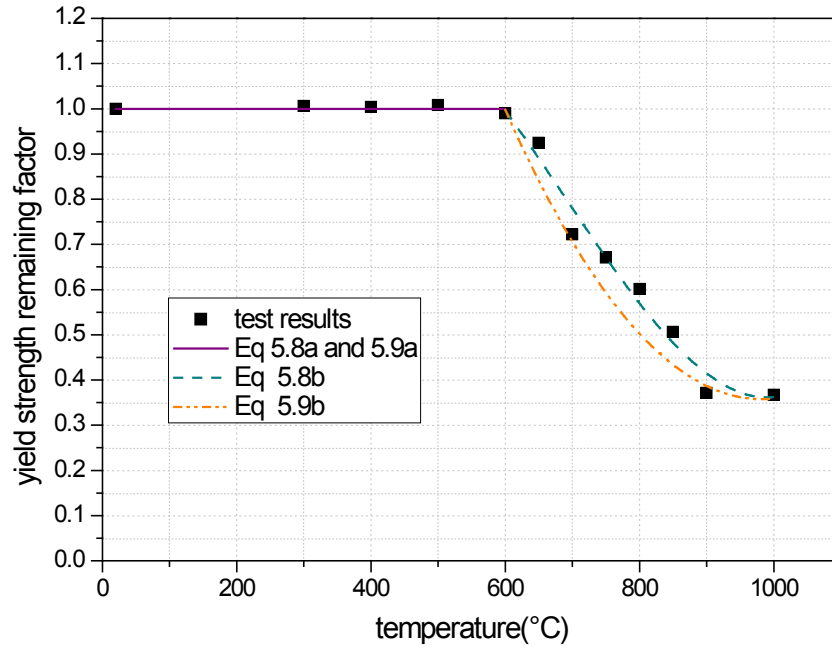
Fig.5.21. Comparison of predicted yield strength remaining factor from Eqs.5.8 and 5.9 with test results.

5.4.4.3 Ultimate strength

$$20 \leq \theta \leq 600, \; \frac{f_{uP\theta}}{f_{u20}} = 1.0 \quad (5.10a)$$

$$600 < \theta < 800, \; \frac{f_{uP\theta}}{f_{u20}} = -1.292 \times 10^{-5}\theta^2 - 1.578 \times 10^{-2}\theta - 3.834 \quad (5.10b)$$

$$800 \leq \theta \leq 1000, \; \frac{f_{uP\theta}}{f_{u20}} = 7.762 \times 10^{-6}\theta^2 - 1.568 \times 10^{-2}\theta + 8.564 \quad (5.10c)$$

Due to the abrupt increase of the post-fire ultimate strength of S960 around 800°C, 3 equations are proposed to predict the post-fire ultimate strength of S960 after cooling down from fire temperatures up to 1000°C. Fig. 5.22 shows that a good agreement exists between the predictions of Eq.5.10 and test results of the post-fire remaining ultimate strength.
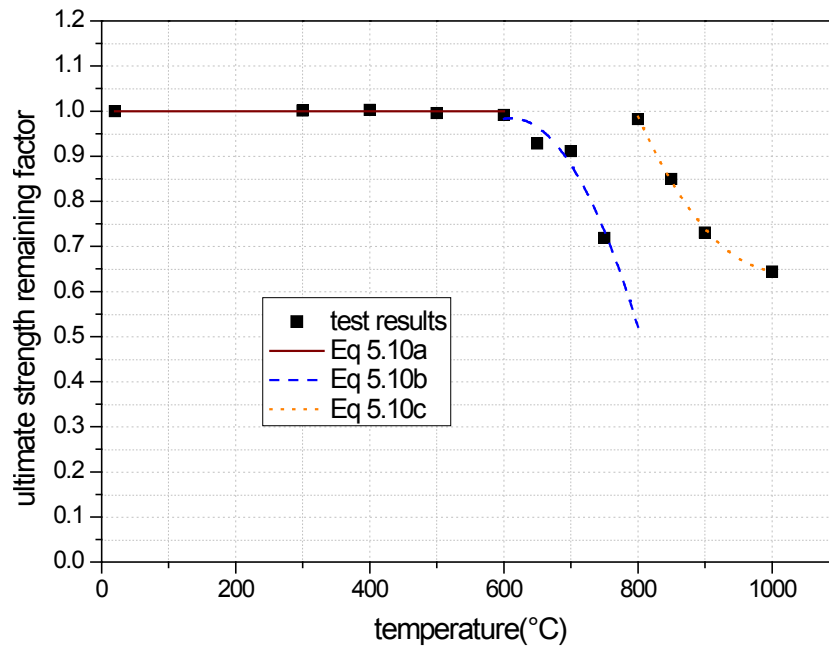
Fig.5.22. Comparison of predicted ultimate strength remaining factor from Eq.5.10 with test results.

5.5 CONCLUSION

This chapter presents detailed experimental studies on the post-fire material properties of high strength steel S460, S690 and S960. Steady state tensile tests were carried out after cooling down from various fire temperatures up to 1000°C, to reveal the remaining elastic modulus, yield strength, ultimate strength and post-fire stress–strain curves of S460, S690 and S960 after fire. The results show that the steel grade and manufacture method have significant influence on the post-fire remaining mechanical properties of structural steels. Hence, the recommendations of BS5950 obtained mainly from mild steels on the reuse of steel structures exposed to fire are not directly applicable to high strength steel or very high strength steel members. Unique recommendations for the reuse of steel members made of high strength steel or very high strength steel should be proposed in the current practical design standards for steel structures. In addition, it is found that the post-fire mechanical properties of HSS S460, S690 and S960 are not affected until they are exposed to fire temperatures above 600°C. So, if the distortions of steel members made of S460, S690 and S960 remain within the tolerance limits after fire, they can be considered to be reused. For the reuse based on conservative consideration, it is suggested using 90% of its nominal mechanical properties if the steel member made of S460, S690 or S960 is cooled down after having been exposed to fire temperatures below 600°C. To easily evaluate the remaining mechanical properties of S460, S690 and S960 after cooling down from temperatures beyond 600°C up to 1000°C, some separate predictive equations are proposed

131

to determine their post-fire elastic modulus, yield strengths and ultimate strengths correspondingly. The application of such accurate remaining mechanical properties will lead to appropriate post-fire evaluation and safe reuse of steel structures with members made of HSS S460, S690 or S960 after exposure to fire.

5.6 REFERENCES

[1] Outinen J, Kaitila O, Makelainen P, High-temperature testing of structural steel and modelling of structures at fire temperatures. Helsinki, Finland: Helsinki Univ. of Technology Laboratory of Steel Structures; 2001.

[2] Outinen J, Mechanical properties of structural steels at high temperatures and after cooling down [PhD thesis]. Helsinki, Finland: Helsinki Univ. of Technology; 2007.

[3] Outinen J, Makelainen P, Mechanical properties of structural steel at elevated temperatures and after cooling down. Fire Mater. 2004;28:237-51.

[4] Lange J, Wohlfeil N, Examination of the mechanical properties of the microalloyed grain refined steel S 460 at elevated temperatures. Bautechnik. 2007;84:711-20.

[5] Schneider R, Lange J, Constitutive equations of structural steel S460 at high temperatures. Nordic steel construction conference 2009. Sweden: 2009. p. 204-11.

[6] Schneider R, Lange J, Constitutive equations and empirical creep law of structural steel S460 at high temperatures. In: Kodur V, Franssen JM, editors. Structures in fire 2010. East Lansing: DEStech Publication, Inc.; 2010. p. 703-10.

[7] Schneider R, Lange J, Material and creep behaviour of S460 in case of fire-experimental investigation and analytical modeling. In: Wald F, Horova K, Jirku J, editors. International conference application of structural fire engineering. Prague: Cost; 2011. p. 55-60.

[8] Young B, Chen J, Uy B, Behavior of high strength structural steel at elevated temperatures. J Struct Eng-Asce. 2006;132:1948-54.

[9] B.S. Institution, BS5950, Structural use of steelwork in building, Part 8: Code of practice for fire resistant design, London, 1998.

[10] CEN, Eurocode 3 - Design of steel structures - Part 1-2: General rules - Structural fire design, in, CEN, Brussels, 2005.

[11] CEN, Eurocode 3 - Design of steel structures - Part 1-12: Additional rules for the extension of EN 1993 up to steel grades S700, in, CEN, Brussels, 2004.

[12] CEN, EN 10025-3, Hot rolled products of structural steels - Part 3: Technical delivery conditions for normalized/normalized rolled weldable fine grain structural steels, in, Brussels, 2004.

[13] CEN, EN 10002-5, Metallic materials-Tensile testing-Part 5: Method of testing at elevated temperature, Brussels, 1992.

[14] ASTM, E21-09, Standard test methods for elevated temperature tension tests of metallic materials, West Conshohocken, United States, 2009.

[15] J.Witteveen, L. Twilt, F.S.K. Bijlaard. Theoretical and experimental analysis of steel structures at elevated temperatures. International association for bridge and structural engineering, Tokyo, September 6-11th, 1976.

[16] AISC, Specification for structural steel buildings, American Institution of Steel Construction, Chicago, 2005.

[17] ASCE, Structural fire protection, New York, 1992.

[18] AS, AS 4100, Australian Standards: Steel structures, Sydney, Australia, 1998.

[19] CEN, EN 10025-6: Hot rolled products of structural steels - Part 6: Technical delivery conditions for flat products of high yield strength structural steels in the quenched and tempered condition, Brussels, 2009.

[20] X. Qiang, F.S.K. Bijlaard, M.H. Kolstein, Post-fire mechanical properties of high strength structural steels S460 and S690, Engineering Structures, 35 (2012) 1–10.

[21] X. Qiang, F.S.K. Bijlaard, M.H. Kolstein, Post-fire performance of very high strength steel S960, Journal of Constructional Steel Research, 80 (2013) 235–242.

Part III

Full-scale behaviour of high strength steel endplate connections in fire and after fire

Chapter 6

Experimental study on HSS endplate connections at ambient temperature and in fire

6.1 INTRODUCTION

In the present chapter, the behaviour of high strength steel endplate connections at ambient temperature and in fire is studied via full scale tests. Tests on 7 endplate connections were conducted at elevated temperature 550°C under steady state as well as at ambient temperature, to observe their performances at ambient and elevated temperatures. In the series of connection specimens, 3 endplate connections were made of mild steels for comparison with high strength steel endplate connections. The parameters investigated were the endplate thickness and the endplate material. All specimens were designed to confine failure to the connections (particularly to the endplates in tensile zone) rather than the beam or column. The moment-rotation characteristic, rotation capacity and failure mode of high strength steel endplate connections in fire and at ambient temperature were obtained through tests and compared with those of mild steel endplate connections. The descriptions of the experimental program and results are given below.

6.2 TEST PROGRAMME

6.2.1 Test specimen

In this experimental study, the strengths of the endplate connections are designed according to Eurocode 3 part: 1-8 Design of joints [1]. In the endplate connections, the endplates are made of high strength steels (S690 and S960) while the beam and column are made of Q345 (mild structural steel, the nominal yield stress of which is 345MPa, similar to S355). The beam sections

used herein are HW300×300 [2] (comparable to European Section HE320A) while the column sections are HW400×400 [2] (comparable to European Section HE300M); their detailed dimensions are presented in Appendix A. For comparison, the connections with endplates made of mild steels Q235 (mild structural steel, the nominal yield stress of which is 235MPa, similar to S235) and Q345 are also included herein. In this experimental study, there are two series of endplate connections. In each of them, the load bearing capacities of the connections are designed to be similar, while the endplate materials and thicknesses vary. In order to compare the behaviour of endplate connections in fire with that at ambient temperature, the tests at ambient temperature on each concerned endplate connection were conducted as well. The overall dimension of the endplate connection test specimen is shown in Fig. 6.1, while the endplate materials and thicknesses of the specimens are shown in Table 6.1 and the detailed drawing of all components of test specimens is presented in Appendix A. Two stiffeners were welded on each side of the beam web at loading point for applying load, as shown in Fig. 6.1(a). The welds between endplate and beam are 45°-fillet welds, which were made in the workshop in a down-hand position. The welding material used for specimens with endplates made of mild steels Q235 and Q345 is ER50-6, while that for specimens with endplates made of high strength steels S690 and S960 is ER76-G. The chemical compositions of these two welding electrodes are listed in Table 6.2, while their mechanical properties are presented in Table 6.3. Since the yield strength of electrode ER50-6 is 439MPa, the welds for specimens with endplates made of mild steels Q235 and Q345 are overmatched. The yield strength of electrode ER76-G is 735MPa, similar to that of HSS S690; hence the welds for specimens with endplate made of HSS S690 are matched welding while those for specimens with endplate made of HSS S960 are under matched. Therefore the weld sizes used for endplates made of mild steels (Q235 and Q345) are 8mm, while those for endplates made of high strength steels (S690 and S960) are 10mm for compensation.

a) Endplate connection   b) endplate

Fig.6.1. Dimension of endplate connection specimen.

Table 6.1: Test specimens and fire test conditions

Connection ID	Endplate material	Endplate thickness (mm)	Electrode	Weld type	Weld Size (mm)	Temperature (°C) of specimens
1-1 A	Q235	20	ER50-6	overmatched	8	20
1-2 A	S690	12	ER76-G	matched	10	20
1-3 A	S960	10	ER76-G	under matched	10	20
2-1 A	Q235	25	ER50-6	overmatched	8	20
2-2 A	Q345	20	ER50-6	overmatched	8	20
2-3 A	S690	15	ER76-G	matched	10	20
2-4 A	S960	12	ER76-G	under matched	10	20
1-1 E	Q235	20	ER50-6	overmatched	8	550
1-2 E	S690	12	ER76-G	matched	10	550
1-3 E	S960	10	ER76-G	under matched	10	550
2-1 E	Q235	25	ER50-6	overmatched	8	550
2-2 E	Q345	20	ER50-6	overmatched	8	550
2-3 E	S690	15	ER76-G	matched	10	550
2-4 E	S960	12	ER76-G	under matched	10	550

Table 6.2: Chemical compositions of the electrodes (%)

Electrode	C	S	Mn	P	Si	Cr	Ni	Mo	V	Cu
ER50-6	0.08	0.015	1.45	0.018	0.96	0003	0.02	0.002	0.004	0.10
ER76-G	0.08	0.009	1.66	0.01	0.56	0.09	1.32	0.46	-	-

Table 6.3: Mechanical properties of the electrodes

Electrode	Yield strength (MPa)	Tensile strength (MPa)	Elongation (%)	Impact test		
				Temperature (°C)	Impact value	
ER50-6	439	510	26.40	-30	88	106	98
ER76-G	735	790	21.50	-40	123	123	132

6.2.2 Test set-up

Fig. 6.2. Fire test furnace.

All fire tests were conducted in a gas furnace (4.5m×3.0m×1.7m) as shown in Fig. 6.2. Since applying a tensile load under fire conditions is more stable than applying a compressive load, the connection specimens were designed to be located upside down in order to easily apply the tensile load from the outside of the furnace, as shown in Fig. 6.3. The members below the furnace cover are in fire during fire tests, while those above the furnace cover are out of the fire field at ambient temperature, see Fig. 6.3.
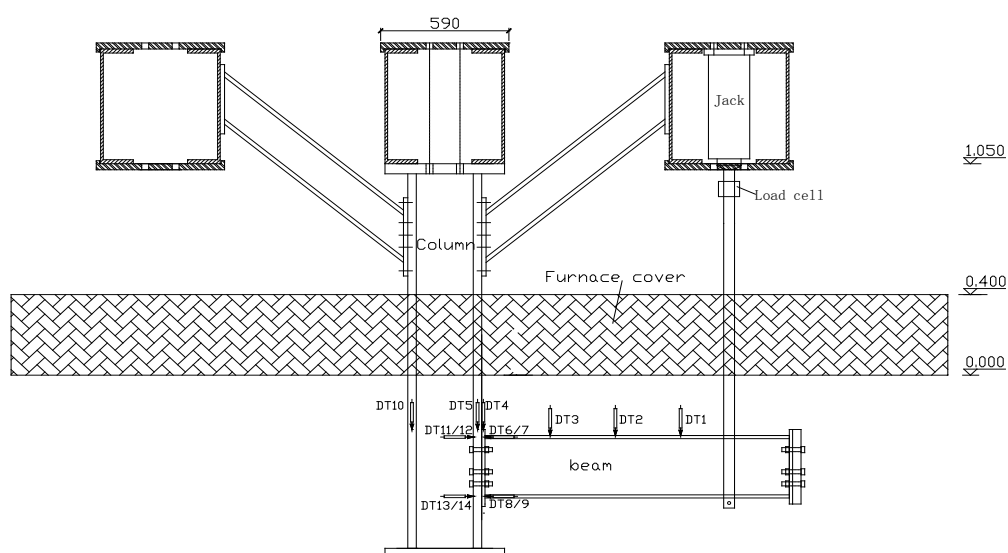

Fig.6.3. Fire test set-up.

6.2.3 Displacement measurements

In the fire tests, 3 vertical displacement sensors (DT1~DT3) were used to obtain the vertical displacement of the beam, as shown in Fig. 6.4. According

to the vertical displacements of beam, the rotation of beam can be calculated. In order to record the displacement of column, 2 vertical displacement sensors (DT5 and DT10) were arranged as shown in Fig. 6.4. According to the displacement of column, the rotation of column can be calculated. In order to measure the displacement of endplate, one vertical displacement sensor (DT4) and 4 horizontal displacement sensors (DT6~DT9) were placed, as shown in Fig. 6.4. According to the displacement of endplate, the rotation of endplate can be calculated. Based on the displacements of the aforementioned components, the rotation of endplate connection in tests can be obtained. Another way of obtaining the rotation of connection was also designed via using four extra horizontal displacement sensors (DT11-DT14) together with the four horizontal displacement sensors DT6-DT9. The two methods of measuring rotation of endplate connection were used to validate each other, which will be presented hereafter in Section 6.3.2.
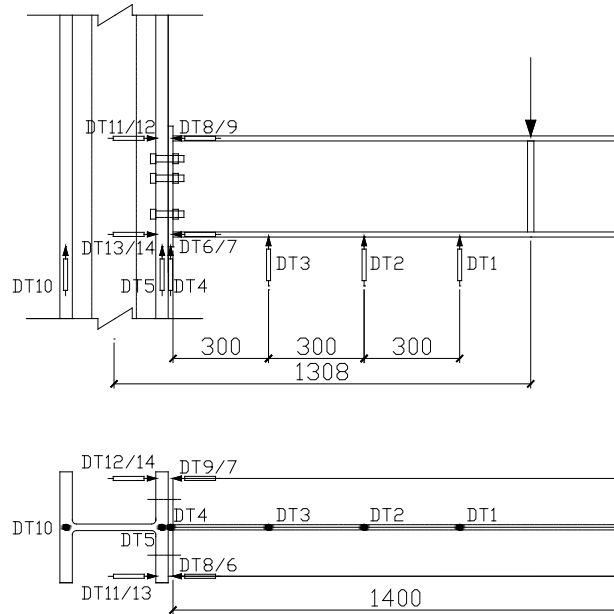

Fig.6.4. Arrangement of displacement sensors.

6.2.4 Test procedure

Before performing the full-scale tests, all equipment was calibrated by skilled technicians. After the installation of each test specimen and measuring equipment, all test equipment was checked by trial loading at ambient temperature. After everything went well, the real tests were started. The full-scale fire tests on endplate connections were conducted under steady state fire condition. The specimens were firstly heated to a pre-selected elevated temperature (550°C) at a constant heating rate 10°C/min, which corresponds to a natural fire to buildings. When the temperature of the concerned components

141

reached the pre-selected elevated temperature, the mechanical load (moment for the connection, see Fig. 6.5) was applied to the specimen at this constant elevated temperature until failure occurred. During loading, displacement control was used by controlling the displacement of piston of the hydraulic actuator at a constant rate 10mm/min. The displacements of beam, column and endplate and the rotation of connection in fire were obtained and recorded. After tests, the final deformation state of connections can be observed.
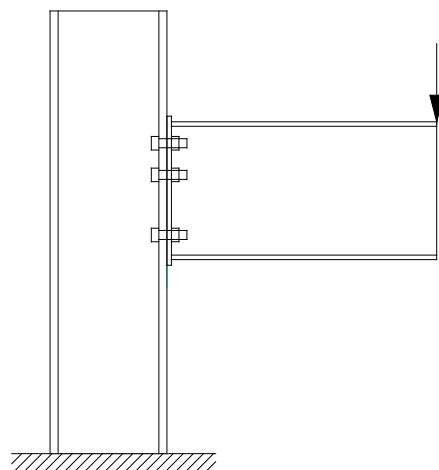

Fig. 6.5. Force application.

6.3 EXPERIMENTAL RESULTS

6.3.1 Deformation at the end of tests

For all endplate connections, both at ambient temperature and in fire, their final deformation states were photographed at the end of tests and are presented in Appendix B of this thesis.

6.3.1.1 At ambient temperature

An overall description on components of all connections at the end of the tests is listed in Table 6.4. As an example, the detailed illustrations on the final deformation state of specimen 1-1 A (Q235 20mm) at ambient temperature are presented in Fig.6.6. It can be seen that the failure was concentrated in the endplate, and the bolts remained almost straight until very large deformation on the endplate appeared. Damage to the endplate started as significant bending; after very large plastic bending deformation of the endplate, the two rows of bolts in tension tore some bearing materials around the bolt holes. It corresponds to a rapid drop in resistance of the connection, as shown in Fig.6.12 and Fig.6.16. After very large bending deformation of the endplate, some threads stripped off the bolts in the top tensile row. The broken bolt in the

second tensile row as shown in Fig.6.6 (d) and (e) was due to the cut during removing the specimen after tests.
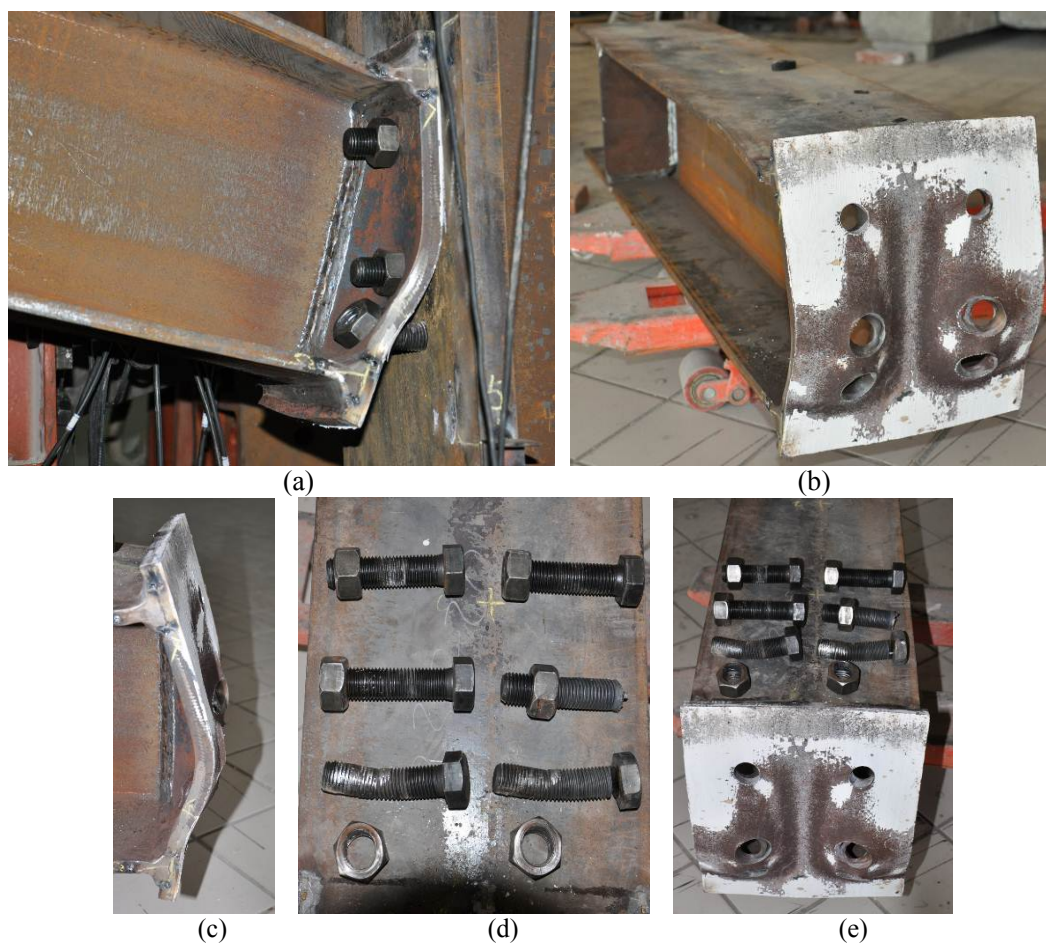

| (a) | (b) |

| (c) | (d) | (e) |

Fig.6.6. Final deformation state of connection 1-1A (Q235 20mm) at ambient temperature.

Table 6.4: Description of components at the end of ambient-temperature tests

Test ID	Endplate material	Endplate thickness (mm)	Endplate yielding	Fracture of bolts in top tensile row	Nuts in top tensile row stripped off	Weld failure in heat affected zone	Bolts in compression almost straight
1-1 A	Q235	20	Yes	No	No	No	Yes
1-2 A	S690	12	Yes	No	Yes	No	Yes
1-3 A	S960	10	Yes	No	No	Yes	Yes
2-1 A	Q235	25	Yes	Yes	No	No	Yes
2-2 A	Q345	20	Yes	Yes	No	No	Yes
2-3 A	S690	15	Yes	Yes	No	No	Yes
2-4 A	S960	12	Yes	Yes	No	No	Yes

6.3.1.2 At elevated temperatures

An overall description of the components of all connections at the end of elevated-temperature tests is listed in Table 6.5.

143

Table 6.5: Description of components at the end of elevated-temperature tests

Test ID	Endplate material	Endplate thickness (mm)	Endplate yielding	Fracture of bolts in top tensile row	Nuts in top tensile row stripped off	Weld failure in heat affected zone	Bolts in compression almost straight
1-1 E	Q235	20	Yes	Yes	No	No	Yes
1-2 E	S690	12	Yes	Yes	No	No	Yes
1-3 E	S960	10	Yes	Yes	No	No	Yes
2-1 E	Q235	25	Yes	Yes	No	No	Yes
2-2 E	Q345	20	Yes	Yes	No	No	Yes
2-3 E	S690	15	Yes	Yes	No	No	Yes
2-4 E	S960	12	Yes	Yes	No	No	Yes

(a) (b) (c)

(d)
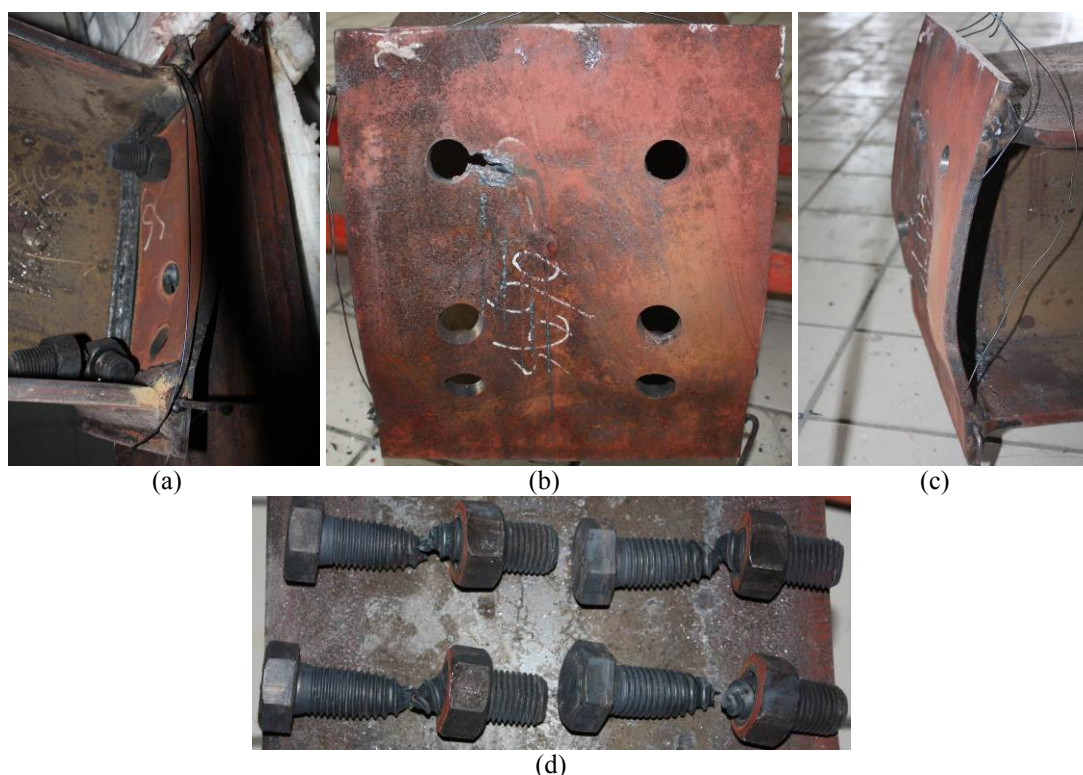
Fig.6.7. Final deformation state of connection 1-2 E (S690 12mm) at elevated temperature 550°C.

As an example, the observed final deformation state of connection 1-2 E (S690 12mm) at elevated temperature 550°C is presented in Fig.6.7. It can be seen that the failure started from the bending of the endplate, and the bolts remained almost straight until very large plastic deformation on the endplate appeared. After very large bending deformation of endplate, the two rows of bolts in tension were gradually pulled apart, with no obvious breaking point, as shown in Fig.6.7 (d). It corresponds to the decline phase in resistance of this connection, as shown in Fig.6.14 and Fig.6.17. For the bolts in compression, they remained straight in tests. The picture of bolts in compression after removing from the specimens after tests was not taken, because the deformed bolts in tension were ruined during removing.

6.3.2 Moment - rotation relationship of endplate connection

The behaviour of a steel beam-to-column joint is usually represented by M-ϕ curve. The rotational deformation of a joint results from the in-plane bending moment M, and it includes the rotational deformation of the connection as well as the shear deformation of the column web panel zone. (The definition of joint and connection is shown in Fig.6.8.) The connection rotational deformation consists of the deformation of the fastening elements (bolts, endplate, etc.) and the deformation of the column web. The rotational deformation of a connection ϕ is defined as the relative rotation between the beam and column axes, see Fig. 6.9, which is equal to:

$$\phi = \theta_b - \theta_c \tag{6.1}$$

This deformation is only due to the force transferred by the beam flanges that are induced by the bending moment M $(M=F \times L)$ acting on the beam.
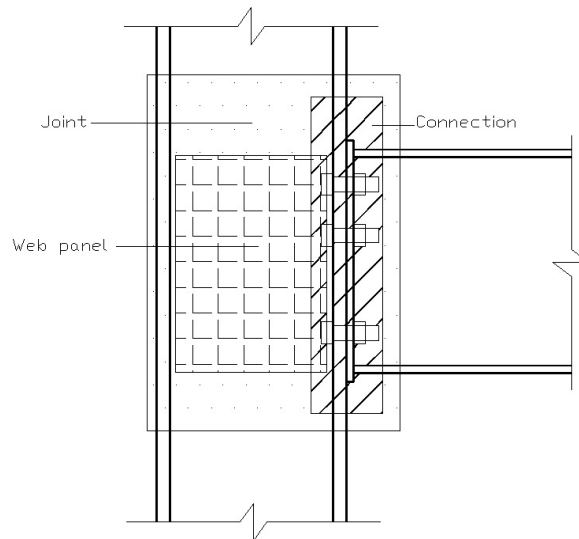

Fig.6.8. Definition of joint and connection.

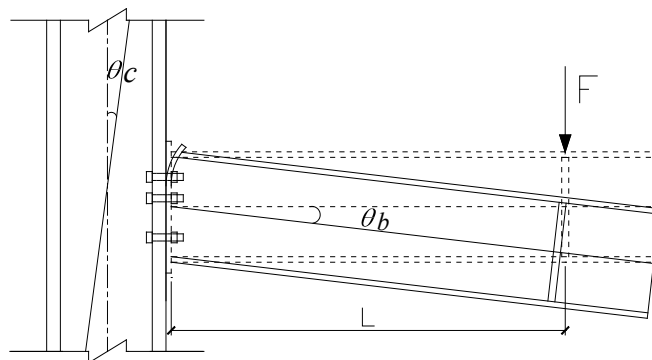Fig.6.9. Endplate connection rotation deformation.

The beam rotation θ_b can be calculated by the following equations:

$$\theta_b = \arctan\frac{\left|\delta_{DT1}\right|-\left|\delta_{DT4}\right|}{900} = \arctan\frac{\left|\delta_{DT2}\right|-\left|\delta_{DT4}\right|}{600} = \arctan\frac{\left|\delta_{DT3}\right|-\left|\delta_{DT4}\right|}{300} = \arctan\frac{\left|\delta_{DT6}\right|+\left|\delta_{DT9}\right|}{h_b - t_{fb}}$$

(6.2)

where δ_{DT1-3} are the vertical displacements of beam measured by LVDT DTi, δ_{DT4} is the vertical displacements of endplate, while δ_{DT6} and δ_{DT9} are the horizontal displacements of beam flanges, see Fig.6.4, h_b is the height of beam section while t_{fb} is the thickness of beam flange. In Eq. (6.2), the deformation of the beam is contributed not only by the deformation itself, but also by the deformation of the column, the deformation of the panel zone and the deformation of connection components. In this experimental study, the column hardly deforms as it behaves almost like a rigid element, which will be validated afterwards.

In tests, the endplate vertical displacement obtained from LVDT DT4 was found very small and not in a range comparable with those from other LVDTs. For illustration, the relationship of applied mechanical load and vertical displacement readings of LVDTs DT1-4 for connection specimen S960 10mm at ambient temperature is shown in Fig.6.10 while the relationship of moment and beam rotation computed according to Eq. (6.2) is presented in Fig.6.11. It can be seen that good agreements exist except the results from DT3, since the displacement sensor DT3 is located closer to the endplate. In this region, the beam theory is not valid and the stress distribution is not smooth. Therefore, the results from displacement sensors DT1 and DT4 are used for further analysis.

The column rotation θ_c can be calculated by the following equations:

$$\theta_c = \arctan\frac{\left|\delta_{DT5}\right|+\left|\delta_{DT10}\right|}{h_c - t_{fc}} = \arctan\frac{\left|\delta_{DT11}\right|+\left|\delta_{DT13}\right|}{h_b - t_{fb}}$$

(6.3)

where h_c is the height of column section and t_{fc} is the thickness of column flange, while h_b is the height of beam section and t_{fb} is the thickness of beam flange; δ_{DT5} and δ_{DT10} are the vertical displacements of column while δ_{DT11} and δ_{DT13} are horizontal ones, see Fig.6.4. The relationship of moment and column rotation computed according to Eq. (6.3) for connection specimen S960

146

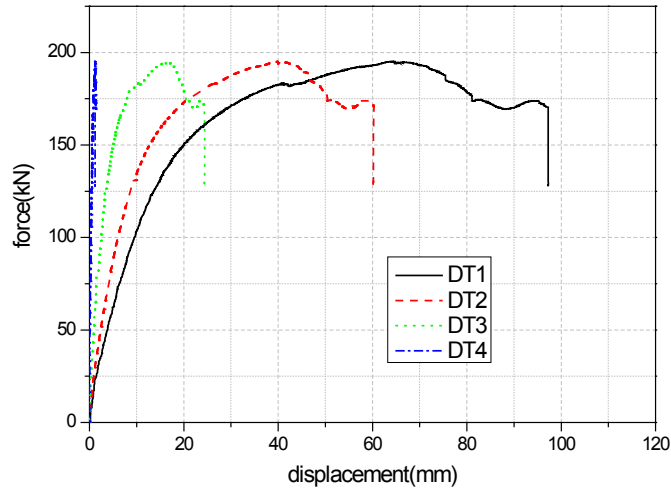10mm at ambient temperature is illustrated in Fig.6.12, where good agreement can be observed.

Fig.6.10. Vertical displacement readings of LVDTs DT1-4 for specimen S960 10mm at ambient temperature.
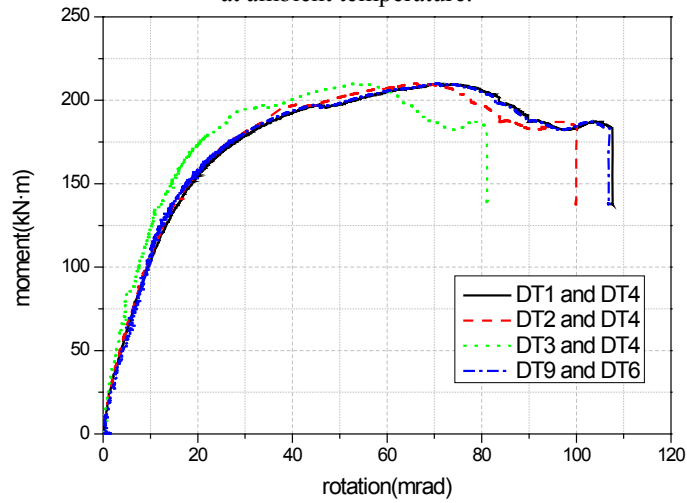

Fig.6.11. Beam rotation computed from the displacement readings for specimen S960 10mm at ambient temperature.
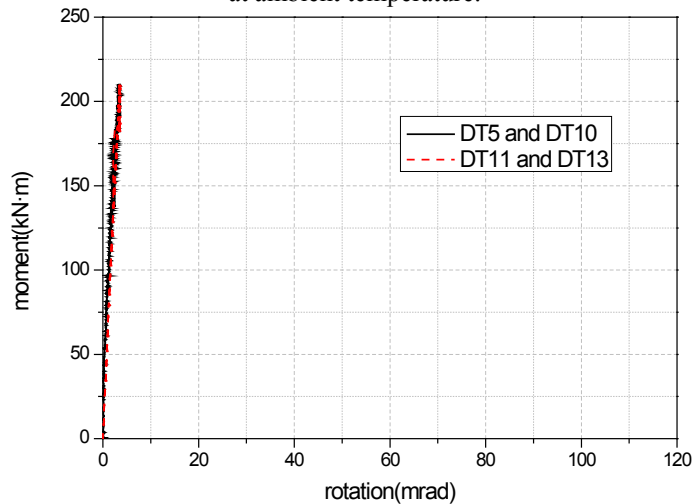

Fig.6.12. Column rotation computed from the displacement readings for specimen S960 10mm at ambient temperature.

What is more, the maximum rotation capacity ϕ_C of a connection, which is defined as the maximum rotation of the moment-rotation characteristic, is illustrated in Fig.6.13, while $\phi_{M\,max}$ is the rotation of connection corresponding to the maximum load level. The rotations of various endplate connections obtained from this experimental study are described hereafter in this section.
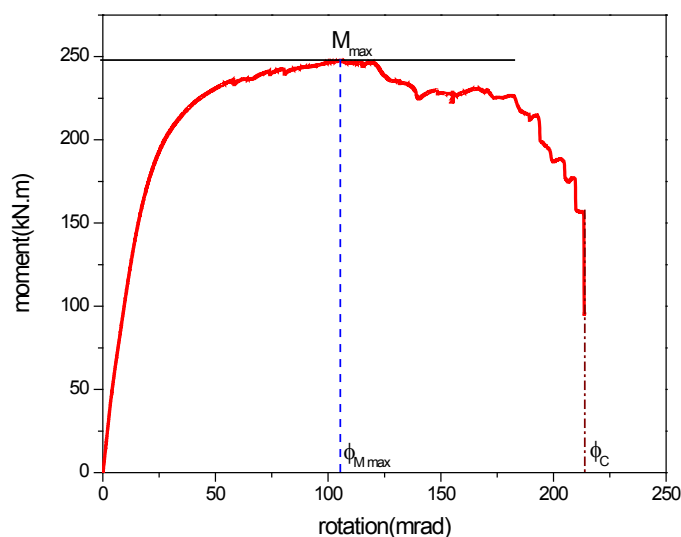

Fig.6.13. Definition of connection rotation capacity.

6.3.2.1 Effect of endplate material and thickness vary at ambient temperature

The load bearing capacity and connection rotation of various connections at ambient temperature obtained from experiments are presented in Table 6.6. The moment-rotation comparison of connections in Series 1 at ambient temperature is shown in Fig.6.14. It can be seen that the load bearing capacity of connection 1-2 A (S690 12mm) is similar to that of connection 1-1 A (Q235 20mm) while the rotational capacity of the former is higher than the latter. In tests, the connection 1-3 A (S960 10mm) at ambient temperature failed due to cracking of the endplate at the heat affected zone of welds after moderate amount of plastic deformation of the endplate, see Fig.B.3 in Appendix B. Hence its rotation capacity is relatively low and not included in the comparison. It highlights that special attention should be paid for the proper design of welds for very thin steel members made of very high strength steels. The moment-rotation comparison of connections in Series 2 at ambient temperature is presented in Fig.6.15.

Table 6.6: Characteristics of connections at ambient temperature

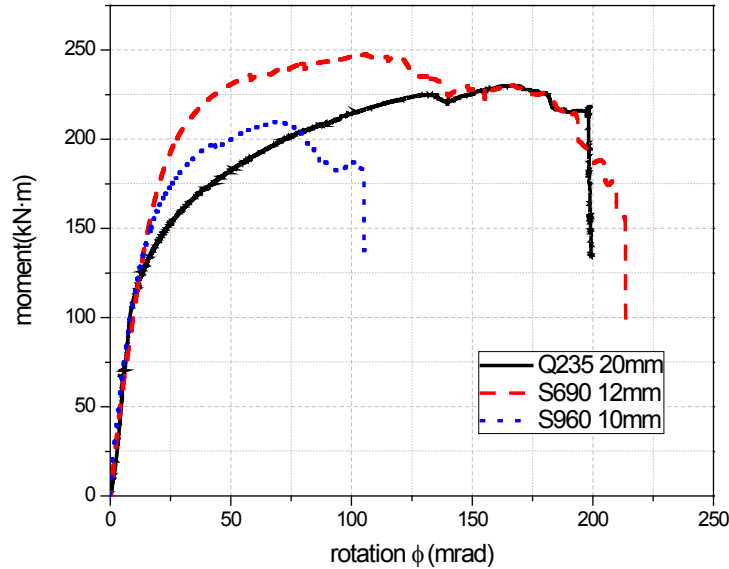| Series | Connection ID | Endplate | | Peak Load | | Connection rotation |
		Material	Thickness (mm)	Moment (kN·m)	Force (kN)	ϕ_C (mrad)
1	1-1 A	Q235	20	229.93	213.69	199
	1-2 A	S690	12	247.85	230.34	214
	1-3 A	S960	10	209.86	195.04	105
2	2-1 A	Q235	25	287.00	266.73	114
	2-2 A	Q345	20	277.25	257.67	115
	2-3 A	S690	15	272.71	253.45	101
	2-4 A	S960	12	264.32	245.65	105

Fig.6.14. Moment-rotation comparison of connections in Series 1 at ambient temperature.
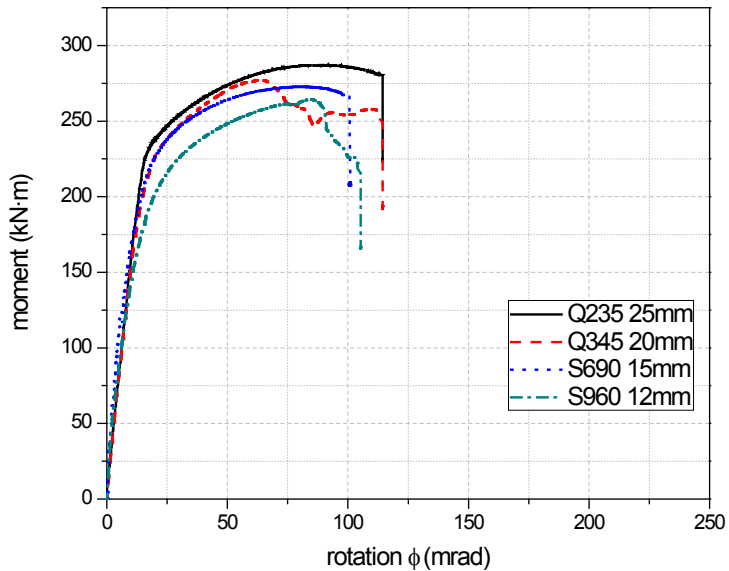

Fig.6.15. Moment-rotation comparison of connections in Series 2 at ambient temperature.

6.3.2.2 Effect of endplate material and thickness vary at elevated temperature

The load bearing capacity and connection rotation of various connections at elevated temperature 550°C obtained from experiments are presented in Table

6.7. The moment-rotation comparison of connections Series 1 at elevated temperature 550°C is shown in Fig.6.16. It can be seen that the load bearing capacities of connection 1-2 E (S690 12mm) and connection 1-3 E (S960 10mm) are higher than that of connection 1-1 E (Q235 20mm), but still in the comparable range. The rotational capacities at elevated temperature 550°C of the three connections in Series 1 are similar to each other. The moment-rotation relationships of connections in Series 2 at elevated temperature 550°C are shown in Fig.6.17. It can be found that the load bearing capacities at elevated temperature 550°C of the four connections in Series 2 are similar to each other, while the rotational capacities of connection 2-2 E (Q345 20mm), connection 2-3 E (S690 15mm) and connection 2-4 E (S960 12mm) are comparable and much higher than that of connection 2-1 E (Q235 25mm).

Table 6.7: Characteristics of connections at elevated temperature 550°C

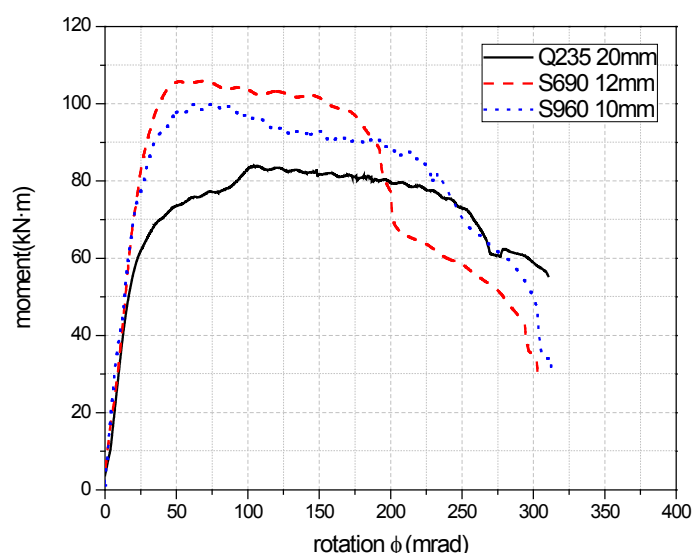| Series	Connection ID	Endplate		Peak load		Connection rotation
		Material	Thickness (mm)	Moment (kN · m)	Force (kN)	ϕ_C (mrad)
1	1-1 E	Q235	20	83.91	77.98	314
	1-2 E	S690	12	105.92	98.44	304
	1-3 E	S960	10	100.05	92.98	313
2	2-1 E	Q235	25	120.40	111.90	191
	2-2 E	Q345	20	111.16	103.31	313
	2-3 E	S690	15	120.78	112.25	330
	2-4 E	S960	12	113.18	105.19	320

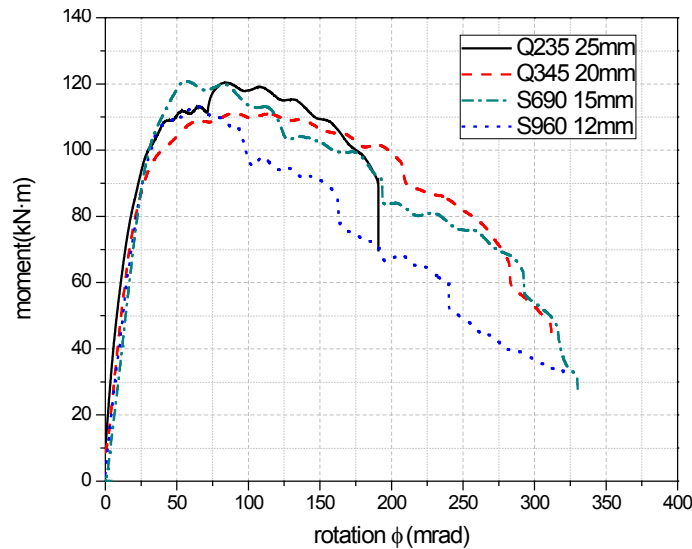Fig.6.16. Moment-rotation comparison of connections Series 1 at elevated temperature 550°C.

Fig.6.17. Moment-rotation comparison of connections Series 2 at elevated temperature 550°C.

A conclusion can be drawn that in endplate connections a proper thinner endplate made of high strength steel can achieve similar load bearing capacity and higher (or at least comparable) rotational capacity both at ambient temperature and at elevated temperatures in comparison to a thicker endplate made of mild steel.

6.3.2.3 Effect of endplate thickness varies at ambient temperature

To state the influence of endplate thickness, the moment-rotation curves of connections with the same endplate material (Q235, S690 and S960) are shown in Fig.6.18-6.20. It can be observed that for endplate connections of which the endplates are made of the same steel material, with a thicker endplate the connection can achieve higher load bearing capacity but its rotational capacity is reduced obviously at ambient temperature. The connections made of S960 as shown in Fig.6.20 are the exception, because of the early cracking of the endplate at the heat affected zone of welds after some plastic deformations on the endplate for connection S960 10mm, see Fig.B.3 in Appendix B.
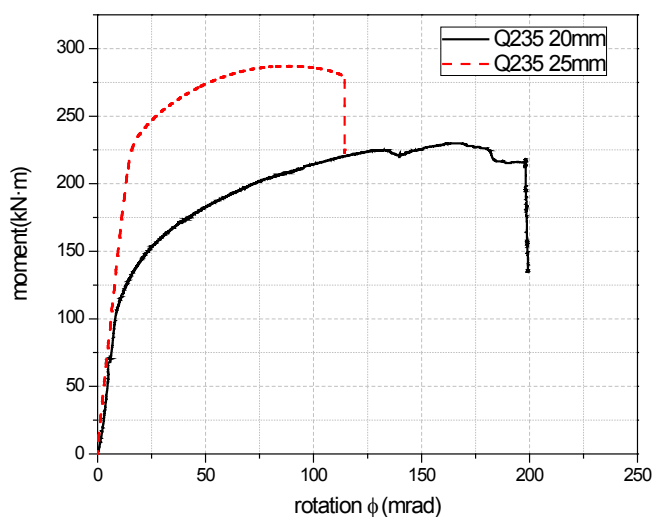
Fig.6.18. Effect of endplate thickness in connections with endplate made of Q235 at ambient temperature.
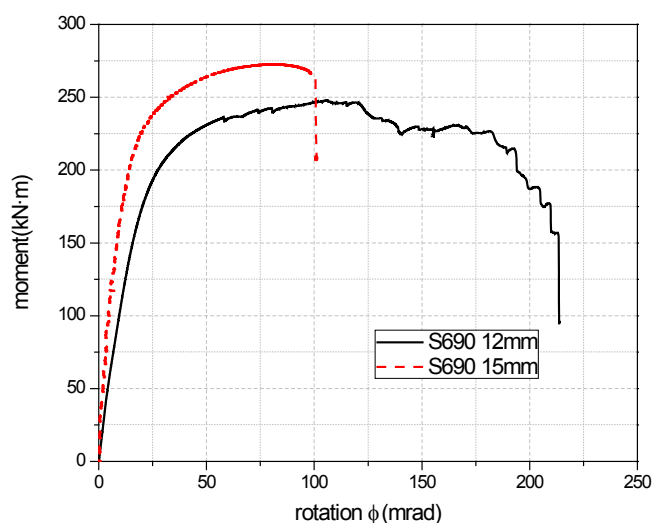

Fig.6.19. Effect of endplate thickness in connections with endplate made of S690 at ambient temperature.
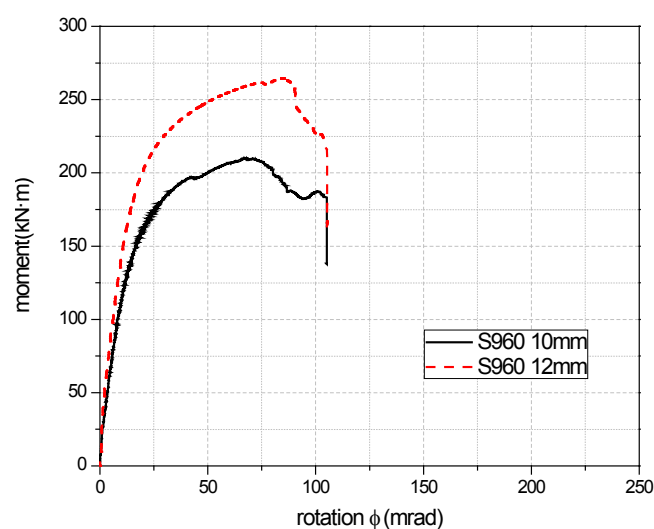

Fig.6.20. Effect of endplate thickness in connections with endplate made of S960 at ambient temperature.

6.3.2.4 Effect of endplate thickness varies at elevated temperature

To state the influence of endplate thickness, the moment-rotation curves at elevated temperature 550°C of connections with the same endplate material are shown in Figs.6.21-6.23 for Q235, S690 and S960 respectively. It can be found that for endplate connections of which the endplates are made of mild steel Q235, with a thicker endplate the connection can achieve higher load bearing capacity at elevated temperature but its rotational capacity at elevated temperature is reduced.
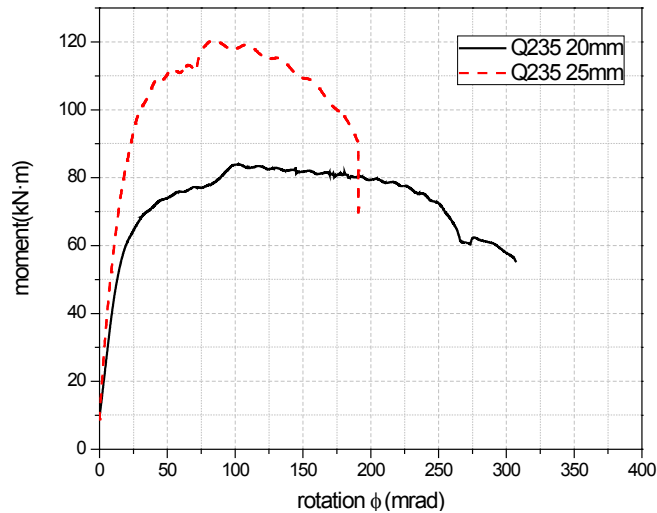

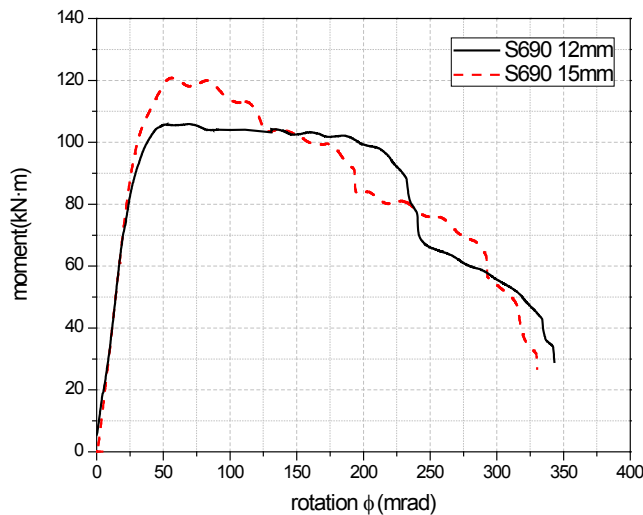Fig.6.21. Effect of endplate thickness in connections with endplate made of Q235 at elevated temperature 550°C.

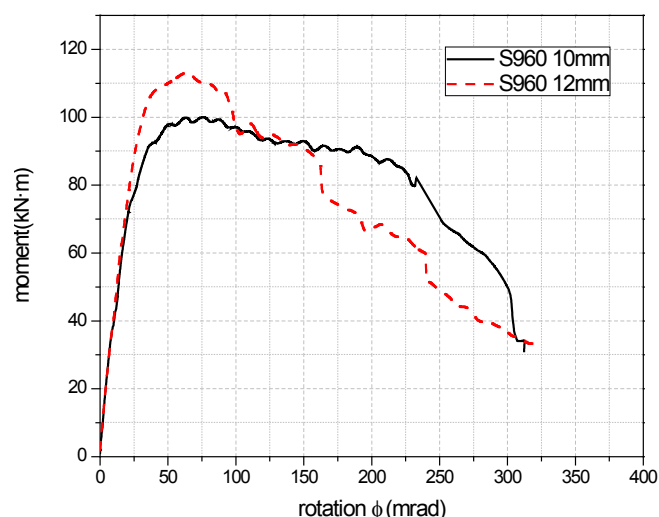Fig.6.22. Effect of endplate thickness in connections with endplate made of S690 at elevated temperature 550°C.

Fig.6.23. Effect of endplate thickness in connections with endplate made of S960 at elevated temperature 550°C.

6.3.3 Rotation capacity of endplate connections

The connection rotations for all endplate connections at ambient and elevated temperatures obtained from tests are presented in Tables 6.8 and 6.9 respectively.

Table 6.8: Connection rotation at ambient temperature obtained in tests

Series	Connection ID	Endplate		Connection rotation	
		Material	Thickness (mm)	$\phi_{M\,max}$ (mrad)	ϕ_C (mrad)
	1-1 A	Q235	20	168	199
1	1-2 A	S690	12	105	214
	1-3 A	S960	10	69	105
	2-1 A	Q235	25	89	134
2	2-2 A	Q345	20	63	130
	2-3 A	S690	15	83	101
	2-4 A	S960	12	85	105

Table 6.9: Connection rotation at elevated temperature 550°C obtained in tests

Series	Connection ID	Endplate		Connection rotation	
		Material	Thickness (mm)	$\phi_{M\,max}$ (mrad)	ϕ_C (mrad)
	1-1 E	Q235	20	106	314
1	1-2 E	S690	12	69	304
	1-3 E	S960	10	76	313
	2-1 E	Q235	25	84	191
2	2-2 E	Q345	20	90	313
	2-3 E	S690	15	58	330
	2-4 E	S960	12	64	320

6.4 DISCUSSION

6.4.1 Failure modes

According to Eurocode 3 Part:1-8 [1], there are 3 failure modes for endplate connections. Mode 1 is complete yielding of endplate or column flange, Mode

2 is bolt failure with yielding of endplate or column flange, while Mode 3 is bolt failure. Mode 3 is considered to be brittle and should be avoided in practical design. The failure modes of all endplate connections can be obtained via theoretical analysis based on the rules of Eurocode 3 Part:1-8 [1]. The detailed analysis procedure is presented in Appendix C of this thesis.

6.4.1.1 At ambient temperature

The failure modes of endplate connections at ambient temperature obtained from theoretical analysis based on Eurocode 3 Part:1-8 [1] and experimental study are listed in Table 6.10. It can be observed that good agreement exists between theoretical analysis and experimental study.

Table 6.10: Failure modes of endplate connections at ambient temperature

Connection ID	Endplate		Failure mode	
	Material	Thickness (mm)	EC3	Test
1-1 A	Q235	20	Mode 1	Mode 1
1-2 A	S690	12	Mode 1	Mode 1
1-3 A	S960	10	Mode 1	Mode 1
2-1 A	Q235	25	Mode 2	Mode 2
2-2 A	Q345	20	Mode 2	Mode 2
2-3 A	S690	15	Mode 2	Mode 2
2-4 A	S960	12	Mode 2	Mode 2

6.4.1.2 At elevated temperatures

Table 6.11: Failure modes of connections at elevated temperature 550°C

Connection ID	Endplate		Failure mode	
	Material	Thickness (mm)	EC3	Test
1-1 E	Q235	20	Mode 2	Mode 2
1-2 E	S690	12	Mode 2	Mode 2
1-3 E	S960	10	Mode 2	Mode 2
2-1 E	Q235	25	Mode 2	Mode 2
2-2 E	Q345	20	Mode 2	Mode 2
2-3 E	S690	15	Mode 2	Mode 2
2-4 E	S960	12	Mode 2	Mode 2

The failure modes of endplate connections at elevated temperature 550°C obtained from theoretical analysis based on Eurocode 3 Part:1-8 [1] and experimental study are listed in Table 6.11. It can be found that there is good agreement between theoretical analysis and experimental study.

It is worthwhile to mention that the failure modes of all connections in series 1 turned from Mode 1 at ambient temperature to Mode 2 at elevated temperature 550°C. This phenomenon attributes to the fact that the reduction of material properties of bolts in fire is quicker than that of structural steels, according to

the reduction factors of material properties of bolts and mild steels in fire recommended in Eurocode 3 Part:1-2 [3] and the experimental results on the material properties reduction factors of high strength steels in fire as presented in Chapter 4.

Further, it can be found that in each connection series both at ambient and at elevated temperatures the failure modes of connections are the same. Thus all in all, in endplate connections an optimal design using a thinner high strength steel endplate can achieve the same failure mode, similar load bearing capacity and comparable or even higher rotation capacity in comparison to an endplate connection with thicker mild steel endplate. This experimental study offers reliable understandings on performance of high strength steel endplate connections both in fire and at ambient temperature. It probably opens a perspective using high strength steels instead of mild steels in practical structural design to some extent.

6.4.2 Plastic flexural resistance of endplate connections

Eurocode 3 part 1-8 [1] gives quantitative rules for the prediction of plastic flexural resistance (design moment resistance) $M_{j,Rd}$ of beam-to-column connections. The prediction based on Eurocode 3 was performed on all test connection specimens at ambient and elevated temperatures. The detailed procedure and results are presented in Appendix C.

For experimental study, a question arises on how to determine the plastic flexural resistance $M_{j,R}$ from a specific test result. In literature, Steenhuis and Snijder et al. [4] give an overview of approaches how to determine the plastic flexural resistance $M_{j,R}$ from a test result. Jaspart [5] proposes that the plastic flexural resistance can be read at the vertical axis from a test moment-rotation curve by drawing a secant line through the part of the test curve with post-limit stiffness, see Fig.6.24. Alternatively, Zanon and Zandonini [6] give a definition of plastic flexural resistance $M_{j,R}$ as shown in Fig.6.25, where the plastic flexural resistance $M_{j,R}$ corresponds to the intersection of the initial stiffness and the post-limit stiffness. Weynand [7] suggests another definition. In his case, the initial stiffness of the connection is assessed as the elastic stiffness of the M-Φ curve. Then, a secant stiffness is determined as the initial stiffness divided by a fixed stiffness modification coefficient η. The plastic

flexural resistance $M_{j,R}$ is defined as the moment level, where this secant stiffness intersects with the experiment $M\text{-}\Phi$ curve, as illustrated in Fig.6.26.
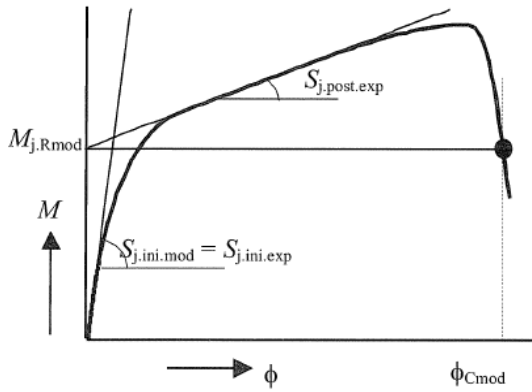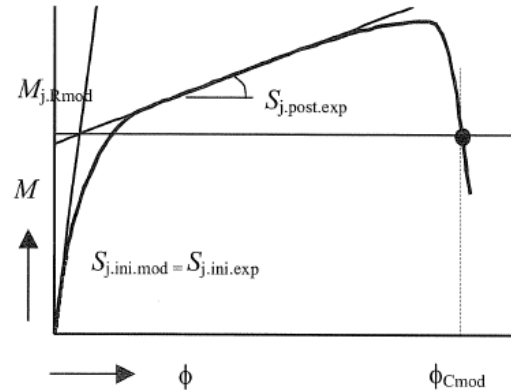

Fig.6.24. $M_{j,R}$ according to Jaspart[5].   Fig.6.25. $M_{j,R}$ according to Zanon and Zandonini [6].
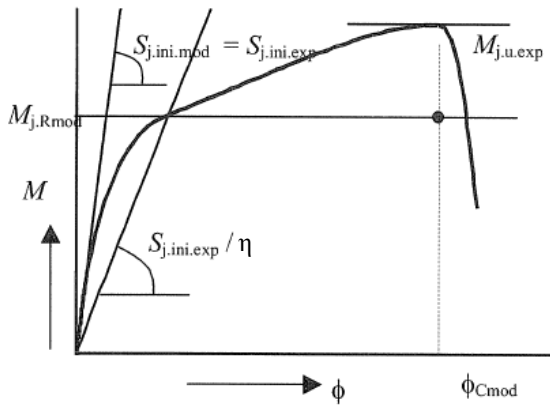

Fig.6.26. $M_{j,R}$ according to Weynand[7].

Eurocode 3 part 1-8 [1] includes Weynand's proposal [7], as a simplified method to obtain the plastic flexural resistance of connections. In the simplified method, the initial rotational stiffness of the connection ($S_{j,ini}$) and the moment-rotation curve are used to obtain the plastic flexural resistance value. Firstly, the secant stiffness (S_j) is calculated by Eq.6.4, where stiffness modification coefficient η is 2 for beam-to-column bolted endplate connections, as illustrated in Table 5.2 of Eurocode 3 part 1-8 [1]. Then the plastic flexural resistance can be obtained by the intersection of the moment rotation curve and a straight line from the origin with slope S_j.

$$S_j = S_{j,ini} / \eta \tag{6.4}$$

In this thesis, Zanon and Zandonini's proposal is employed as Method 1 to obtain the plastic flexural resistance $M_{j,Rd,test,1}$ of the endplate connection from an experimental moment-rotation curve. For comparison, the simplified method recommended in Eurocode 3 part 1-8 [1] is used as Method 2 to obtain the plastic flexural resistance $M_{j,Rd,test,2}$ (for instance see Fig.6.27). The plastic flexural resistances of endplate connections obtained from experimental study

through these two methods are compared with the predictions of Eurocode 3, as shown in Figs.6.27-6.40.

6.4.2.1 At ambient temperature:

The plastic flexural resistances of all endplate connections at ambient temperature obtained from this experimental study are compared with the theoretical predictions of Eurocode 3, as listed in Table 6.12. It can be observed that reasonable agreements exist between the theoretical predictions and experimental results. Via Ratio$_3$, presented in Table 6.12, the observation can be found that $M_{j,Rd,test,1}$ obtained based on Zanon and Zandonini's definition is generally smaller than $M_{j,Rd,test,2}$, which is defined according to Weynand's proposal and the simplified method recommend by Eurocode 3. By comparing $M_{j,Rd,test,1}$ with the predicted plastic flexural resistance according to Eurocode 3, it can be seen that the predictions of Eurocode 3 are generally on the non-conservative side when the test result is obtained based on Zanon and Zandonini's definition. However, the comparison of $M_{j,Rd,test,2}$ with the predicted plastic flexural resistance according to Eurocode 3 shows that the predictions of Eurocode 3 are generally on the conservative side.

Table 6.12: Evaluation of plastic flexural resistance of connections at ambient temperature

Test ID	Connections	$M_{j,Rd,EC3}$ (kN·m)	$M_{j,Rd,test,1}$ (kN·m)	$M_{j,Rd,test,2}$ (kN·m)	Ratio$_1$= $\dfrac{M_{j,Rd,EC3}}{M_{j,Rd,test,1}}$	Ratio$_2$= $\dfrac{M_{j,Rd,EC3}}{M_{j,Rd,test,2}}$	Ratio$_3$= $\dfrac{M_{j,Rd,test,1}}{M_{j,Rd,test,2}}$
1-1 A	Q235 20mm	167.07	155.61	153.20	1.074	1.091	1.016
1-2 A	S690 12mm	176.04	207.18	222.73	0.850	0.790	0.930
1-3 A	S960 10mm	170.62	159.98	181.98	1.067	0.938	0.879
2-1 A	Q235 25mm	245.14	243.15	259.41	1.008	0.945	0.937
2-2 A	Q345 20mm	239.79	235.79	255.04	1.017	0.940	0.925
2-3 A	S690 15mm	248.54	225.92	233.22	1.100	1.066	0.969
2-4 A	S960 12mm	234.17	199.65	202.987	1.173	1.154	0.984

Note:

$M_{j,Rd,EC3}$ is the predicted plastic flexural resistance according to Eurocode 3;

$M_{j,Rd,test,1}$ is the test obtained plastic flexural resistance according to Zanon and Zandonini's evaluation method;

$M_{j,Rd,test,2}$ is the test obtained plastic flexural resistance according to Weynand's evaluation method.

Fig.6.27 compares the plastic flexural resistance $M_{j,Rd}$ predicted by Eurocode 3 with the tested moment-rotation curve of connection 1-1 A (Q235 20mm), and with the test obtained plastic flexural resistances $M_{j,Rd,test,1}$ and $M_{j,Rd,test,2}$. It can be seen that $M_{j,Rd,EC3}$ is slightly higher than $M_{j,Rd,test,1}$ and $M_{j,Rd,test,2}$ for connection 1-1 A (Q235 20mm) at ambient temperature.

The plastic flexural resistance $M_{j,Rd}$ of connection 1-2 A (S690 12mm) predicted by Eurocode 3 is compared with the tested moment-rotation curve and experimentally obtained plastic flexural resistances $M_{j,Rd,test,1}$ and $M_{j,Rd,test,2}$, as shown in Fig.6.28. It can be observed that the plastic flexural resistance $M_{j,Rd,test,1}$ obtained based on Zanon and Zandonini's definition is smaller than that of $M_{j,Rd,test,2}$ obtained according to Weynand's definition. What is more, the prediction of Eurocode 3 $M_{j,Rd,EC3}$ is conservative in comparison to $M_{j,Rd,test,1}$ and $M_{j,Rd,test,2}$ for connection 1-2 A (S690 12mm) at ambient temperature.

As shown in Fig.6.29, the plastic flexural resistance $M_{j,Rd}$ of connection 1-3 A (S960 10mm) predicted according to Eurocode 3 is compared with the tested moment-rotation curve and experimentally obtained plastic flexural resistances $M_{j,Rd,test,1}$ and $M_{j,Rd,test,2}$. It can be found that the plastic flexural resistance $M_{j,Rd,test,1}$ obtained based on Zanon and Zandonini's definition is smaller than that of $M_{j,Rd,test,2}$ obtained according to Weynand's definition. Moreover, the prediction of Eurocode 3 $M_{j,Rd,EC3}$ is between $M_{j,Rd,test,1}$ and $M_{j,Rd,test,2}$ for connection 1-3 A (S960 10mm) at ambient temperature.

The comparison of the plastic flexural resistance $M_{j,Rd}$ predicted by Eurocode 3 with the tested results by two definition methods for the four connections in Serries 2 at ambient temperature are presented in Figs.6.30-6.33.
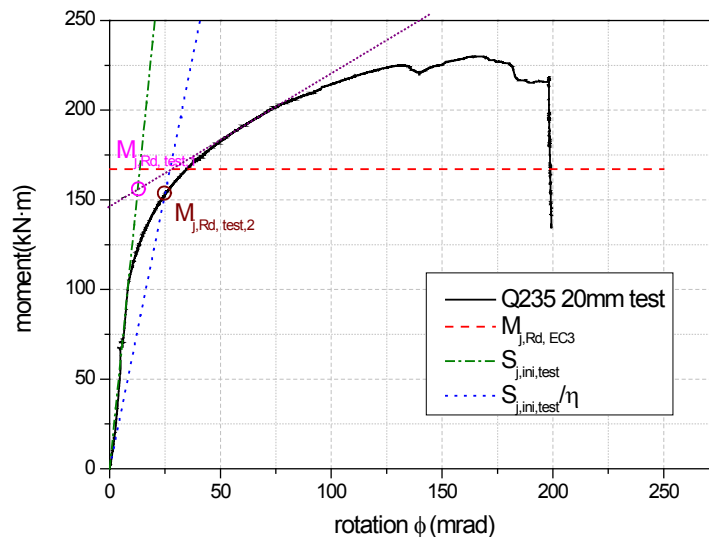

Fig.6.27. Comparison on plastic flexural resistance of 1-1 A (Q235 20mm) at ambient temperature.
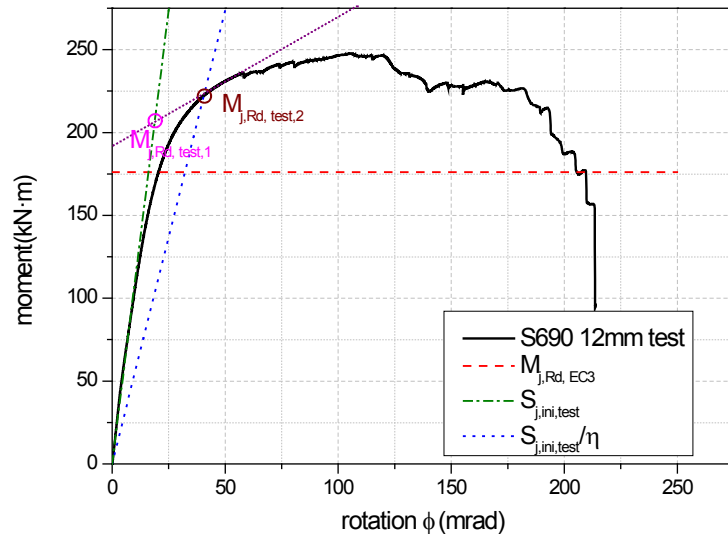
Fig.6.28. Comparison on plastic flexural resistance of 1-2 A (S690 12mm) at ambient temperature.
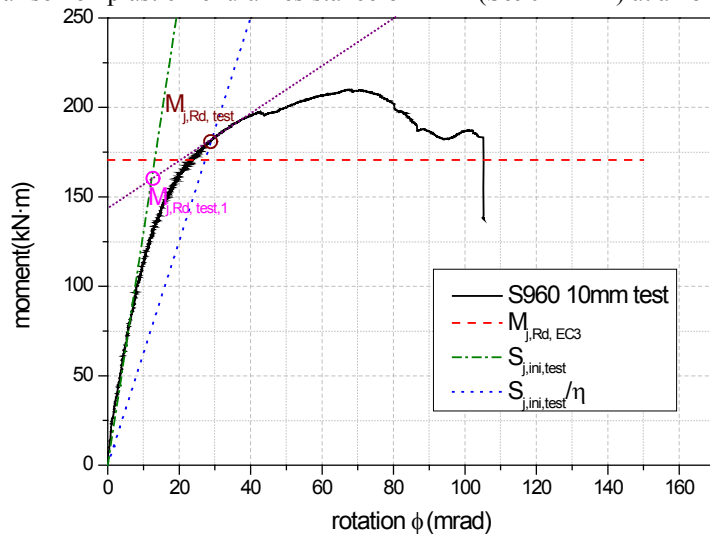

Fig.6.29. Comparison on plastic flexural resistance of 1-3 A (S960 10mm) at ambient temperature.
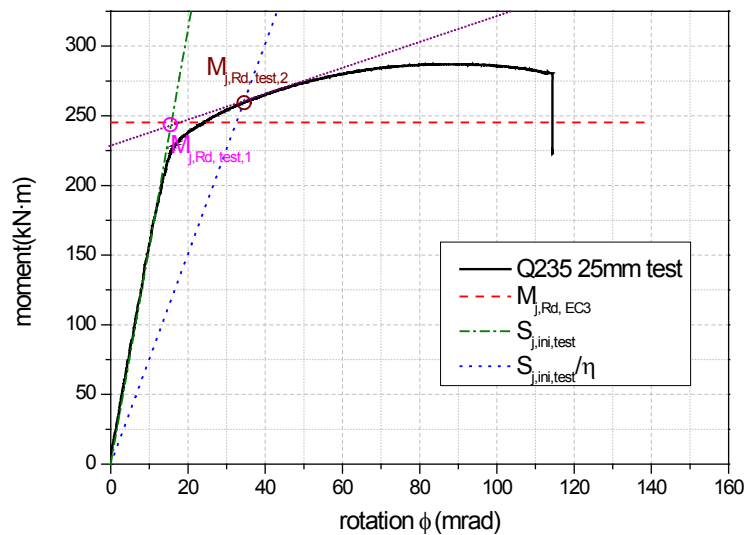

Fig.6.30. Comparison on plastic flexural resistance of Q235 25mm at ambient temperature (2-1A).
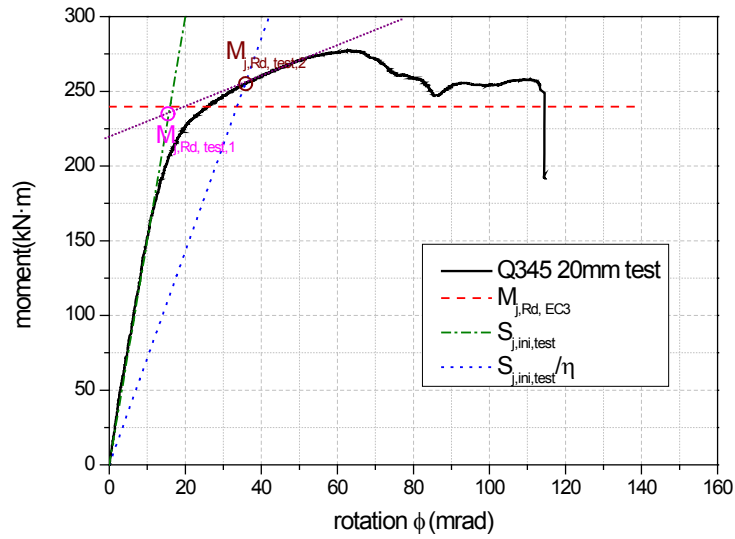
Fig.6.31. Comparison on plastic flexural resistance of Q345 20mm at ambient temperature (2-2A).
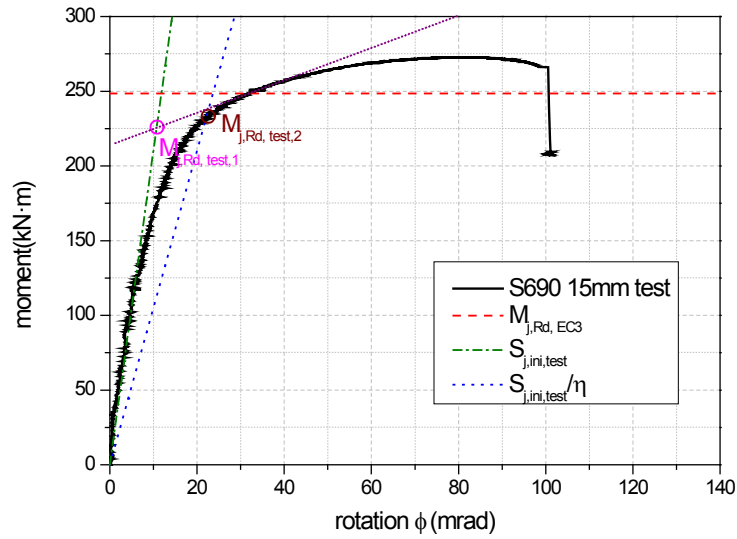

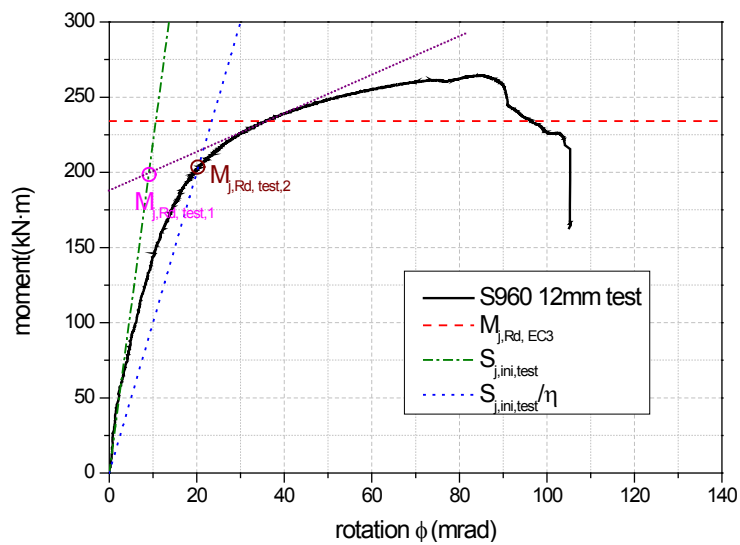Fig.6.32. Comparison on plastic flexural resistance of S690 15mm at ambient temperature (2-3A).

Fig.6.33. Comparison on plastic flexural resistance of S960 12mm at ambient temperature (2-4A).

161

6.4.2.2 At elevated temperature 550°C:

The plastic flexural resistances of all endplate connections at elevated temperature 550°C are compared with the theoretical predictions of Eurocode 3, as listed in Table 6.13. It can be seen that reasonable agreements exist between the theoretical predictions and the experimental results.

Table 6.13: Evaluation of design moment resistance of connections at elevated temperature 550°C

Test ID	Connections	$M_{j,Rd,EC3}$ (kN·m)	$M_{j,Rd,test,1}$ (kN·m)	$M_{j,Rd,test,2}$ (kN·m)	Ratio$_1$= $\dfrac{M_{j,Rd,EC3}}{M_{j,Rd,test,1}}$	Ratio$_2$= $\dfrac{M_{j,Rd,EC3}}{M_{j,Rd,test,2}}$	Ratio$_3$= $\dfrac{M_{j,Rd,test,1}}{M_{j,Rd,test,2}}$
1-1 E	Q235 20mm	76.77	68.13	72.94	1.127	1.053	0.934
1-2 E	S690 12mm	89.90	89.99	105.38	0.999	0.853	0.854
1-3 E	S960 10mm	95.26	84.68	93.74	1.125	1.016	0.903
2-1 E	Q235 25mm	109.29	106.50	108.79	1.026	1.005	0.979
2-2 E	Q345 20mm	107.37	104.68	105.86	1.026	1.014	0.989
2-3 E	S690 15mm	105.94	101.25	120.02	1.046	0.883	0.844
2-4 E	S960 12mm	105.41	104.83	111.90	1.006	0.942	0.937

Note:

$M_{j,Rd,EC3}$ is the predicted plastic flexural resistance according to Eurocode 3;

$M_{j,Rd,test,1}$ is the test obtained plastic flexural resistance according to Zanon and Zandonini's evaluation method;

$M_{j,Rd,test,2}$ is the test obtained plastic flexural resistance according to Weynand's evaluation method.

By comparing Ratio$_3$, presented in Table 6.13, it can be found that $M_{j,Rd,test,1}$ obtained based on Zanon and Zandonini's definition is generally smaller than $M_{j,Rd,test,2}$, which is defined according to Weynand's proposal as well as the simplified method recommended by Eurocode 3. By comparing $M_{j,Rd,test,1}$ with the predicted plastic flexural resistance by Eurocode 3, see Ratio$_1$ as presented in Table 6.13, it can be seen that the predictions of Eurocode 3 are generally non-conservative when the test result is obtained based on Zanon and Zandonini's definition.

However, the comparison of $M_{j,Rd,test,2}$ with the predicted plastic flexural resistance by Eurocode 3 shows that the predictions of Eurocode 3 are generally on the conservative side, when the definition of the test result is based on Weynand's proposal and the simplified method recommended by Eurocode 3.

The comparison of the plastic flexural resistance $M_{j,Rd}$ predicted by Eurocode 3 with the experimentally obtained plastic flexural resistances $M_{j,Rd,test,1}$ and

$M_{j,Rd,test,2}$ for these seven endplate connections at elevated temperature 550°C are presented in Figs.6.34-6.40.

Fig.6.34. Comparison on plastic flexural resistance of 1-1 E (Q235 20mm) at elevated temperature 550°C.

Fig.6.35. Comparison on plastic flexural resistance of 1-2 E (S690 12mm) at elevated temperature 550°C.

Fig.6.36. Comparison on plastic flexural resistance of 1-3 E (S960 10mm) at elevated temperature 550°C.
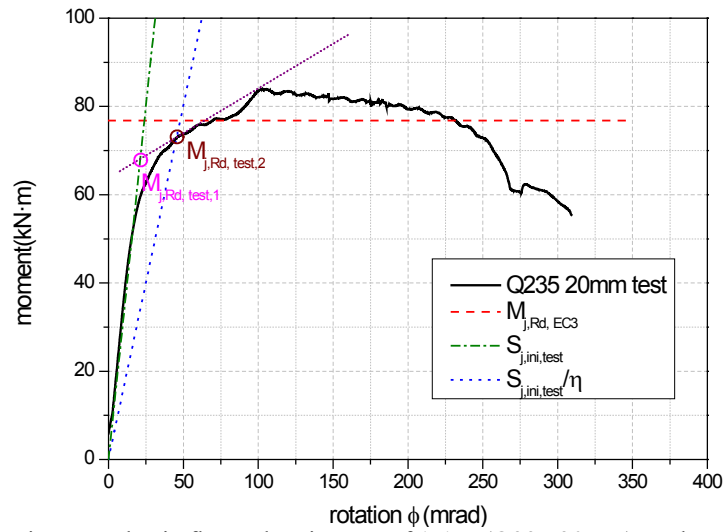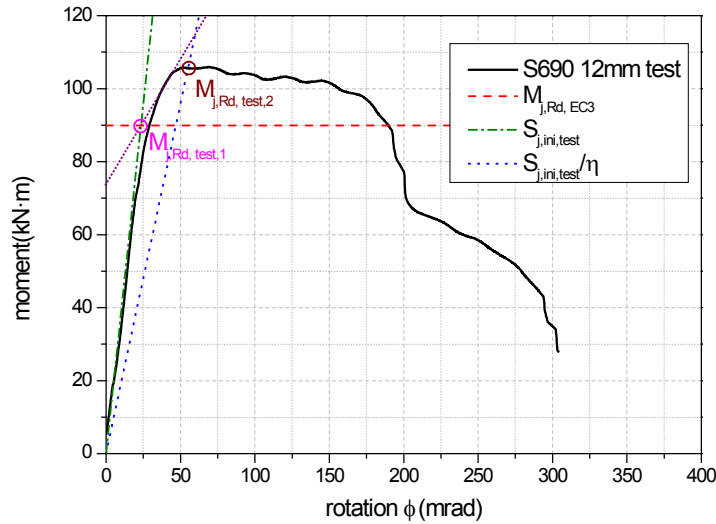
Fig.6.37. Comparison on plastic flexural resistance of 2-1 E (Q235 25mm) at elevated temperature 550°C.

Fig.6.38. Comparison on plastic flexural resistance of 2-2 E (Q345 20mm) at elevated temperature 550°C.

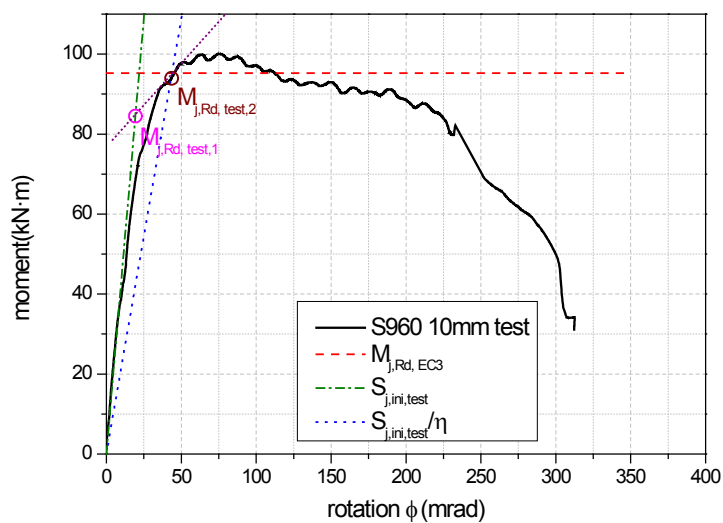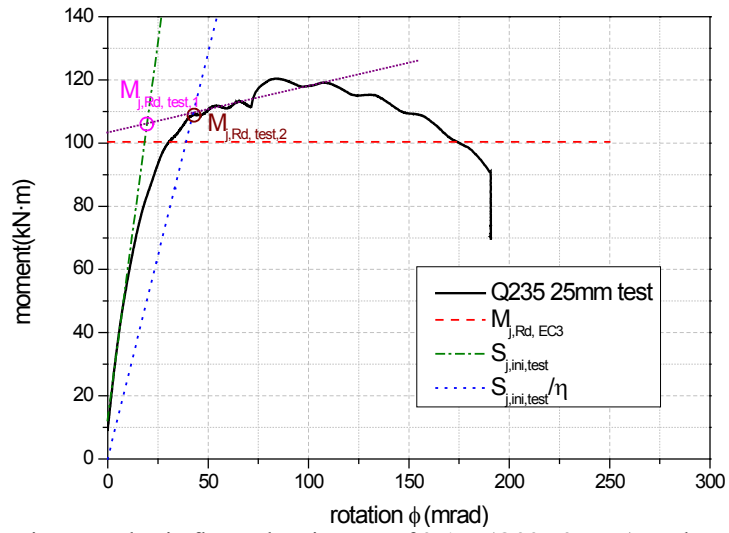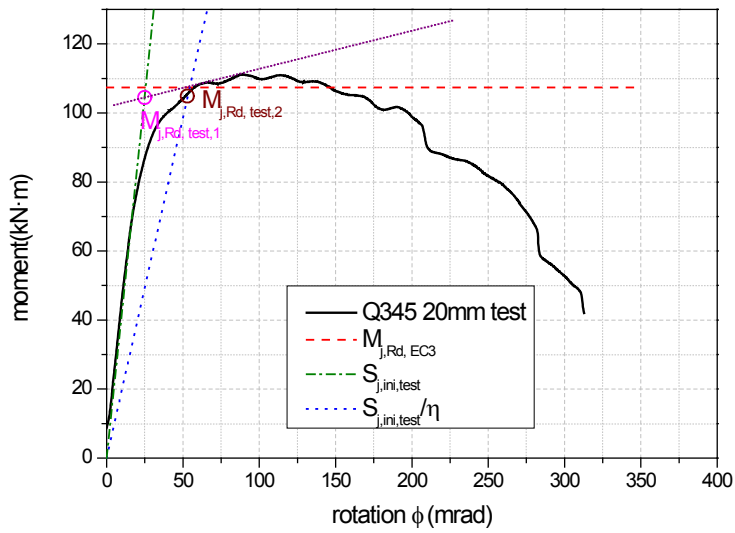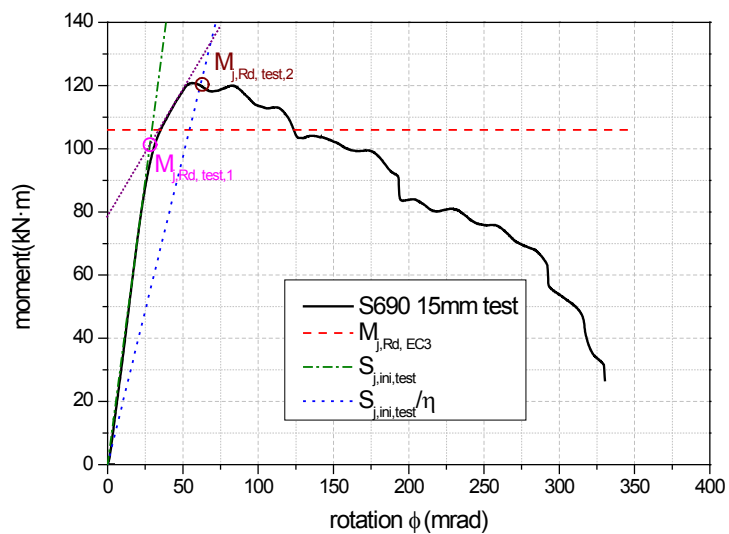Fig.6.39. Comparison on plastic flexural resistance of 2-3 E (S690 15mm) at elevated temperature 550°C.
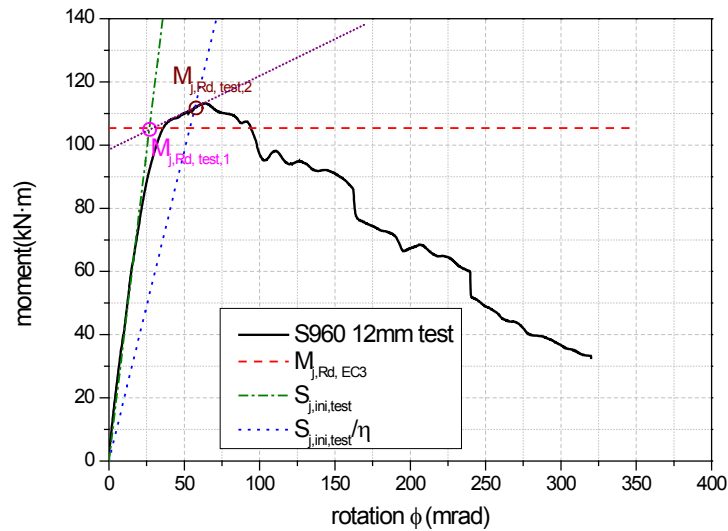
Fig.6.40. Comparison on plastic flexural resistance of 2-4 E (S960 12mm) at elevated temperature 550°C.

6.4.3 Rotation capacity of endplate connections

Eurocode 3 part 1-8 [1] states that at ambient temperature a bolted endplate connection may be assumed to have sufficient rotation capacity for plastic analysis, provided that both of the following conditions are satisfied: i) the moment resistance of the connection is governed by the resistance of either the column flange in bending or the endplate in bending; ii) the thickness t of either the column flange or the endplate (not necessarily the same basic component as in (i)) satisfies:

$$t \leq 0.36d\sqrt{\frac{f_{u,b}}{f_y}} \tag{6.5}$$

where d is the bolt diameter, $f_{u,b}$ is the tensile strength of the bolt and f_y is the yield stress of the relevant basic component (column flange or the endplate). The verification of these guidelines in Eurocode 3 part 1-8 [1] with the characterization of the rotation capacity of endplate connections obtained from tests is conducted. It can be found that the first condition is guaranteed for all specimens (the connection moment resistance is always governed by the resistance of the endplate in bending), while the second condition, Eq. (6.5) is not satisfied for all specimens, as listed in Table 6.14.

Table 6.14:Verification of the guidelines of EC3 on rotation capacity at ambient temperature

Connection ID	Endplate		
	Material	Thickness t_{ep} (mm)	Max thickness t_{ep} (mm) according to EC3
1-1 A	Q235	20	18
1-2 A	S690	12	11
1-3 A	S960	10	9
2-1 A	Q235	25	18
2-2 A	Q345	20	15
2-3 A	S690	15	11
2-4 A	S960	12	9

In literature it is generally accepted that a minimum of 40-50mrad ensures "sufficient rotation capacity" of a bolted joint in a partial strength scenario [8-10]. Wilkinson et al. [10] suggested that a connection in steel moment resisting frames in a seismic area must develop a minimum plastic rotation of 30mrad. What is more, Girao Coelho [9] conducted experimental study on endplate connections at ambient temperature, with endplates made of S355 (3 specimens with different geometries) and S690 (1 specimen). In her tests, only one specimen with endplate made of S355 satisfied with the criterion of Eurocode 3 part 1-8, while all her test results easily met with the "40-50" mrad criterion. For the present experimental study, Table 6.6 shows that the maximum rotation capacities ϕ_C of all specimens at ambient temperature in this study are much higher than 40-50mrad, even for all specimens the rotations at maximum load $\phi_{M\,max}$ guarantee this condition as well. Therefore, the Eurocode 3 [1] current provisions seem too conservative on rotation capacity of bolted endplate connections. In addition, the current provisions on sufficient rotation capacity of connections in Eurocode 3 were mainly obtained from bolted connections made of mild steels, and they need to be calibrated when applied to connections made of high strength steels or very high strength steels. In order to establish more accurate criteria for connections made of high strength steels, further work such as more repetitive tests as well as parametric study are still required in practice.

The maximum rotation capacity ϕ_C at elevated temperature 550°C of all specimens in this experimental study is higher in comparison to that at ambient temperature. For all specimens at elevated temperature 550°C, the connection rotation at maximum load $\phi_{M\,max}$ is higher than 40-50mrad, which is the minimum connection rotation to be considered to have sufficient rotation capacity for partial strength connections. Hence the rotation capacity of high strength steel endplate connections in fire is considered to be sufficient, which guarantees the ductility and fire safety of steel structures using endplate connections made of high strength steel.

6.5 CONCLUSION

Fire tests on 7 endplate connections of which the endplates are made of high strength steels (or mild steels for comparison) were reported in this chapter. As reference, the full scale tests on these 7 endplate connections at ambient temperature were also conducted and presented herein. All specimens were designed to trigger failure in the endplate connections rather than in beam or column. The following conclusions can be drawn from this experimental study:

1. The load bearing capacity as well as rotation capacity of endplate connections is dependent on the combination of endplate material and endplate thickness.

2. For endplate connections the endplates of which are made of the same steel material, with a thicker endplate the connection can achieve higher load bearing capacity but its rotational capacity is reduced obviously at both ambient temperature and elevated temperatures. This is valid for both mild steels (i.e. Q235) and high strength steels (i.e. S690 and S960).

3. The accuracy of Eurocode 3 for plastic flexural resistance of endplate connections both at ambient temperature and in fire is acceptable, no matter the endplate is made of mild steels or high strength structural steels.

4. The plastic flexural resistance of connections based on the definition of Zanon and Zandonini is generally smaller than that according to Weynand's proposal as well as the simplified method recommend by Eurocode 3. This conclusion is valid for all endplate connections in this experimental study (both mild steel endplate connections and high strength steel endplate connections) at ambient and elevated temperatures.

5. The Eurocode 3 current provisions on rotation capacity of bolted connections seem too conservative, which were mainly obtained from connections made of mild steels. They need to be calibrated when applied to connections made of high strength steels and very high strength steels.

6. The rotation capacity of high strength steel endplate connections in fire is considered to be sufficient, which guarantees the ductility and fire safety of steel structures using connections made of high strength steel.

7. In endplate connections, a proper design using a relatively thin high strength steel endplate can achieve the same failure mode, similar load bearing capacity and comparable or even higher rotation capacity, both

at ambient temperature and in fire, in comparison to a connection with relatively thick mild steel endplate.

8. This experimental study opens a perspective of using high strength steels to take place of mild steels in structural design. For practical applications and fire-resistance design of other types of connections and structural members, more research work (such as tests on more types of connections and parametric studies) should be further conducted on the behaviour of high strength steel structures in fire.

6.6 REFERENCES

[1] European Committee for Standardization (CEN), EN 1993-1-8, Eurocode3: Design of steel structures, Part 1-8: Design of joints, Brussels , 2005.

[2] Chinese Committee for Standardization, GB/T 11256-2005, The hot-rolled H and cut T section, China, 2005.

[3] CEN, Eurocode 3 - Design of steel structures - Part 1-2: General rules - Structural fire design, in, CEN, Brussels, 2005.

[4] C.M. Steenhuis, A.C.W.M. Vrouwenvelder, F.van Herwijnen, H.H. Snijder, Definitions of resistance and deformation capacity for non-sway steel and composite structures, Heron, Vol.47, No.1 (2002).

[5] J.P. Jaspart, Study of the semi-rigidity of beam-to-column joints and its influence on the resistance and stability of steel buildings, PhD thesis, Liège University, 1991.

[6] P. Zanon, R. Zandonini, Experimental analysis of end plate connections, Proceedings of the state of the art workshop on connections and the behaviour of strength and design of steel structures, Cachan, pp.41-51, 1988.

[7] K. Weynand, Sicherheits- und Wirtschaftlichkeitsuntersuchungen zur Anwendung nachgiebiger Anschlüsse im Stahlbau. Heft 35, Shaker Verlag, Aachen, 1997.

[8] Ana M. Girão Coelho, Luís Simões da Silva, Frans S. K. Bijlaard, Ductility analysis of bolted extended end plate beam-to-column connections in the framework of the component method, Steel and composite structures, 6, 33-53(2006).

[9] Ana M. Girão Coelho, Characterization of the ductility of bolted end plate beam-to-column steel connections, PhD thesis, University of Coimbra, 2004.

[10] S. Wilkinson, G. Hurdman, A. Crowther, A moment resisting connection for earthquake resistant structures, J Constr Steel Res, 62, 295–302 (2006).

Chapter 7

Numerical analysis of HSS endplate connections at ambient temperature and in fire

7.1 INTRODUCTION

This chapter describes a numerical modelling of high strength steel endplate connections in fire. For comparison, the behaviour of mild steel endplate connections has been modelled as well. The endplate connections modelled in this chapter are exactly the same with those used in the experimental study presented in Chapter 6. The performances of various endplate connections at ambient temperature were also simulated as reference. This present chapter introduces the main characteristics of the finite element model, such as geometry, materials, mesh, element, contact interaction and analysis progress etc. This numerical modelling is validated against the experimental results shown in Chapter 6.

7.2 FINITE ELEMENT MODEL DISCRIPTION

The finite element software package ABAQUS 6.8 [1] was employed to numerically simulate the behaviour of endplate connections both at ambient temperature and at elevated temperatures.

7.2.1 Geometric Details

The geometric details of all connections' components modelled in FEM are the same as those of the test specimens as presented in Chapter 6. Because the geometric details, load, temperature distribution and boundary conditions of the endplate connection are symmetric, half of the endplate connection was modelled, to reduce computer costs and shorten computing time. The

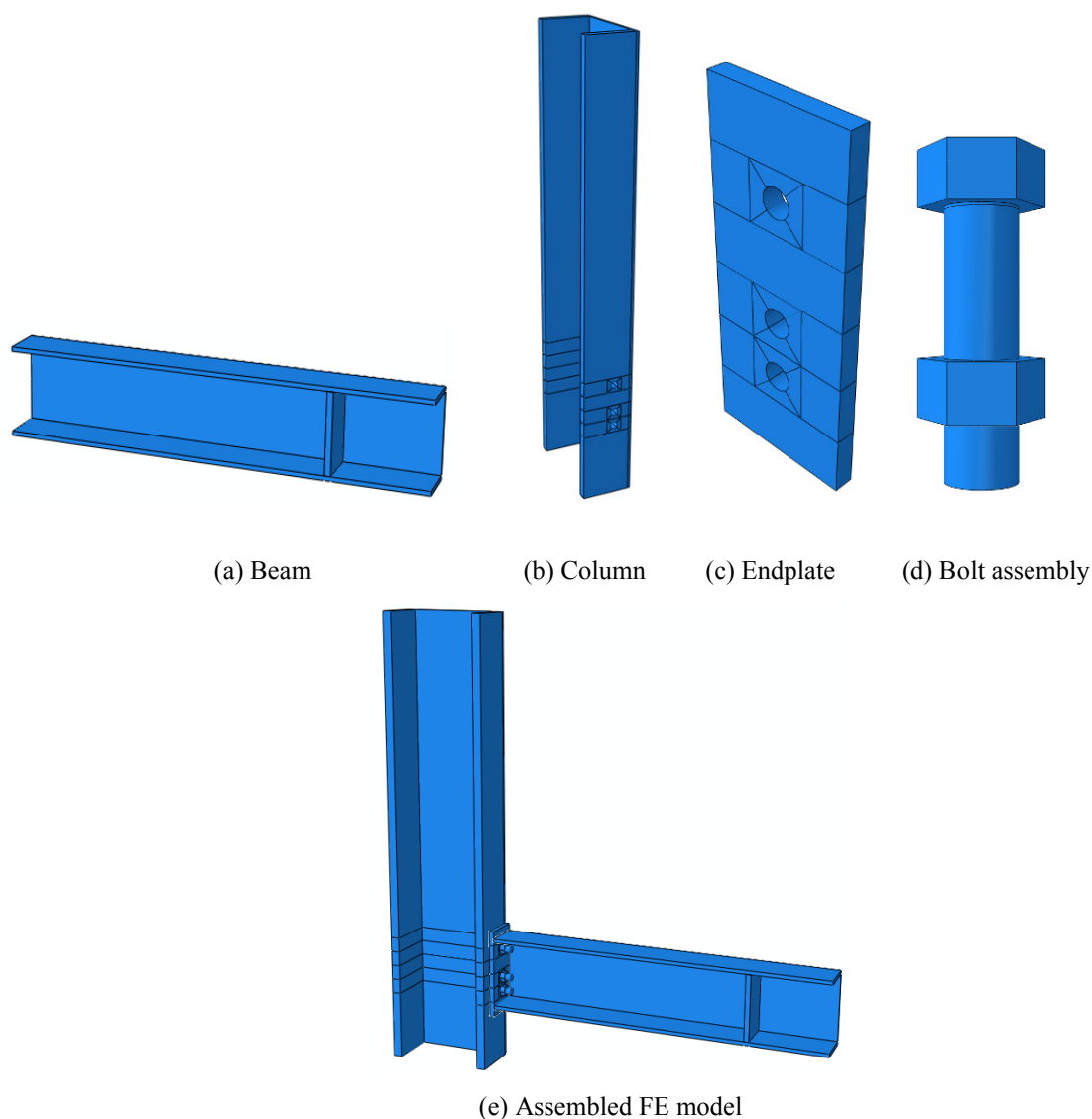components of this FE model are shown in Fig. 7.1, including beam, column, endplate, bolt shank and nut.

(a) Beam   (b) Column   (c) Endplate   (d) Bolt assembly

(e) Assembled FE model

Fig.7.1. FE model.

7.2.2 Mesh Generation and Element Type

There were 7 surface-to-surface contact interactions and 7 tie interactions in this FE model, and the materials were endowed with non-linear properties (detailed information is presented afterwards in Section 7.2.5). These make this numerical analysis sensitive to mesh, so the mesh should be fine enough. To capture accurate stress distribution in the region around bolt holes where yielding is likely to initiate, an intensive mesh was created in the vicinity of bolt holes, as shown in Fig. 7.2(c).

(a) Beam   (b) Column   (c) Endplate   (d) Bolt assembly
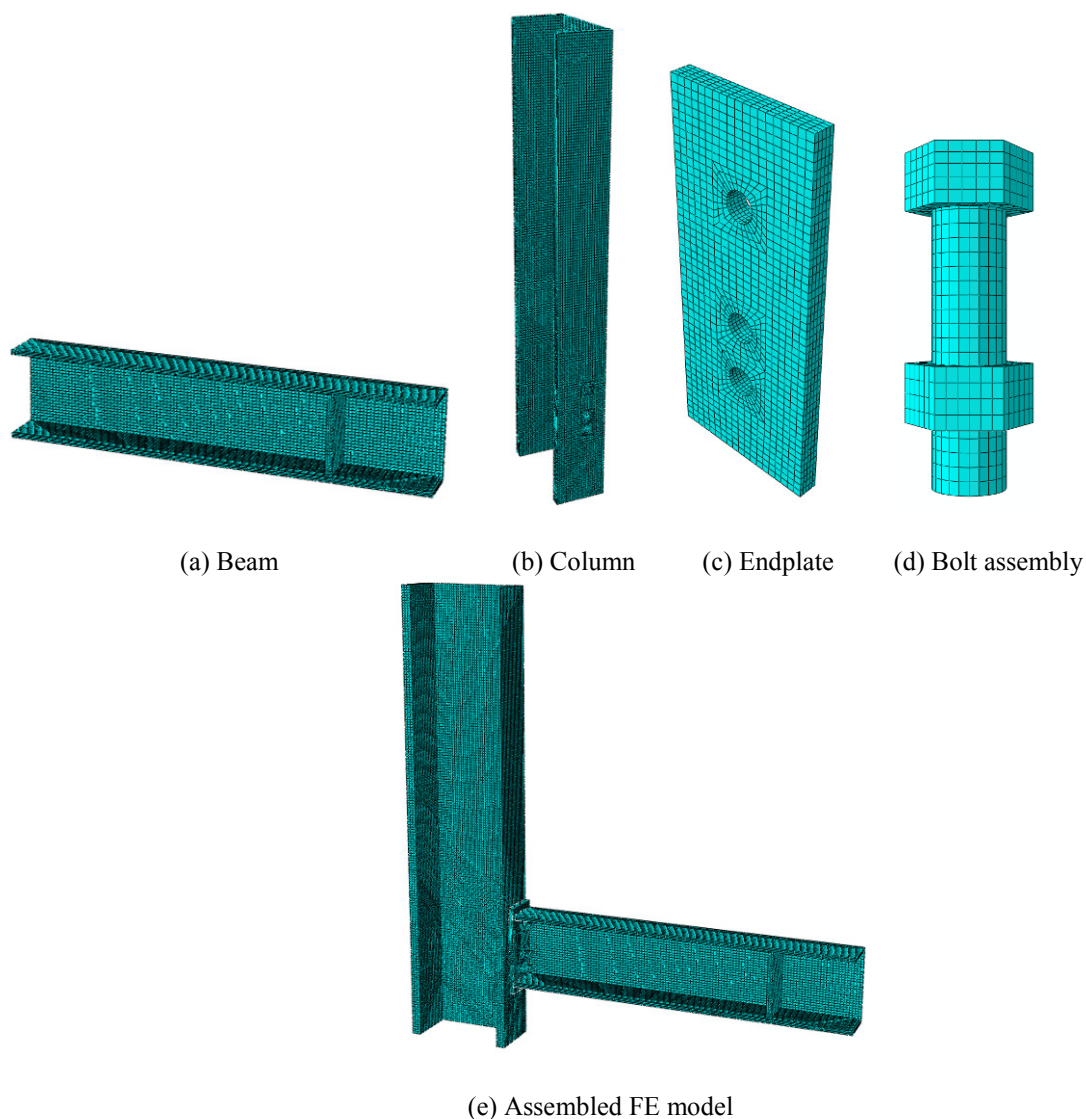
(e) Assembled FE model

Fig.7.2. Mesh generation of FE model.

The whole connection was modelled using C3D8I elements. In the ABAQUS package, the first letter or letters of an element's name indicate to which family the element belongs, hence C3D8I is a continuum (solid) element. As shown in Fig.7.3, C3D8I is 8-node brick element having nodes only at its corners, which uses linear interpolation in each direction and is often called linear element or first-order element. The last symbol of the element's name means full integration (8 Gauss points) and incompatible modes.
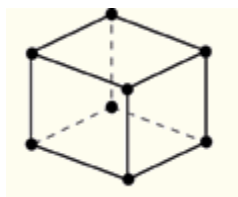

Fig.7.3. Linear 8-node brick element C3D8 in ABAQUS [1].

The ABAQUS package contains a large variety of hexahedron (brick), shell, contact and beam elements endowed with different features depending on the application. In literature, Bursi and Jaspart [2, 3] compared three 8-node brick elements:

(1) The C3D8 element with full integration (8 Gauss points), is accurate in the constitutive law integration, but the shear locking phenomenon is commonly associated with it when simulating bending-dominated structures.

(2) The C3D8R element with reduced integration (1 Gauss point), supplies a remedy for the shear locking problem caused by using C3D8, but the rank-deficiency of the stiffness matrix may produce spurious singular (hour glassing) modes, which can often make the elements unfeasible.

(3) The C3D8I element with full integration (8 Gauss points) and incompatible modes, has 13 additional degrees of freedom and the primary effect of these degrees of freedom is to eliminate the parasitic shear stresses that are observed in regular displacement elements in analyzing bending-dominated problems [1]. In addition, these degrees of freedom are also able to eliminate artificial stiffening due to Poisson's effect in bending. In regular displacement elements, the linear variation of the axial stress due to bending is accompanied by a linear variation of the stress perpendicular to the bending direction, which leads to incorrect stresses and an overestimation of the stiffness. The incompatible modes prevent such a stress from occurring [1].

Through comparison with the aforementioned three brick elements, the C3D8I elements are found to perform particularly well both in the elastic and inelastic regimes, and are suitable for representing the bending-dominated behaviour of a structure [2], therefore employed herein in this numerical model.

7.2.3 Contact Interaction and Analysis Process

(a) bolts-to-column flange   (b) column flange-to-endplate   (c) endplate-to-nuts
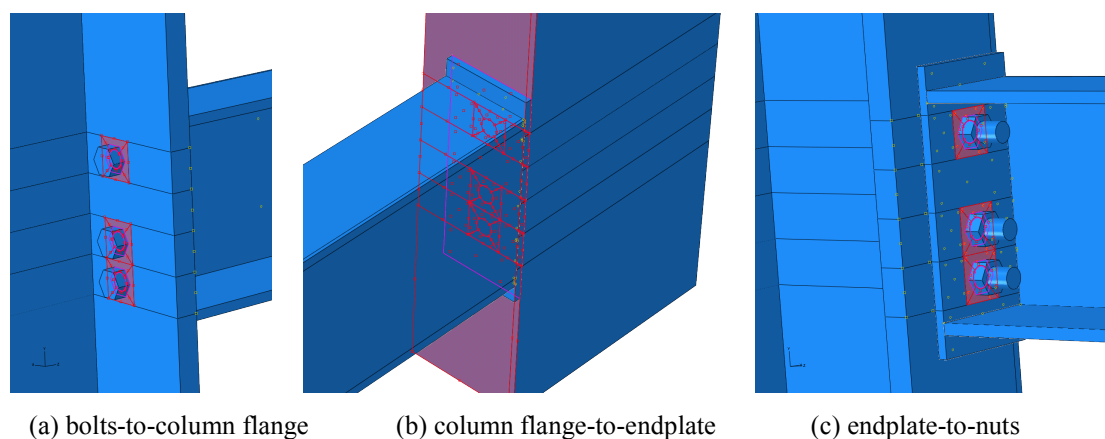Fig.7.4. Contact pairs in FE model.

The contact pairs in the endplate connection comprised the bolts-to-column flange, column flange-to-endplate, endplate-to-nuts, see Fig.7.4, where the red contact surfaces are master surfaces while the purple ones are slave surfaces. The nuts were tied to the corresponding bolt shanks, see Fig.7.5. Surface-to-surface contact, with a small sliding option, was used for all contact surfaces to fully transfer load. To handle contact interaction problem, the whole analysis process comprised five steps. In the first step, the bolts and endplate were restrained of all direction freedoms temporarily, and then a very small pretension was applied to every bolt for temporarily restraining the bolt assembly. The temperature field for all components was 20°C. In the second step, the bolts and the endplate were freed from any temporary restraint. In the third step, the length of every bolt was fixed. In the fourth step, the temperature field for all components was modified to 550°C. (For the analysis at ambient temperature, the temperature field was kept constant.) In the fifth step, an equivalent vertical surface traction converted from the vertical load was applied to the beam flange at the stiffener for loading. The first three steps helped contact interactions to be established smoothly, which is effective to decrease calculation time and eliminate errors.

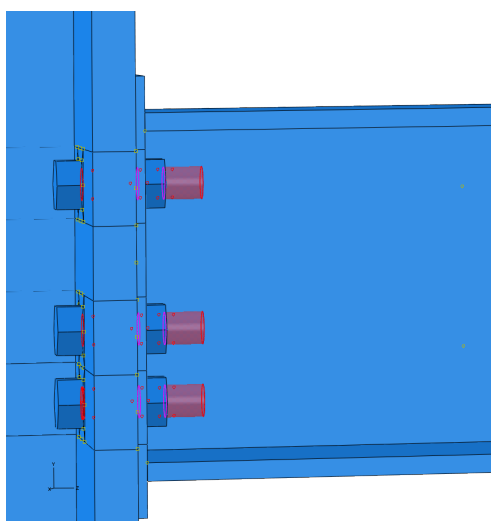Fig.7.5. Tie constraints between bolt shanks and nuts in FE model.

7.2.4 Welds

The welds between endplate and beam were treated by tie constraint instead of physically solid modelling, as shown in Fig. 7.6., in order to simplify the FE model.
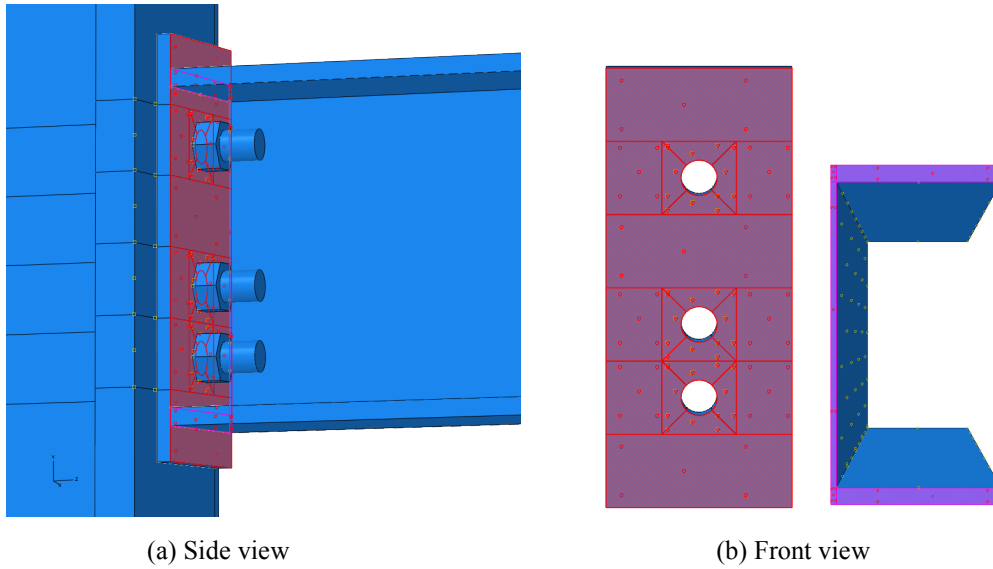
<div align="center">

(a) Side view   (b) Front view

Fig.7.6. Tie constraint between endplate and beam.

</div>

7.2.5 Material Properties

In this FE modelling, the material properties of mild steels (including Q235 and Q345) at ambient temperature were obtained according to tensile tests on the mild steel materials used in full-scale tests; their material properties at elevated temperatures were obtained according to the recommended reduction factors of structural steels in fire from Eurocode 3 part 1-2 [4]. The material properties of Grade 8.8 bolts at ambient and elevated temperatures used herein were those reported by the University of Sheffield [3-6]. The material properties of HSS S690 and S960 at ambient and elevated temperatures input herein were obtained from material tests presented in Chapter 4 and reference [9]. The yield and ultimate strengths of HSS S690 and S960 at ambient temperature offered by the steel supplier are shown in Table 7.1. An overall description of stress-strain curves of bolts and various structural steels at ambient temperature is presented in Fig.7.7.

The input mechanical properties of various materials in this FE modelling are actual strain and actual stress. The actual strain and actual stress were calculated according to Eqs (7.3) and (7.4), based on the engineering strain and engineering stress obtained from material tests (via Eqs (7.1) and (7.2)).

$$\varepsilon_{eng} = \frac{\Delta l}{l_0} \tag{7.1}$$

$$\sigma_{eng} = \frac{F}{A_0} \tag{7.2}$$

$$\varepsilon_{true} = \int_{l_0}^{l} \frac{dl}{l} = \ln(\frac{l}{l_0}) = \ln(1 + \varepsilon_{eng}) \qquad (7.3)$$

$$\sigma_{true} = \frac{F}{A} = \frac{F}{A_0 \frac{l_0}{l}} = \sigma_{eng}(1 + \varepsilon_{eng}) \qquad (7.4)$$

Table 7.1: Strengths of S690 and S960 at ambient temperature offered by steel supplier

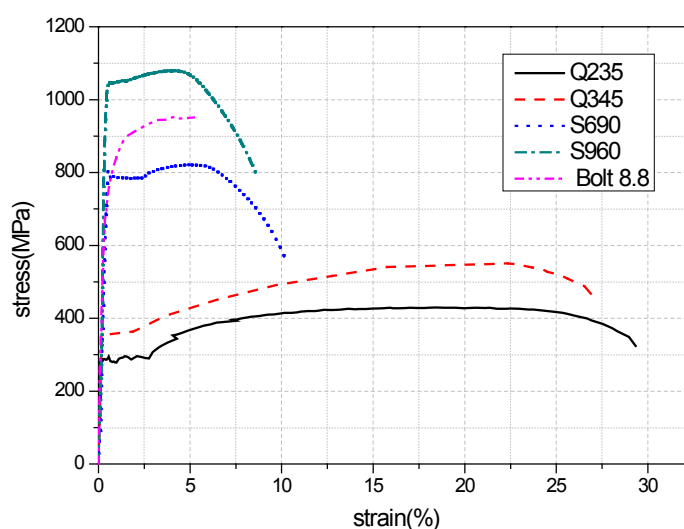| HSS	Yield strength (MPa)	Ultimate strength (MPa)
S690	799	843
S960	1043	1111

Fig.7.7. Stress-strain curves of various materials at ambient temperature.

7.2.6 Failure Criterion based on Deformation

The deformation capacity of a T-stub in bolted endplate connections is related to the endplate/bolt resistance ratio and is eventually determined by bolt fracture or cracking of the endplate material. In both situations, the modelling of the failure condition can be evaluated by assuming that cracking occurs when the ultimate strain ε_u is attained, either at the bolt or at the endplate/column flange.

Ana Girao Coelho et al. [10, 11] have proposed a failure criterion for the assessment of T-stub connections collapse. As a component of the T-stub connection, the bolt is subjected to combined tension and bending. In this case, the strain distribution at the bolt critical section changes from the symmetric case described in Fig. 7.8(a) to the case illustrated in Fig. 7.8(b). The bolt axis direction is no longer a principal direction. However, if a similar failure

175

criterion is adopted to the single bolt in tension respecting to the maximum average principal strain, i.e. $\varepsilon_{11,av,b} = \varepsilon_{u,b}$ (where $\varepsilon_{u,b}$ is the ultimate strain of the bolt), the deformation capacity of the bolt in combined tension and bending can be determined. It has been concluded that since the bolt, as a T-stub element, is subjected to combined tension and bending deformations, failure should be assessed by comparison of the maximum average principal strain, $\varepsilon_{11,av,b}$ with $\varepsilon_{u,b}$. Similarly, the failure of endplate or column flange is also based on the average principal strain reaching the ultimate strain of its material. This failure criterion based on deformation is employed in this numerical study.
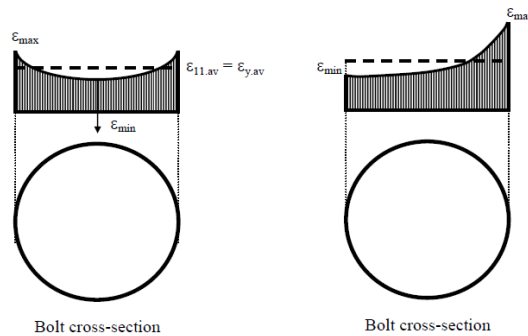
(a) Bolt under pure axial tension.   (b) Bolt under combined tension and bending.

Fig.7.8. Sketch of the strain distribution within a bolt cross-section [11].

7.3   VALIDATIONS   AGAINST   EXPERIMENTAL RESULTS

Validations of the numerical modelling were performed against the experimental results on endplate connections both at ambient temperature and at elevated temperatures.

7.3.1 Deformation at the End of Ambient-temperature Test

The comparisons on final deformation states of all connections at the end of the tests at ambient temperature between numerical simulations and experimental results were performed. For example, Fig. 7.9 and Fig 7.10 present the comparisons on deformation of the connection 2-3 A (S690 15mm) at the end of the test and its components after failure at ambient temperature, via comparing the experimental final deformation state and the numerical contour plots of Mises stress. It can be observed that good agreement exists on final deformation of connection 2-3 A (S690 15mm) at ambient temperature. Although the current numerical model can not simulate the fracture of the bolts, it is able to reveal the location where the fracture initiates and evolves, as

shown in Fig. 7.10 (c). Similar observations can be found for all 7 connection specimens at ambient temperature.
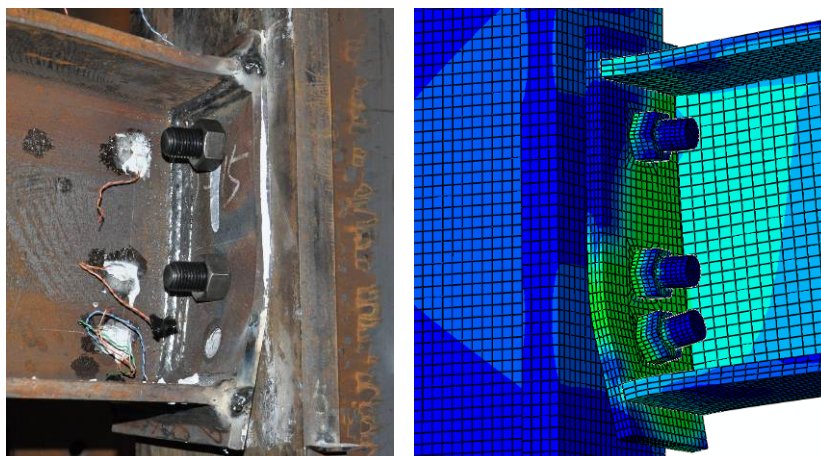

Fig.7.9. Comparison on final deformation state of connection 2-3 A (S690 15mm) at ambient temperature.

(a) Endplate front view

(b) Endplate side view

(c) Bolts
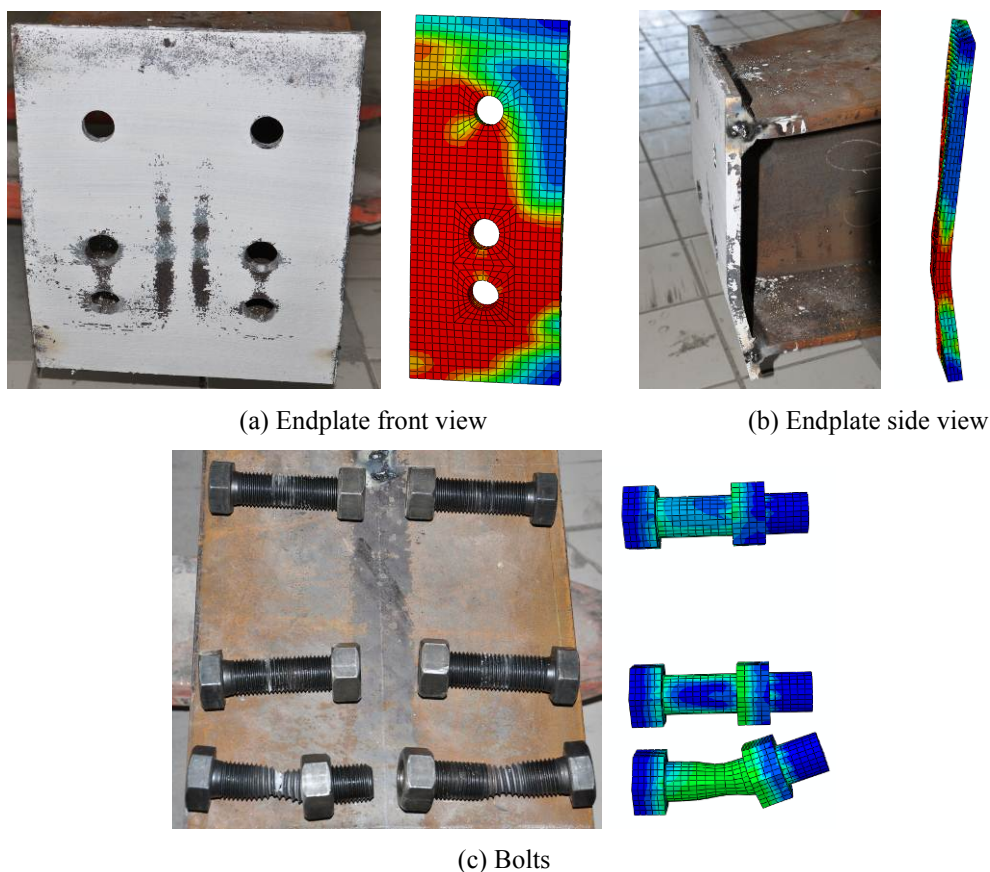
Fig.7.10. Comparison on components of 2-3 A (S690 15mm) after failure at ambient temperature.

In numerical modelling, the equivalent plastic strain (PEEQ, as simplified by ABAQUS) indicates whether the material is currently yielding or not. The contour plots of equivalent plastic strain (PEEQ) obtained from numerical modelling of specimens after failure at ambient temperature are compared with their experimental final deformation as well. For instance, the comparison for connection 2-4 A (S960 12mm) is shown in Fig.7.11, where good agreements

between experimental results and numerical modelling exist. Similarly, good agreements can be found for all tested connection specimens at ambient temperature.
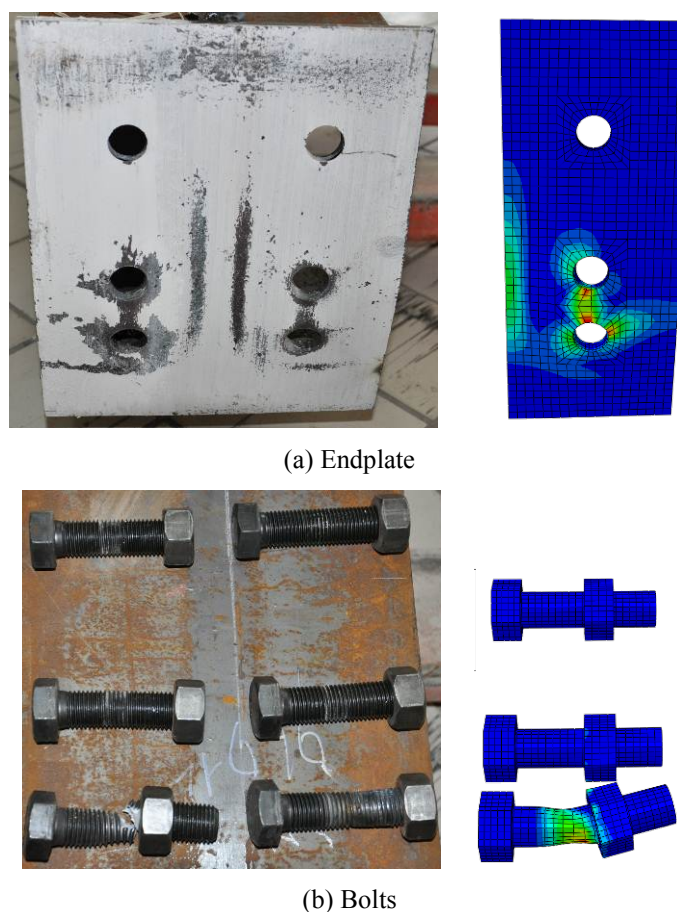

(a) Endplate

(b) Bolts

Fig.7.11. Experimental final deformation and numerically predicted PEEQ of 2-4 A (S960 12mm) at ambient temperature.

7.3.2 Deformation at the End of Elevated-temperature Test

The comparisons on final deformation states of all connections at the end of the tests at elevated temperature 550°C between numerical simulations and experimental results were conducted as well. Fig. 7.12 and Fig 7.13 show the comparisons on experimental final deformation states of connection 2-3 E (S690 15mm) and its components (for instance) after failure at elevated temperature 550°C with corresponding contour plots of Mises stress obtained from numerical modelling at elevated temperature 550°C. It can be found that good agreements exist on the final deformation state of connection 2-3 E (S690 15mm) at elevated temperature 550°C. Although the current numerical model cannot simulate the fracture of the bolts, it is able to reveal the location where the fracture initiates and evolves, as shown in Fig. 7.13 (c). The current FE model stops when the first failure of components occurs, i.e. the bolts in the top

tensile row for this connection in fire. In the experimental study, after failure of the bolts in the top tensile row, the bolts in the second tensile row experienced significant bending deformation until failure occurred. But in the present numerical study, it is not possible to simulate the failure of bolts in the second tensile row and the corresponding deformations of other components following the failure of bolts in the top tensile row. Similar conclusions can be drawn for all 7 connection specimens at elevated temperature 550°C.
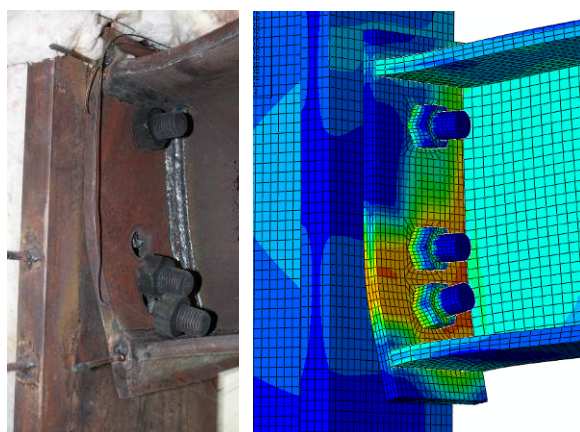

Fig.7.12. Comparison on final deformation state of connection 2-3 E (S690 15mm) at elevated temperature 550°C.

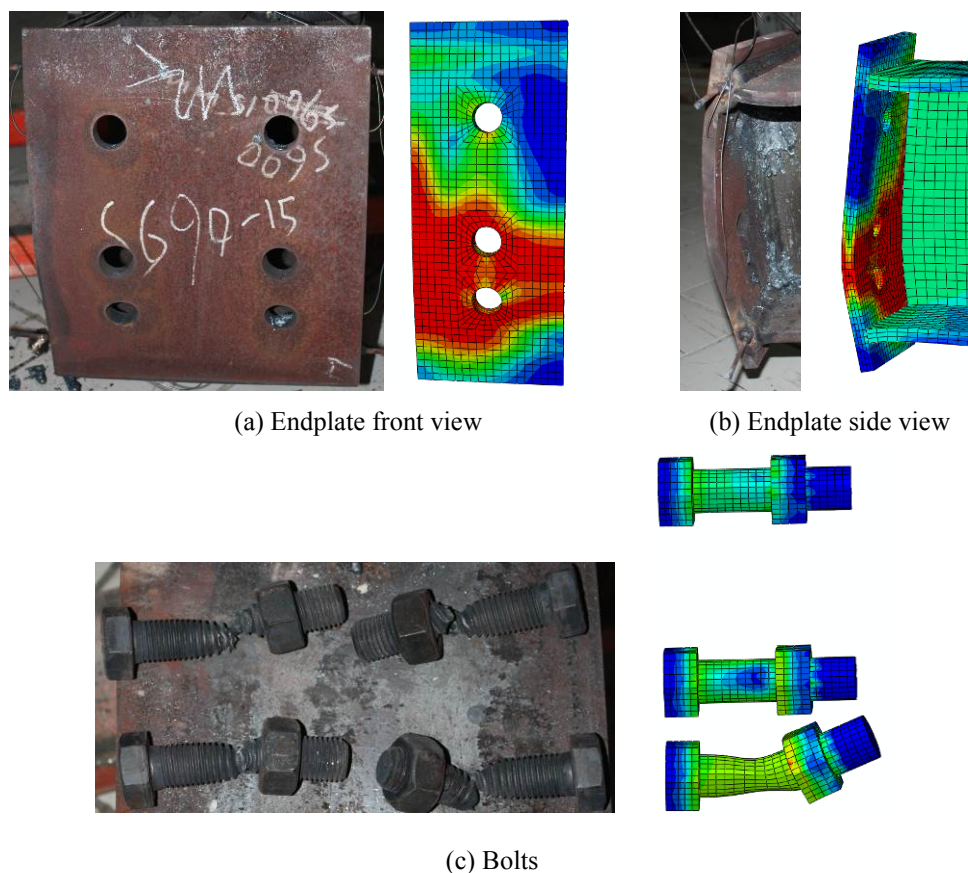(a) Endplate front view   (b) Endplate side view

(c) Bolts

Fig.7.13. Comparison on components of 2-3 E (S690 15mm) after failure at elevated temperature 550°C.

The contour plots of equivalent plastic strain (PEEQ) obtained from numerical modelling of specimens after failure at elevated temperature 550°C are compared with their experimental final deformation as well. For example, the comparison for connection 2-4 E (S960 12mm) is shown in Fig.7.14, in which there are good agreements between experimental results and numerical modelling. Similarly, good agreements can be found for all tested connection specimens at elevated temperature 550°C.

(a) Endplate

(b) Bolts
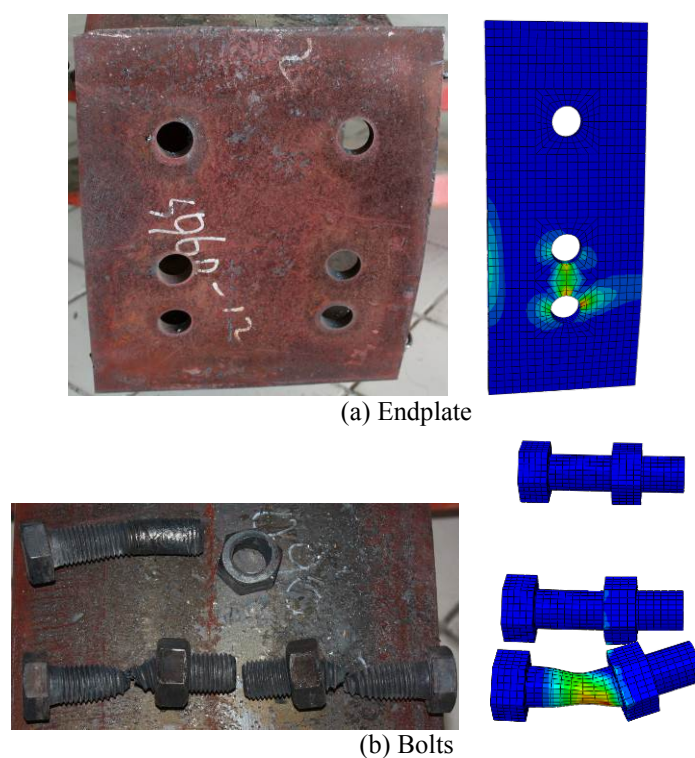
Fig.7.14. Test final deformation and numerical PEEQ of 2-4 E (S960 12mm) at 550°C.

7.3.3 Moment-rotation Characteristic at Ambient Temperature

The comparisons of numerical modelling and experimental study on the moment-rotation relationship of various endplate connections (both HSS endplate connections and mild steel endplate connections) at ambient temperature are shown in Fig. 7.15-7.21.

Fig.7.15. Moment-rotation comparison of 1-1 A (Q235 20mm) at ambient temperature.

Fig.7.16. Moment-rotation comparison of 1-2 A (S690 12mm) at ambient temperature.

Fig.7.17. Moment-rotation comparison of 1-3 A (S960 10mm) at ambient temperature.

Fig.7.18. Moment-rotation comparison of 2-1 A (Q235 25mm) at ambient temperature.

Fig.7.19. Moment-rotation comparison of 2-2 A (Q345 20mm) at ambient temperature.

Fig.7.20. Moment-rotation comparison of 2-3 A (S690 15mm) at ambient temperature.
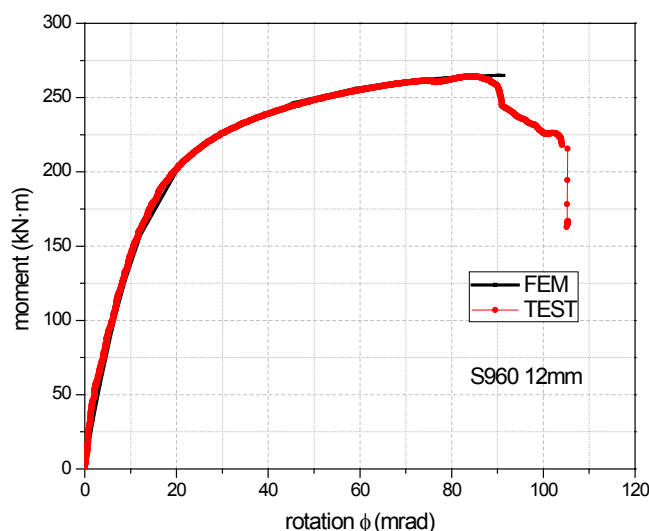
Fig.7.21. Moment-rotation comparison of 2-4 A (S960 12mm) at ambient temperature.
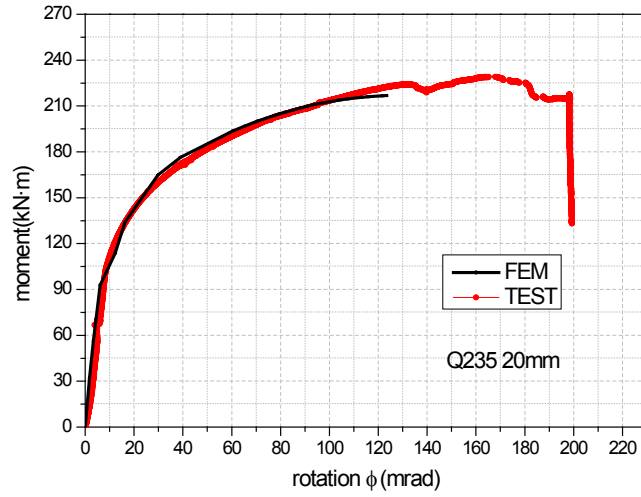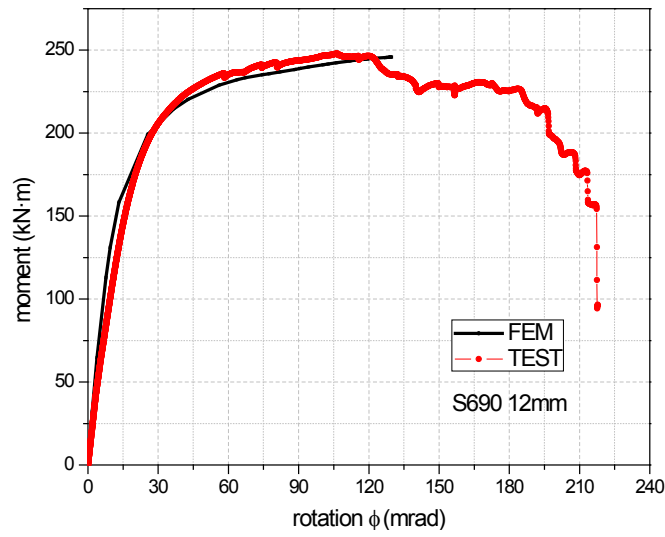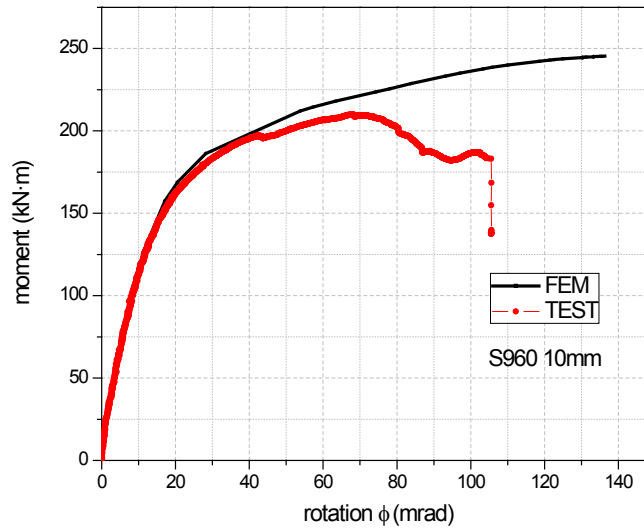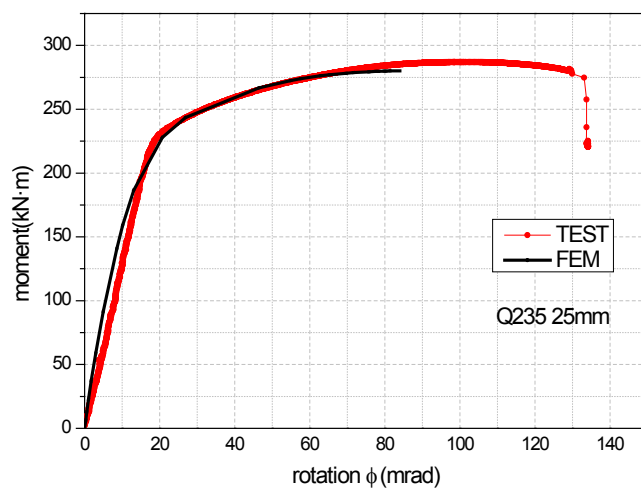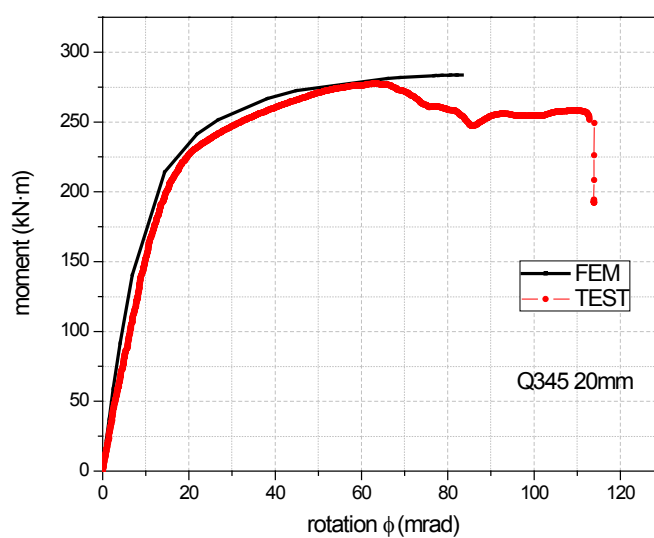
It can be seen that good agreements exist in general. For instance, as shown in Fig.7.21, the numerical moment-rotation relationship agrees very well with that from experimental result on initial stiffness, load bearing capacity and the connection rotation at the maximum load level $\phi_{M\max}$. However, this current numerical analysis stops when the maximum average principal strain of bolts or endplate/column flange achieves the ultimate strain of its material, which is the failure criterion used herein. So this current FE model cannot simulate the descending stage of moment-rotation curves obtained in tests, hence it is not able to simulate the final connection rotation capacity ϕ_C. It is worthwhile to note that for connection 1-3 A (S960 10mm) when the connection rotation is within 40mrad, the numerically predicted moment-rotation relationship agrees the test result very well, but in excess of 40mrad there are some deviations. It is because the endplate thickness of this connection (S960 10mm) is very thin (the thinnest in all connection specimens), so in tests the heat effect during welding on the mechanical properties of the endplate in the heat affected zone is relatively obvious and results in cracking on the endplate at the heat affected zone after some plastic deformations of endplate (see Fig.B.3 in Appendix B). But in this numerical simulation, the heat affect during welding on mechanical properties of the endplate has not been taken into consideration. This is the reason why the peak load and rotation capacity of the numerical result are higher than those of the experimental result for connection 1-3 A (S960 10mm).

Table 7.2: Validation of numerical study against experimental study at ambient temperature

Connection ID	Endplate		Peak moment (kN · m)		Deviation of peak moment (%) (absolute value)
	Material	Thickness (mm)	Tests	FEM	
1-1 A	Q235	20	229.93	216.85	5.69
1-2 A	S690	12	247.85	248.04	0.08
1-3 A	S960	10	*210.27*	245.42	*14.32*
2-1 A	Q235	25	287.00	280.14	2.39
2-2 A	Q345	20	277.25	283.73	2.34
2-3 A	S690	15	272.71	279.52	2.50
2-4 A	S960	12	264.32	265.01	0.26

The peak load of various endplate connections at ambient temperature obtained from numerical modelling are validated with the experimental results and listed in Table 7.2. It can be found that the maximum deviation of the peak moment between numerical modelling and experimental result is 5.69% for all connection specimens at ambient temperature (not taking consideration of the results for connection 1-3 A (S960 10mm)), which means good agreements exist.

7.3.4 Moment-rotation Characteristic at Elevated Temperature

The comparisons of numerical modelling and experimental study on the moment-rotation relationship of various endplate connections (both HSS endplate connections and mild steel endplate connections) at elevated temperature 550°C are shown in Fig. 7.22-7.28.

Fig.7.22. Moment-rotation comparison of 1-1 E (Q235 20mm) at elevated temperature 550°C.

Fig.7.23. Moment-rotation comparison of 1-2 E (S690 12mm) at elevated temperature 550°C.

Fig.7.24. Moment-rotation comparison of 1-3 E (S960 10mm) at elevated temperature 550°C.

Fig.7.25. Moment-rotation comparison of 2-1 E (Q235 25mm) at elevated temperature 550°C.

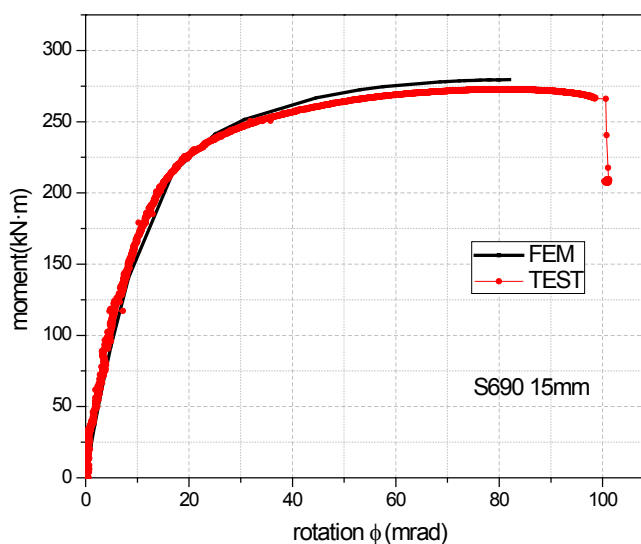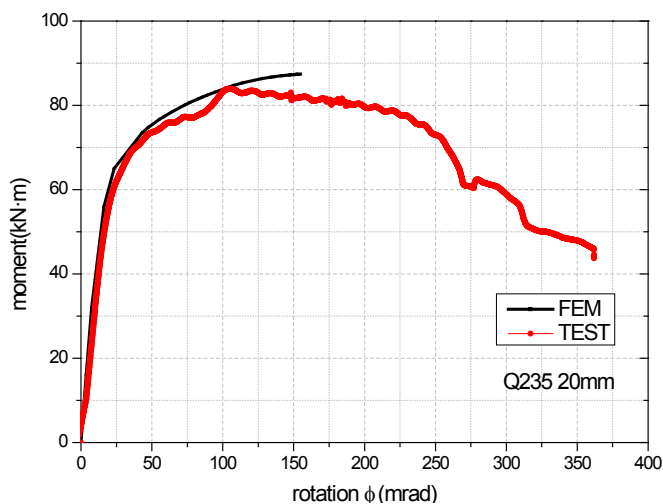Fig.7.26. Moment-rotation comparison of 2-2 E (Q345 20mm) at elevated temperature 550°C.
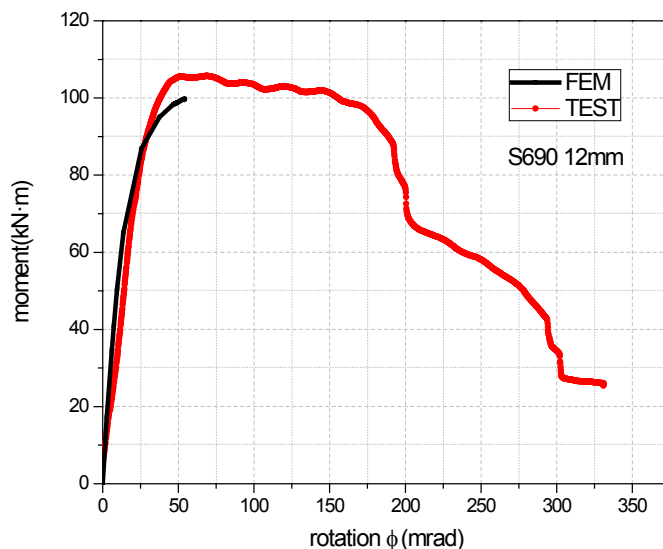

Fig.7.27. Moment-rotation comparison of 2-3 E (S690 15mm) at elevated temperature 550°C.
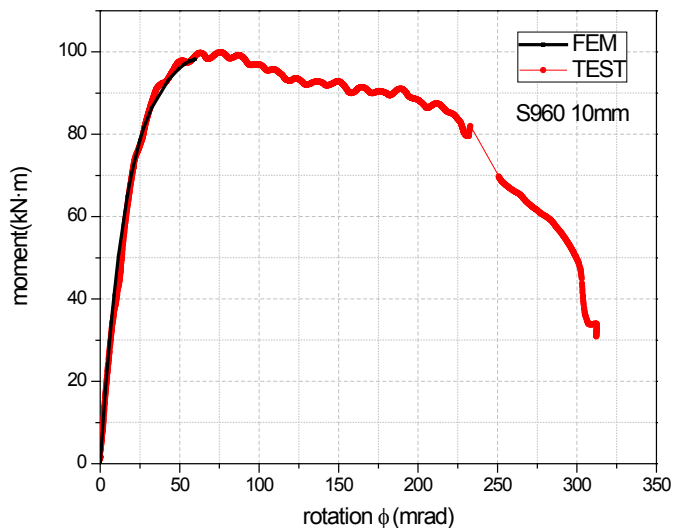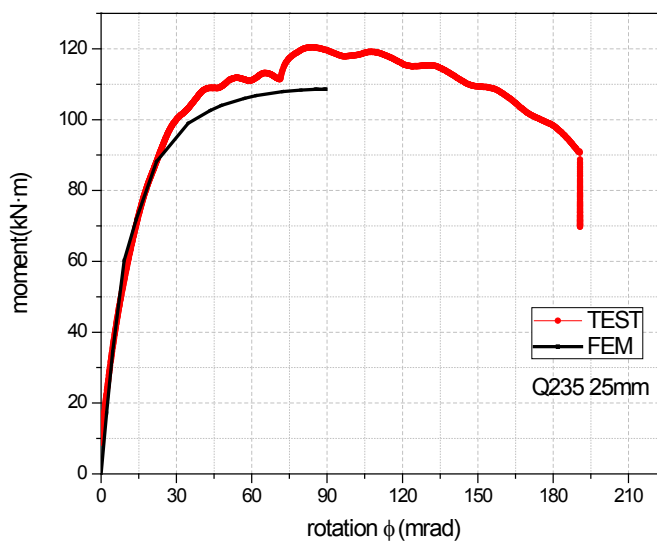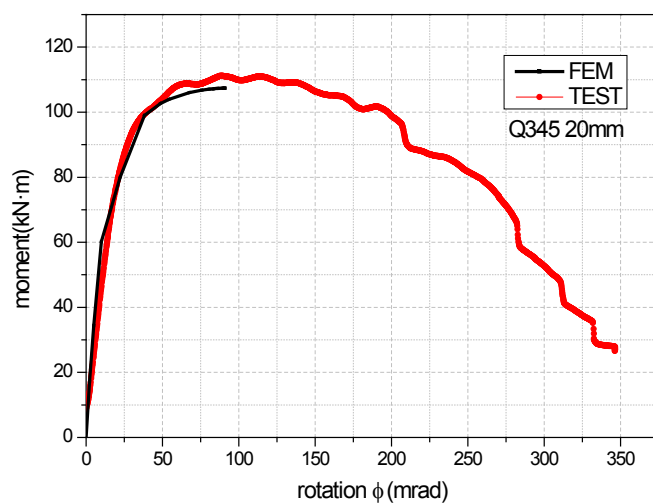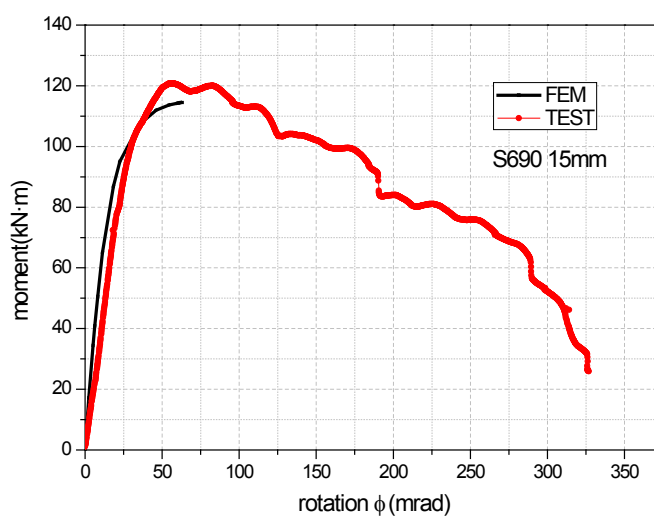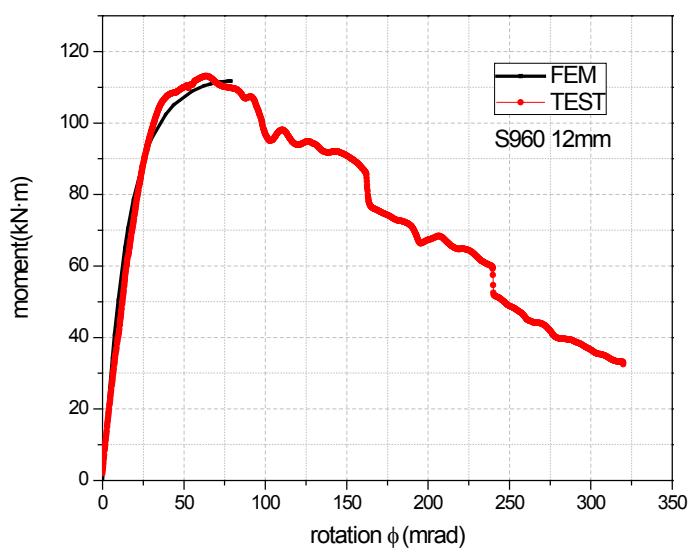

Fig.7.28. Moment-rotation comparison of 2-4 E (S960 12mm) at elevated temperature 550°C.

Table 7.3: Validation of numerical study against experimental study at elevated temperature 550°C

Connection ID	Endplate		Peak moment (kN · m)		Deviation of peak moment (%) (absolute value)
	Material	Thickness (mm)	Tests	FEM	
1-1 E	Q235	20	83.91	87.39	4.15
1-2 E	S690	12	105.92	99.74	5.83
1-3 E	S960	10	100.05	98.23	1.82
2-1 E	Q235	25	120.40	108.60	9.80
2-2 E	Q345	20	111.16	107.37	3.41
2-3 E	S690	15	120.78	114.52	5.18
2-4 E	S960	12	113.18	111.79	1.23

It can be found that the numerical modelling agrees very well with that from the experimental study on initial stiffness, peak moment and the connection rotation at the maximum load level $\phi_{M\,max}$ for all endplate connections at elevated temperature. The peak moments of various endplate connections at elevated temperature 550°C obtained from numerical modelling are validated with the experimental results and listed in Table 7.3. It can be observed that the maximum deviation of the peak moment between numerical modelling and experimental result is 9.80% for all connection specimens at elevated temperature 550°C.

Hence this numerical model is verified to be able to simulate the behaviour of endplate connections with reasonable accuracy at ambient and elevated temperatures.

7.3.5 Stress Distribution State

The stress distribution state of the endplate connection at any time point in fire or during loading at ambient temperature can be obtained by this proposed numerical analysis. For endplate connections at ambient temperature, contour plots of the Mises stress on the endplate, for instance connection 1-2 A (S690 12mm) as shown in Fig. 7.29, clearly show a similar stress distribution and yielding of the endplate at the locations where the yield line pattern was observed in tests. It can be seen there is good agreement between numerical modelling and experimental results on the yield line pattern of endplate connection at ambient temperature. A similar conclusion can also be obtained for endplate connections in fire as well, as presented in Fig. 7.30 taking connection 1-2 E (S690 12mm) for example. Hence, this numerical model can be used with confidence to predict the stress distribution of the endplate connection both at ambient temperature and in fire, which is not easily feasible for full-scale tests especially under fire conditions.
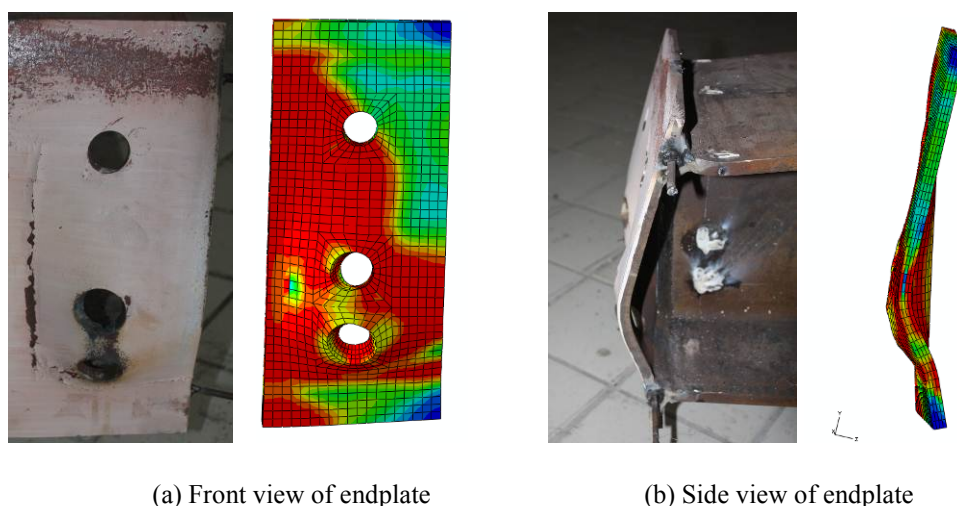
(a) Front view of endplate   (b) Side view of endplate

Fig.7.29. Stress state at the end of test and yield line pattern of 1-2 A (S690 12mm) at ambient temperature.
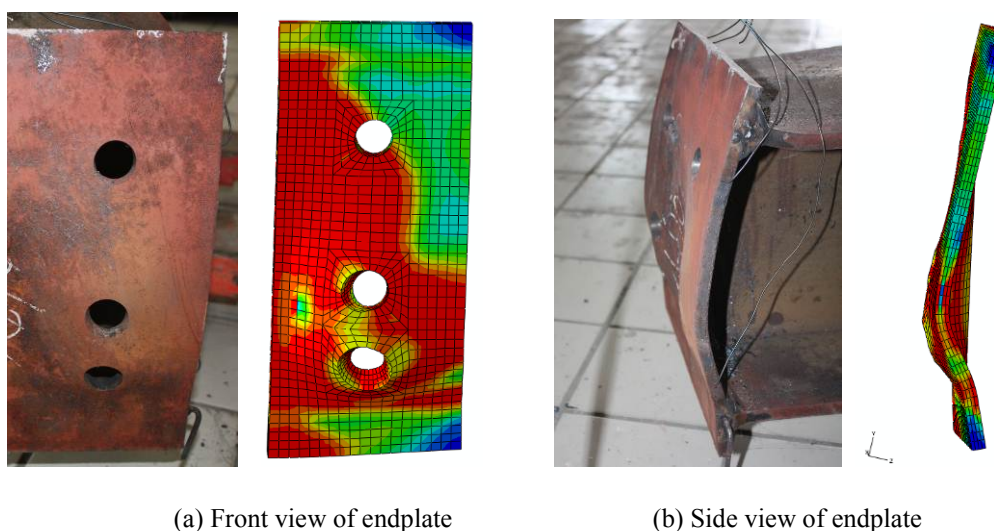
(a) Front view of endplate   (b) Side view of endplate

Fig.7.30. Stress state at the end of test and yield line pattern of 1-2 E (S690 12mm) at elevated temperature 550°C.

7.4 CONCLUSION

This chapter reports on a FE modelling of endplate connections using ABAQUS/Standard, in order to study the performance of high strength steel endplate connections at ambient and elevated temperatures. Validation of the numerical modelling against all representative experimental results conducted on the moment-rotation relationship, final deformation and yield line pattern of connections shows good agreements exist. Therefore, the numerical analysis method proposed herein can be used with confidence to predict the behaviour of high strength steel endplate connections in fire as well as at ambient temperature. The following conclusions can be drawn.

The challenge of numerical modelling contact interactions considering material and geometric non-linear effects has been solved successfully. The proposed FE modelling is verified appropriate to simulate both high strength steel and mild steel endplate connections at ambient and elevated temperatures. Based on this, the FE modelling can be used to predict stress distribution of high strength steel endplate connections both at ambient temperature and in fire, which is not easy to achieve in full-scale tests especially under fire conditions.

Moreover, parametric study can be further performed using this verified numerical model to investigate the performances of high strength steel endplate connections under various fire conditions, via inputting proper mechanical properties of high strength steels in fire. Hence the proposed numerical modelling may be used as a benchmark for further investigation on improving the behaviour of steel connections under fire conditions and fire safety of steel structures.

By the present modelling method, the first critical component of endplate connections can be identified, but the occurrence of component fracture as well as the subsequent failure on other components cannot be predicted. To improve this numerical simulation, solid modelling of welds, considering the heat effect of welds and taking into account fracture features on components are of importance in future numerical research.

7.5 REFERENCES

[1] Abaqus Analysis User's Manual, 6.8 version.

[2] O.S. Bursi, and J.P. Jaspart, Benchmarks for finite element modelling of bolted steel connections, Journal of Constructional Steel Research, 43 (1997) No. 1-3: 17-42.

[3] O.S. Bursi, and J.P. Jaspart, Basic issues in the finite element simulation of extended end plate connections, Computers and Structures, 69 (1998) 361-382.

[4] European Committee for Standardization (CEN), EN 1993-1-2, Eurocode3: Design of steel structures, Part 1-2: General rules - Structural fire design, Brussels , 2005.

[5] Y. Hu, J.B. Davison, I.W. Burgess and R.J. Plank, Experimental Study on Flexible End Plate Connections in Fire, Proc. 5th European Conference on Steel Structures, Graz, Austria, 1007-1012.

[6] Y. Hu, J.B. Davison, I.W. Burgess and R.J. Plank, Comparative Study of the Behaviour of BS 4190 and BS EN ISO 4014 Bolts in Fire, ICSCS 2007, Manchester, 587-592.

[7] Y. Hu, Robustness of flexible endplate connections under Fire Conditions, PhD thesis, University of Sheffield, UK, 2009.

[8] Y. Theodorou, Mechanical properties of grade 8.8 bolts at elevated temperatures. Master's dissertation. University of Sheffield, UK, 2003.

[9] X. Qiang, F.S.K. Bijlaard, M.H. Kolstein, Dependence of mechanical properties of high strength steel S690 on elevated temperatures, Construction and Building Materials, 30 (2012) 73–79.

[10] A.M. Girão Coelho, F.S.K. Bijlaard, L. Simões da Silva, On the deformation capacity of beam-to-column bolted connections, Document ECCSTWG 10.2-02-003, European Convention for Constructional Steelwork – Technical Committee 10: Structural connections (ECCS-TC10), 2002.

[11] A.M. Girão Coelho, Characterization of the ductility of bolted end plate beam-to-column steel connections, PhD thesis, University of Coimbra, 2004.

Chapter 8

Experimental study on HSS endplate connections after fire

8.1 INTRODUCTION

In the present chapter, the behaviour of high strength steel endplate connections after cooling down from fire is studied through full scale tests. Tests on two series of endplate connections (in total 7 connection specimens) were conducted after cooling down from fire temperature 550°C to evaluate their performance after fire. In each connection series, one or two endplate connections made of mild steels were included for comparison. The parameters investigated were endplate thickness and endplate material. The specimens were designed to trigger failure to the connections (particularly to the endplates) rather than beam or column. The post-fire moment-rotation characteristic, rotation capacity and final deformation state of high strength steel endplate connections after fire were obtained by means of tests and compared with those of mild steel endplate connections after fire. Furthermore, the post-fire behaviour of high strength steel endplate connections was compared with that at ambient temperature without fire exposure to evaluate the residual performance after fire. The descriptions on the test program and test results are given below.

8.2 TEST PROGRAMME

8.2.1 Test specimen

In this experimental study on the behaviour of endplate connections after fire, the endplate connections are designed according to Eurocode 3: Part 1:8 [1], the details of which are exactly the same with that introduced in Chapter 6. In the endplate connections, the endplates are made of high strength steels (S690 and S960) while the beam and column are made of Q345 (similar to S355). The beam sections used in this experimental study are HW300×300 [2] (h=300mm, b=300mm, t_w=10mm, t_f=15mm, comparable to European Section HE320A)

while the column sections are HW400×400 [2] (*h*=428mm, *b*=407mm, t_w=20mm, t_f=35mm, comparable to European Section HE400M). For comparison, the connections with endplates made of mild steels Q235 (similar to S235) and Q345 (similar to S355) are also included herein. In order to compare the behaviour of endplate connections after fire with that without exposure to fire, the tests at ambient temperature without fire exposure on each concerned endplate connection are included as well. The detailed drawing of endplate connection test specimen is shown in Appendix A, while the characteristics and test conditions of the specimens are shown in Table 8.1. The welds between endplate and beam are continuous 45°-fillet welds, which were done in workshop in a down-hand position. The weld sizes for endplates made of mild steels are 8mm, while those for endplates made of high strength steels are 10mm. The welding material used for specimens with endplates made of mild steels Q235 and Q345 is ER50-6, while that for specimens with endplates made of high strength steels S690 and S960 is ER76-G. The chemical compositions of these two welding electrodes are listed in Table 6.2, while their mechanical properties are presented in Table 6.3.

Table 8.1: Test specimens and post-fire test conditions

Connection ID	Endplate material	Endplate thickness (mm)	Electrode	Weld type	Highest fire temperature (°C) specimens exposed to in post-fire tests
1-1 P	Q235	20	ER50-6	overmatched	550
1-2 P	S690	12	ER76-G	matched	550
1-3 P	S960	10	ER76-G	under matched	550
2-1 P	Q235	25	ER50-6	overmatched	550
2-2 P	Q345	20	ER50-6	overmatched	550
2-3 P	S690	15	ER76-G	matched	550
2-4 P	S960	12	ER76-G	under matched	550

8.2.2 Test set-up and procedure

The heating process was conducted in the furnace in the same way as in fire tests, see Fig.6.2 and Fig.6.3. The specimen was firstly heated to 550°C at a constant heating rate 10°C/min (which corresponds to normally protected steel members in fire), after the temperature of connection components achieved 550°C and being stable, the heating was stopped and the specimens began to cool down to ambient temperature. After cooling down, the post-fire connection specimens were loaded at ambient temperature until failure to evaluate the residual load bearing capacity, displacement, rotation, and failure modes of HSS endplate connections after cooling down from fire. The loading method was the same with that at ambient temperature introduced in Chapter 6. Before tests, all equipment was examined by trial loading at ambient

temperature. During trial loading, the displacements and applied force were checked. When everything went well, formal loading was started. During loading, displacement control was used via controlling the displacement of the piston of the hydraulic actuator at 10mm/min. The displacements of beam, column and endplate, the rotation of connection, and failure mode of connection after fire were obtained and recorded. For post-fire tests, the displacement measurement was the same as that of fire tests and tests at ambient temperature. The arrangement of displacement sensors is shown in Fig.6.4.

8.3 EXPERIMENTAL RESULTS AND DISCUSSION

8.3.1 Deformation at the end of tests

For all endplate connections after fire, their final deformation states were photographed at the end of tests at ambient temperature after cooling down from fire and presented in Appendix B of this thesis. An overall description on components of all connections at the end of tests is given in Table 8.2.

Table 8.2: Description of components at the end of post-fire tests

Test ID	Endplate material	Endplate thickness (mm)	Endplate yielding	Fracture of bolts in top tensile row	Nuts in top tensile row stripped off	Weld failure in heat affected zone	Bolts in compression almost straight
1-1 P	Q235	20	Yes	No	No	No	Yes
1-2 P	S690	12	Yes	No	Yes	No	Yes
1-3 P	S960	10	Yes	No	No	Yes	Yes
2-1 P	Q235	25	Yes	Yes	No	No	Yes
2-2 P	Q345	20	Yes	Yes	No	No	Yes
2-3 P	S690	15	Yes	Yes	No	No	Yes
2-4 P	S960	12	Yes	No	Yes	No	Yes

(a)　　　　　　　　(b)　　　　　　　　(c)
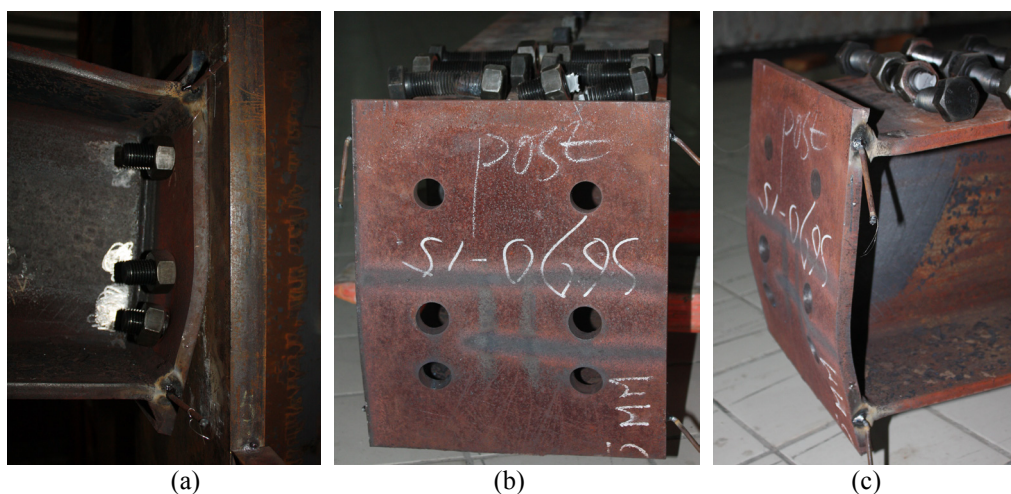
(d)
Fig.8.1. Final deformation state of connection 2-3 P (S690 15mm) after fire.

As an example, the final deformation state of connection 2-3 P (S690 15mm) after cooling down from fire temperature 550°C is shown in Fig.8.1. It can be found that the endplate has a moderate amount of bending deformation. After some plastic deformations of the endplate, failure occurred on the bolts of the top row in tension, as shown in Fig.8.1 (d). It corresponds to the descending phase in resistance of the connection as illustrated in Fig.8.3 and Fig.8.5. The bolts in the second tensile row and bolts in compression remained almost straight in tests.

8.3.2 Failure modes

The failure modes of all endplate connections can be predicted by theoretical analysis based on Eurocode 3 Part:1-8 [1], by employing the post-fire remaining factors of S690 and S960 obtained by material tests, shown in Chapter 5, and that for mild steels recommended in British standard BS5950 [3]. The detailed procedure of this theoretical analysis is shown in Appendix C of this thesis.

The failure modes of endplate connections after cooling down from 550°C obtained from theoretical analysis and experimental study are listed in Table 8.3. It can be observed that good agreement exists between theoretical analysis and experimental study.

Table 8.3: Failure modes of endplate connections after cooling down from 550°C

Connection ID	Endplate		Failure mode	
	Material	Thickness (mm)	EC3	Test
1-1 P	Q235	20	Mode 1	Mode 1
1-2 P	S690	12	Mode 1	Mode 1
1-3 P	S960	10	Mode 1	Mode 1
2-1 P	Q235	25	Mode 2	Mode 2
2-2 P	Q345	20	Mode 2	Mode 2
2-3 P	S690	15	Mode 2	Mode 2
2-4 P	S960	12	Mode 2	Mode 2

Table 8.4: Effect of post fire on failure modes of endplate connections in tests

Series	Endplate		Failure mode	
	Material	Thickness (mm)	Ambient temperature	Post fire
1-1	Q235	20	Mode 1	Mode 1
1-2	S690	12	Mode 1	Mode 1
1-3	S960	10	Mode 1	Mode 1
2-1	Q235	25	Mode 2	Mode 2
2-2	Q345	20	Mode 2	Mode 2
2-3	S690	15	Mode 2	Mode 2
2-4	S960	12	Mode 2	Mode 2

The post-fire failure modes of endplate connections observed after tests were compared with those at ambient temperature without fire exposure, as presented in Table 8.4. It can be found that after cooling down from 550°C the failure mode of each endplate specimen is the same as its failure mode at ambient temperature without fire exposure. So the failure mode is not affected after cooling down from elevated temperatures up to 550°C, which is valid for both mild steel endplate connections and high strength steel endplate connections.

8.3.3 Moment- rotation relationship of endplate connections after fire

As mentioned above, the behaviour of a steel beam-to-column connection is represented by an M- ϕ curve. The rotational deformation of a connection, ϕ, is defined as the relative rotation between the beam and column axes, which can be calculated according to Eqs. (6.1), (6.2) and (6.3).

8.3.3.1 Effect of endplate material and thickness vary

The peak load and connection rotation Φ_C of various connections after cooling down from fire temperature 550°C obtained from experiments are presented in Table 8.5. The moment-rotation comparison of connections in Series 1 after fire is shown in Fig.8.2. It can be seen that their load bearing capacities are similar, while the maximum rotational capacity of connection 1-2 P (S690 12mm) is higher than that of connection 1-1 P (Q235 20mm). In tests, the post-fire connection S960 10mm failed due to cracking of the endplate at the heat affected zone of welds after a moderate amount of plastic deformation on the endplate. Therefore, its rotation capacity is relatively low and not included in the comparison. The moment-rotation comparison of connections in Series 2 after cooling down from fire is presented in Fig.8.3. It can be found that the post-fire load bearing capacities of connections in Series 2 are similar to each other. The post-fire rotational capacities of connections 2-1 P (Q235 25mm), 2-2 P (Q345 20mm) and 2-3 P (S690 15mm) are in a comparable range, while

that of connection 2-4 P (S960 12mm) is higher than the others in connection series 2.

Table 8.5: Characteristics of connections after cooling down from fire temperature 550°C

Connection ID	Endplate		Peak load		Connection rotation
	Material	Thickness (mm)	Moment (kN • m)	Force (kN)	Φ_C (mrad)
1-1 P	Q235	20	255.56	237.51	249
1-2 P	S690	12	226.67	210.66	397
1-3 P	S960	10	230.80	214.50	147
2-1 P	Q235	25	272.59	253.34	150
2-2 P	Q345	20	272.35	253.11	139
2-3 P	S690	15	261.79	243.30	141
2-4 P	S960	12	252.85	234.99	238

A conclusion can be drawn that in endplate connections a proper thinner endplate made of high strength steel can achieve similar post-fire load bearing capacity and higher (or at least comparable) post-fire maximum rotational capacity in comparison with a thicker endplate made of mild steel.
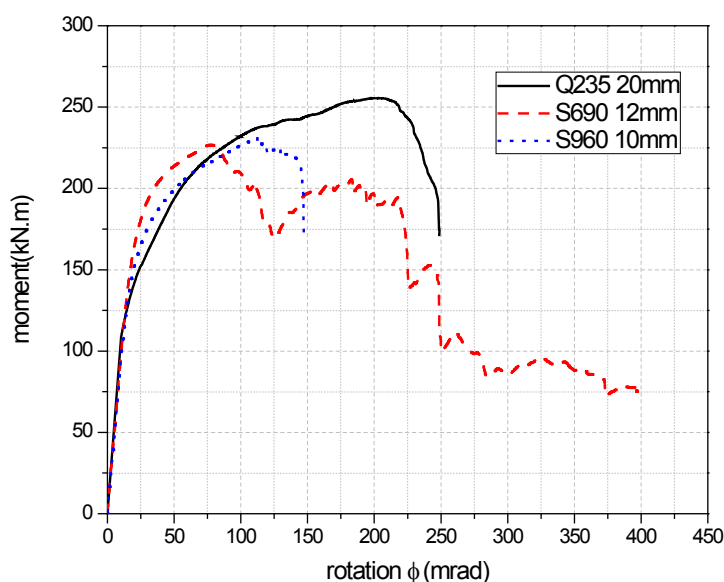

Fig.8.2. Moment-rotation comparison of connections Series 1 after cooling down from fire.
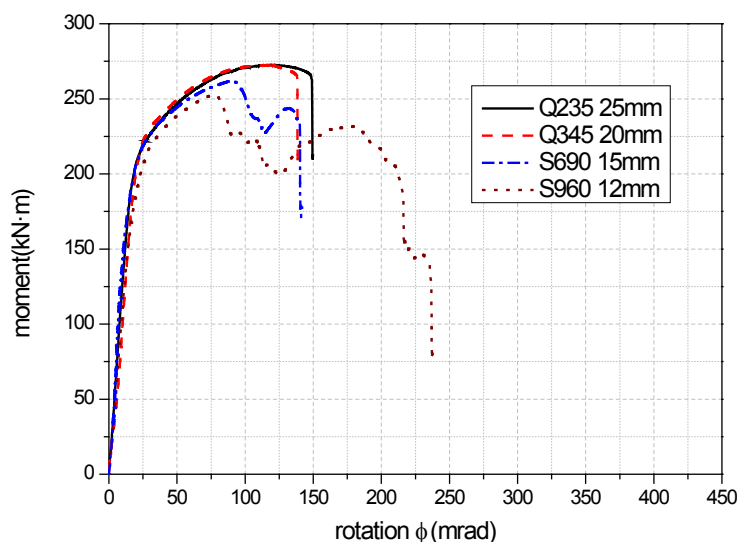
Fig.8.3. Moment-rotation comparison of connections Series 2 after cooling down from fire.

8.3.3.2 Effect of endplate thickness varies

For post-fire behaviour of endplate connections of which the endplates are made of the same steel material, the effect of variations on endplate thicknesses after fire when the endplate is made of Q235, S690 and S960 is shown in Fig.8.4-Fig.8.6 respectively. It can be observed that for endplate connections of which the endplates are made of the same steel material, with a thicker endplate the connection can achieve higher post-fire load bearing capacity, but its rotational capacity after fire is reduced obviously. The endplate connections made of S960 as shown in Fig.8.16 are the exception, because of the early cracking of the endplate at the heat affected zone of welds for connection S960 10mm.
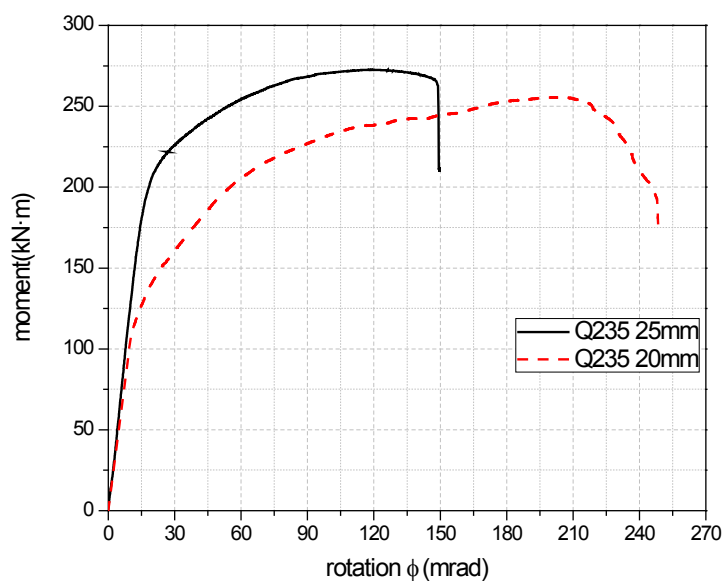
Fig.8.4. Effect of endplate thickness in connections with endplate made of Q235 after fire.
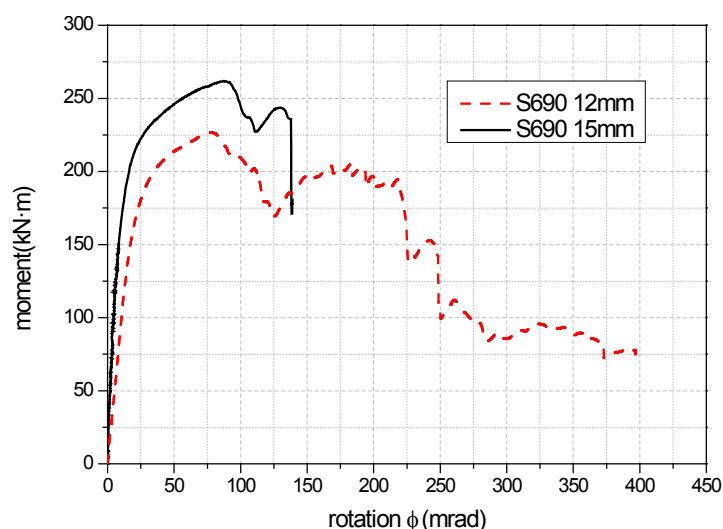
Fig.8.5. Effect of endplate thickness in connections with endplate made of S690 after fire.
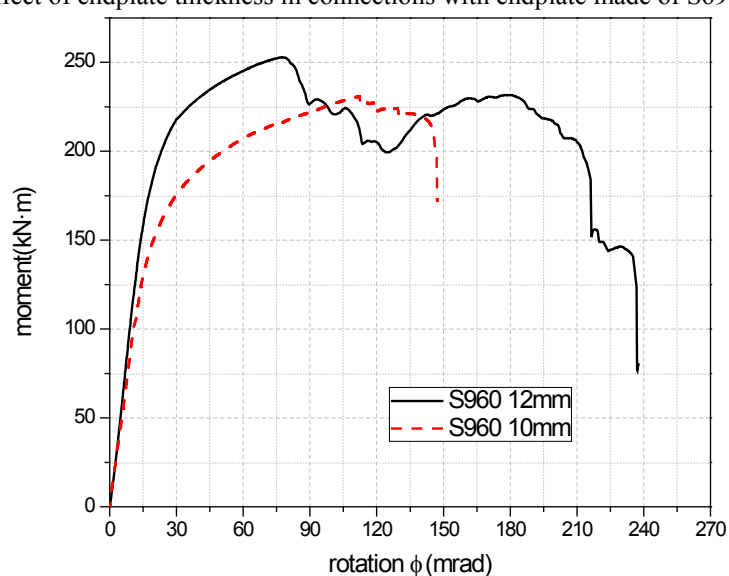
Fig.8.6. Effect of endplate thickness in connections with endplate made of S960 after fire.

8.3.3.3 Post-fire effect on endplate connections

In order to investigate the post-fire effect on the behaviour of endplate connections, comparison on moment-rotation relationship of connection 1-1 P (Q235 20mm) after cooling down from fire temperature 550°C with that at ambient temperature without fire exposure is presented in Fig.8.7. The comparisons for the other endplate connections are shown in Fig.8.8-Fig.8.12 respectively. The behaviour of connection 1-3 P (S960 10mm) is excluded herein, also because of its early cracking on the endplate at the heat affected zone.
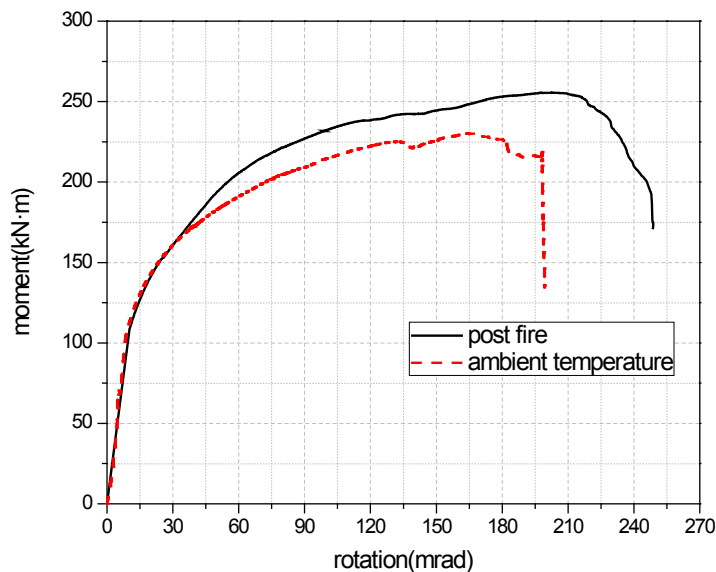
Fig.8.7. Effect of post fire to 550°C on connection 1-1 P (Q235 20mm).
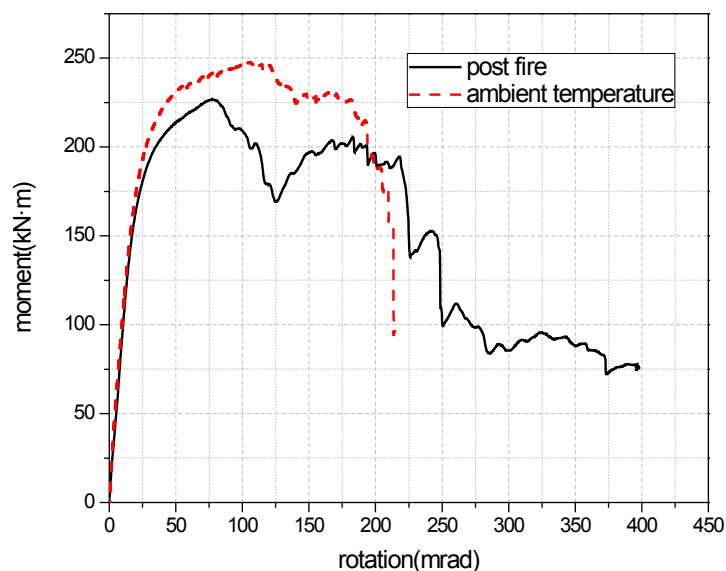
Fig.8.8. Effect of post fire to 550°C on connection 1-2 P (S690 12mm).

Fig.8.9. Effect of post fire to 550°C on connection 2-1 P (Q235 25mm).

Fig.8.10. Effect of post fire to 550°C on connection 2-2 P (Q345 20mm).

Fig.8.11. Effect of post fire to 550°C on connection 2-3 P (S690 15mm).

Fig.8.12. Effect of post fire to 550°C on connection 2-4 P (S960 12mm).

Table 8.6: Post-fire effect on behaviour of endplate connections

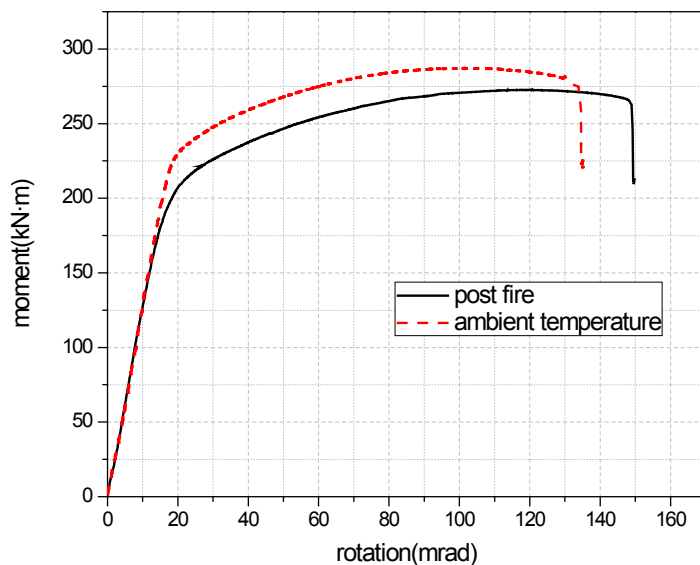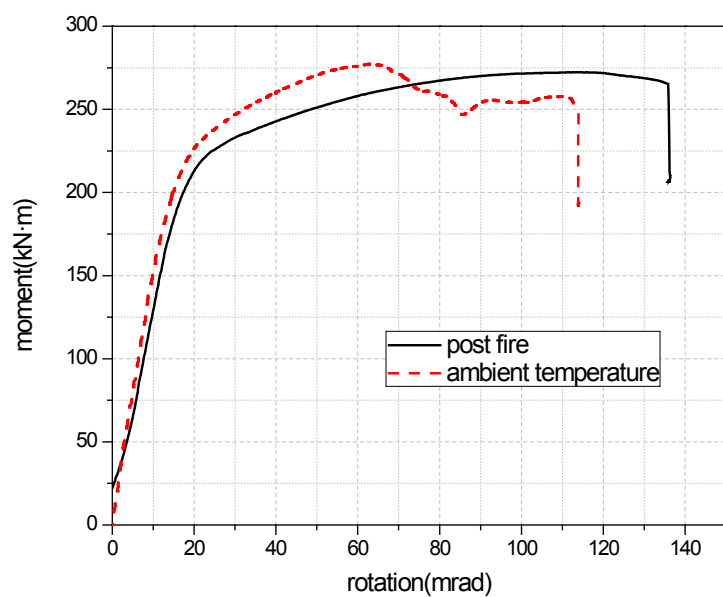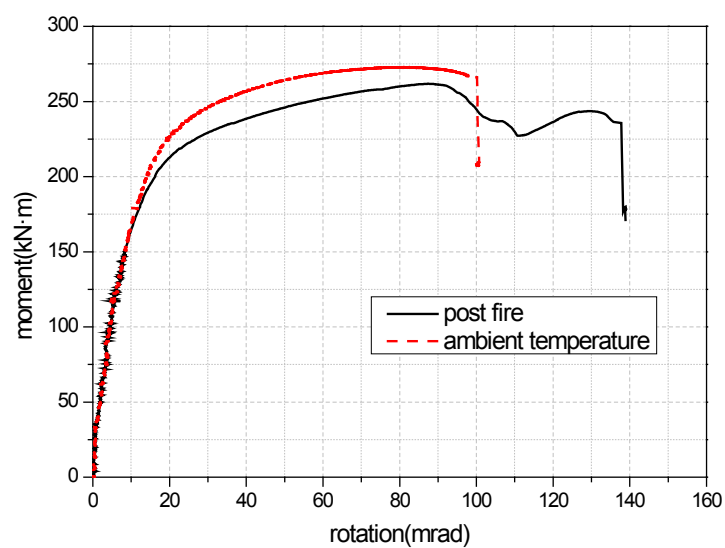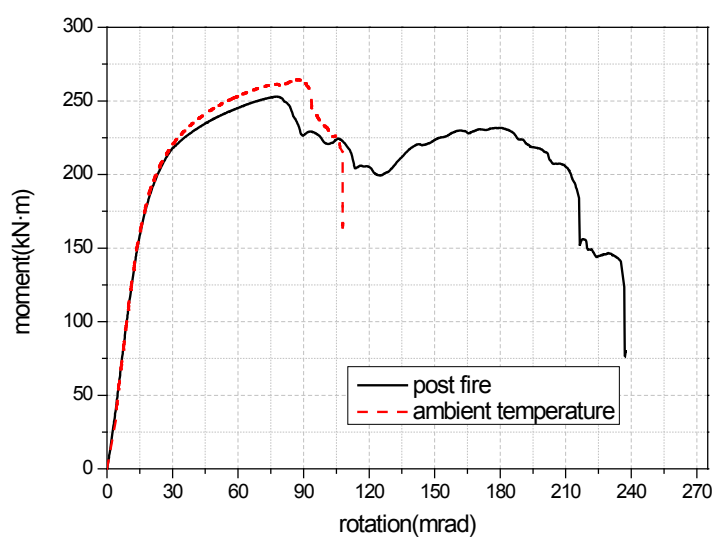| Endplate Connections			Peak moment (kN • m)			Connection rotation capacity Φ_C (mrad)		
Test ID	Mate -rial	Thickness (mm)	After fire	Ambient temperature	Reduction (%)	After fire	Ambient temperature	Improvement (%)
1-1 P	Q235	20	255.56	229.93	-11.15	249	199	25.13
1-2 P	S690	12	226.67	247.85	8.55	397	214	85.51
2-1 P	Q235	25	272.59	287.00	5.02	150	114	31.58
2-2 P	Q345	20	272.35	277.25	1.77	139	115	20.87
2-3 P	S690	15	261.79	272.71	4.00	141	101	39.60
2-4 P	S960	12	252.85	264.32	4.34	238	105	126.67

Table 8.6 summarizes the post-fire effect on various endplate connections, including the reduction of residual load bearing capacity and improvements of rotational capacity Φ_C after fire. It can be found that for all endplate connections, the residual load bearing capacities after fire is more than 90% of their original load bearing capacities at ambient temperature without fire exposure. It means endplate connections can regain more than 90% of their original load bearing capacities after cooling down from fire temperature 550°C. This important finding is valid for both high strength steel endplate connections and mild steel endplate connections. It is very promising for the reuse of steel structures with endplate connections after fire. It might be necessary to keep in mind that the increase of residual load bearing capacity of connection 1-1 P (Q235 20mm) after fire attributes to the deviation of material properties of endplate Q235 of which the thickness is 20mm.

What is more, the rotational capacity of high strength steel endplate connections after cooling down from fire temperature 550°C is found to be improved in comparison to that at ambient temperature without fire exposure. As mentioned in Chapter 6, it is generally accepted that a minimum of 40-50mrad rotation ensures "sufficient rotation capacity" of a bolted joint in a partial strength scenario [4, 5]. Wilkinson et al. suggested that a connection in steel moment resisting frames in a seismic area must develop a minimum plastic rotation of 30mrad [6]. In this experimental study, the post-fire rotation capacity is higher than 100mrad for all endplate connection specimens. Hence the post-fire rotation capacity of high strength steel endplate connections is proved sufficient after cooling down from fire temperature 550°C. This conclusion is also valid for the post-fire rotational capacity of mild steel endplate connections.

8.3.4 Plastic flexural resistance

In theoretical predictions of plastic flexural resistance (design moment resistance) of endplate connections based on Eurocode 3 [1], the remaining factor 0.9 for post-fire yield strength of mild steels is used, as recommended in British standard BS 5950 [3]. For high strength steels, based on the results of experimental study as presented in Chapter 5, 0.9 is employed as remaining factor of yield strength after cooling down from fire temperatures below 600°C. For the bolts of Grade 8.8, test results reported by Guobiao Lou et al.[7] are used. The plastic flexural resistances of all endplate connections after fire obtained from tests defined according to two methods (Zanon and Zandonini's method [8] and Weynand's method [9]) are compared with the theoretical predictions of Eurocode 3 [1], as illustrated in Table 8.7.

It can be observed that good agreements exist between the theoretical predictions and experimental results. Via Ratio 3 presented in Table 8.7, the observation can be found that $M_{j,Rd,test,1}$, obtained based on Zanon and Zandonini's definition, is generally smaller than $M_{j,Rd,test,2}$, which is defined according to Weynand's proposal and the simplified method recommend by Eurocode 3. The comparison of $M_{j,Rd,test,2}$ with the predicted plastic flexural resistance according to Eurocode 3 shows that the predictions of Eurocode 3 are generally at the conservative side when the test result is obtained based on Weynand's evaluation method. However, when the test obtained plastic flexural resistance is defined according to Zanon and Zandonini's method, the predictions of Eurocode 3 are not as conservative as the former, but still on the conservative side in general. This validates that the accuracy of Eurocode 3 is acceptable when used to predict the plastic flexural resistance of endplate connections after fire, no matter the endplate is made of mild steels or high strength structural steels.

The comparisons of the plastic flexural resistance $M_{j,Rd}$ predicted by Eurocode 3 with the experimentally obtained plastic flexural resistances $M_{j,Rd,test,1}$ and $M_{j,Rd,test,2}$ for all seven connections after cooling down from fire temperature 550°C are presented in Figs.8.13-8.19.

Table 8.7: Evaluation of plastic flexural resistance after cooling down from 550°C

Test ID	Connections	$M_{j,Rd,EC3}$ (kN·m)	$M_{j,Rd,test,1}$ (kN·m)	$M_{j,Rd,test,2}$ (kN·m)	Ratio$_1$= $\dfrac{M_{j,Rd,EC3}}{M_{j,Rd,test,1}}$	Ratio$_2$= $\dfrac{M_{j,Rd,EC3}}{M_{j,Rd,test,2}}$	Ratio$_3$= $\dfrac{M_{j,Rd,test,1}}{M_{j,Rd,test,2}}$
1-1 P	Q235 20mm	150.36	164.98	161.21	0.911	0.933	1.023
1-2 P	S690 12mm	158.93	190.17	205.88	0.836	0.772	0.924
1-3 P	S960 10mm	153.56	175.67	194.24	0.874	0.791	0.904
2-1 P	Q235 25mm	223.06	227.59	233.18	0.980	0.957	0.976
2-2 P	Q345 20mm	211.12	232.07	238.41	0.910	0.886	0.973
2-3 P	S690 15mm	228.32	216.43	227.73	1.055	1.003	0.950
2-4 P	S960 12mm	222.11	215.80	228.26	1.029	0.973	0.945

Note:

$M_{j,Rd,EC3}$ is the predicted plastic flexural resistance according to Eurocode 3;

$M_{j,Rd,test,1}$ is the test obtained plastic flexural resistance according to Zanon and Zandonini's evaluation method;

$M_{j,Rd,test,2}$ is the test obtained plastic flexural resistance according to Weynand's evaluation method.
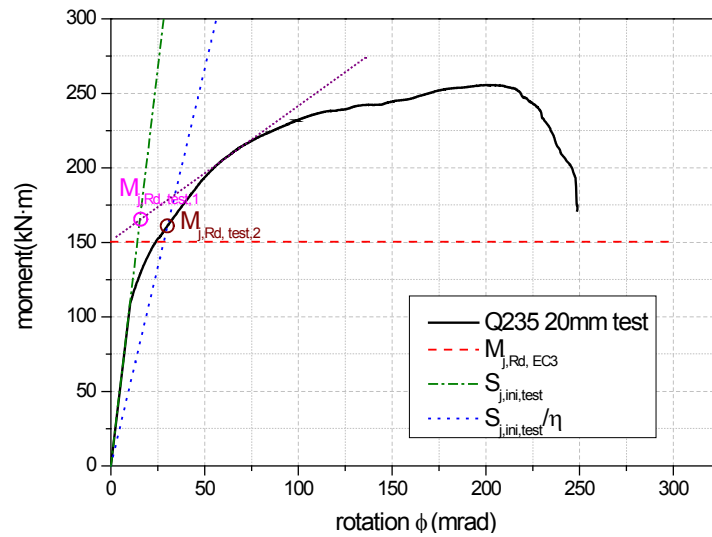
Fig.8.13. Comparison on plastic flexural resistance of connection 1-1 P (Q235 20mm) after fire.
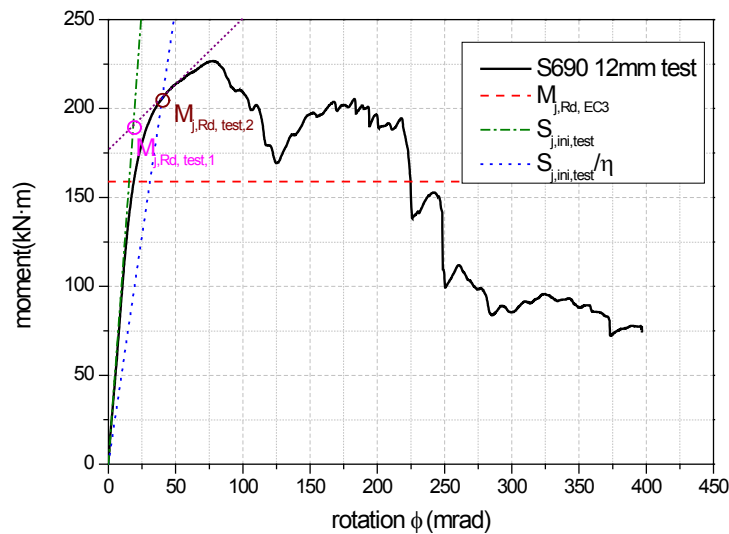
Fig.8.14. Comparison on plastic flexural resistance of connection 1-2 P (S690 12mm) after fire.
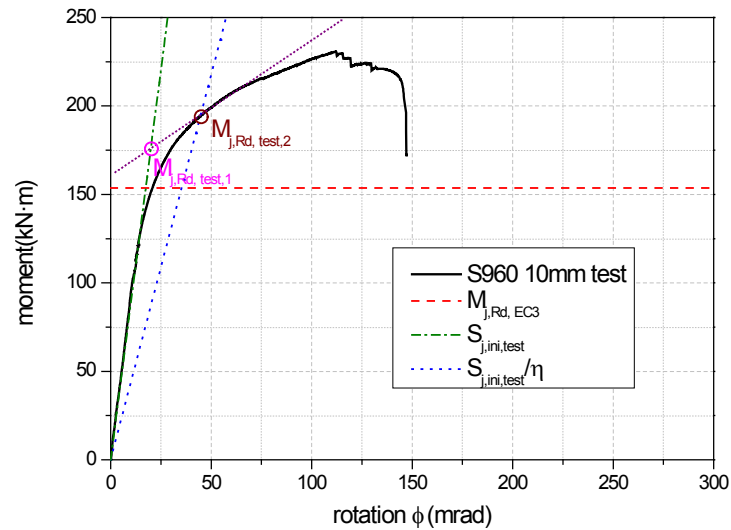
Fig.8.15. Comparison on plastic flexural resistance of connection 1-3 P (S960 10mm) after fire.
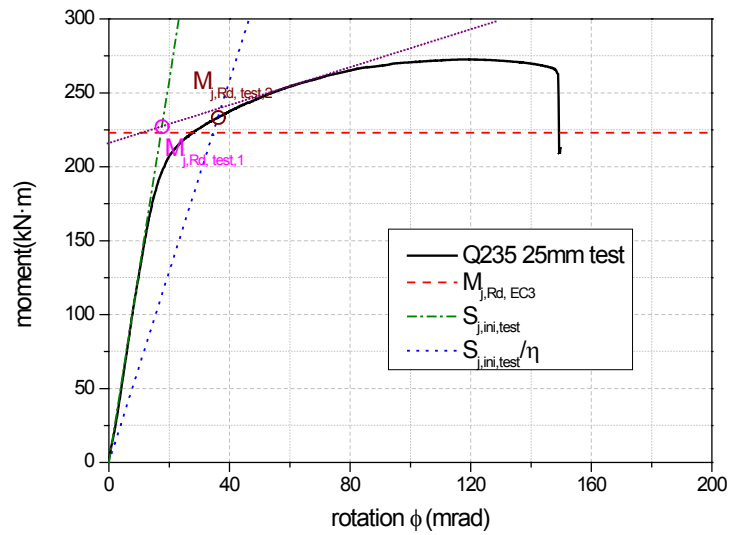
Fig.8.16. Comparison on plastic flexural resistance of connection 2-1 P (Q235 25mm) after fire.
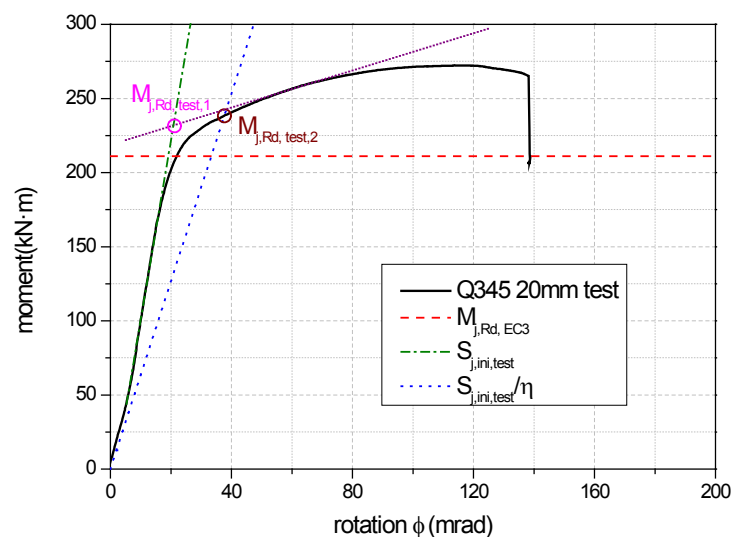
Fig.8.17. Comparison on plastic flexural resistance of connection 2-2 P (Q345 20mm) after fire.
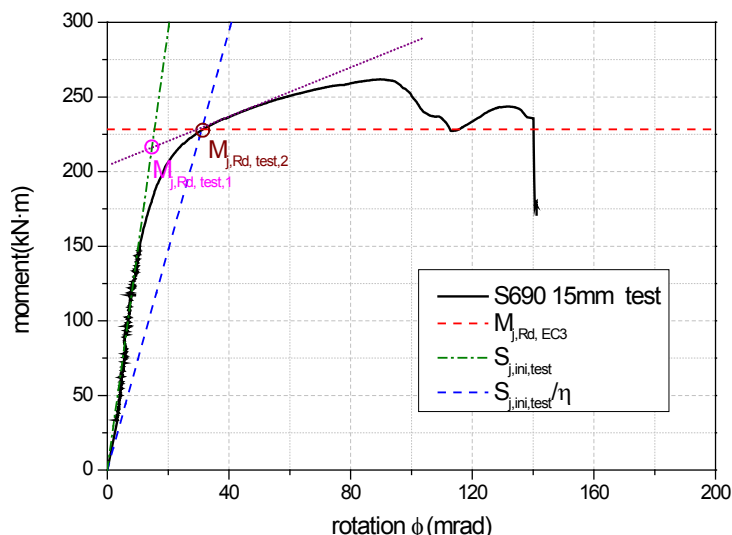
Fig.8.18. Comparison on plastic flexural resistance of connection 2-3 P (S690 15mm) after fire.
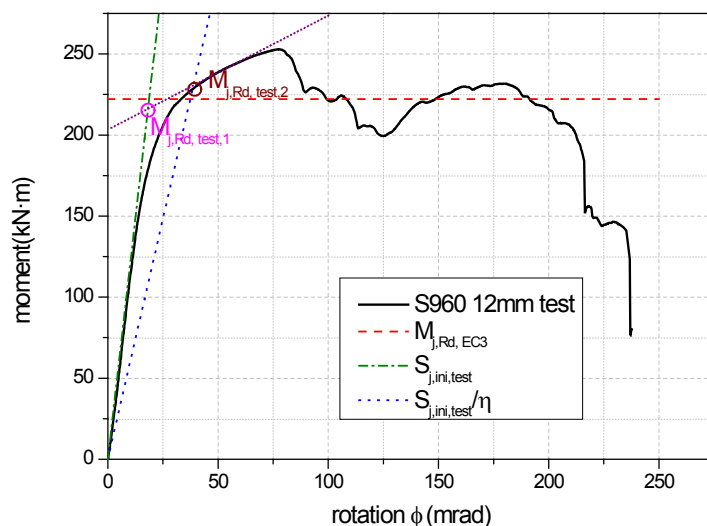
Fig.8.19. Comparison on plastic flexural resistance of connection 2-4 P (S960 12mm) after fire.

8.4 CONCLUSION

Full scale post-fire tests on 7 endplate connections of which the endplates are made of high strength steel (or mild steels for comparison) are introduced in this chapter. All specimens are designed to trigger failure in the connections rather than in beam or column. The post-fire behaviour of various endplate connections after cooling down from 550°C is compared with their performance at ambient temperature without fire exposure and presented herein. The post-fire test results are compared with theoretical predictions of Eurocode 3 as well.

The following conclusions can be drawn from this experimental study:

1. The post-fire load bearing capacity as well as rotation capacity of endplate connections is dependent on the combination of endplate material and endplate thickness.

2. For post-fire endplate connections the endplates of which are made of the same steel material, with a thicker endplate the connection can achieve higher load bearing capacity after fire, but its post-fire rotation capacity is reduced obviously after cooling down from fire. This is valid for connections of which the endplates are made of both mild steels (i.e. Q235) and high strength steels (i.e. S690 and S960).

3. The rotation capacity of high strength steel endplate connections after fire is proved to be sufficient, which guarantees the post-fire ductility and safety of steel structures using endplate connections made of high strength steel after cooling down from fire temperatures below 550°C.

4. In endplate connections, a proper design using a thinner high strength steel endplate can achieve the same failure mode, similar residual load bearing capacity and comparable or even higher rotation capacity after cooling down from fire, in comparison with a connection with thicker mild steel endplate.

5. It is found that high strength steel endplate connection can regain more than 90% of its original load bearing capacity after cooling down from fire temperature 550°C. This important finding is very promising for the reuse of steel structures with high strength steel endplate connections after fire.

6. The accuracy of Eurocode 3 for plastic flexural resistance of endplate connections is validated to be acceptable when used to predict post-fire behaviour, no matter the endplate is made of mild steels or high strength structural steels.

7. This experimental study can be used as a benchmark for evaluation on post-fire performance of high strength steel endplate connections. It widens a perspective of using high strength steels to take place of mild steels in structural design of endplate connections. For practical applications and post-fire evaluation of other types of connections or structural members made of high strength steels, more research work (such as tests on more types of connections and parametric study) should be further conducted on the behaviour of high strength steel structures after fire.

8.5 REFERENCES

[1] European Committee for Standardization (CEN), BS EN 1993-1-8, Eurocode3: Design of steel structures, Part 1-8: Design of joints. British Standards Institution, Brussels , 2005.

[2] Chinese Committee for Standardization, GB/T 11256-2005, The hot-rolled H and cut Tsection, China, 2005.

[3] B.S. Institution, BS5950, Structural use of steelwork in building, Part 8: Code of practice for fire resistant design, London, 1998.

[4] Ana M. Girão Coelho, Luís Simões da Silva, Frans S. K. Bijlaard, Ductility analysis of bolted extended end plate beam-to-column connections in the framework of the component method, Steel and composite structures, 6, 33-53(2006).

[5] Ana M. Girão Coelho, Characterization of the ductility of bolted end plate beam-to-column steel connections. PhD thesis, University of Coimbra, 2004.

[6] S. Wilkinson, G. Hurdman, A. Crowther, A moment resisting connection for earthquake resistant structures. J Constr Steel Res, 62, 295–302 (2006).

[7] G. Lou, S. Yu and R.Wang, Experimental study of mechanical properties of high-strength bolts after fire. Proceedings of the Sixth International Conference Structures in Fire 2010, pp.679-686, East Lansing, USA, 2010.

[8] P. Zanon, R. Zandonini, Experimental analysis of end plate connections, Proceedings of the state of the art workshop on connections and the behaviour of strength and design of steel structures, Cachan, pp.41-51, 1988.

[9] K. Weynand, Sicherheits- und Wirtschaftlichkeitsuntersuchungen zur Anwendung nachgiebiger Anschlüsse im Stahlbau. Heft 35, Shaker Verlag, Aachen, 1997.

Chapter 9

Numerical analysis on HSS endplate connections after fire

9.1 INTRODUCTION

This chapter presents a numerical study on high strength steel endplate connections after fire carried out using the commercial package ABAQUS 6.8 [1]. For comparison, the post-fire behaviour of mild steel endplate connections has been modelled as well. The endplate connections modelled in this chapter are exactly the same as those in the experimental study presented in Chapter 8, the geometric details of which are presented in Appendix A. The final deformation state, moment-rotation characteristics and stress distribution of endplate connections after fire are obtained from numerical modelling. Further, the accuracy of this numerical modelling is validated against the experimental results described in Chapter 8.

9.2 FINITE ELEMENT MODEL DISCRIPTION

9.2.1 Geometric Details

The geometric details of all connections' components modelled in FEM are the same with those of the test specimens as presented in Chapter 8. Because the geometric details, load, temperature distribution and boundary conditions of the endplate connection are symmetric, half of the endplate connection is modelled, to reduce computer costs and computing time. The components of this FE model are the same with those in fire as described in Chapter 7, see Fig. 7.1, including beam, column, endplate, bolt shank and nut.

9.2.2 Mesh Generation and Element Type

There are 7 surface-to-surface contact interactions and 7 tie interactions in this FE model, and the materials are endowed with non-linear properties. These make this analysis sensitive to mesh, so the mesh should be fine enough in this model. To capture accurate stress distribution in the region around bolt holes

where yielding would likely to initiate, an intensive mesh was created in the vicinity of bolt holes, as shown in Fig. 7.2(c). The whole connection was modelled using C3D8I element, because of its excellence in simulating contact interactions, non-linear material properties and stress concentrations. The detailed description of C3D8I element has been introduced in Section 7.2.2. The mesh generation of this FE model is the same with that for fire performance simulation in Chapter 7, see Fig.7.2.

9.2.3 Contact Interaction and Analysis Process

The contact pairs in this numerical model comprise the bolts-to-column flange, column flange-to-endplate, endplate-to-nuts, as same as that shown in Fig.7.4. The nuts were tied to the corresponding bolt shanks. Surface-to-surface contact, with a small sliding option, was employed for all contact surfaces to fully transfer load. To handle contact interaction problem, the whole analysis process comprised 5 analysis steps. In the first step, the bolts and endplate were temporarily restrained of all direction freedoms, and then a very small temporary load was applied to every bolt for restraining the bolt pairs temporarily. In the second step, the bolts and the endplate were freed from any temporary restraint. In the third step, the length of every bolt was fixed. In the fourth step, the temperature field for all components was set to 20°C, where the material properties used in this model were post-fire mechanical properties of structural steels after cooling down from fire temperature 550°C. In the fifth step, an equivalent vertical surface traction converted from the vertical load was applied to the beam flange at the stiffener for loading, see Fig.7.1 (e). The first three analysis steps helped contact interactions to be established smoothly, which is effective to decrease calculation time and eliminate errors. The failure criterion employed herein is based on deformation by assuming that cracking occurs when the ultimate strain ε_u of the material (either endplate or bolt) is reached, as presented in detail in Section 7.2.6.

9.2.4 Welds

The welds between endplate and beam were treated by tie constraint instead of physically solid modelling, as same as that shown in Fig.7.6, in order to simplify this FE model.

9.2.5 Material Properties

In this FE modelling, the material properties of mild steels (including Q235 and Q345) after cooling down from fire temperature 550°C are 90% of their

original mechanical properties at ambient temperature without fire exposure, according to the recommendation on post-fire residual factor of S235 and S275 from British Standard 5950: Part 8 [2]. The post-fire material properties of Grade 8.8 bolt assembly are 90% of their original mechanical properties at ambient temperature without fire exposure. The material properties of Grade 8.8 bolt assembly at ambient temperature without fire exposure input herein are in accordance with those reported by the University of Sheffield in literature [3-6], and the remaining factors of mechanical properties of Grade 8.8 bolt assembly after fire reported by Guobiao Lou et al.[7] are employed herein. The material properties of high strength steels S690 and S960 after cooling down from fire input in this FE model were obtained by experimental study presented in Chapter 5 and references [8, 9].

9.3 VALIDATIONS AGAINST EXPERIMENTAL RESULTS

Validations of this numerical modelling were performed against the experimental results on high strength steel and mild steel endplate connections after cooling down from fire temperature 550°C, to verify the accuracy of the proposed numerical model.

9.3.1 Deformation at the End of Post-fire Test

The numerically simulated final deformation states of all endplate connections after cooling down from fire temperature 550°C were compared with those obtained from experimental study described in Chapter 8. Fig. 9.1 and Fig. 9.2 present the comparisons on the final deformation state of connection 2-3 P (S690 15mm) and its components after failure at ambient temperature after cooling down from fire temperature 550°C, as an example. It can be seen that good agreements exist on final deformation of connection 2-3 P (S690 15mm) after fire. Although the current numerical model cannot simulate the fracture of the bolts, it is able to reveal the location where the fracture initiates and evolves, as shown in Fig. 9.2 (c). Similar conclusions can be drawn for all 7 connection specimens after cooling down from fire.
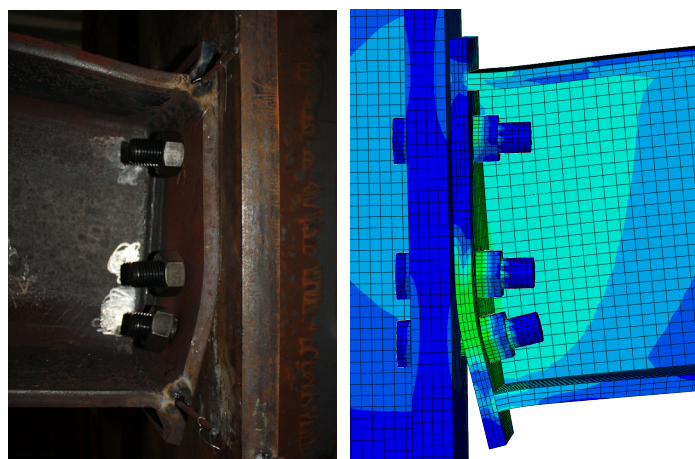
Fig.9.1. Comparison on final deformation state of connection 2-3 P (S690 15mm) after cooling down from fire temperature 550°C.

(a) Endplate front view   (b) Endplate side view

(c) Bolts
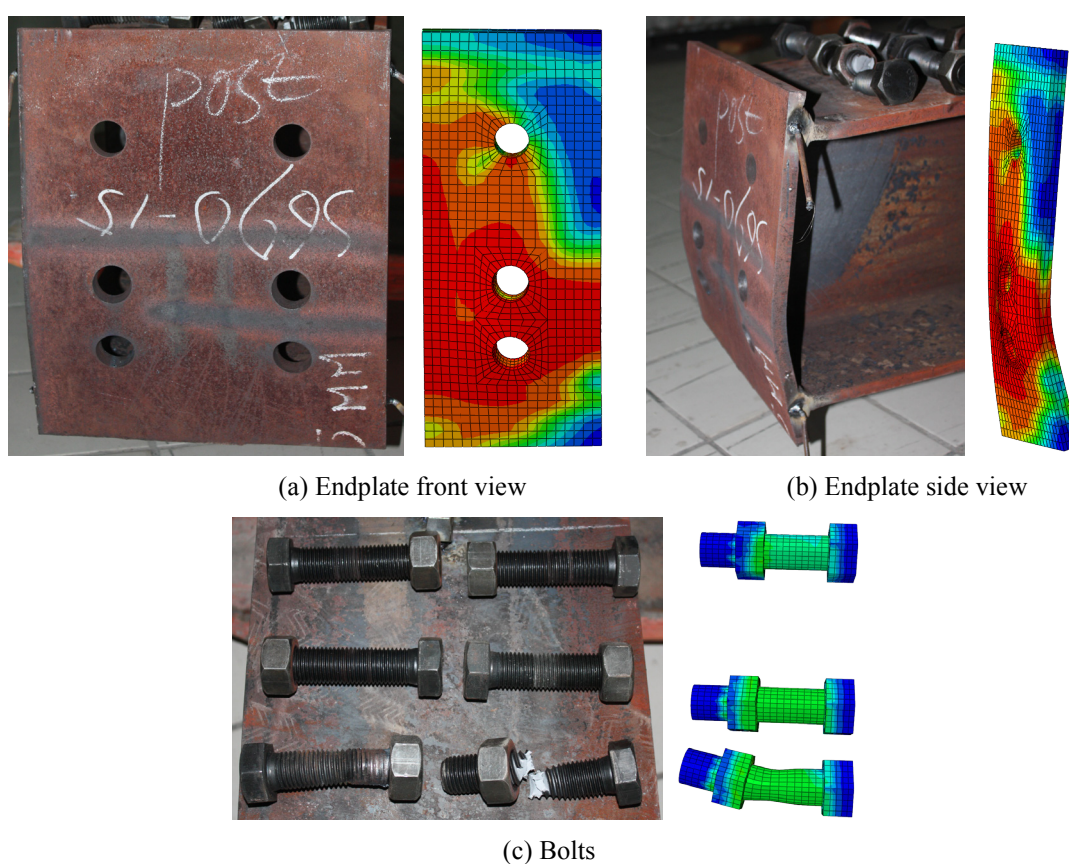
Fig.9.2. Comparison on post-fire components of connection 2-3 P (S690 15mm) after failure.

In numerical modelling, the equivalent plastic strain (PEEQ, as simplified by ABAQUS) indicates whether the material is currently yielding or not. The contour plots of equivalent plastic strain (PEEQ) obtained from numerical modelling of specimens after post-fire failure are compared with their experimental final deformation as well. For instance, the comparison for connection 2-3 P (S690 15mm) is shown in Fig.9.3, where good agreements between experimental results and numerical modelling exist.
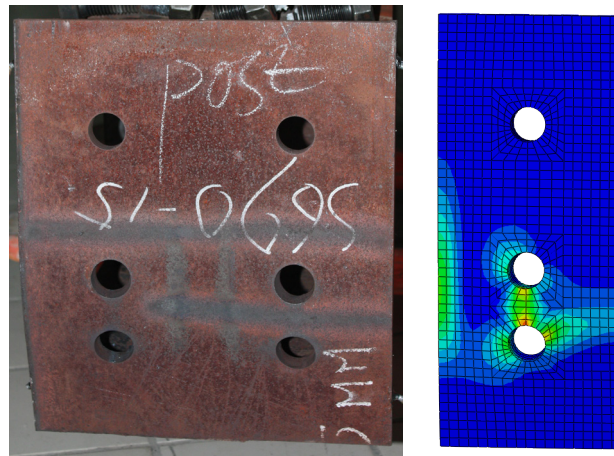
(a) Endplate
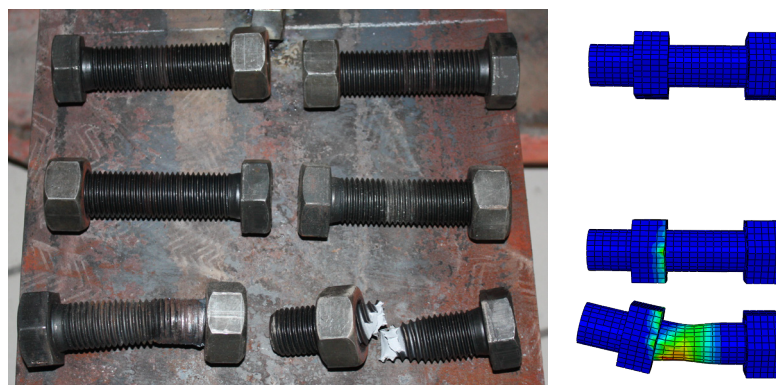
(b) Bolts

Fig.9.3. Experimental final deformation and numerically predicted PEEQ of connection 2-3 P (S690 15mm) at cooling down from 550°C.

9.3.2 Moment-rotation Characteristic after Fire

The comparisons of numerical modelling and experimental study on the moment-rotation relationship of various endplate connections (both HSS endplate connections and mild steel endplate connections) after cooling down from fire temperature 550°C are shown in Fig. 9.4- Fig. 9.10.
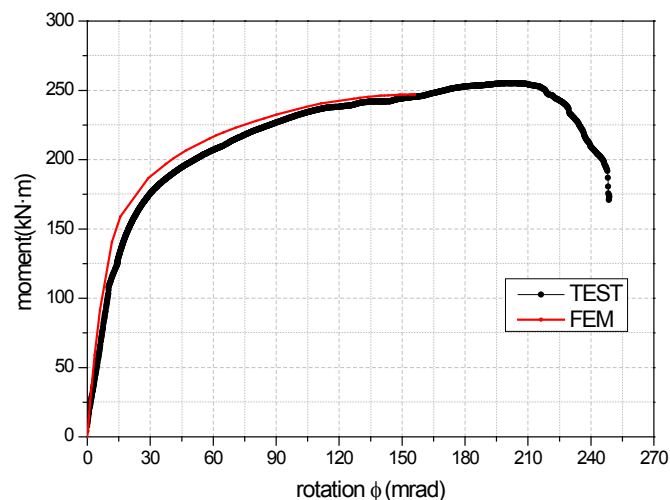
Fig.9.4. Moment-rotation comparison of 1-1 P (Q235 20mm) after cooling down from 550°C.

213
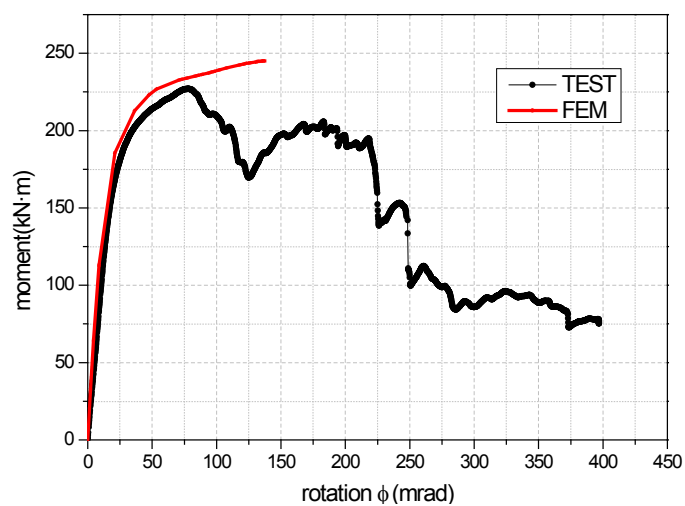
Fig.9.5. Moment-rotation comparison of 1-2 P (S690 12mm) after cooling down from 550°C.
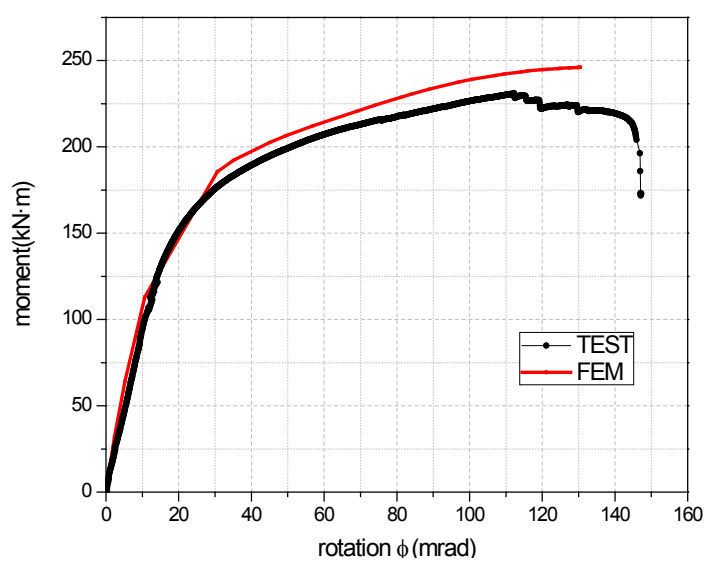
Fig.9.6. Moment-rotation comparison of 1-3 P (S960 10mm) after cooling down from 550°C.
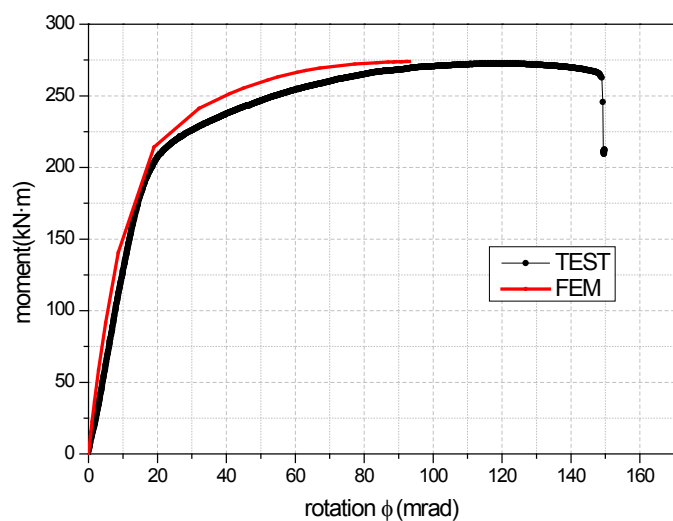
Fig.9.7. Moment-rotation comparison of 2-1 P (Q235 25mm) after cooling down from 550°C.
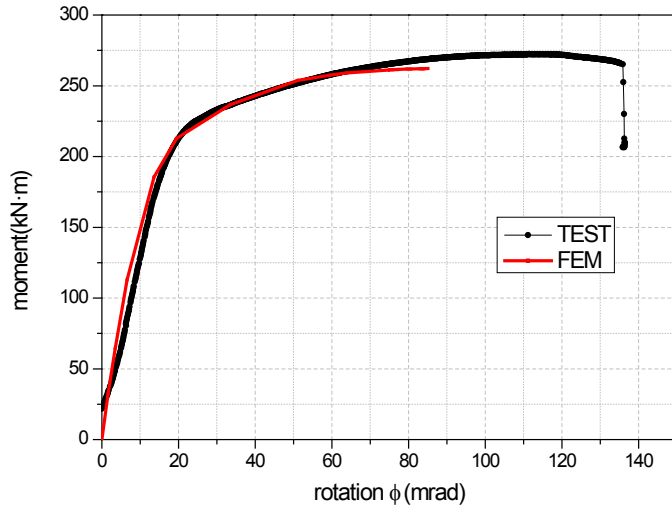
Fig.9.8. Moment-rotation comparison of 2-2 P (Q345 20mm) after cooling down from 550°C.
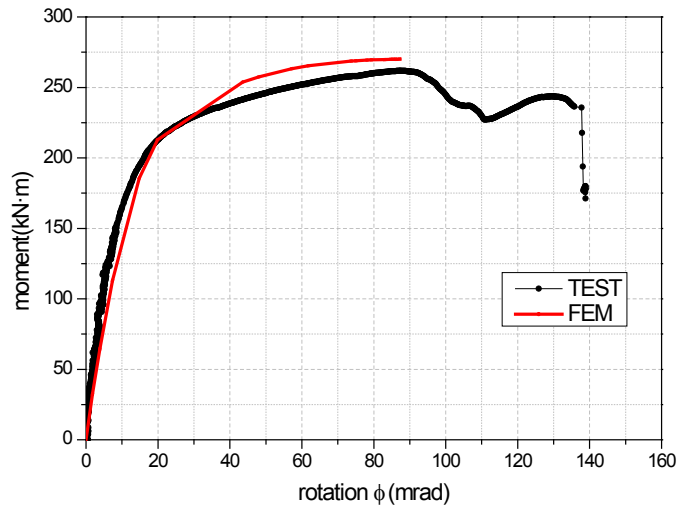
Fig.9.9. Moment-rotation comparison of 2-3 P (S690 15mm) after cooling down from 550°C.
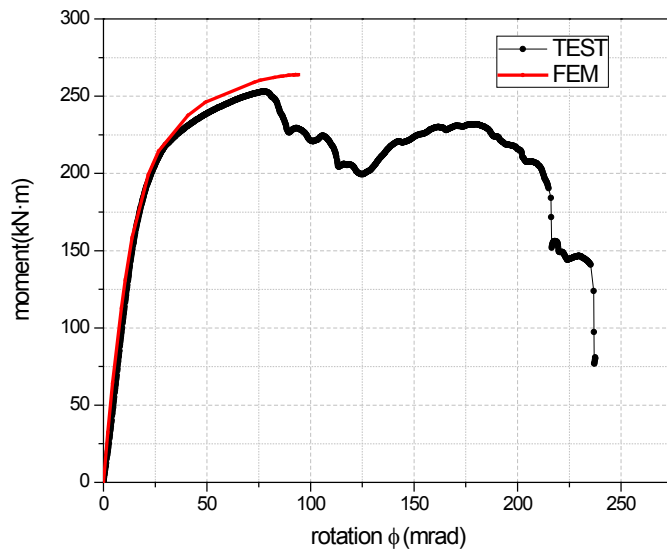
Fig.9.10. Moment-rotation comparison of 2-4 P (S960 12mm) after cooling down from 550°C.

It can be seen that good agreements exist between numerical modelling and test results for all test specimens. For instance, as shown in Fig. 9.10, the

numerically simulated moment-rotation relationship agrees very well with that from experimental results on post-fire initial stiffness, post-fire load bearing capacity and post-fire connection rotation at the maximum load level $\phi_{M\max}$. However, this current FE model cannot simulate the descending stage of moment-rotation curves obtained in tests; hence it is not able to simulate the post-fire connection rotation capacity ϕ_C.

Table 9.1: Validation of numerical study against experimental study after cooling down from fire temperature 550°C

Connection ID	Endplate		Peak moment (kN • m)		Deviation of peak moment (%)
	Material	Thickness (mm)	Tests	FEM	
1-1 P	Q235	20	255.56	247.11	3.31
1-2 P	S690	12	226.67	245.11	8.14
1-3 P	S960	10	-	246.17	-
2-1 P	Q235	25	272.59	273.96	0.50
2-2 P	Q345	20	272.35	262.14	3.75
2-3 P	S690	15	261.79	270.06	3.16
2-4 P	S960	12	252.85	264.01	4.41

The post-fire peak load of various endplate connections after cooling down from fire temperature 550°C obtained from numerical modelling are validated with the experimental results and listed in Table 9.1. It is worthwhile mentioning that the results for connection S960 10mm are excluded in the comparison of peak load because of its early cracking on the endplate at the heat affected zone of welds in post-fire tests. It can be found that the maximum deviation of the post-fire peak load between numerical modelling and experimental result is 8.14% for all connection specimens. The differences between numerical modelling and experimental study might attribute to the deviations of material properties of structural steels and temperature field distribution in various components of connection specimens when they are exposed to fire in full-scale tests. It is validated that the numerical model proposed here can simulate the post-fire performance of endplate connections with reasonable accuracy, which is valid for both high strength steel endplate connections and mild steel endplate connections.

9.3.3 Stress Distribution State

The stress distribution state of endplate connections at any time point during loading after cooling down from fire can be obtained by this proposed numerical analysis, in the form of contour plots of the Mises stress. For example, Fig. 9.11 and Fig. 9.12 show the contour plots of the Mises stress on components of connection 1-2 P (S690 12mm), in which the stress distribution

on the components can be observed. Fig. 9.11 also compares the post-fire yield line pattern of endplate between that from numerical modelling and test result. It can be seen that good agreement exists. The same conclusion can be drawn from the comparisons of numerical modelling and test results for all tested connection specimens. Therefore, this numerical model can be used with confidence to predict the stress distribution and yield line pattern of the endplate connections after fire.

(a) Front view of endplate   (b) Side view of endplate
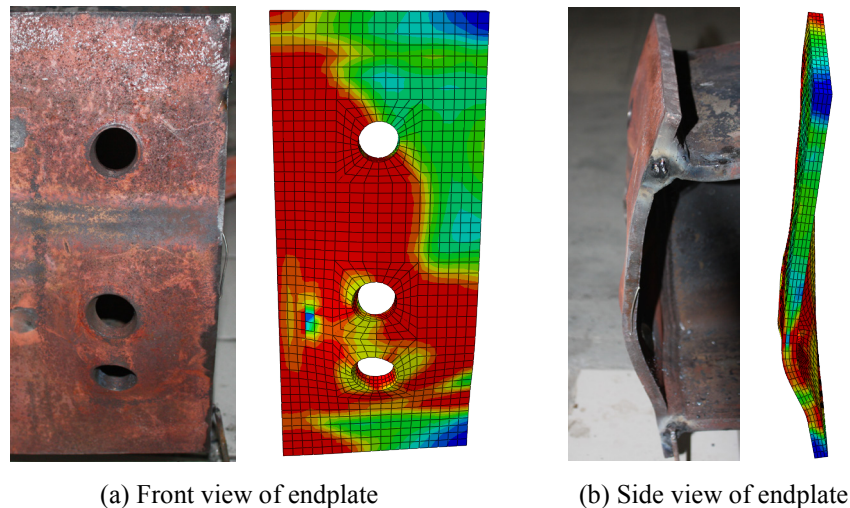
Fig.9.11. Stress state at the end of test and yield line pattern for endplate of 1-2 P (S690 12mm) after cooling down from fire.

Fig.9.12. Stress state at the end of test for bolts in top tensile row of 1-2 P (S690 12mm) after cooling down from fire.

9.4 CONCLUSION

This chapter reports on a numerical study of endplate connections using ABAQUS/Standard, in order to investigate the performance of high strength steel endplate connections after fire. Validation of this numerical modelling against all representative experimental results conducted on moment-rotation relationship, final deformation state and yield line pattern of endplate connections shows good agreements exist. Hence the numerical analysis method proposed herein can be used with confidence to predict the behaviour of high strength steel endplate connections after cooling down from fire. The following conclusions can be drawn.

The challenge of numerical modelling contact interactions considering material and geometric non-linear effects has been solved successfully. The proposed FE modelling is validated appropriate to simulate both high strength steel and mild steel endplate connections after fire. Based on this, the FE modelling can be used with confidence to predict stress distribution of high strength steel endplate connections after cooling down from fire, which is not easy to achieve for all connection components in full-scale tests. What is more, parametric study can be further performed using this numerical model to investigate the post-fire performances of high strength steel endplate connections after cooling down from various fire temperatures, via inputting proper mechanical properties of high strength steels after fire, for instance that of S460, S690 and S960 after cooling down from various fire temperatures presented in Chapter 5. Thus the proposed numerical model may be used as a basis for further investigation on evaluating the behaviour of post-fire steel connections and fire safety of steel structures with high strength steel members after fire.

By the present modelling method, the first critical component of endplate connections can be identified, but the occurrence of component fracture as well as the subsequent failure on other components cannot be predicted. To improve this numerical simulation, solid modelling of welds and taking into account fracture features on components are of importance in future numerical study.

9.5 REFERENCES

[1] Abaqus Analysis User's Manual, 6.8 version.

[2] B.S. Institution, BS5950, Structural use of steelwork in building, Part 8: Code of practice for fire resistant design, London, 1998.

[3] Y. Hu, J.B. Davison, I.W. Burgess and R.J. Plank, Experimental Study on Flexible End Plate Connections in Fire, Proc. 5th European Conference on Steel Structures, Graz, Austria, 1007-1012.

[4] Y. Hu, J.B. Davison, I.W. Burgess and R.J. Plank, Comparative Study of the Behaviour of BS 4190 and BS EN ISO 4014 Bolts in Fire, ICSCS 2007, Manchester, 587-592.

[5] Y. Hu, Robustness of flexible endplate connections under Fire Conditions, PhD thesis, University of Sheffield, UK, 2009.

[6] Theodorou Y, Mechanical properties of grade 8.8 bolts at elevated temperatures. Master's dissertation. University of Sheffield, UK, 2003.

[7] G. Lou, S. Yu and R.Wang, Experimental study of mechanical properties of high-strength bolts after fire. Proceedings of the Sixth International Conference Structures in Fire 2010, pp.679-686, East Lansing, USA, 2010.

[8] X. Qiang, F.S.K. Bijlaard, M.H. Kolstein, Post-fire mechanical properties of high strength structural steels S460 and S690, Engineering Structures, 35 (2012) 1–10.

[9] X. Qiang, F.S.K. Bijlaard, M.H. Kolstein, Post-fire performance of very high strength steel S960, Journal of Constructional Steel Research, 80 (2013) 235–242.

Chapter 10

Conclusions and recommendations

The aim of this research is to reveal more information and understanding on behaviour and failure mechanisms of high strength steel endplate connections (combining high strength steel endplates with either mild steel or high strength steel beams and columns in endplate connections) in fire and after fire, for an effective application of high strength structural steels in civil engineering as well as enhancing the fire safety of steel structures.

The research work consists of three main parts: (Part I) numerical validation of research idea; (Part II) experimental study on mechanical properties of high strength structural steels in fire and after fire; (Part III) full-scale behaviour of high strength steel endplate connections in fire and after fire. In the following section, the main outcome of each part of this research is presented, while in the final section some recommendations for future research work in this field are proposed.

10.1 CONCLUSIONS

Part I: Numerical validation of research idea

The main goal of this part is to reveal how connections behave in fire when combining high strength steel endplate with mild steel beam and column in endplate connections.

The challenge of numerical modelling contact interactions was solved successfully, considering material and geometric non-linear effects. The proposed FE modelling was verified appropriate to simulate mild steel endplate connections at ambient and elevated temperatures with reasonable accuracy. On this basis, the performances of HSS endplate connections at ambient temperature and at elevated temperatures were further predicted and compared with those of mild steel one.

It is found that a proper thinner HSS endplate can enhance the connection's ductility both at ambient temperature and at elevated temperatures, and simultaneously achieve almost the same moment resistance as a mild steel endplate connection. The proposed research idea, combining HSS with mild steel in connections, may be used for further investigation of improving the behaviour of steel connections under fire conditions as well as promoting the application of HSS in civil engineering.

Part II: Experimental study on mechanical properties of high strength structural steels in fire and after fire

(a) In fire

The comparison of HSS S460, S690 and S960 with mild steels shows that the deterioration of mechanical properties of structural steels at elevated temperatures is dependent on steel grades and manufacture method. Comparison with current European, American, Australian and former British design standards for steel structures shows that no current design standard may be used conservatively to conduct fire-resistance design of steel structures with high strength steel S460N, S690 or S960. Therefore, unique predictive equations calculating reduction factors of mechanical properties for HSS S460N, S690 and S960 at elevated temperatures were proposed and recommended for safe practical design and structural analysis. Furthermore, in tests necking always happened before tensile failure and no brittle failure mode was observed for all specimens made of HSS S460, S690 and S960 at various elevated temperatures up to 700°C, which is promising for the fire safety of steel structures with members made of HSS.

(b) After fire

The experimental results show that the steel grade has a significant influence on the post-fire residual mechanical properties of structural steels. Thus, the recommendations of the former British standard BS5950, obtained mainly from mild steels, on the reuse of steel structures exposed to fire are not appropriate to be used directly for high strength steel or very high strength steel members. Unique recommendations for the reuse of steel members made of high strength steel or very high strength steel should be proposed in the practical design standards. In addition, it is found that the post-fire material properties of S460, S690 and S960 are not affected until they are exposed to fire temperatures above 600°C. So, if the distortions of steel members made of HSS S460, S690

and S960 after fire remain within the tolerance limits, they can be considered to be reused. For the reuse based on conservative consideration, it is suggested using 90% of its nominal mechanical properties if the steel member made of HSS S460, S690 or S960 is cooled down after exposure to fire temperatures below 600°C. To easily evaluate the residual mechanical properties of S460, S690 and S960 after cooling down from temperatures beyond 600°C up to 1000°C, some separate predictive equations were proposed to determine their post-fire elastic modulus, yield strengths and ultimate strengths. The application of such accurate residual mechanical properties will lead to appropriate post-fire evaluation and safe reuse of steel structures with members made of HSS S460, S690 or S960 after being exposed to fire.

This part of the research also highlights the necessity of more research works on mechanical properties at elevated temperatures as well as after cooling down from fire for all high strength structural steel grades used in construction, since it is found that the deterioration of mechanical properties of structural steels in fire and after fire is dependent on steel grade and manufacture.

Part III: Full-scale behaviour of high strength steel endplate connections in fire and after fire

(a) In fire

The following conclusions can be drawn from the experimental study. The moment resistance as well as rotation capacity of endplate connections is dependent on the combination of endplate material and endplate thickness. For endplate connections of which the endplates are made of the same steel material, with a thicker endplate the connection can achieve higher moment resistance but its rotational capacity is reduced obviously at both ambient temperature and elevated temperatures. This is proved valid for both mild steels (i.e. Q235) and high strength steels (i.e. S690 and S960). The current provisions of Eurocode 3 on rotation capacity of bolted connections seem too conservative, which were mainly obtained from connections made of mild steels. They need to be checked when applied to connections made of high strength steels or very high strength steels. Maybe more repetitive tests are of help to propose an unique provision for rotation capacity of HSS bolted connections. The rotation capacity of high strength steel endplate connections in fire is proven sufficient (based on the generally accepted sense that a minimum of 40-50mrad ensures "sufficient rotation capacity" of a partial-

strength bolted joint), which guarantees the ductility and safety of steel structures using connections made of high strength steel under fire conditions. Moreover, it is found that in endplate connections a proper design using a thinner high strength steel endplate can achieve the same failure mode, similar moment resistance and comparable or even higher rotation capacity both at ambient temperature and in fire, in comparison to a connection with thicker mild steel endplate.

Further, the proposed FE modelling was verified appropriate to simulate both high strength steel and mild steel endplate connections at ambient and elevated temperatures. Based on this, the FE modelling can be used to predict stress distribution of high strength steel endplate connections both at ambient temperature and under fire conditions, which is not easy to achieve in full-scale tests especially in fire. What is more, parametric study can be further performed using this numerical model to investigate the performances of high strength steel endplate connections under various fire conditions, via inputting accurate mechanical properties of high strength structural steels in fire. Therefore the proposed numerical modelling may be used for further investigation on improving the behaviour of steel connections under fire conditions and fire safety of entire steel structures.

(b) After fire

The following conclusions can be drawn from this post-fire experimental study. Firstly the post-fire moment resistance as well as rotation capacity of endplate connections is dependent on the combination of endplate material and endplate thickness. For post-fire endplate connections of which the endplates are made of the same steel material, with a thicker endplate the connection can achieve higher moment resistance after fire but its post-fire rotation capacity is reduced obviously after cooling down from fire. This is valid for connections of which the endplates are made of both mild steels (i.e. Q235) and high strength steels (i.e. S690 and S960). The post-fire rotation capacity of high strength steel endplate connections has been proven to be sufficient, which guarantees the post-fire ductility and safety of steel structures using connections made of high strength steel after cooling down from fire temperatures. Further it is found that in endplate connections a proper design using a thinner high strength steel endplate can achieve the same failure mode, similar residual moment resistance and comparable or even higher rotation capacity after cooling down from fire, in comparison to a connection with thicker mild steel endplate. Furthermore, it is found that high strength steel endplate connections can regain more than

90% of their original moment resistance after cooling down from fire temperature 550°C. This important finding is very promising for the reuse of steel structures with high strength steel endplate connections after fire exposure. This experimental study can be used as a basis for evaluation of post-fire performance of high strength steel endplate connections. It widens a perspective of using high strength steels to take place of mild steels in the structural design of endplate connections.

What is more, the proposed FE modelling is validated appropriate to simulate both high strength steel and mild steel endplate connections after fire. Based on this, the numerical modelling can be used with confidence to predict stress distribution of high strength steel endplate connections after cooling down from fire, which is not easy to achieve for all connection components in full-scale tests. Moreover, parametric study can be further carried out using this numerical model to investigate the post-fire performances of high strength steel endplate connections after cooling down from various fire temperatures, through inputting proper mechanical properties of high strength steels after fire. Thus the proposed numerical model may be used as a basis for further investigation on evaluating the behaviour of post-fire steel connections and possibility of reuse of the steel structures with high strength steel members after fire.

10.2 RECOMMENDATIONS

Based on this research, the following remarks can be recommended for future research and practical application.

The deterioration of mechanical properties of structural steels at elevated temperatures is dependent on steel grade and manufacture method. Hence the current design standards for steel structures, which were mainly obtained from mild steels previously, may not be conservatively applied to high strength structural steels. The recommendations on reduction factors of structural steels under fire conditions in current leading design standards for steel structures (i.e. Eurocode 3, AISC, ASCE, AS 4100 and BS 5950 et al.) should be verified before applying to high strength structural steels. Some unique proposals for high strength structural steels should be introduced in current leading design standards.

The post-fire material properties of HSS S460, S690 and S960 are not affected until they are exposed to fire temperatures above 600°C. So, if the distortions of steel members made of HSS S460, S690 and S960 remain within the tolerance limits after fire, they can be considered to be reused. For the practical reuse based on conservative consideration, it is suggested using 90% of its nominal mechanical properties if the steel member made of HSS S460, S690 or S960 is cooled down after the exposure to fire temperatures below 600°C.

In endplate connections, a proper design using a thinner high strength steel endplate can achieve the same failure mode, similar moment resistance and comparable or even higher rotation capacity both in fire and after cooling down from fire, in comparison with a connection with thicker mild steel endplate. Therefore, the optimizing design of combining high strength structural steels with mild steels is of value in enhancing the fire safety of steel structures and their performance after fire. On this basis, more research ideas in combining high strength structural steels with mild steels in steel structures, to achieve the optimizing design, can be further proposed and investigated.

The current provisions of Eurocode 3 on rotation capacity of bolted connections seem too conservative, which were mainly obtained from connections made of mild steels. They need to be calibrated when applied to connections made of high strength steels or very high strength steels. More repetitive tests are of help to propose an unique provision in current leading design standards for rotation capacity of HSS bolted connections.

Results from fire tests of isolated connections provide important fundamental data on the behaviour of connections, but do not truly reflect the actual behaviour of connections in building structures in the event of a fire, due to the absence of structural continuity. Thus, the numerical simulation of connections and further entire structural frames subjected to fire and after fire is of importance as an alternative research methodology of expensive and size-limited full-scale fire tests.

Temperature gradients between different structural components in practical fires are of significance in influencing the distribution of force and deformation. In numerical modelling, it is suggested to simulate the temperature gradients for more accurate modelling. Of course, this might involve some additional knowledge on building physics beyond structural

engineering, such as on the heat transfer, thermal conductivity, thermal convection and so on.

By the present numerical modelling method, the first critical component of endplate connections can be identified, but the occurrence of component fracture as well as the subsequent failure on other components cannot be predicted. To improve this numerical simulation, solid modelling of welds and taking into account fracture features on components are of value in future research.

This research opens a perspective of using high strength structural steels to take place of mild steels in structural design. Due to the availability of high strength structural steel sheets in the current market, this full-scale experimental study was limited to several high strength steel grades with certain thicknesses. A further numerical parametric study based on the proposed FE model will be of value to perform the optimizing design and to fully understand the behaviour of HSS endplate connections in fire and after fire. For practical applications, fire-resistance design and post-fire evaluation of other types of connections (rather than endplate connections) and structural members, more research works should be further conducted on the behaviour of high strength steel structures in fire as well as after fire, such as the researches on high strength cast steel joints, columns made of HSS and HSS tubular members in offshore structures etc.

Appendixes

Column: HW400*400

8M20

8M20

Endplate connection

Beam: HW300*300

6M27

6M27

Beam

Beam :HW300*300

6M27

① endplate of beam

② stiffener of beam

Beam Section

endplate connection and beam

| 2012-01-1 | TU DELFT | No.: 1/3 | Size: A4 |

Column right side

Column left side

③ endplate of column

1860

550

310 60 120 163 100 130 211

8φ22

6φ29

75 75

Column left side

1860

550

163 100 130 211

8φ22

75 75

③ endplate of column

210 210

550 550

428

70 70

20

4φ32

407

35

550

210 210

550

70 70

4φ32

550

column and its endplate

2012-01-1

TU DELFT

No.: 2/3

Size: A4

Loading plate ⓐ

1700*100*10

1700

200   1300   200

100

6×Φ23

---

⑤ endplate

493

60   163   100   130   40

300

75 75

8Φ22

6

---

inclined strut ⓒ

HW200*200

8M20

105   283   105

20

60 163 100 130

45°

493

6

⑤

779

1101.67

HW200*200

④

8M20

105   283   105

20

40 130 100 163 60

493

6

---

④ endplate

40   130   100   163   60

300

75 75

8Φ22

493

6
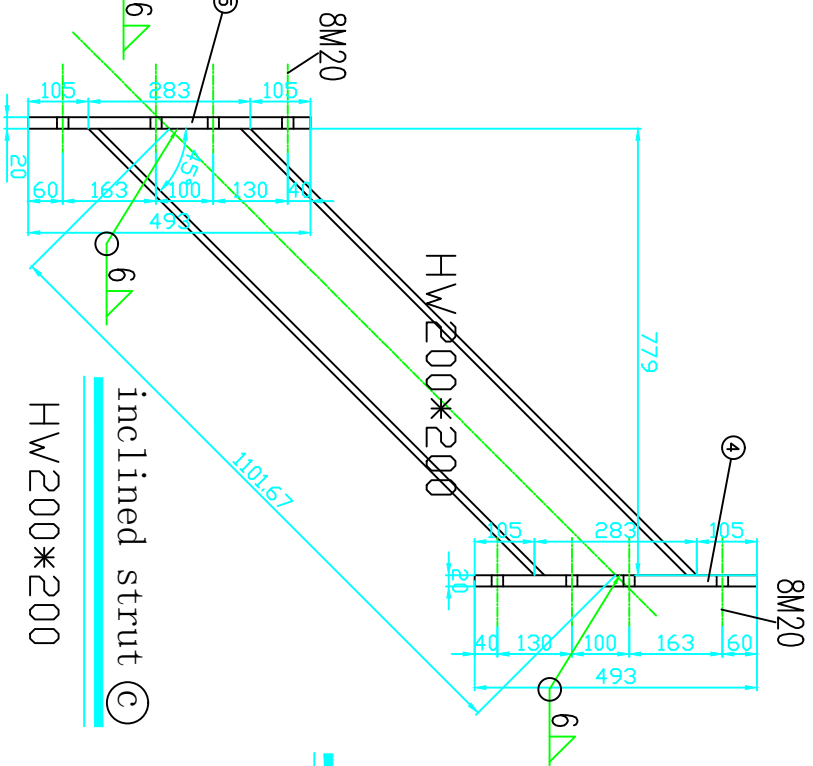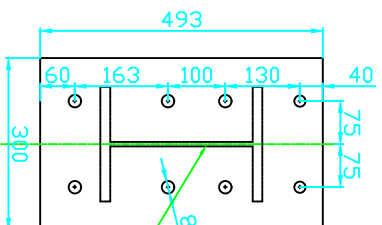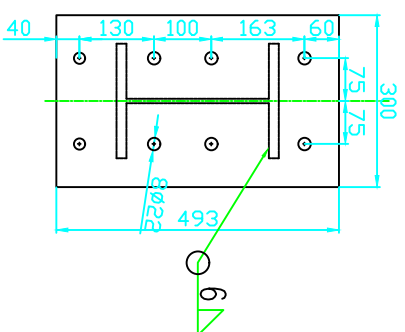
Loading accessories

| TU DELFT | No.: 3/3 |
| 2012-01-1 | Size: A4 |

Appendix B:

Deformations of endplate connections at the end of tests

B.1 At ambient temperature

For all endplate connections, their final deformation states were photographed at the end of ambient-temperature tests and presented below.

<table>
<tr><td>(a)</td><td>(b)</td></tr>
<tr><td>(c)</td><td>(d)</td><td>(e)</td></tr>
</table>

Fig.B.1. Final deformation state of connection 1-1 A (Q235 20mm) at ambient temperature.

The detailed illustrations on the final deformation state of Q235 20mm at ambient temperature are presented in Fig.B.1. It can be seen that the failure was concentrated in the endplate, and the bolts remained almost straight until very

large deformation on endplate appeared. Damage to the endplate started as significant bending; after very large plastic bending deformation of the endplate, the two rows of bolts in tension tore some bearing material from the bolt holes. It corresponds to a rapid drop in resistance of the connection, as shown in Fig.6.12 and Fig.6.16. After very large bending deformation of the endplate, some threads stripped off the bolts in the top tensile row. For the bolts in the second tensile row and bolts in compression, they remained straight in tests. The broken bolt in the second tensile row as shown in Fig.B.1 (d) and (e) was cut during removing specimen after tests.

| (a) | (b) |
| (c) | (d) | (e) |

Fig.B.2. Final deformation state of connection 1-2 A (S690 12mm) at ambient temperature.

The detailed final deformation state of S690 12mm at ambient temperature is shown in Fig.B.2. It can be seen that the failure was concentrated in the endplate, and the bolts remained almost straight until very large deformation on the endplate appeared. Deformation of the endplate started as significant bending; after very large bending deformation of endplate the two rows of bolt holes in tension got extended. Finally, the nuts stripped off the bolts in the top tensile row. It corresponds to a rapid drop in resistance of the connection, as shown in Fig.6.12 and Fig.6.17. For the bolts in the second tensile row and bolts in compression, they remained almost straight in tests. The picture of bolts after removing from the specimens after tests was not taken, because the

bolts in the top tensile row were ruined during removing and the other two rows of bolts remained almost straight.
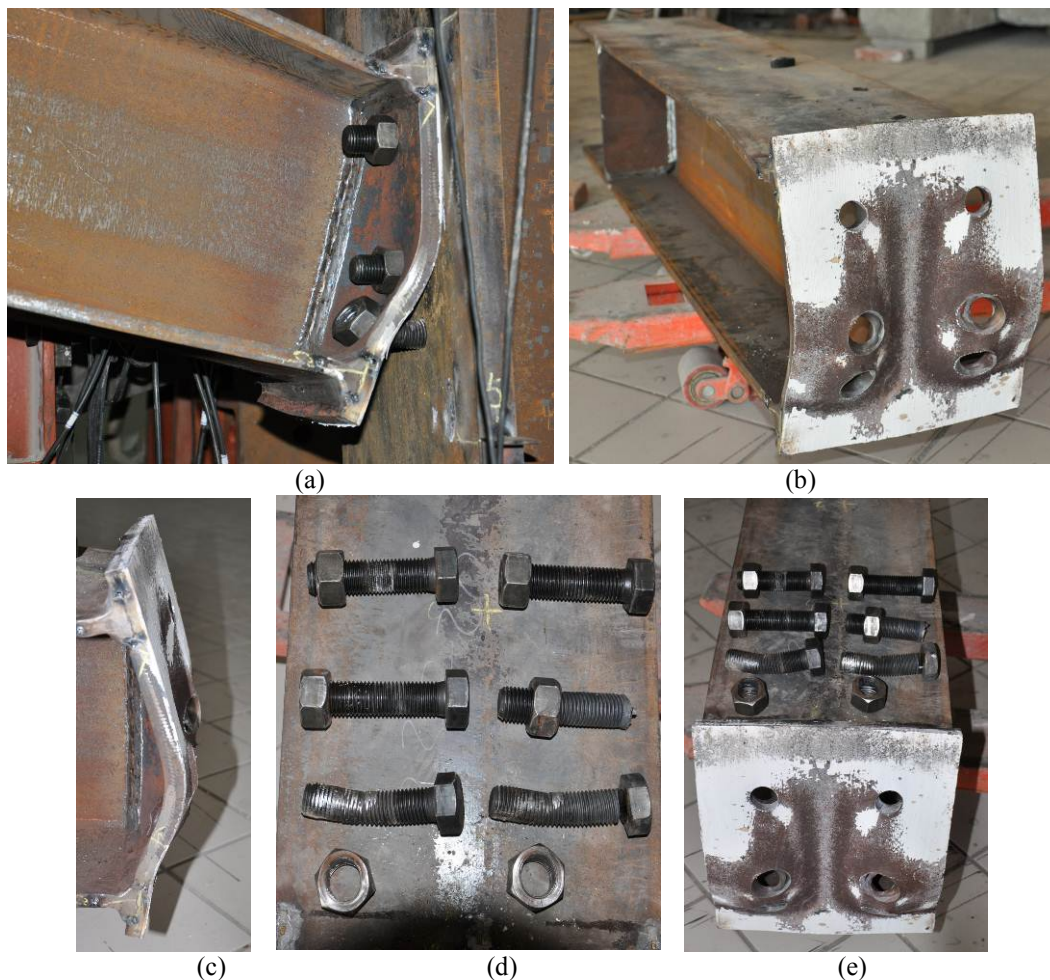

Fig.B.3. Final deformation state of connection 1-3 A (S960 10mm) at ambient temperature.

The detailed final deformation state of S960 10mm at ambient temperature is described in Fig.B.3. The endplate can be seen to have a moderate amount of plastic bending deformation. After some plastic deformation of endplate and extensions of bolt holes in the tension zone, cracking appeared on the endplate at the heat affected zone of the welds, as shown in Fig.B.3 (b) and (c). It attributes to the quality of the welds between endplate and beam. Since the thickness of endplate is very thin only 10mm (the thinnest in all specimens for this study), the effect of heating during welding on this endplate is more obvious than thicker endplates. For all bolts in this specimen at ambient temperature, they remained straight in tests. The damage of bolts in the top tensile row as shown in Fig.B.3 (e) was due to the cutting during removing the specimen after tests.
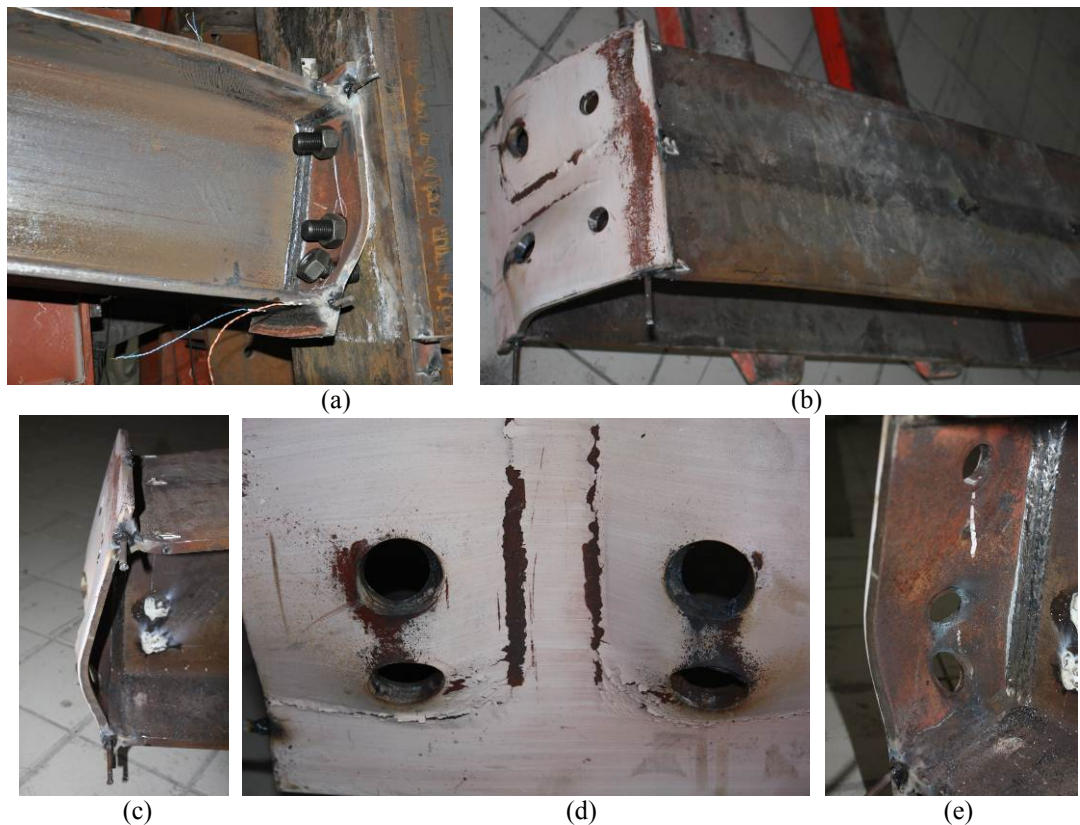
Fig.B.4. Final deformation state of connection 2-1 A (Q235 25mm) at ambient temperature.

The final deformation state of Q235 25mm at ambient temperature is presented in Fig.B.4. It can be observed that the endplate has a moderate amount of bending deformation. After some plastic deformation of the endplate, failure occurred on the bolts of the tensile top row, as shown in Fig.B.4 (d) and (e). It corresponds to the rapid drop in resistance of the connection as illustrated in Fig.6.13 and Fig.6.16. For the bolts in the second tensile row and bolts in compression, they remained almost straight in tests.

(d)   (e)   (f)
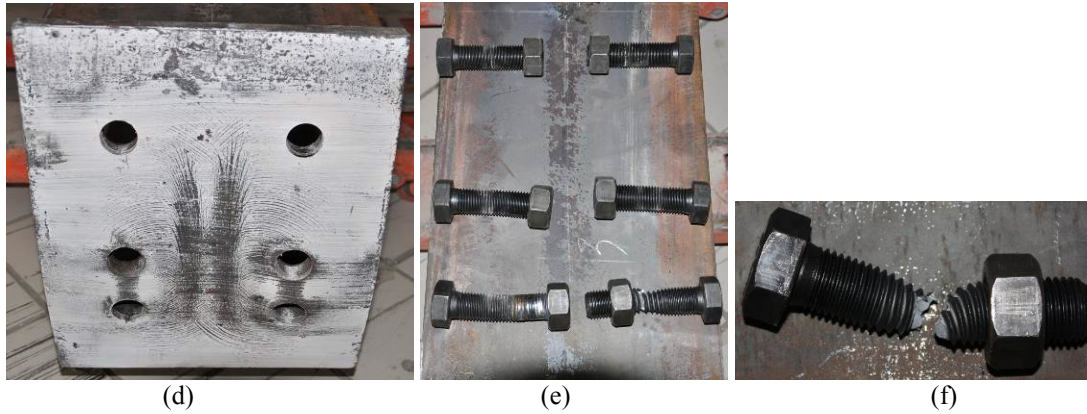
Fig.B.5. Final deformation state of connection 2-2 A (Q345 20mm) at ambient temperature.

The final deformation state of Q345 20mm at the end of the ambient-temperature test is shown in Fig.B.5, which is similar to that of Q235 25mm. It can be seen that the endplate also has a moderate amount of bending deformation. After some plastic bending deformation of the endplate, failure occurred on the bolts of the top row in tension, as shown in Fig.B.5 (e) and (f). It corresponds to the rapid drop in resistance of the connection as illustrated in Fig.6.13. As to the bolts in the second tensile row and bolts in compression, they remained almost straight in tests.

(a)   (b)

(c)   (d)   (e)   (f)
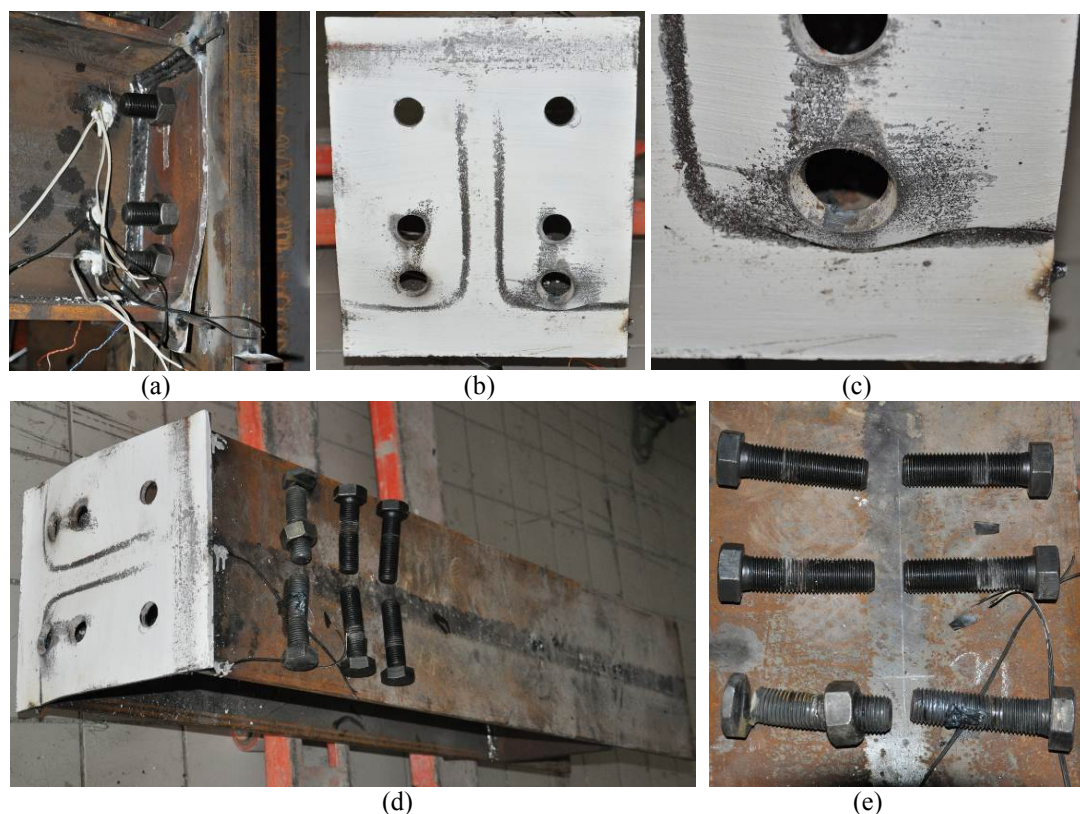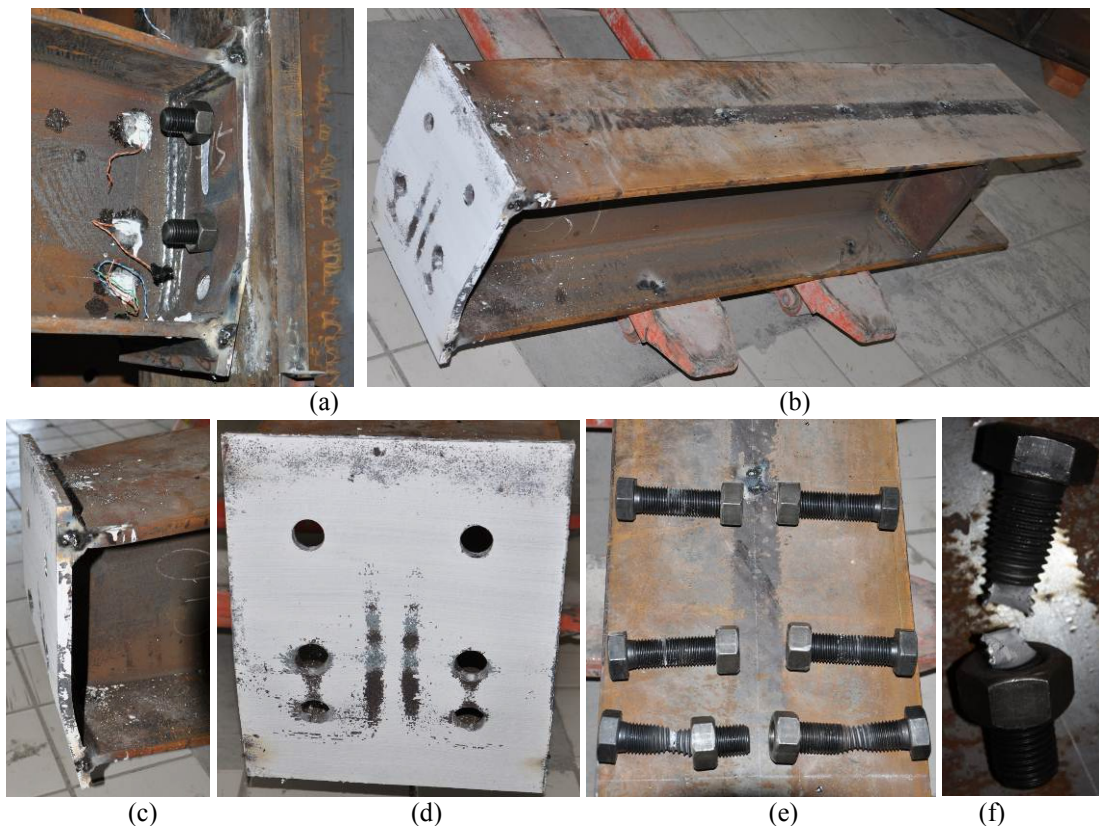
Fig.B.6 Final deformation state of connection 2-3 A (S690 15mm) at ambient temperature.

The final deformation state of S690 15mm at ambient temperature is shown in Fig.B.6, which is similar to that of Q235 25mm and Q345 20mm. It can be

239

found that the endplate has a moderate amount of bending deformation as well. After some plastic bending deformation of the endplate, failure occurred on the bolts of the top row in tension, as shown in Fig.B.6 (e) and (f). It corresponds to the rapid drop in resistance of this connection as illustrated in Fig.6.13 and Fig.6.17. For the bolts in the second tensile row and bolts in compression, they remained almost straight in tests.

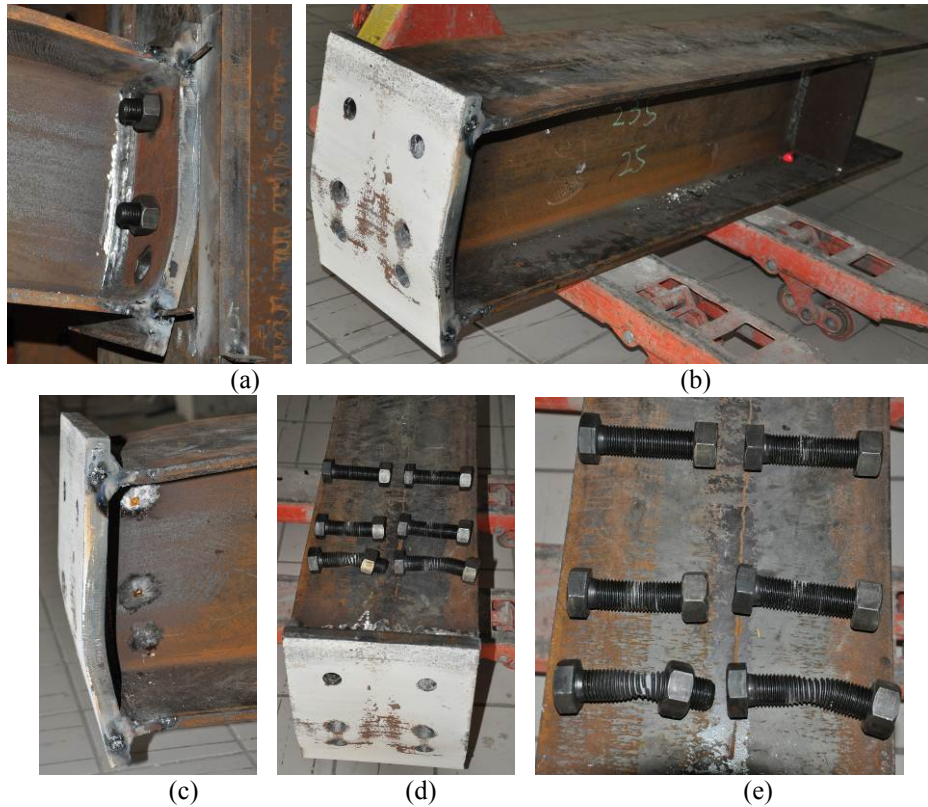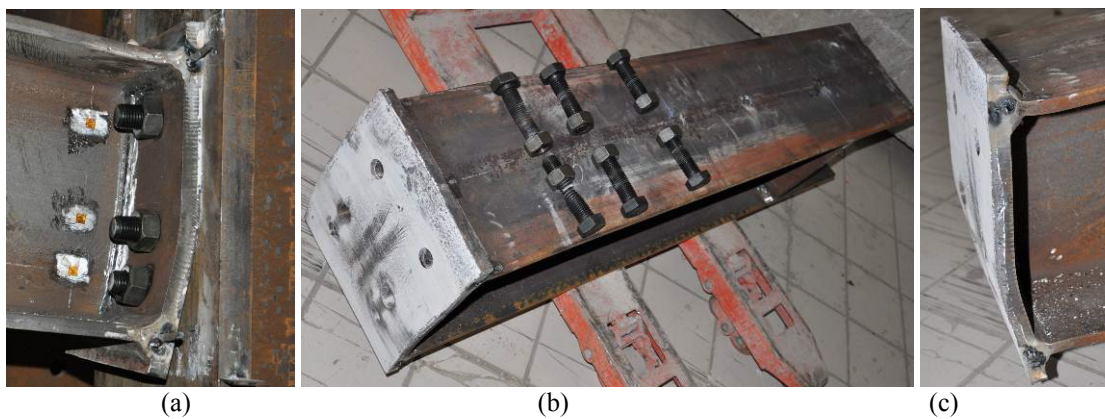|		
(a)	(b)	(c)
(d)	(e)	
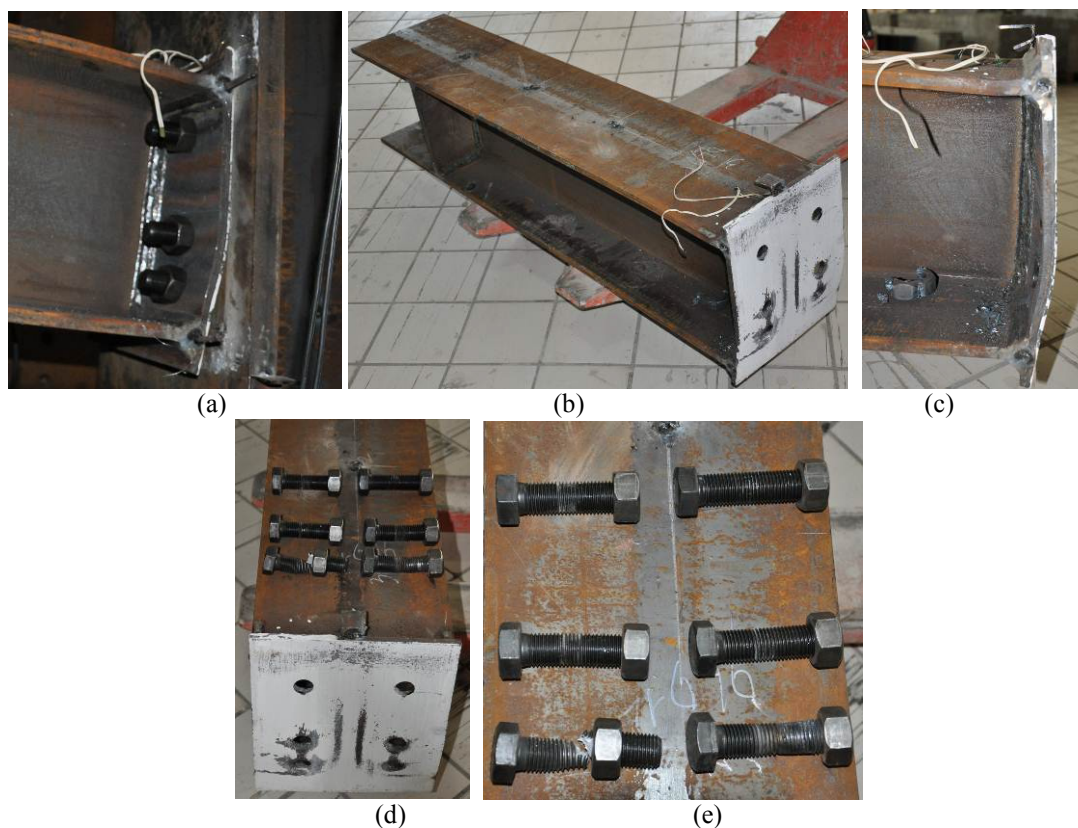
Fig.B.7. Final deformation state of connection 2-4 A (S960 12mm) at ambient temperature.

The final deformation state of S960 12mm at ambient temperature is shown in Fig.B.7. It can be observed that the endplate has a moderate amount of bending deformation as well. After some plastic bending deformation of the endplate, failure occurred on the bolts of the top row in tension, as shown in Fig.B.7 (d) and (e). It corresponds to the rapid drop in resistance of the connection as illustrated in Fig.6.13 and Fig.6.18. For the bolts in the second tensile row and bolts in compression, they remained almost straight in tests.

B.2 At elevated temperatures

(a)	(b)	(c)
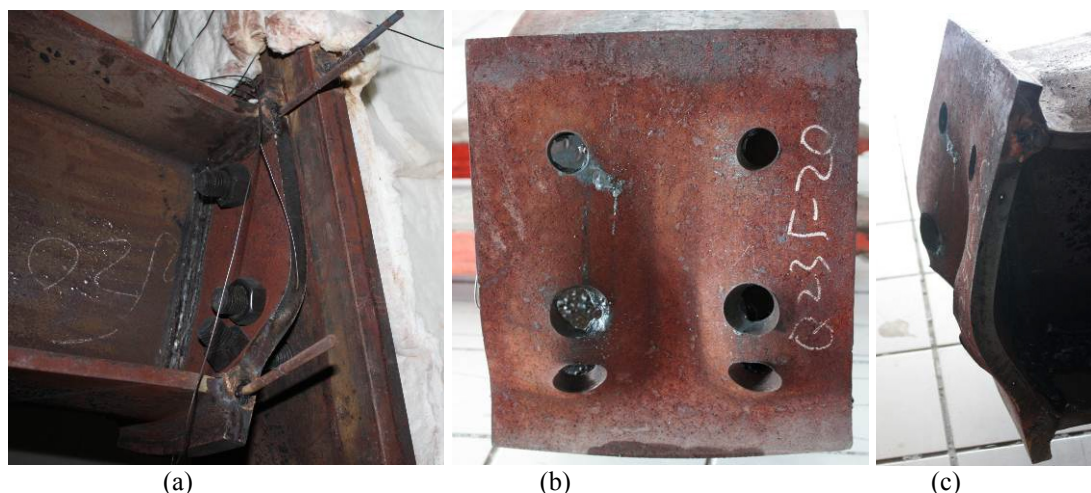
Fig.B.8. Final deformation state of connection 1-1 E (Q235 20mm) at elevated temperature 550°C.

The detailed illustrations on the final deformation state of Q235 20mm at the end of the test at elevated temperature 550°C are presented in Fig.B.8. It can be seen that the failure was concentrated in the endplate, and the bolts remained almost straight until very large plastic deformation on the endplate appeared. Damage to the endplate started as significant bending; after very large bending deformation, the two rows of bolts in tension extended the corresponding bolt holes. Finally, the bolts in the top tensile rows had acquired significant bending deformations until final failure. It corresponds to a rapid drop in resistance of the connection, as shown in Fig.6.14 and Fig.6.19. As to the bolts in compression, they remained straight in tests. The picture of bolts after removing from the specimens after tests was not taken because the deformed bolts in tension were ruined during removing.

(a)	(b)	(c)

(d)

Fig.B.9. Final deformation state of connection 1-2 E (S690 12mm) at elevated temperature 550°C.

The detailed final deformation state of S690 12mm at elevated temperature 550°C is presented in Fig.B.9. It can be found that the failure was started from the bending of endplate, and the bolts remained almost straight until very large plastic deformation on the endplate appeared. After very large bending deformation of the endplate, the two rows of bolts in tension were gradually pulled apart, with no obvious breaking point, as shown in Fig.B.9 (d). It corresponds to the decline phase in resistance of this connection, as shown in Fig.6.14 and Fig.6.20. For the bolts in compression, they remained straight in tests. The picture of bolts in compression after removing from the specimens after tests was not taken because the deformed bolts in tension were ruined during removing.

(a)   (b)   (c)

Fig.B.10. Final deformation state of connection 1-3 E (S960 10mm) at elevated temperature 550°C.

The final deformation state of S960 10mm at elevated temperature 550°C is shown in Fig.B.10. It can be observed that damage to the endplate started as significant bending, and after very large bending deformation of endplate, the top row of bolts in tension was gradually pulled apart, with no obvious breaking point as shown in Fig.B.10 (c). It corresponds to the decline phase in resistance of the connection, as shown in Fig.6.14 and Fig.6.21. As for the bolts in the second tensile row, they experienced visible bending deformation. For the bolts in compression, they remained almost straight in tests.

(a)   (b)   (c)   (d)
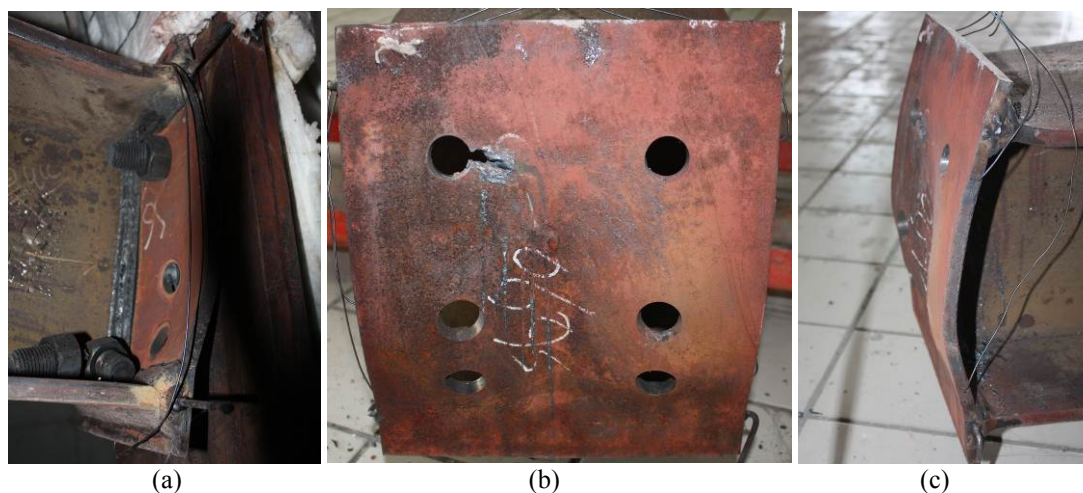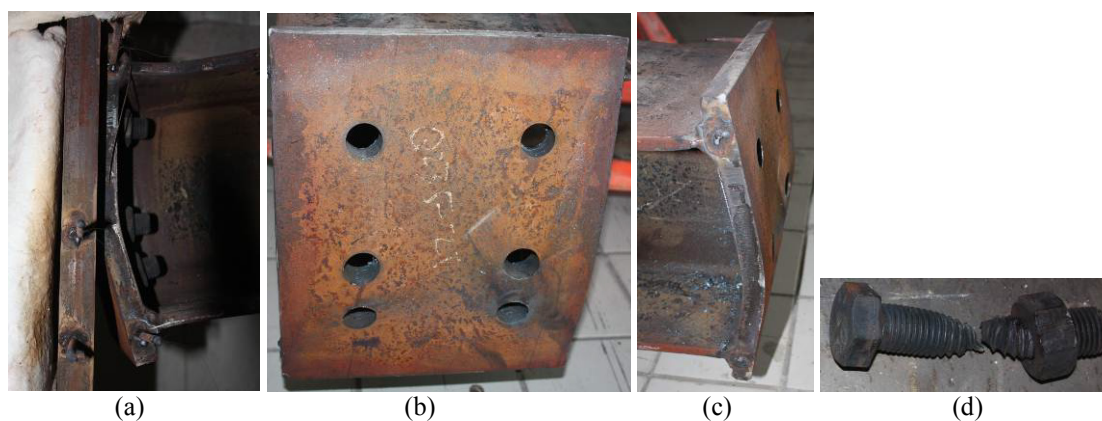
Fig.B.11. Final deformation state of connection 2-1 E (Q235 25mm) at elevated temperature 550°C.

The final deformation state of Q235 25mm at elevated temperature 550°C is shown in Fig.B.11. It can be found that damage to the endplate started from significant bending; after large bending deformation of endplate, the top row of bolts in tension was gradually pulled apart. It corresponds to the decline phase in resistance of the connection, as shown in Fig.6.15 and Fig.6.19. For the bolts in the second tensile row, they experienced bending deformations. As to the bolts in compression, they remained almost straight in tests.

(a)   (b)   (c)

(d)
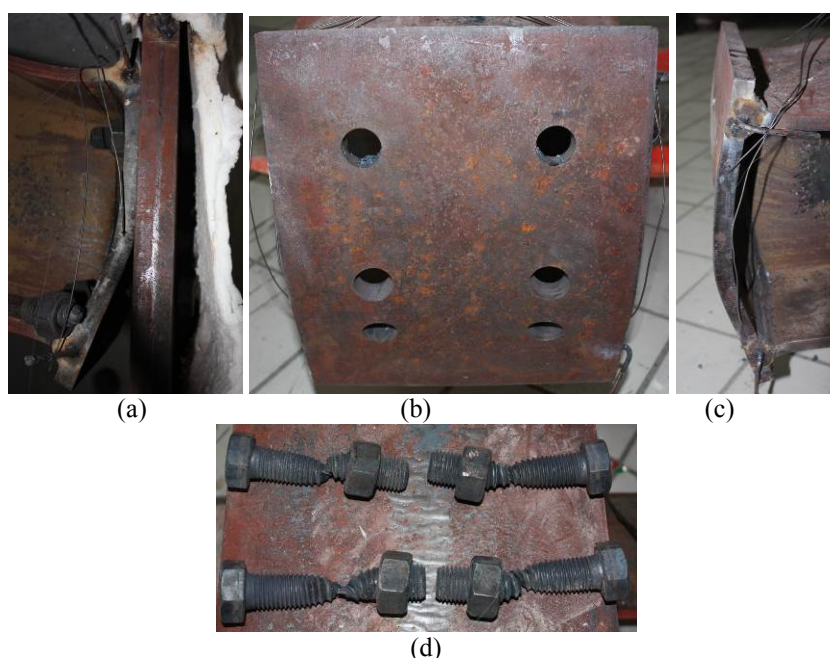
Fig.B.12. Final deformation state of connection 2-2 E (Q345 20mm) at elevated temperature 550°C.

The detailed illustrations on the final deformation state of Q345 20mm at elevated temperature 550°C are presented in Fig.B.12. It can be seen that damage to the endplate started from significant bending, and after large bending deformation of endplate, the two rows of bolts in tension were gradually pulled apart, without obvious breaking point as shown in Fig.B.12 (d). It corresponds to the decline phase in resistance of the connection, as shown in Fig.6.15. As for the bolts in compression, they remained almost straight in tests.
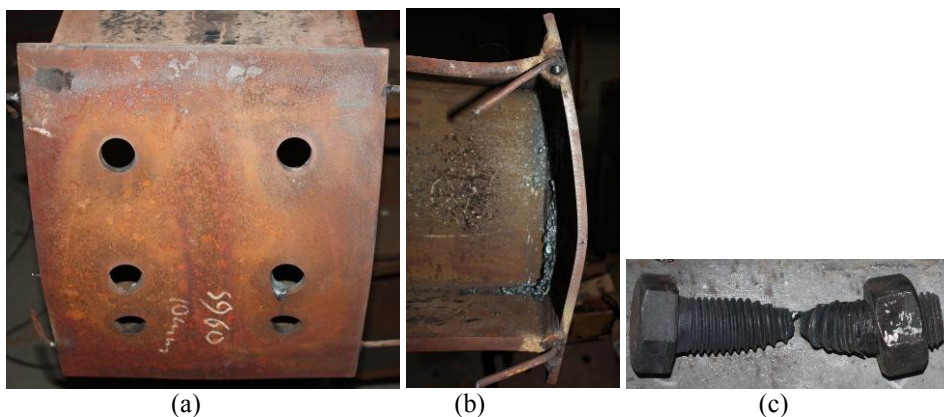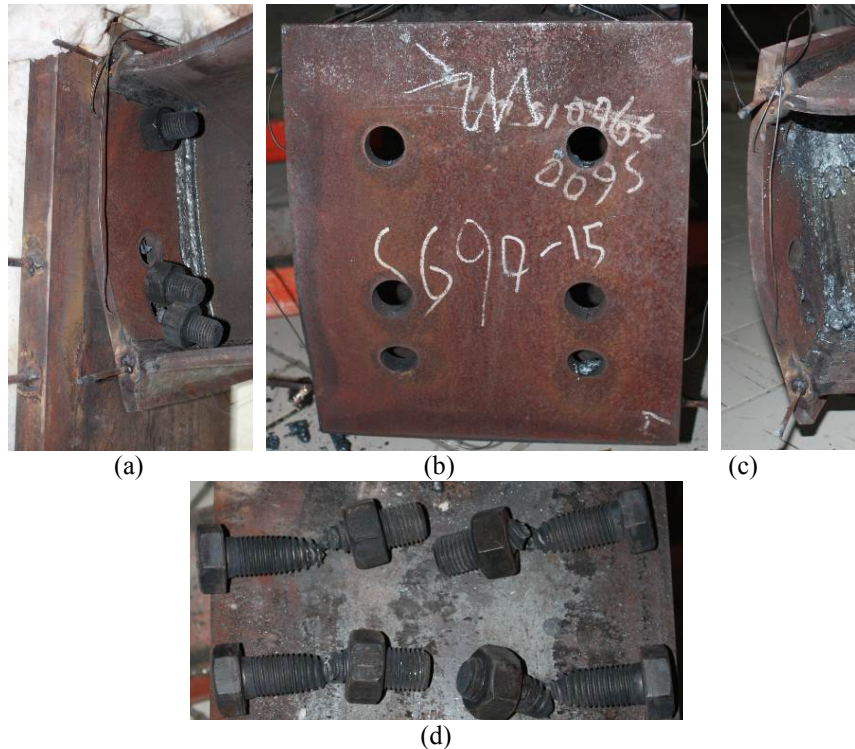
Fig.B.13. Final deformation state of connection 2-3 E (S690 15mm) at elevated temperature 550°C.

The detailed final deformation state of S690 15mm at elevated temperature 550°C is shown in Fig.B.13. It can be seen that damage to the endplate started from significant bending; after large bending deformation of the endplate, the two rows of bolts in tension were gradually pulled apart, without obvious breaking point as shown in Fig.B.13 (d). It corresponds to the decline phase in resistance of the connection, as shown in Fig.6.20. As to the bolts in compression, they remained almost straight in tests.
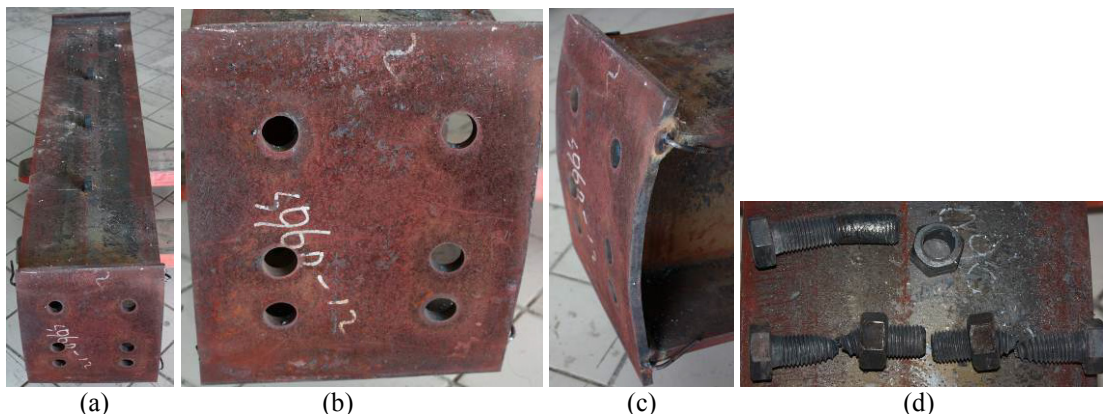
Fig.B.14. Final deformation state of connection 2-4 E (S960 12mm) at elevated temperature 550°C.

The final deformation state of S960 12mm at elevated temperature 550°C is illustrated in Fig.B.14. It can be observed that damage to the endplate started from significant bending; after large bending deformation of the endplate, the top row of bolts in tension was gradually pulled apart, without obvious breaking point, as shown in Fig.B.14 (d). It corresponds to the decline phase in

resistance of the connection, as shown in Fig.6.21. For the bolts in the second tensile row, they experienced bending deformation. As to the bolts in compression, they remained almost straight in tests.

B.3 After cooling down from fire

For all endplate connections in post-fire test, their final deformation states were photographed at the end of tests at ambient temperature after cooling down from fire and presented in Fig.B.15-B.21.

(a) (b) (c)
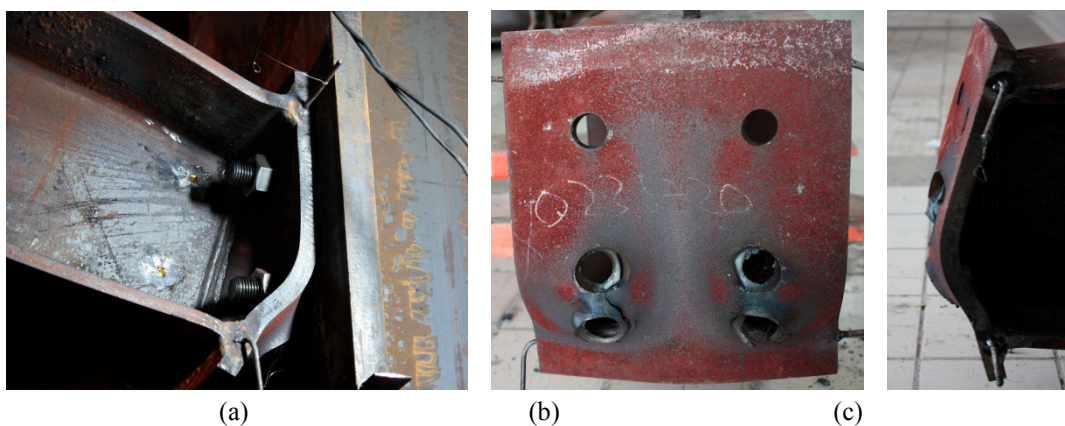
Fig.B.15. Final deformation state of connection 1-1 P (Q235 20mm) after fire.

(a) (b) (c)

(d) (e)
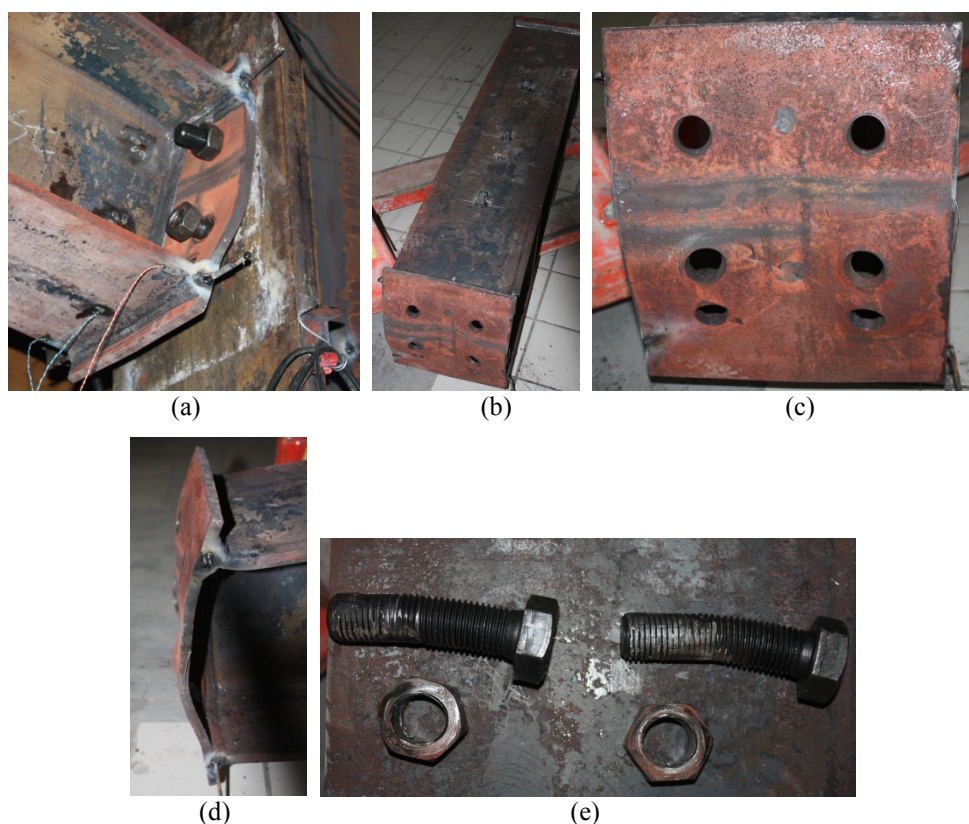
Fig.B.16. Final deformation state of connection 1-2 P (S690 12mm) after fire.

(a)　　　　　　　　(b)　　　　　　　　(c)

(d)　　　　　　　　(e)
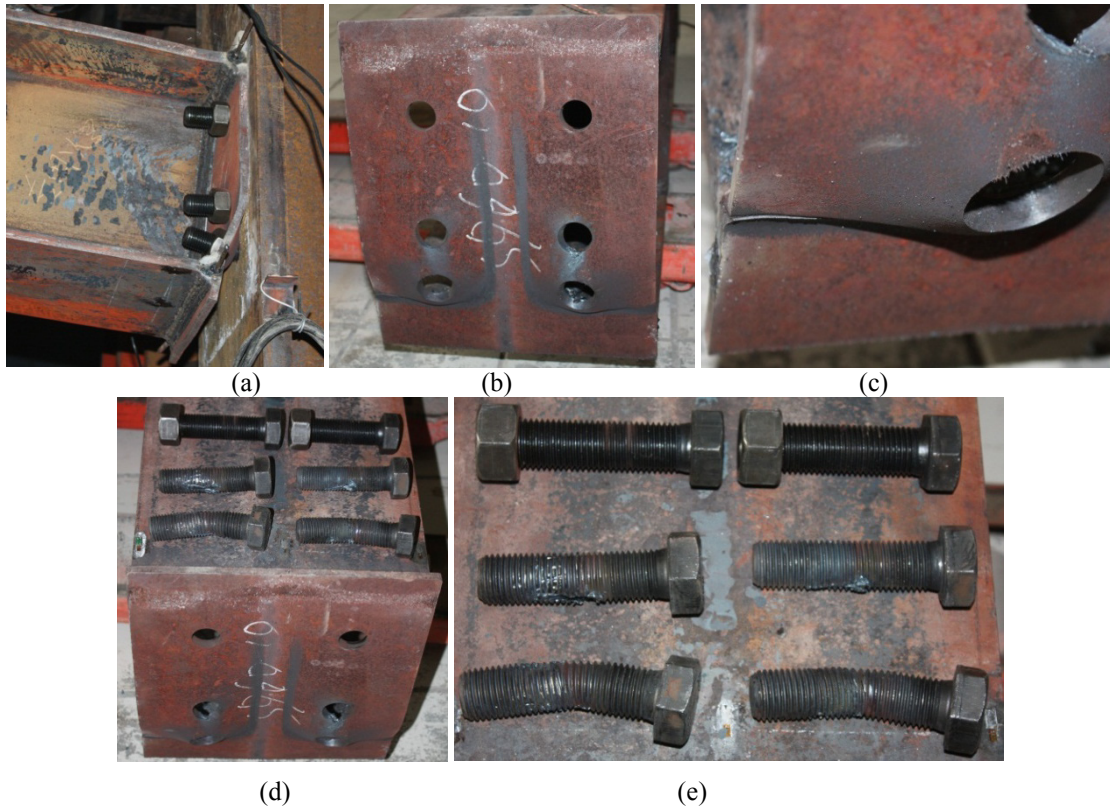
Fig.B.17. Final deformation state of connection 1-3 P (S960 10mm) after fire.

(a)　　　　　　　　(b)　　　　　　　　(c)

(d)
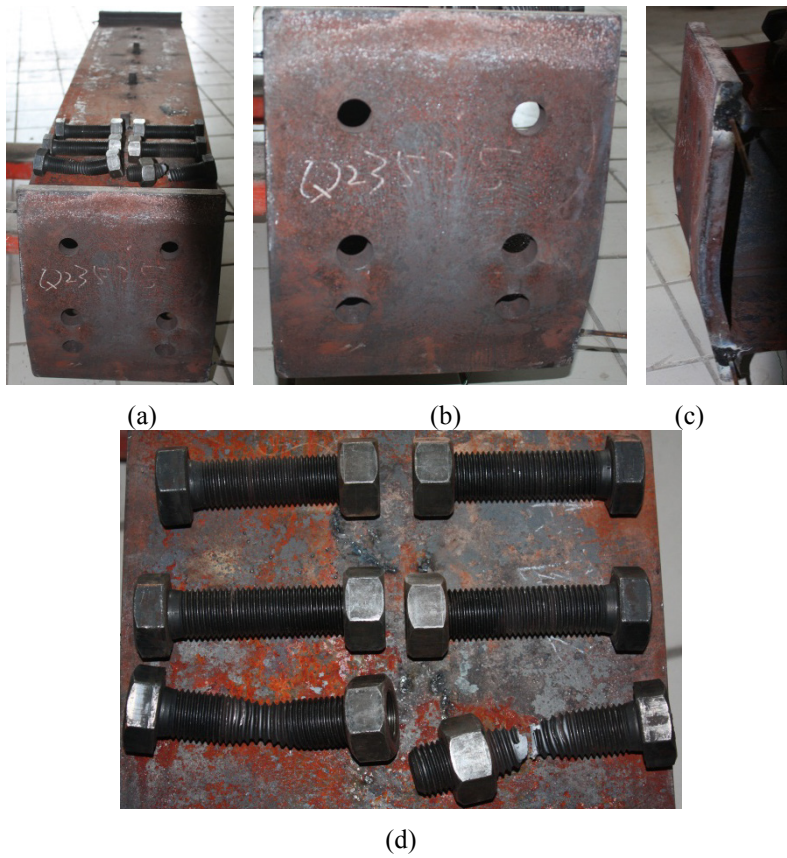
Fig.B.18. Final deformation state of connection 2-1 P (Q235 25mm) after fire.

(a)   (b)   (c)

(d)   (e)
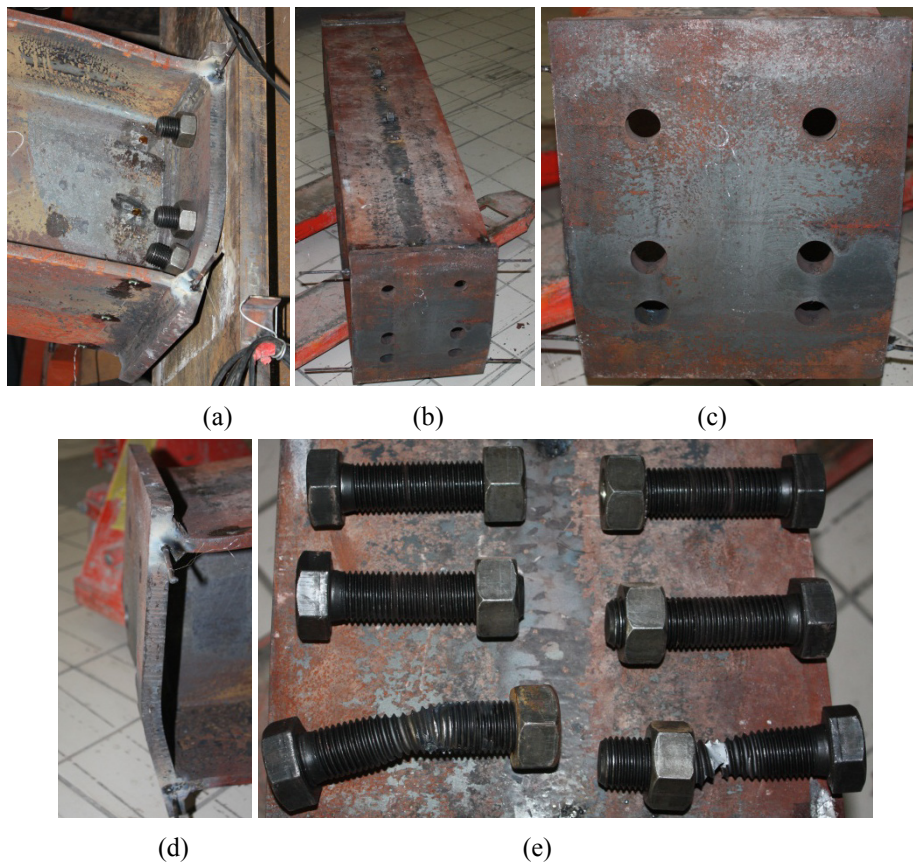
Fig.B.19. Final deformation state of connection 2-2 P (Q345 20mm) after fire.

(a)   (b)   (c)

(d)
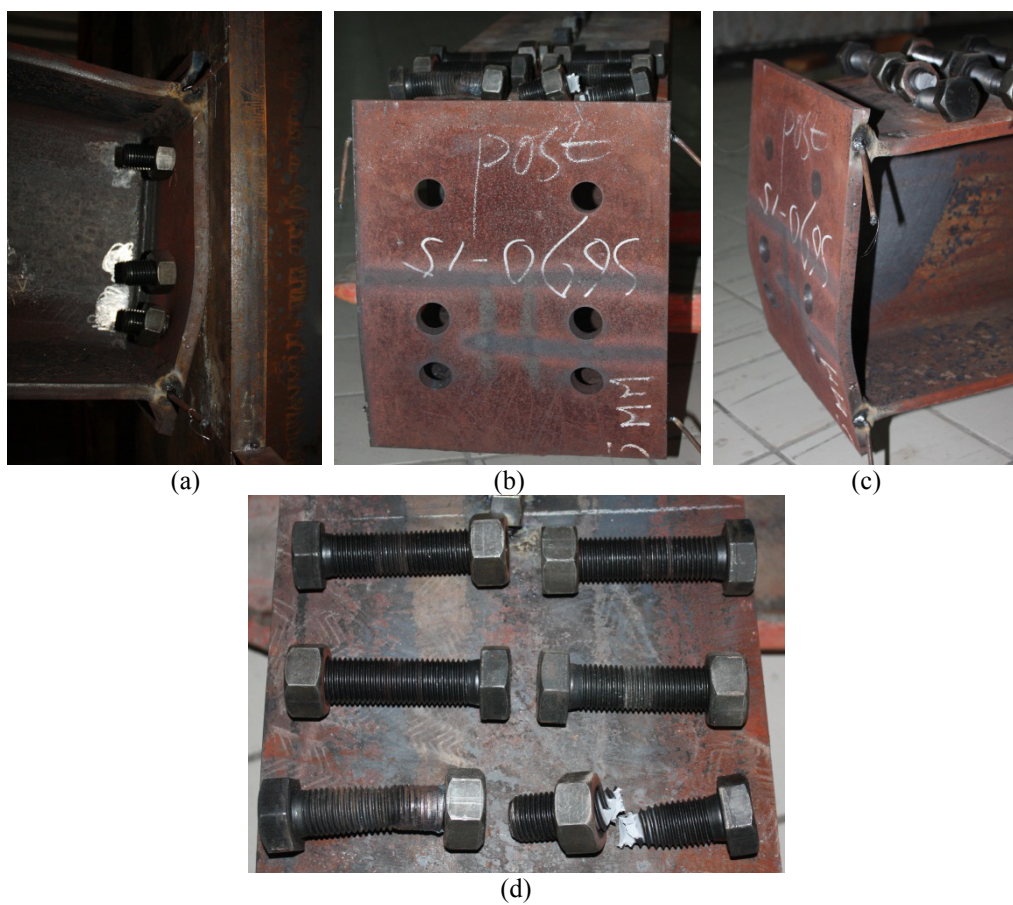
Fig.B.20. Final deformation state of connection 2-3 P (S690 15mm) after fire.

247

(a)   (b)   (c)

(d)   (e)
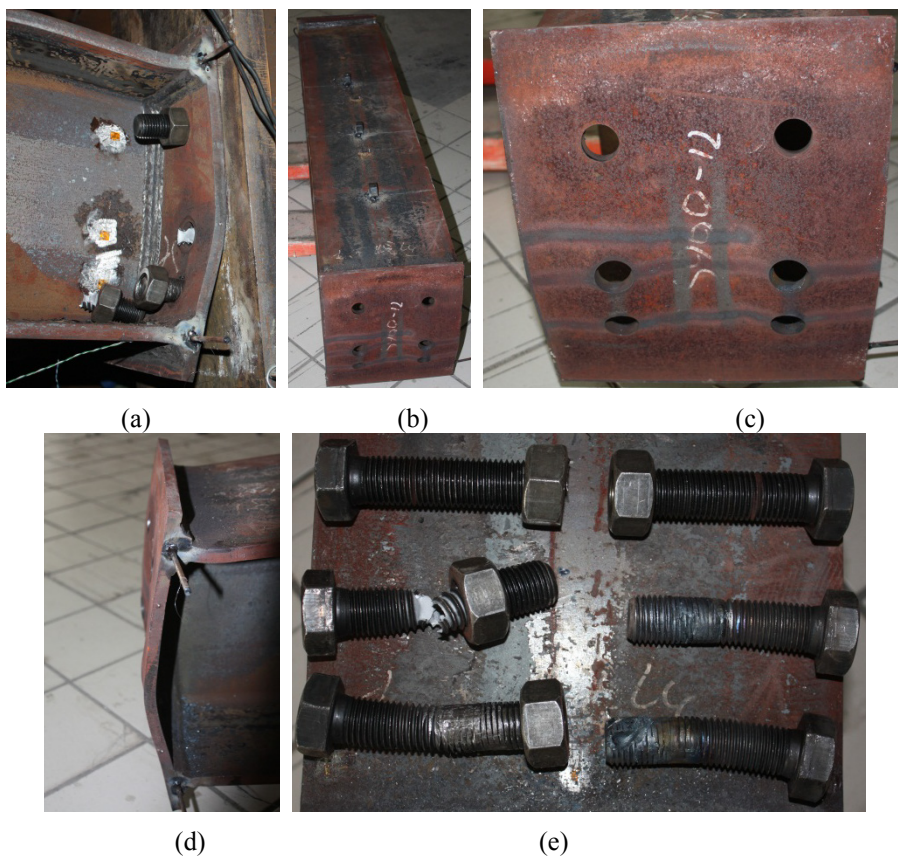
Fig.B.21. Final deformation state of connection 2-4 P (S960 12mm) after fire.

Appendix C:

Endplate connection calculation based on Eurocode 3

Components description

Column section: HW400*400, h=428mm, b=407mm, t_w= 20mm, t_f =35mm, r=27mm.
Beam section: HW300*300, h=300mm, b=300mm, t_w= 10mm, t_f =15mm, r=27mm.
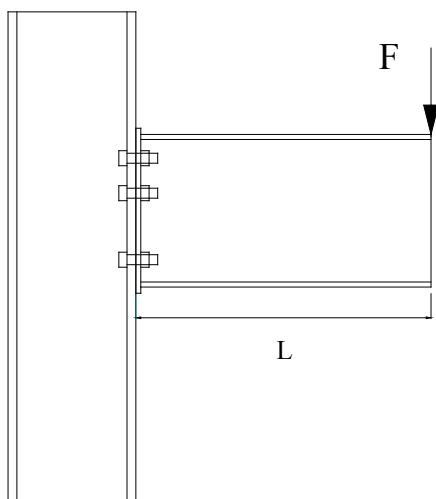
Fig.C.1 Specimen and applied force
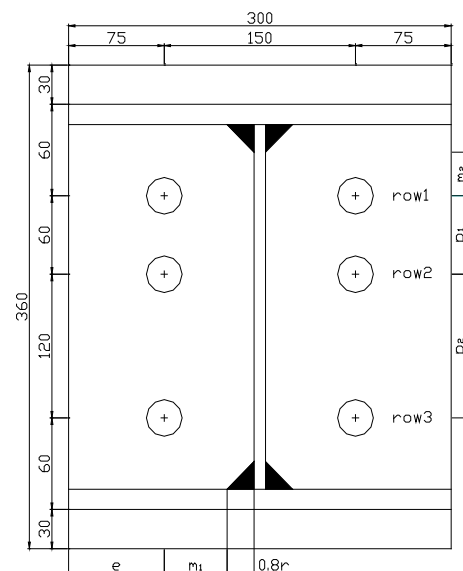
Fig.C.2 Endplate geometry

Experimental conditions:

At ambient temperature and at elevated temperature 550°C.

1. Bolts calculation

Each bolt resistance:

Shear resistance: $F_{v,Rd} = \dfrac{\alpha_v f_{ub} A_s}{\gamma_{M2}}$

249

Tension resistance: $F_{t,Rd} = \dfrac{k_2 f_{ub} A_s}{\gamma_{M2}}$

1) S8.8 M27 Bolt tension resistance

$$F_{t,Rd} = \frac{k_2 f_{ub} A_s}{\gamma_{M2}} = \frac{0.9 \times 800 \times \dfrac{\pi}{4} \times 27^2}{1.25} = 329.792 kN$$

2) S8.8 M27 Bolt shear resistance

$$F_{v,Rd} = \frac{\alpha_v f_{ub} A_s}{\gamma_{M2}} = \frac{0.6 \times 800 \times \dfrac{\pi}{4} \times 27^2}{1.25} = 219.861 kN$$

2. Endplate in bending calculation

1) Effective length of endplate

e=75mm

m_1=75-5-0.8*13=59.6mm

m_2=60-15-0.8*13=34.6mm

p_1=60mm

p_2=120mm

$$\lambda_1 = \frac{m_1}{m_1 + e} = \frac{59.6}{59.6 + 75} = 0.443$$

$$\lambda_2 = \frac{m_2}{m_1 + e} = \frac{34.6}{59.6 + 75} = 0.257$$

$\therefore \alpha = 7.111$

① Bolt-row considered individually

   a) Circular patterns failure mode

   Every row l_{eff}=2πm=2$\pi$$m_1$=374.48mm

   b) Non-circular patterns failure mode

   Row 1: l_{eff1}=αm=7.111*59.6= 423.82mm > 374.48mm

   Row 2: l_{eff2}=4m+1.25e=4*59.6+1.25*75=332.15mm

   Row 3: l_{eff3}=4m+1.25e=4*59.6+1.25*75=332.15mm

② Bolt-row considered as part of a group of bolt-rows

   a) Circular patterns failure mode

   Group 1+2: l_{eff}=2(πm+p_1) =2(59.6π+60) =494.48mm

   Group 2+3: l_{eff}=2(πm+p_2) =2(59.6π+120) =614.48mm

   Group 1+2+3: l_{eff}= 2(πm+ p_1+p_2) = 2(59.6π+60+120) =734.48mm

   b) Non-circular patterns failure mode

Group 1+2: $l_{eff}= \alpha\, m + p_1 = 483.82mm < 494.48mm$

Group 2+3: $l_{eff}= \alpha\, m + p_2 = 543.82mm < 614.48mm$

Group 1+2+3: $l_{eff}= 2\alpha\, m + p_1 + p_2 - (4m+1.25e) = 695.48mm < 734.48mm$

∴ In group, $l_{eff1} = 374.48mm$

$l_{eff1+2} = 483.82mm$

$l_{eff1+2+3} = 695.48mm$

2) Tensile resistance

Failure Mode 1: complete yielding of the flange $F_{T,1,Rd} = \dfrac{4M_{Pl,1,Rd}}{m}$

Failure Mode 2: bolt failure with yielding of the flange

$$F_{T,2,Rd} = \frac{2M_{Pl,2,Rd} + n\sum F_{t,Rd}}{m+n}$$

Failure Mode 3: bolt failure $F_{T,3,Rd} = \sum F_{t,Rd}$

Where, $F_{t,Rd}$ is the tension resistance of a bolt; $M_{Pl,i,Rd} = 0.25\sum l_{eff,i}\, t_f^2 f_y / \gamma_{M0}$;

$n = e_{min}$ but $n \le 1.25m$, so $n = 74.5mm$ herein.

Connections series 1:

a) At ambient temperature

The design tensile resistance of the endplate in bending on individual bolt rows and group of bolt rows is obtained as the minimum of the three failure mode values of tensile resistances $F_{T,1,Rd}$, $F_{T,2,Rd}$ and $F_{T,3,Rd}$. The failure mode can be obtained by comparing the value of $F_{T,1,Rd}$, $F_{T,2,Rd}$ and $F_{T,3,Rd}$. The design tensile resistance of the endplate on individual bolt rows is shown in the last column of the table below, and the design tensile resistance of endplate on the group of bolt rows is shown in grey background.

Table C.1: Design resistance of endplate connections in series 1 at room temperature

End plate	t_f	Bolt rows	$l_{eff,1}$ (mm)	$l_{eff,2}$ (mm)	$M_{Pl,1,Rd}$	$M_{Pl,2,Rd}$	$F_{T,1,Rd}$ (kN)	$F_{T,2,Rd}$ (kN)	$F_{T,3,Rd}$ (kN)	Failure mode	Bolt row	Plastic flexural resistance (kN)
Q235	20	1	374	424	8800	9960	591	607	824		1	590.62
		1+2	484	484	11370	11370	763	1086	1649	Mode 1	2	172.45
		1+2+3	695	695	16344	16344	1097	1618	2473		3	333.83
S690	12	1	374	424	9302	10528	615	624	824		1	615.06
		1+2	484	484	12018	12018	807	1095	1649	Mode 1	2	191.53
		1+2+3	695	695	17276	17276	1159	1632	2473		3	352.86
S960	10	1	374	424	8988	10172	603	610	824		1	603.19
		1+2	484	484	11612	11612	779	1089	1649	Mode 1	2	176.12
		1+2+3	695	695	16692	16692	1120	1623	2473		3	340.93

b) At elevated temperature 550°C

Table C.2: Design resistance of endplate connections in series 1 at elevated temperature 550°C

End plate	t_f	Bolt rows	$l_{eff,1}$ (mm)	$l_{eff,2}$ (mm)	$M_{Pl,1,Rd}$	$M_{Pl,2,Rd}$	$F_{T,1,Rd}$ (kN)	$F_{T,2,Rd}$ (kN)	$F_{T,3,Rd}$ (kN)	Failure mode	Bolt row	Plastic flexural resistance (kN)
Q235	20	1	374	424	5500	6225	369	271	322		1	271.48
		1+2	484	484	7106	7106	477	463	643	Mode 2	2	191.78
		1+2+3	695	695	10215	10215	686	688	965		3	222.30
S690	12	1	374	424	4958	5611	333	262	322		1	262.32
		1+2	484	484	6406	6406	430	453	643	Mode 2	2	167.58
		1+2+3	695	695	9208	9208	618	673	965		3	188.08
S960	10	1	374	424	5294	5991	355	268	322		1	267.99
		1+2	484	484	6839	6839	459	459	643	Mode 2	2	191.02
		1+2+3	695	695	9831	9831	660	683	965		3	200.81

c) After cooling down from elevated temperature 550°C

Table C.3: Design resistance of endplate connections in series 1 after cooling down from elevated temperature 550°C

End plate	t_f	Bolt rows	$l_{eff,1}$ (mm)	$l_{eff,2}$ (mm)	$M_{Pl,1,Rd}$	$M_{Pl,2,Rd}$	$F_{T,1,Rd}$ (kN)	$F_{T,2,Rd}$ (kN)	$F_{T,3,Rd}$ (kN)	Failure mode	Bolt row	Plastic flexural resistance (kN)
Q235	20	1	374	424	7920	8964	532	557	763		1	531.56
		1+2	484	484	10233	10233	687	1000	1525	Mode 1	2	155.20
		1+2+3	695	695	14709	14709	987	1490	2288		3	300.44
S690	12	1	374	424	8372	9475	562	565	763		1	561.87
		1+2	484	484	10816	10816	726	1008	1525	Mode 1	2	164.05
		1+2+3	695	695	15548	15548	1044	1503	2288		3	317.58
S960	10	1	374	424	8089	9155	543	560	763		1	542.87
		1+2	484	484	10451	10451	701	1003	1525	Mode 1	2	158.51
		1+2+3	695	695	15022	15022	1008	1495	2288		3	306.84

Connections series 2:

a) At room temperature

Table C.4: Design resistance of endplate connections in series 2 at room temperature

End plate	t_f	Bolt rows	$l_{eff,1}$ (mm)	$l_{eff,2}$ (mm)	$M_{Pl,1,Rd}$	$M_{Pl,2,Rd}$	$F_{T,1,Rd}$ (kN)	$F_{T,2,Rd}$ (kN)	$F_{T,3,Rd}$ (kN)	Failure mode	Bolt row	Design resistance (kN)
Q235	25	1	374	424	13750	15562	923	690	824		1	690.14
		1+2	484	484	17765	17765	1192	1181	1649	Mode 2	2	490.90
		1+2+3	695	695	25537	25537	1714	1755	2473		3	532.86
Q345	20	1	374	424	12920	14622	867	676	824		1	676.12
		1+2	484	484	16692	16692	1120	1165	1649	Mode 2	2	444.14
		1+2+3	695	695	23994	23994	1610	1732	2473		3	490.09
S690	15	1	374	424	14535	16450	975	703	824		1	703.38
		1+2	484	484	18778	18778	1260	1196	1649	Mode 2	2	492.78
		1+2+3	695	695	26993	26993	1812	1777	2473		3	580.57
S960	12	1	374	424	12942	14647	869	677	824		1	676.50
		1+2	484	484	16721	16721	1122	1165	1649	Mode 2	2	445.71
		1+2+3	695	695	24036	24036	1613	1733	2473		3	490.94

b) At elevated temperature550°C

Table C.5: Design resistance of endplate connections in series 2 at elevated temperature 550°C

End plate	t_f	Bolt rows	$l_{eff,1}$ (mm)	$l_{eff,2}$ (mm)	$M_{Pl,1,Rd}$	$M_{Pl,2,Rd}$	$F_{T,1,Rd}$ (kN)	$F_{T,2,Rd}$ (kN)	$F_{T,3,Rd}$ (kN)	Failure mode	Bolt row	Design resistance (kN)
Q235	25	1	374	424	8594	9726	577	321	322		1	320.70
		1+2	484	484	11103	11103	745	523	643	Mode 2	2	201.32
		1+2+3	695	695	15961	15961	1071	774	965		3	251.08
Q345	20	1	374	424	8075	9139	542	315	322		1	314.93
		1+2	484	484	10432	10432	700	513	643	Mode 2	2	197.93
		1+2+3	695	695	14996	14996	1006	760	965		3	246.70
S690	15	1	374	424	7747	8768	520	309	322		1	309.40
		1+2	484	484	10009	10009	672	507	643	Mode 2	2	197.15
		1+2+3	695	695	14387	14387	966	750	965		3	243.94
S960	12	1	374	424	7623	8627	512	307	322		1	307.31
		1+2	484	484	9849	9848	661	504	643	Mode 2	2	196.85
		1+2+3	695	695	14157	14157	950	747	965		3	242.90

c) After cooling down from elevated temperature 550°C

Table C.6: Design resistance of endplate connections in series 2 after cooling down from elevated temperature 550°C

End plate	t_f	Bolt rows	$l_{eff,1}$ (mm)	$l_{eff,2}$ (mm)	$M_{Pl,1,Rd}$	$M_{Pl,2,Rd}$	$F_{T,1,Rd}$ (kN)	$F_{T,2,Rd}$ (kN)	$F_{T,3,Rd}$ (kN)	Failure mode	Bolt row	Design resistance (kN)
Q235	25	1	374	424	12375	14006	831	633	763		1	632.58
		1+2	484	484	15989	15989	1073	1086	1525	Mode 2	2	440.49
		1+2+3	695	695	22983	22983	1543	1614	2288		3	469.44
Q345	20	1	374	424	11628	13160	780	620	763		1	619.96
		1+2	484	484	15023	15023	1008	1071	1525	Mode 2	2	388.27
		1+2+3	695	695	21595	21595	1449	1593	2288		3	441.08
S690	15	1	374	424	13081	14805	878	644	763		1	644.49
		1+2	484	484	16900	16900	1134	1099	1525	Mode 2	2	454.95
		1+2+3	695	695	24294	24294	1630	1633	2288		3	531.03
S960	12	1	374	424	11648	13183	782	620	763		1	620.30
		1+2	484	484	15049	15049	1010	1072	1525	Mode 2	2	389.68
		1+2+3	695	695	21632	21632	1452	1594	2288		3	380.00

3. Beam flange and web in compression

The compression resistance of a beam flange and the adjacent compression zone of the beam web may be assumed to act at the level of the centre of compression, as calculated below.

$$F_{c,fb,Rd} = \frac{M_{c,Rd}}{h - t_{fb}}$$

where: h is the depth of the beam; $M_{c,Rd}$ is the moment resistance of the beam cross-section, can be calculated as $M_{c,Rd} = \frac{W_{Pl} f_{yb}}{\gamma_{M0}}$; t_{fb} is the flange thickness of the beam.

So herein, $F_{c,fb,Rd} = \frac{M_{c,Rd}}{h - t_{fb}} = \frac{\frac{W_{Pl} f_{yb}}{\gamma_{M0}}}{h - t_{fb}} = \frac{\frac{1628 \times 10^3 \times 345}{1.0}}{300 - 15} = \frac{561660}{285} = 1970.74 kN$

4. Column web panel in shear

Shear resistance of the unstiffened column web panel:

$$V_{wp,Rd} = \frac{0.9 f_{y,wc} A_{vc}}{\sqrt{3} \times \gamma_{M0}} = \frac{0.9 \times 345 \times [(428 - 35 \times 2) \times 20]}{\sqrt{3} \times 1.0} = 1283.554 kN$$

5. Design moment resistance and design force of the endplate connections

$M_{j,Rd} = \sum_r h_r F_{tr,Rd}$, where: $F_{tr,Rd}$ is the effective tension resistance of bolt-row r; h_r is the distance from bolt-row r to the centre of compression; r is the bolt-row number.

$\therefore$ The design applied force F_{Rd} to be used in the tests can be calculated as:

$$F_{Rd} = \frac{M_{j,Rd}}{L} .$$

Connections series 1:

a) At room temperature

Table C.7: Design moment and force resistance of endplate connections in series 1 at room temperature

Endplate material	t_f (mm)	$F_{t,1,Rd}$ (kN)	$F_{t,2,Rd}$ (kN)	h_1(mm)	h_2(mm)	$M_{j,Rd}$ (kN·mm)	F_{Rd} (kN)
Q235	20	590.62	172.45	232.5	172.5	167067.26	155.27
S690	12	615.06	191.53	232.5	172.5	176038.99	163.61
S960	10	603.19	176.12	232.5	172.5	170621.88	158.57

b) At elevated temperature 550°C

Table C.8: Design moment and force resistance of endplate connections in series 1 at elevated temperature 550°C

Endplate material	t_f (mm)	$F_{t,1,Rd}$ (kN)	$F_{t,2,Rd}$ (kN)	h_1(mm)	h_2(mm)	$M_{j,Rd}$ (kN·mm)	F_{Rd} (kN)
Q235	20	248.45	110.19	232.5	172.5	76773.18	71.35
S690	12	262.32	167.58	232.5	172.5	89898.76	83.55
S960	10	267.99	191.02	232.5	172.5	95258.99	88.53

c) After cooling down from elevated temperature 550°C

Table C.9: Design moment and force resistance of endplate connections in series 1 after cooling down from elevated temperature 550°C

Endplate material	t_f (mm)	$F_{t,1,Rd}$ (kN)	$F_{t,2,Rd}$ (kN)	h_1(mm)	h_2(mm)	$M_{j,Rd}$ (kN·mm)	F_{Rd} (kN)
Q235	20	531.56	155.20	232.5	172.5	150360.53	139.74
S690	12	561.87	164.05	232.5	172.5	158934.28	147.71
S960	10	542.87	158.51	232.5	172.5	153559.69	142.71

Connections series 2:

a) At room temperature

Table C.10: Design moment and force resistance of endplate connections in series 2 at room temperature

Endplate material	t_f (mm)	$F_{t,1,Rd}$ (kN)	$F_{t,2,Rd}$ (kN)	h_1(mm)	h_2(mm)	$M_{j,Rd}$ (kN·mm)	F_{max} (kN)
Q235	25	690.14	490.90	232.5	172.5	245137.80	227.82
Q345	20	682.44	470.29	232.5	172.5	239792.33	222.86
S690	15	703.38	492.78	232.5	172.5	248540.40	230.99
S960	12	676.50	445.71	232.5	172.5	234171.23	217.63

b) At elevated temperature 550°C

Table C.11: Design moment and force resistance of endplate connections in series 2 at elevated temperature 550°C

Endplate material	t_f (mm)	$F_{t,1,Rd}$ (kN)	$F_{t,2,Rd}$ (kN)	h_1(mm)	h_2(mm)	$M_{j,Rd}$ (kN·mm)	F_{max} (kN)
Q235	25	320.70	201.32	232.5	172.5	109291.25	101.57
Q345	20	314.93	197.93	232.5	172.5	107365.24	99.78
S690	15	309.40	197.15	232.5	172.5	105943.55	98.46
S960	12	307.31	196.85	232.5	172.5	105405.65	97.96

c) After cooling down from elevated temperature 550°C

Table C.12: Design moment and force resistance of endplate connections in series 2 after cooling down from elevated temperature 550°C

Endplate material	t_f (mm)	$F_{t,1,Rd}$ (kN)	$F_{t,2,Rd}$ (kN)	h_1(mm)	h_2(mm)	$M_{j,Rd}$ (kN·mm)	F_{max} (kN)
Q235	25	632.58	440.49	232.5	172.5	223059.25	207.30
Q345	20	619.96	388.27	232.5	172.5	211116.88	196.21
S690	15	644.49	454.95	232.5	172.5	228322.61	212.20
S960	12	620.30	451.52	232.5	172.5	222107.22	206.42

Curriculum vitae

Personal Information

Name	Xuhong Qiang
Date of birth	April 3rd, 1984
Gender	Female
Nationality	Chinese
Email	qiangxuhong1984@gmail.com

Education Background

Sep. 2002 - July 2006   Bachelor in Civil Engineering with honors
Major in Building Engineering
Dalian University of Technology
Dalian, Liaoning Province, China

Sep.2006 – Sep. 2008   MSc in Structural Engineering with honors
Major in Steel Structures
Tongji University
Shanghai, China

Work Experience

Nov. 2008 – July 2013   PhD researcher in Structural Engineering
Research on high strength steel endplate connections
in steel structures under fire conditions and after fire
Delft University of Technology
Delft, the Netherlands

List of Publications

I. Journal publications:

1）Xuhong Qiang, Yongfeng Luo, Zhun Luo, Lihua Zhang.Experimental study on the material capability of steel structural members after fire. Chinese Journal of Civil Engineering, 2009, 42（7）:28-35.（in Chinese)

2）Xuhong Qiang, Yongfeng Luo, Jiaqin He, Lihua Zhang.Experimental study on the behaviour of high-strength bolted connection after fire. Chinese Journal of Building Strucure,2010,40（8）:116-120.(in Chinese)

3）Xuhong Qiang, Frans S.K. Bijlaard, Henk Kolstein. Post-fire mechanical properties of high strength structural steels S460 and S690. **Engineering Structures**, 2012, 35: 1-10.

4）Xuhong Qiang, Frans S.K. Bijlaard, Henk Kolstein. Dependence of mechanical properties of high strength steel S690 on elevated temperatures. **Construction and Building Materials**, 2012, 30: 73-79.

5）Xuhong Qiang, Frans S.K. Bijlaard, Henk Kolstein. Deterioration of mechanical properties of high strength structural steel S460N under steady state fire condition. **Materials & Design**, 2012, 36: 438- 442.

6）Xuhong Qiang, Frans S.K. Bijlaard, Henk Kolstein. Deterioration of mechanical properties of high strength structural steel S460N under transient state fire condition. **Materials & Design,** 2012, 40: 521-527.

7）Xuhong Qiang, Frans S.K. Bijlaard, Henk Kolstein. Numerical prediction of combining HSS with mild steel in endplate connections at ambient and elevated temperatures. **Advanced Science Letters**, 2012,10:72-79.

8）Xuhong Qiang, Frans S.K. Bijlaard, Henk Kolstein. Post-fire performance of very high strength steel S960. **Journal of Constructional Steel Research,** 2013, 80: 235-242.

9）Xuhong Qiang, Frans S.K. Bijlaard, Henk Kolstein. Elevated-temperature mechanical properties of high strength steel S460N: experimental study & design recommendations. **Fire Safety Journal,** 2013, 55:15-21.

10）Xuhong Qiang, Frans S.K. Bijlaard, Henk Kolstein. Material behaviour of high strength structural steel S460 in fire and after fire. **IES Journal Part A: Civil & Structural Engineering,** 2013, Volume 6, No. 2:104-111 (recommended to this journal by the chair of ICASS 2012 International Conference, accepted after peer-review)

11）Xuhong Qiang, Frans S.K. Bijlaard, Henk Kolstein, Leen Twilt. Numerical analysis of High strength steel endplate connections at ambient and elevated temperatures. **Journal of Structural Fire Engineering**. (in press, selected by the chief editor of this journal from ASFE 2011 International Conference, accepted after peer-review)

Under review：

12）Xuhong Qiang, Frans S.K. Bijlaard, Henk Kolstein. Behaviour of beam-to-column high strength steel endplate connections under fire conditions - Part 1: Experimental study. **Engineering Structures.**

13) Xuhong Qiang, Frans S.K. Bijlaard, Henk Kolstein. Behaviour of beam-to-column high strength steel endplate connections under fire conditions - Part 2: Numerical study. **Engineering Structures.**

II.   Conference Publications

14) Xuhong Qiang, Yongfeng Luo, Jiaqin He, Lihua Zhang. Experimental study on web-bolted flanged-welded connections after fire. Second National Conference on Construction of Steel Structures. 2008, Guangzhou, China.

15) Xuhong Qiang, Frans S.K. Bijlaard, Henk Kolstein, Leen Twilt. Modelling of HSS endplate connections: achievements and perspectives. SEMC 2010, The Fourth International Conference on Sturcutral Engineering, Mechanics and Computation, 2010, Cape Town, South Africa. **(SEMC 2010 Young Researcher Fellowship Award)**

16) Xuhong Qiang, Frans S.K. Bijlaard, Henk Kolstein, Leen Twilt. Numerical Modelling of HSS Endplate Connections at Elevated Temperatures. The 6th International Conference on Structures in Fire, SiF'10, 2010, East Lansing, USA.

17) Xuhong Qiang, Frans S.K. Bijlaard, Henk Kolstein. Numerical analysis of HSS Endplate Connections at ambient and elevated temperatures. International Conference on Applications of Structural Fire Engineering, ASFE 2011, Prague, Czech Republic. (selected by **Journal of Structural Fire Engineering**)

18) Xuhong Qiang, Frans S.K. Bijlaard, Henk Kolstein. Elevated temperature effect on elastic modulus of high strength steel S690. International Conference on Advances in Construction Materials through Science and Engineering, RILEM 2011, Hong Kong.

19) Xuhong Qiang, Frans S.K. Bijlaard, Henk Kolstein. Material behaviour of high strength steel S460 in fire and after fire. The 7th International Conference on Advances in Steel Structures, ICASS 2012, Nanjing, China. (selected by **IES Journal Part A: Civil & Structural Engineering**)

20) Xuhong Qiang, Frans S.K. Bijlaard, Henk Kolstein. Material behaviour of high strength steel S690 in fire and after fire. The 7th International Conference on Structures in Fire, SiF'12, 2012, Zurich, Switzerland.

21) Xuhong Qiang, Frans S.K. Bijlaard, Henk Kolstein. Predictive equations for high strength structural steel S690 exposed to fire. The 10th International Conference on Advances in Steel Concrete Composite and Hybrid Structures, ASCCS 2012, Singapore.